FACULDADE DE ENGENHARIA DA UNIVERSIDADE DO PORTO

Design and Development of a Robotic Lower-Limb Rehabilitation Support System for Seated and Supine Rehabilitation

Sandro Daniel Oliveira



Master in Bioengineering

Supervisor: Prof. Vítor Hugo Machado Oliveira Pinto, PhD

October 11, 2026

© Sandro Oliveira, 2026

Resumo

A crescente necessidade de serviços de reabilitação, associada a condições que podem causar limitações motoras persistentes, impulsiona o desenvolvimento de tecnologias que auxiliam na execução de exercícios repetitivos e controlados. Os sistemas robóticos podem ajudar neste processo, permitindo controlar o movimento, acompanhar o utilizador e ajustar a assistência conforme as suas capacidades. Esta dissertação teve como objetivo conceber, desenvolver e avaliar experimentalmente um sistema robótico ajustável para auxiliar na reabilitação do membro inferior. O sistema destina-se a pessoas com mobilidade limitada e à realização de exercícios em posições sentada ou deitada, procurando simultaneamente limitar a massa, o custo e a complexidade mecânica do sistema.

Foi desenvolvido um protótipo para um único membro inferior, com três articulações ativas correspondentes à anca, ao joelho e ao tornozelo. A estrutura mecânica tem segmentos ajustáveis para a coxa e perna. O dimensionamento foi definido com base em requisitos biomecânicos e antropométricos. A atuação e a monitorização da posição articular usam motores e *encoders* magnéticos absolutos. Seis canais de eletromiografia ajudam a estimar a participação voluntária do utilizador, sendo usados para identificar a intenção de movimento e a intensidade da ativação muscular.

Foram implementados dois modos de reabilitação. No modo passivo, as articulações seguem trajetórias cíclicas predefinidas. No modo ativo-assistido, a intenção de movimento, a contribuição voluntária e a posição articular são usadas para ajustar a referência de movimento e a assistência robótica por meio de uma estratégia *assist-as-needed*. A arquitetura também inclui mecanismos de segurança baseados em software e uma aplicação de computador para configuração, calibração e monitorização do sistema.

A avaliação experimental foi realizada de forma progressiva, começando pela validação individual das funções mecânicas, de atuação, sensorização, controlo e segurança, seguida de testes de integração. Nos ensaios sem carga, o sistema executou os modos de reabilitação passivo e ativo-assistido e permitiu a operação integrada das três articulações, incluindo movimentos simultâneos. Durante a posterior avaliação com o membro inferior mecanicamente acoplado ao protótipo, ocorreu a fratura da placa-guia da coxa durante o primeiro movimento passivo da anca, revelando uma limitação da robustez estrutural da configuração atual.

De forma geral, os resultados demonstram a viabilidade funcional da arquitetura proposta ao nível de prova de conceito. As funções de sensorização, atuação, controlo e segurança apresentaram o comportamento esperado nas condições avaliadas, mas a limitação identificada durante o ensaio com carga evidencia a necessidade de desenvolvimento mecânico adicional e de nova validação estrutural antes da utilização do sistema nas condições de reabilitação pretendidas.

Palavras-chave: reabilitação robótica • membro inferior • controlo *assist-as-needed* • eletromiografia de superfície • interação humano–robô

Abstract

The growing need for rehabilitation services, associated with conditions that can cause persistent motor limitations, drives the development of technologies that assist in the performance of repetitive and controlled exercises. Robotic systems can help in this process. They make it possible to control movement, monitor the user and adjust the assistance according to their capabilities. This dissertation aimed to design, develop and experimentally evaluate an adjustable robotic system to support lower-limb rehabilitation. The system is intended for people with limited mobility and for exercises performed in seated or lying positions, while simultaneously aiming to limit the mass, cost and mechanical complexity of the system.

A prototype was developed for a single lower limb, with three active joints corresponding to the hip, knee and ankle. The mechanical structure has adjustable thigh and shank segments. The dimensions were defined based on biomechanical and anthropometric requirements. Actuation and joint-position monitoring use motors and absolute magnetic encoders. Six electromyography channels help estimate the user's voluntary participation and are used to identify movement intention and the intensity of muscle activation.

Two rehabilitation modes were implemented. In passive mode, the joints follow predefined cyclic trajectories. In active-assisted mode, movement intention, voluntary contribution and joint position are used to adjust the movement reference and robotic assistance through an assist-as-needed strategy. The architecture also includes software-based safety mechanisms and a computer application for system configuration, calibration and monitoring.

The experimental evaluation was carried out progressively, starting with the individual validation of the mechanical, actuation, sensing, control and safety functions, followed by integration tests. During unloaded tests, the system performed both passive and active-assisted rehabilitation modes and allowed the integrated operation of the three joints, including simultaneous movements. During the subsequent evaluation with the lower limb mechanically coupled to the prototype, the thigh guide plate fractured during the first passive hip movement, revealing a limitation in the structural robustness of the current configuration.

Overall, the results demonstrate the functional feasibility of the proposed architecture at the proof-of-concept level. The sensing, actuation, control and safety functions behaved as expected under the evaluated conditions, but the limitation identified during the loaded test highlights the need for further mechanical development and additional structural validation before the system can be used under the intended rehabilitation conditions.

Keywords: robotic rehabilitation • lower limb • assist-as-needed control • surface electromyography • human–robot interaction

The United Nations Sustainable Development Goals

The development of the robotic lower-limb rehabilitation support system presented in this dissertation relates to several objectives of the United Nations Sustainable Development Goals (SDGs). The strongest connections arise from the healthcare application of the prototype, the technological development involved in its implementation, and the effort to design a rehabilitation solution that can accommodate users with limited mobility and different anthropometric characteristics.

The most relevant goals for the present work are SDG 3 (Good Health and Well-being), SDG 9 (Industry, Innovation and Infrastructure), and SDG 10 (Reduced Inequalities). Their relationship with the dissertation is summarised in Table 1.

The connection with SDG 3 is mainly associated with the rehabilitation purpose of the system, whereas SDG 9 reflects the engineering and technological development carried out throughout the dissertation. SDG 10 is related to the effort to design the prototype for users with different physical characteristics and for rehabilitation situations in which conventional standing or gait-based approaches may not be appropriate. Since the system remains a proof-of-concept prototype, these contributions should be understood as design and technological contributions rather than as demonstrated clinical outcomes.

Table 1: Sustainable Development Goals related to the developed rehabilitation system.

SDG	Goal	Relevant Target	How the Dissertation Addresses the Target
3	Good Health and Well-being	**Target 3.8**: Achieve universal health coverage, including access to quality essential health-care services and financial risk protection.	The work develops a robotic system intended to support lower-limb rehabilitation in seated and lying positions, including users with limited mobility who may not be able to participate in standing or gait-based rehabilitation. Cost was also considered throughout development, with the aim of limiting the financial requirements of the proposed rehabilitation solution.
9	Industry, Innovation and Infrastructure	**Target 9.5**: Enhance scientific research and technological capabilities and encourage innovation.	The dissertation involved the design, implementation and experimental evaluation of an integrated robotic rehabilitation system. The developed prototype combines an adjustable three-joint mechanical structure, actuation, magnetic joint-position sensing, six-channel electromyography acquisition, passive and active-assisted rehabilitation control, assist as needed, safety mechanisms and a desktop application within a common architecture.
10	Reduced Inequalities	**Target 10.2**: Empower and promote the social, economic and political inclusion of all, irrespective of age, disability or other status.	The system was designed for users with limited mobility and for rehabilitation situations in which standing or gait-based training may not be possible. Its seated and lying configurations allow rehabilitation to be considered for users with more restricted functional capabilities, while the adjustable thigh and shank sections were designed to accommodate users with different anthropometric characteristics.

Agradecimentos

Obrigado ao Professor Vítor Hugo Pinto por todo o acompanhamento e apoio ao longo da minha dissertação, em especial pela disponibilidade constante e pelo rumo claro que ajudou a dar a este trabalho.

Obrigado aos meus amigos, aos que conheci na faculdade e aos que fiz em casa, pela companhia e por todas as memórias.

Obrigado aos meus avós por todo o carinho.

Obrigado à minha namorada pela companhia diária, por todo o apoio e pelo crescimento em conjunto.

O mais sincero e profundo obrigado aos meus pais, sem os quais nada seria possível, por tudo o que sou.

Sandro Oliveira

"Happiness is the richest thing we will ever own."

Donald Duck

Contents

1 Introduction **1**
- 1.1 Context . . . 1
- 1.2 Motivation . . . 2
- 1.3 Objectives . . . 3
- 1.4 Contributions . . . 3
- 1.5 Dissertation Structure . . . 4

2 Theoretical Background **6**
- 2.1 Lower-limb rehabilitation and clinical motivation . . . 6
- 2.2 Robotic systems in lower-limb rehabilitation . . . 7
- 2.3 Design requirements for seated and lying lower-limb rehabilitation systems . . . 9
- 2.4 Lower-limb biomechanics and anthropometry . . . 10
- 2.5 Mechanical architecture, adjustability and human-robot alignment . . . 14
- 2.6 Actuation technologies for lower-limb rehabilitation systems . . . 16
- 2.7 Sensing technologies for lower-limb rehabilitation systems . . . 18
- 2.8 Control strategies for lower-limb rehabilitation systems . . . 22
- 2.9 Research gap . . . 25
- 2.10 Summary . . . 25

3 System Development and Implementation **27**
- 3.1 System Overview . . . 27
- 3.2 Mechanical Structure . . . 30
  - 3.2.1 Overall Mechanical Architecture . . . 30
  - 3.2.2 Anthropometric Adjustability . . . 34
  - 3.2.3 Joint Design and Alignment . . . 39
  - 3.2.4 Human-Robot Interfaces . . . 42
  - 3.2.5 Manufacturing and Assembly . . . 43
- 3.3 Actuation System . . . 44
  - 3.3.1 Joint Torque Estimation . . . 44
  - 3.3.2 Motor and Gearbox Selection . . . 46
  - 3.3.3 Motor Drivers and Power Electronics . . . 49
- 3.4 Joint Position Sensing . . . 50
  - 3.4.1 Encoder Selection . . . 50
  - 3.4.2 Mechanical Integration . . . 50
  - 3.4.3 Encoder Acquisition and Calibration . . . 51
- 3.5 EMG Acquisition and Processing . . . 53
  - 3.5.1 Sensor Placement . . . 53
  - 3.5.2 Signal Acquisition . . . 55

3.5.3 EMG Calibration and Normalisation . . . 56
3.5.4 Movement Intention Detection . . . 58
3.6 Control System . . . 59
3.6.1 Control Architecture . . . 60
3.6.2 High-Level Control . . . 62
3.6.3 Mid-Level Control . . . 62
3.6.4 Low-Level Motor Control . . . 69
3.6.5 Communication Architecture . . . 70
3.7 Safety Implementation . . . 71
3.8 Desktop Application . . . 72
3.9 Final System Integration . . . 75
3.10 Summary . . . 78

4 Experimental Validation and Results **81**
4.1 Validation Methodology . . . 81
4.2 Mechanical and Functional Validation . . . 81
4.2.1 Anthropometric Adjustment . . . 82
4.2.2 Joint Range of Motion . . . 83
4.2.3 Structural and Assembly Assessment . . . 85
4.3 Actuation and Joint-Position Validation . . . 86
4.3.1 Actuator Movement Tests . . . 86
4.3.2 Encoder Operation . . . 87
4.3.3 Joint-Position Tracking . . . 89
4.4 EMG and Movement-Intention Validation . . . 91
4.4.1 Calibration Evaluation . . . 92
4.4.2 Movement-State Classification . . . 92
4.4.3 Movement-Intensity Estimation . . . 94
4.5 Control-System Validation . . . 95
4.5.1 Passive Rehabilitation . . . 96
4.5.2 Active-Assisted Rehabilitation . . . 98
4.6 Safety and Fault-Handling Validation . . . 105
4.6.1 Joint and Speed Limits . . . 105
4.6.2 Communication Loss . . . 107
4.6.3 Encoder Fault . . . 109
4.6.4 Actuator Tracking Fault . . . 112
4.6.5 Emergency Stop and Recovery . . . 113
4.7 Integrated System Validation . . . 118
4.7.1 Single-Joint Integration . . . 118
4.7.2 Multi-Joint Integration . . . 121
4.7.3 System Evaluation Under Mechanical Loading . . . 124
4.8 Discussion . . . 125
4.9 Summary . . . 127

5 Conclusions and Future Work **129**
5.1 General Conclusions . . . 129
5.2 Limitations . . . 130
5.3 Future Work . . . 131

References **133**

A Calculation Details **139**
A.1 Anthropometric Calculations . . . 139
A.2 Preliminary Joint Torque Calculations . . . 139
A.3 Gearbox Output Torque . . . 141
A.4 Final Joint Torque Verification . . . 141

B Technical Drawings **144**
B.1 Structural Plates and Foot Platform . . . 144
B.2 Motor Supports . . . 150
B.3 Encoder Supports . . . 155
B.4 Stationary Support Structure . . . 158

C Additional Validation Results **162**
C.1 Encoder Operation . . . 162
C.1.1 Hip Joint . . . 162
C.1.2 Ankle Joint . . . 162
C.2 Joint-Position Tracking . . . 162
C.2.1 Hip Joint . . . 162
C.2.2 Ankle Joint . . . 166
C.3 EMG and Movement-Intention Validation . . . 168
C.3.1 Hip Joint . . . 168
C.3.2 Ankle Joint . . . 169

D Integrated Validation Circuits **173**
D.1 Single-Joint Knee Circuit . . . 173
D.2 Complete Three-Joint Circuit . . . 175

List of Figures

1.1 Global number of people with conditions that could benefit from rehabilitation, showing the distribution across age groups and the increase in rehabilitation need between 1990 and 2019. Reproduced from Cieza et al. (2020). 2

2.1 Global burden of stroke in the world. Adapted from Feigin et al. (2025). 6
2.2 Bedside lower-limb rehabilitation robot supporting the patient's limb during supine rehabilitation. Reproduced from Z. Wang et al. (2024). 9
2.3 Main anatomical parts of the lower limb (Luu and Nguyen 2026). 11
2.4 Anatomical reference planes (Luu and Nguyen 2026). 12
2.5 Relevant lower-limb anthropometric measurements from ANSUR II. Compiled from Gordon et al. (2015) 13
2.6 Examples of physical interfaces employed to attach lower-limb robotic systems to the user. (a) Fixation using straps and cuffs, (b) a rigid support together with straps, and (c) a moulded shell secured by straps. Panels (a) and (b) are adapted from Andrade et al. (2024); panel (c) is adapted from Sarkisian, Ishmael, and Lenzi (2021). 15
2.7 Examples of power transmission mechanisms used in lower-limb rehabilitation systems are shown: (a) direct-mounted transmission with a speed reducer, (b) gear mechanism, (c) tendon-driven system, (d) push–pull cable mechanism, and (e) chain-and-gear mechanism. Adapted from Aliman, Ramli, and Amiri (2024). . . 19
2.8 Examples of rotary encoder technologies: (a) coded disc used in a mechanical contact encoder, and operating principles of (b) a magnetic encoder and (c) an optical encoder. Adapted from Dynamics Research Corporation (1992) and Seybold et al. (2019). 21
2.9 General hierarchical structure of an exoskeleton control system, consisting of high-level, mid-level and low-level control. Reproduced from Miguel-Fernández et al. (2023). 22
2.10 Main High-level control objectives: (I) assistive control, (II) challenge-based control, and (III) adaptive control. Reproduced from Miguel-Fernández et al. (2023). 23
2.11 Main mid-level control strategies used in lower-limb rehabilitation systems: trajectory-tracking control, neuromuscular control and compliant control. Reproduced from Miguel-Fernández et al. (2023). 24

3.1 Overall architecture of the developed robotic lower-limb rehabilitation support system. 28
3.2 Developed robotic lower-limb rehabilitation support system in the two intended rehabilitation configurations. 29

3.3 Overview of the mechanical design of the developed robotic lower-limb rehabilitation support system. . . . 31
3.4 Models of the structural plates used in the thigh and shank sections. . . . 32
3.5 Model of the foot platform. . . . 32
3.6 Models of the mechanical supports developed for the hip, knee and ankle motors. 33
3.7 Models of the stationary supporting structure and the hip actuator mounting arrangement. . . . 33
3.8 Models of the encoder mounting solutions developed for the hip, knee and ankle motor assemblies. . . . 34
3.9 Assembly of the guide and sliding plates used for longitudinal adjustment. . . . 35
3.10 Main elements of the locking mechanism to fix the relative position of the guide and sliding plates. . . . 36
3.11 Minimum and maximum configurations of the adjustable thigh and shank sections. At maximum length, a 100 mm overlap between plates is observable. . . . 38
3.12 Keyed-shaft geometry and its use in the direct mechanical coupling. . . . 39
3.13 Geometric alignment of the robotic joint axes in the developed prototype. . . . 41
3.14 Interfaces implemented in the prototype using adjustable Velcro straps. . . . 42
3.15 Ethylene-Vinyl Acetate (EVA) foam lining applied to the contact surfaces of the thigh section. . . . 43
3.16 AS5048B Adapter Board used for joint-position sensing. . . . 51
3.17 Example of an AS5048B encoder mounting arrangement. . . . 52
3.18 Anatomical locations of the lower-limb muscles. Adapted from Betts et al. (2022). 54
3.19 MyoWare 2.0 Muscle Sensor (SparkFun Electronics). . . . 56
3.20 Electromyography (EMG) calibration and normalisation procedure. . . . 57
3.21 Control architecture of the developed system and organisation of the high, mid and low-level control functions. . . . 61
3.22 Implemented passive rehabilitation trajectory-generation algorithm. . . . 64
3.23 Implemented active-assisted mid-level control structure. . . . 66
3.24 Overview page of the desktop application. . . . 73
3.25 Patient-management page of the desktop application. . . . 74
3.26 EMG calibration page of the desktop application. . . . 74
3.27 Configuration of the active-assisted and passive rehabilitation modes through the desktop application. . . . 76
3.28 System-settings page of the desktop application. . . . 77
3.29 Advanced diagnostic page of the desktop application. . . . 77

4.1 Minimum and maximum adjustment configurations of the thigh section. . . . 82
4.2 SolidWorks configurations showing the reference geometry and angular measurements used to evaluate the joint Range of Motion (ROM) limits. . . . 84
4.3 Evaluation of the rotation-unwrapping function using the knee actuator. . . . 88
4.4 Step-based and encoder-derived knee joint positions during the multi-position tracking test. . . . 90
4.5 Error after each return to the initial position during the knee joint repeatability tests. 90
4.6 Stationary stability of the encoder-derived knee joint-position measurement. . . . 91
4.7 EMG signals and calibration reference values during rest, flexion and extension. . 92
4.8 Normalised flexor and extensor EMG activation. . . . 93
4.9 Comparison between instructed and detected movement states across repeated relaxed, flexion and extension trials. . . . 94

4.10 Mean maximum estimated movement intensity for low, medium and high voluntary flexion and extension efforts. . . . 94
4.11 Passive rehabilitation validation results, showing the generated reference and the corresponding step-based and encoder-derived knee positions for the three tested configurations. . . . 97
4.12 Angular reference trajectories for the different movement directions and intensity levels. . . . 99
4.13 Reference behaviour in the absence of directional movement intention. . . . 100
4.14 Generated angular reference behaviour at the configured joint limits. . . . 101
4.15 Assistance response to changes in tracking error and movement intensity. . . . 103
4.16 Assisted angular target during the Assist as Needed (AAN) evaluation. . . . 103
4.17 Requested and safe angular targets during the speed-limiting test. . . . 106
4.18 Control response to communication loss and restoration. . . . 108
4.19 System response to a brief interruption of encoder acquisition. . . . 110
4.20 System response to a sustained interruption of encoder acquisition. . . . 111
4.21 System response when encoder acquisition was unavailable during initialisation. . . 111
4.22 System response to brief and sustained tracking errors. . . . 113
4.23 System response during the emergency-stop sequence. . . . 115
4.24 System response during the fault-recovery sequence. . . . 116
4.25 Knee movement during the integrated sensing and control test. T1, T3 and T5 correspond to knee flexion, whereas T2, T4 and T6 correspond to knee extension. Each active phase was followed by a relaxation period. . . . 119
4.26 AAN behaviour during the integrated knee test. T1, T3 and T5 correspond to knee flexion, whereas T2, T4 and T6 correspond to knee extension. . . . 120
4.27 Encoder-derived knee-position variation during the final 1 s of the relaxation period following each single-joint trial. . . . 120
4.28 Detected movement intentions during the multi-joint integration test. T1-T6 correspond to the individual joint trials, whereas T7-T9 correspond to simultaneous multi-joint operation. . . . 122
4.29 Joint-position changes during the simultaneous movement trials. T7 combined hip flexion and knee extension, T8 combined knee extension and ankle dorsiflexion, and T9 combined hip flexion, knee extension and ankle dorsiflexion. . . . 123
4.30 AAN behaviour during the multi-joint integration test. . . . 123
4.31 Thigh guide plate fracture observed during the loaded passive hip rehabilitation test. 125

B.1 Technical drawing of the thigh guide plate. . . . 145
B.2 Technical drawing of the thigh sliding plate. . . . 146
B.3 Technical drawing of the shank guide plate. . . . 147
B.4 Technical drawing of the shank sliding plate. . . . 148
B.5 Technical drawing of the foot platform. . . . 149
B.6 Technical drawing of the hip motor support. . . . 151
B.7 Technical drawing of the knee motor support. . . . 152
B.8 Technical drawing of the ankle motor–encoder support base. . . . 153
B.9 Technical drawing of the ankle motor–encoder support wall. . . . 154
B.10 Technical drawing of the hip encoder support. . . . 156
B.11 Technical drawing of the knee encoder support. . . . 157
B.12 Technical drawing of the hip motor mounting block. . . . 159
B.13 Technical drawing of the stationary support base. . . . 160
B.14 Technical drawing of the stationary support wall. . . . 161

C.1 Rotation-unwrapping results for the hip actuator. 163
C.2 Rotation-unwrapping results for the ankle actuator. 164
C.3 Step-based and encoder-derived hip joint positions during the multi-position tracking test. 165
C.4 Error after each return to the initial position during the hip joint repeatability tests. 165
C.5 Stationary stability of the encoder-derived hip joint-position measurement. 166
C.6 Step-based and encoder-derived ankle joint positions during the multi-position tracking test. 166
C.7 Error after each return to the initial position during the ankle joint repeatability tests. 167
C.8 Stationary stability of the encoder-derived ankle joint-position measurement. . . 167
C.9 EMG signals and calibration reference values for the hip muscle pair. 168
C.10 Normalised flexor and extensor EMG activation for the hip muscle pair. 168
C.11 Comparison between instructed and detected movement states during the hip validation trials. 169
C.12 Mean maximum estimated movement intensity for low, medium and high voluntary hip flexion and extension efforts. 170
C.13 EMG signals and calibration reference values for the ankle muscle pair. 170
C.14 Normalised dorsiflexor and plantarflexor EMG activation for the ankle muscle pair. 171
C.15 Comparison between instructed and detected movement states during the ankle validation trials. 171
C.16 Mean maximum estimated movement intensity for low, medium and high voluntary ankle dorsiflexion and plantarflexion efforts. 172

D.1 Circuit used for the single-joint knee integration test. 174
D.2 Circuit used for the multi-joint integration test and the additional lying-configuration functional check. 176

List of Tables

1 Sustainable Development Goals related to the developed rehabilitation system. . . iv

2.1 Comparison between end-effector and exoskeleton-based rehabilitation systems. . 8
2.2 Reference ranges of motion for the lower limb. Adapted from Luu and Nguyen (2026). 12
2.3 Anthropometric coefficients for the lower-limb segments, based on the data reported by Winter (Winter 2009). 14
2.4 Main mechanical methods for user adaptation and human-robot compatibility in lower-limb rehabilitation systems. 16
2.5 Comparison of the main actuation technologies used in lower-limb rehabilitation systems, based on Aliman, Ramli, and Amiri (2024). 17

3.1 Anthropometric measurements from ANSUR II considered for the dimensional design of the thigh and shank sections (Gordon et al. 2015). 35
3.2 Estimated reference lengths of the thigh and shank used to establish the lower and upper design limits of the prototype. 35
3.3 Plate dimensions and adjustment ranges of the thigh and shank sections. 37
3.4 Specific anthropometric measurements used to define the fixed dimensions of the foot platform. 37
3.5 Specific anthropometric measurements used to define the fixed positions of the hip and ankle joint axes. 40
3.6 Anthropometric values used for the lower and upper design cases in the torque estimations (Gordon et al. 2015). 45
3.7 Preliminary joint torque estimates used for actuator selection. 46
3.8 Specifications of the actuators and gearboxes selected for the three robotic joints. Underlined values indicate the torque considered available for each actuator assembly. 47
3.9 Masses of the actuator assemblies and moving mechanical components considered in the final torque verification. 48
3.10 Final joint torque estimates including gravitational and inertial contributions. . . 48
3.11 Driver configurations used for the three robotic joints. 49
3.12 Surface Electromyography (sEMG) sensor locations. 55
3.13 Conditions used for movement-intention classification. 59
3.14 High-level interpretation of the detected movement states. 62
3.15 Effect of the AAN input variables on assistance. 68
3.16 Structure of the movement-intention message transmitted through the Universal Asynchronous Receiver-Transmitter (UART) connection. 70
3.17 Implemented software safety mechanisms. 72
3.18 Mass of the main components associated with the moving part of the final prototype. 79

3.19 Cost of the main components used in the final prototype. 79

4.1 Designed and measured adjustment dimensions of the thigh and shank sections. . 82
4.2 Comparison between the designed and practical ROM values. 83
4.3 Summary of the actuator movement tests. 86
4.4 Results of the encoder rotation-unwrapping tests. 87
4.5 Results of the multi-position joint tracking tests. 89
4.6 Results of the joint repeatability tests. 90
4.7 Stationary stability of the encoder joint-position measurements. 90
4.8 Classification performance for the tested movement states. 93
4.9 Passive rehabilitation configurations used during validation. 96
4.10 Quantitative position-tracking results for the three passive rehabilitation test configurations. 96
4.11 Comparison between expected and observed reference speeds for different movement intensities. 99
4.12 Comparison of expected and observed AAN outputs under different input conditions. 102
4.13 Results of the joint-position limiting tests. 106
4.14 Comparison of configured and observed safe-target speed limits. 106
4.15 Results of the actuator tracking-fault tests. 112
4.16 Results of the emergency-stop and fault-recovery tests. 117

C.1 Movement-state classification results for the hip. 169
C.2 Movement-state classification results for the ankle. 169

D.1 Main connections used in the single-joint knee circuit. 173
D.2 Actuation Arduino pins used for the motor-driver control signals. 175
D.3 Inter-Integrated Circuit (I^2C) address configuration of the three AS5048B encoders. 175
D.4 Shared connections used in the complete three-joint circuit. 175

List of Acronyms

AAN Assist as Needed

BLDC Brushless DC

COM Centre of Mass

DALY Disability-Adjusted Life Year

EEG Electroencephalography

EMG Electromyography

EVA Ethylene-Vinyl Acetate

I^2C Inter-Integrated Circuit

IMU Inertial Measurement Unit

P10 10th Percentile

P90 90th Percentile

PID Proportional-Integral-Derivative

PLA Polylactic Acid

ROM Range of Motion

sEMG Surface Electromyography

UART Universal Asynchronous Receiver-Transmitter

Chapter 1

Introduction

1.1 Context

The need for rehabilitation represents a significant challenge for global health. Based on data from the Global Burden of Disease Study 2021, approximately 2.56 billion people worldwide were living with a health condition that could benefit from rehabilitation in 2021 (Zhang et al. 2026), corresponding to roughly one third of the global population. As illustrated in Figure 1.1, the need for rehabilitation affects individuals across all age groups and has increased considerably since 1990. Of the conditions contributing to this demand, stroke is especially important since it can cause persistent motor impairments and long-term disability. In 2021, around 93.8 million people worldwide were living with stroke (Feigin et al. 2025).

For many stroke survivors, motor impairments can reduce their capacity to carry out everyday activities and limit their ability to take part in society, having a direct impact on their quality of life (Alt Murphy et al. 2025). As a result, motor rehabilitation is of great importance in restoring functional ability and enhancing the patient's independence. To support this recovery, rehabilitation must include training that is appropriately dosed, repetitive, goal-directed, and progressive, adapted to the patient's particular condition and stage of recovery (Alt Murphy et al. 2025).

Providing this kind of rehabilitation via traditional therapy can be demanding since there is large variation between patients and the clinical resources available are limited, which makes it hard for physiotherapists to deliver the necessary intensity and number of repetitions while at the same time getting quantitative data on the patient's performance (Miguel-Fernández et al. 2023). Robotic rehabilitation systems have emerged as helpful tools that can support repetitive, controlled training while also reducing physical strain on therapists. They are also capable of incorporating sensing and control methods that enable patient performance to be monitored and the level of assistance to be adjusted depending on the rehabilitation task (Miguel-Fernández et al. 2023). Recent evidence has shown that robot-assisted lower-limb training can improve motor function, walking ability, and balance in patients who have had a stroke (H. Wang et al. 2025). Nevertheless, not all patients are initially able to participate in rehabilitation activities that involve standing or walking.

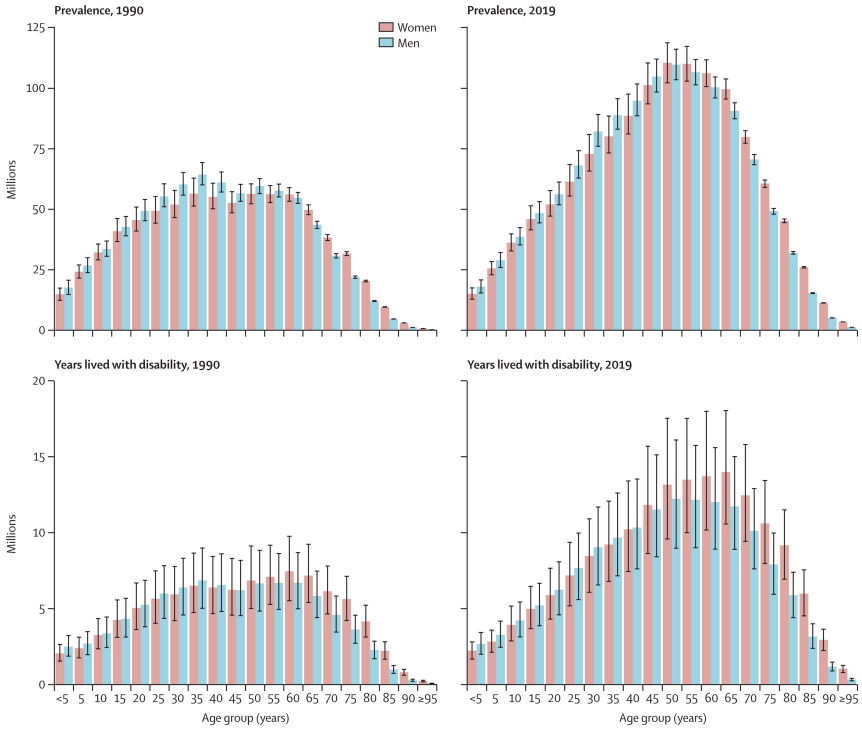


Figure 1.1: Global number of people with conditions that could benefit from rehabilitation, showing the distribution across age groups and the increase in rehabilitation need between 1990 and 2019. Reproduced from Cieza et al. (2020).

Patients who have severe or acute neurological or limb-related conditions might have to stay in bed temporarily or may have inadequate mobility to carry out gait training (D. Wang et al. 2023). In these cases, lower-limb rehabilitation may have to be carried out while the patient is sitting or lying down. These rehabilitation scenarios introduce specific requirements regarding patient positioning, lower-limb support and adaptation to different users.

Despite the technological progress made in this field, several practical limitations remain. Concerns raised by patients and rehabilitation professionals include safety, the use of one-size-fits-all approaches, ease of use, device weight and placement, and cost (Morris et al. 2023).

1.2 Motivation

Conventional rehabilitation remains essential for the recovery of lower-limb motor function, but providing intensive, repetitive and patient-specific training can demand a lot of time and physical energy from rehabilitation professionals. Moreover, since clinical resources are limited it can be difficult to keep up the necessary training dosage and to continuously monitor the patient's performance. Robotic rehabilitation can help address some of these limitations.

However, robotic rehabilitation systems also have their own limitations, since existing solutions can be hard to adapt to different patients and aspects such as device weight, mechanical complexity, ease of use and cost can reduce their practicality and accessibility. This is especially

important in the case of rehabilitation being provided to patients with reduced mobility who may need treatment while seated or lying down.

The motivation for this dissertation is to explore a robotic rehabilitation solution for the lower limbs which retains the key benefits of robotic assistance but at the same time reduces some of the practical limitations of the current systems.

1.3 Objectives

The goal of this dissertation is to design, develop and experimentally evaluate an adjustable robotic lower-limb rehabilitation support system intended for patients with limited mobility undergoing rehabilitation in seated or lying positions, while aiming to limit system mass, cost and mechanical complexity. The system should be capable of providing controlled assistance to lower-limb movements, adapting to different users and incorporating sensing and control strategies that allow the rehabilitation process to respond to the patient's capabilities and level of participation.

To accomplish this overall aim, the following specific objectives were established:

- Specify the biomechanical and anthropometric requirements which should guide the development of the rehabilitation system, such as the relevant joint movements, ranges of motion, user dimensions and expected mechanical loads.
- Design and develop an adjustable mechanical structure suitable for lower-limb rehabilitation in seated and lying positions, and select and integrate an actuation solution capable of producing controlled movements of the lower-limb joints.
- Select and incorporate appropriate sensing technologies to monitor the state of the robotic system and collect information related to the patient's movements and level of involvement during rehabilitation.
- Develop a control architecture capable of providing different degrees of robotic assistance depending on the rehabilitation task and the patient's capabilities, while incorporating appropriate safety measures to ensure that the system operates within the specified limits.
- Develop a functional prototype and experimentally evaluate its main mechanical, sensing and control functions.

1.4 Contributions

This dissertation contributes to the development of a robotic lower-limb rehabilitation support system intended for seated and lying rehabilitation. The main contributions can be divided into physical and scientific and technical contributions.

Physical contributions.

The key physical contribution consists of designing and building a functional prototype for a single lower limb, featuring three joints that are actuated at the hip, knee and ankle. The mechanical structure has adjustable thigh and shank sections, a special foot platform, and custom supports for both the actuators and the joint-position sensors. The prototype was developed using accessible manufacturing methods, with most of the mechanical components produced by 3D printing.

The project also involved selecting and integrating the motor-gearbox assemblies, along with their individual drivers and an Arduino-based electronic system. This architecture separates physiological sensing from actuation and joint-position monitoring. Custom mounting solutions were created for the magnetic encoders, and a six-channel Electromyography (EMG) acquisition arrangement was established to obtain information from opposing muscle pairs associated with the three joints.

Scientific and technical contributions.

The scientific and technical contributions include the application of anthropometric and biomechanical data to the dimensional design and actuator selection of the proposed system. The control architecture incorporates both passive and active-assisted rehabilitation modes in order to support different levels of voluntary user participation. A methodology was established for estimating the torque requirements of the hip, knee and ankle, the estimation first being based on the user's lower limb and then taking into account the masses of the respective robotic components.

Another contribution consists of the development of a movement-intention detection method based on EMG and its incorporation into a hierarchical control architecture. The implemented processing includes individual muscle calibration, normalisation of the signal, classification of the movement states and estimation of movement intensity. These outputs are then used to produce angular references and to adjust the assistance given by the Assist as Needed (AAN) controller. The architecture also features joint-position monitoring and software-based safety mechanisms.

Finally, the dissertation presents a phased experimental methodology for assessing the mechanical structure, actuation, sensing, control and safety features of the prototype. The results from the tests serve as evidence of the way in which the mechanical, actuator and EMG subsystems function under the conditions studied. The contribution of this work is therefore the development and functional evaluation of an integrated rehabilitation-support solution, rather than the demonstration of clinical effectiveness.

1.5 Dissertation Structure

This dissertation is organised into five chapters, followed by appendices which contain additional technical information.

Chapter 1 introduces the context and motivation for the work, defines the main and specific objectives, and presents the contributions of the dissertation.

Chapter 2 provides the theoretical background relevant to lower-limb robotic rehabilitation. This chapter covers the rehabilitation requirements, the existing robotic architectures, lower-limb biomechanics and anthropometry, mechanical design, actuation and sensing technologies, and control strategies. It also points out the main limitations of present systems which justify the development of the proposed solution.

Chapter 3 describes the development and implementation of the robotic lower-limb rehabilitation support system. It presents the mechanical structure and anthropometric adjustment, actuation and sensing, EMG acquisition and processing, and the overall control architecture. The chapter then describes the passive and active-assisted rehabilitation modes, the implemented safety mechanisms, and the graphical user interface developed to operate the system.

Chapter 4 presents the experimental validation of the developed system and discusses the results. The evaluation includes the mechanical and functional behaviour of the prototype, the operation of the actuators and encoders, joint-position control and tracking, the detection of movement intention, passive and active-assisted rehabilitation, safety mechanisms, and the integration of the complete system.

The main outcomes of the dissertation are summarised in Chapter 5, the limitations of the prototype are discussed, and possible directions for future work are identified.

Finally, the appendices provide supplementary technical and experimental material. This includes the expressions used for anthropometric dimensioning and joint-torque estimation, technical drawings of the mechanical components developed in SolidWorks, additional experimental results from the validation procedures presented throughout the dissertation, and circuit diagrams of the relevant electronic systems.

Chapter 2

Theoretical Background

2.1 Lower-limb rehabilitation and clinical motivation

Stroke is one of the main causes of long-term disability and poses a significant concern to global health. Between 1990 and 2021, the absolute number of incident strokes increased by around 70%. During this period, stroke-related deaths, prevalent stroke cases and Disability-Adjusted Life Years (DALYs) also increased considerably. In addition to its health impacts, stroke also carries a significant economic burden, with an estimated global cost of over US$890 billion, which is expected to rise to US$1.6 trillion by 2050. Figure 2.1 provides an overview of the global burden of stroke, based primarily on data from the Global Burden of Disease 2021 Study (Feigin et al. 2025).

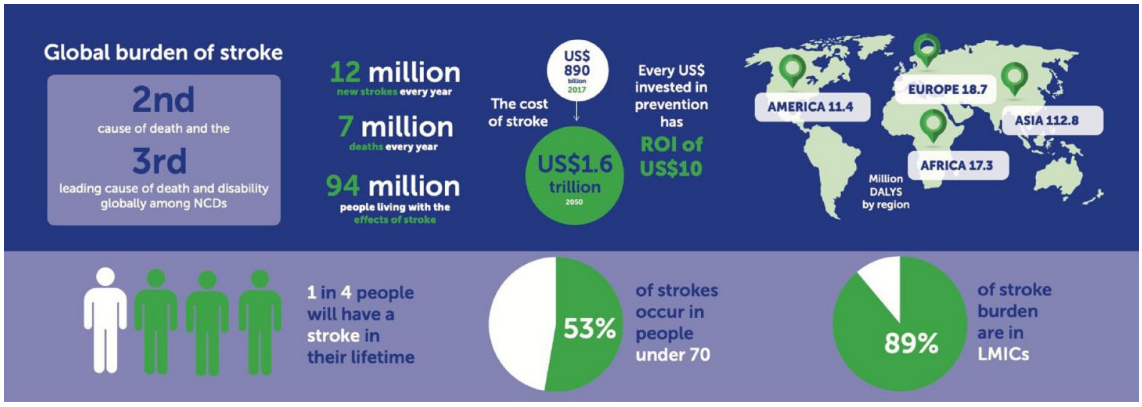


Figure 2.1: Global burden of stroke in the world. Adapted from Feigin et al. (2025).

Stroke can result in long-term motor impairments with varying degrees of severity. In more severe cases, patients can show symptoms such as paralysis, spasticity, abnormal muscle synergies, and compensatory movement patterns (Miguel-Fernández et al. 2023). On the other hand, some patients may retain part of their voluntary motor function while still presenting muscle weakness and limitations in coordination, muscle activation, or movement capacity (Li et al. 2024; Miguel-Fernández et al. 2023). Such impairments can decrease lower-limb mobility and make it harder to carry out everyday movements. Reduced mobility directly affects patients' independence, limiting

their ability to perform activities of daily living and reducing participation in social and community activities (Miguel-Fernández et al. 2023; Alt Murphy et al. 2025).

For this reason, restoring motor function and mobility is one of the main objectives of post-stroke rehabilitation. Physical therapy plays a central role in this process (Li et al. 2024). Regaining the ability to walk is an important objective for many stroke patients. However, lower-limb rehabilitation goes beyond gait recovery. It also focuses on restoring muscle strength and activation, flexibility, and joint Range of Motion (ROM), all of which contribute to improving the functional use of the affected limbs (Li et al. 2024).

Current clinical guidelines state that motor rehabilitation should involve repetitive, goal-directed, progressive and task-specific practice together with an appropriate training dose (Alt Murphy et al. 2025). Repetition allows patients to practise the movements targeted during rehabilitation, while progressive training means that the difficulty level can be increased as their functional ability improves. Yet there is no one particular amount or intensity of training that is best for all patients. The rehabilitation programme should therefore be adapted to the patient's current condition, stage of rehabilitation and functional goals, and adjusted as recovery progresses (Alt Murphy et al. 2025; Li et al. 2024). Patients should continue to take an active role during the training sessions. Giving too much help to patients who still possess some voluntary motor function can decrease their physical involvement and might have a negative impact on motor learning (Miguel-Fernández et al. 2023). Consequently, the amount of support provided during rehabilitation should be enough to help the patient to carry out the movement while preserving as much of their own contribution as possible.

It can be difficult for physiotherapists to give patients repetitive and individualised training via traditional therapy. This is because of the variation between patients, the need to constantly adjust the programme and the limited availability of clinical resources, all of which make it hard to provide the required amount of training while at the same time gathering quantitative data on patient performance (Miguel-Fernández et al. 2023). These limitations have motivated the increasing use of robotic systems as complementary tools in lower-limb rehabilitation.

2.2 Robotic systems in lower-limb rehabilitation

Robotic rehabilitation systems offer several advantages that can help overcome limitations of conventional physical therapy. These systems are able to give controlled and repetitive movements and can support a large number of training repetitions, while at the same time reducing part of the physical strain on therapists. Moreover, since sensors are incorporated, the patient's performance can be monitored quantitatively throughout the entire rehabilitation process, which in turn makes it easier to modify the rehabilitation programme based on the patient's progress (H. Wang et al. 2025; Rodríguez-Fernández, Lobo-Prat, and Font-Llagunes 2021). The way in which the systems handle sensing and control also enables them to change the level of assistance or resistance given during training in accordance with the patient's abilities, ensuring that the task remains appropriately challenging and supporting motor learning and recovery (Miguel-Fernández et al. 2023). Recent

evidence has demonstrated that robot-assisted training of the lower limbs improves motor function, walking ability and balance in stroke patients when compared with standard care (H. Wang et al. 2025).

Although lower-limb rehabilitation robotics are often linked with gait training, their uses go beyond just restoring the ability to walk. This is especially important for patients who have limited motor functions and who may not be able to stand or carry out gait training (Z. Wang et al. 2024). In such cases, robotic systems can help with particular movements of the lower limbs while the patient is either seated or lying down, enabling rehabilitation to focus on motor recovery at various stages of mobility. Different systems have been created for this purpose. For instance, R. Wu et al. (2024) presented an ankle rehabilitation robot that can function with the patient in both a seated and supine position, while the SmartSling developed by D. Wang et al. (2023) was designed to offer lower-limb rehabilitation directly at the bedside.

The way in which robotic assistance is provided is strongly influenced by the system's mechanical design. A common distinction is made between end-effector and exoskeleton-based approaches (H. Wang et al. 2025). In end-effector systems, interaction with the lower limb takes place at a distal contact point, generally the foot, and movement of the limb is caused indirectly via this point of contact. This can lead to a simpler mechanical structure and mean that there is less physical contact between the patient and the robot. When in a stationary or supine position, end-effector-based systems can also incorporate support mechanisms to partially reduce the weight of the lower limb (Z. Wang et al. 2024). Nevertheless, the limited connection with the limb also results in less direct control of the intermediate joints and may cause the movement to depart from the desired rehabilitation path (Yu et al. 2023). Exoskeleton-based systems, by contrast, make use of mechanical structures that follow the various segments of the lower limb and interact more directly with the relevant human joints. This enables more direct control of individual joint movements, but also introduces additional requirements regarding adjustment to the patient's dimensions and correct alignment between the robotic and anatomical joints (Meng et al. 2023; Squartecchia et al. 2026). A comparison between these two approaches is presented in Table 2.1.

Table 2.1: Comparison between end-effector and exoskeleton-based rehabilitation systems.

Architecture	**Human-robot interaction**	**Main advantages**	**Main limitations**
End-effector	Interaction mainly through a distal contact point.	Simpler mechanical structure. Reduced physical contact.	Less direct control of intermediate joints. Possible deviations from the planned trajectory.
Exoskeleton-based	Structure follows the segments of the lower limb. Direct interaction with the anatomical joints.	More direct control of individual joint movements.	Requires anthropometric adjustment and accurate alignment between robotic and anatomical joints.

As shown in Table 2.1, neither approach is generally better, the decision depends on the rehabilitation goals, the patient's functional capabilities, and the conditions in which the system will be used. A system intended to assist joint movement while the patient is seated or lying down has different mechanical and functional requirements from one designed for gait training.

2.3 Design requirements for seated and lying lower-limb rehabilitation systems

When it comes to robotic systems that are designed for use while sitting or lying down, their design has to take into account the specific conditions that occur in these usage environments. In particular, the weight of the lower limb must be considered, since the system may need to support the limb while assisting its movement. In the case of a weak affected limb, supporting it or partly reducing its weight can decrease the load on the joints while moving, thereby reducing the risk of discomfort or injury. For this reason, some rehabilitation robots include dedicated leg-support mechanisms and footrests, as illustrated in Figure 2.2, where the patient's lower limb is supported during supine rehabilitation (Z. Wang et al. 2024).

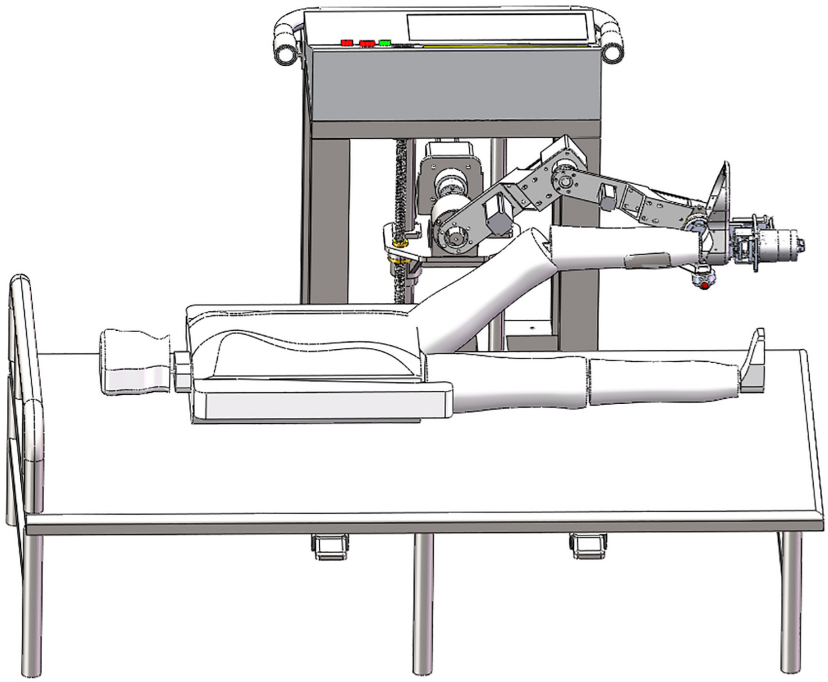


Figure 2.2: Bedside lower-limb rehabilitation robot supporting the patient's limb during supine rehabilitation. Reproduced from Z. Wang et al. (2024).

Another essential requirement is that the system should be capable of being adjusted to suit different rehabilitation positions and patients. Depending on the robotic architecture, this can involve adjusting the height or position of the device relative to the patient (Yu et al. 2023; R. Wu et al. 2024).

Furthermore, the movements caused by the rehabilitation system must also stay within safe limits. The joint ROM refers to the angular range within which a patient's joint can move safely and is thus a crucial factor when determining the working space of a rehabilitation robot (X. Wang et al. 2021). The mechanical design should enable the movements needed for rehabilitation while at the same time preventing the joints from being driven beyond their safe limits. Mechanical limiters can be included in rotational joints as an extra safety feature to physically stop excessive movement (Yu et al. 2023; Meng et al. 2023).

Another key design requirement is to ensure that the patient is properly aligned with the robotic system. The rotation centers of the robotic joints should be as near as possible to the corresponding anatomical joint centers. Misalignment of these axes can lead to unwanted forces at the interface between the patient and the robot, causing discomfort and possibly resulting in secondary injuries (Meng et al. 2023). For this reason, rehabilitation systems can include adjustment mechanisms that allow the robotic joint centers to be aligned with the patient (Meng et al. 2023; R. Wu et al. 2024).

The physical link between the patient and the device must be stable enough without reducing comfort. In order to pass on movement between the robot and the lower limb, rehabilitation systems usually make use of straps, cuffs or foot supports. These attachments should reduce the relative movement between the patient and the device without, however, causing excessive pressure or shear forces on the skin. If the interface is poorly designed it may lead to discomfort, an inconsistent transmission of the assisting forces and, after long use, possible skin injuries (Squartecchia et al. 2026).

Apart from these biomechanical requirements, practical factors such as size, mobility and the ease with which the equipment can be adjusted must also be taken into account. It can be difficult to move large and complicated rehabilitation systems from one clinical setting to another, and they may not be appropriate for use near a bed or in spaces that are limited in size. Compact designs, adjustable parts and mobile bases can enhance the practicality of these devices at the same time as reducing unnecessary mechanical complexity (Yu et al. 2023; D. Wang et al. 2023).

2.4 Lower-limb biomechanics and anthropometry

Figure 2.3 shows that the lower limb may be divided into four main anatomical parts: the pelvis, the thigh, the leg and the foot, connected by the hip, knee and ankle joints, which grant their relative movement (Luu and Nguyen 2026). In biomechanical analysis, the thigh, shank, and foot can be treated as rigid links (X. Wang et al. 2021).

The joints move along the three different anatomical planes (Figure 2.4). The hip joint allows for flexion–extension, abduction–adduction and internal–external rotation, whereas the knee is mainly defined by flexion–extension. At the ankle, the primary movements are dorsiflexion–plantarflexion, inversion–eversion and rotational movements (Luu and Nguyen 2026).

All the joint movements have a well-defined ROM, this being the angular interval within which the joint is capable of moving. The angles of the joints are measured with reference to a standard anatomical position, as shown in Figure 2.4, which is taken as the zero point for motion (Luu and

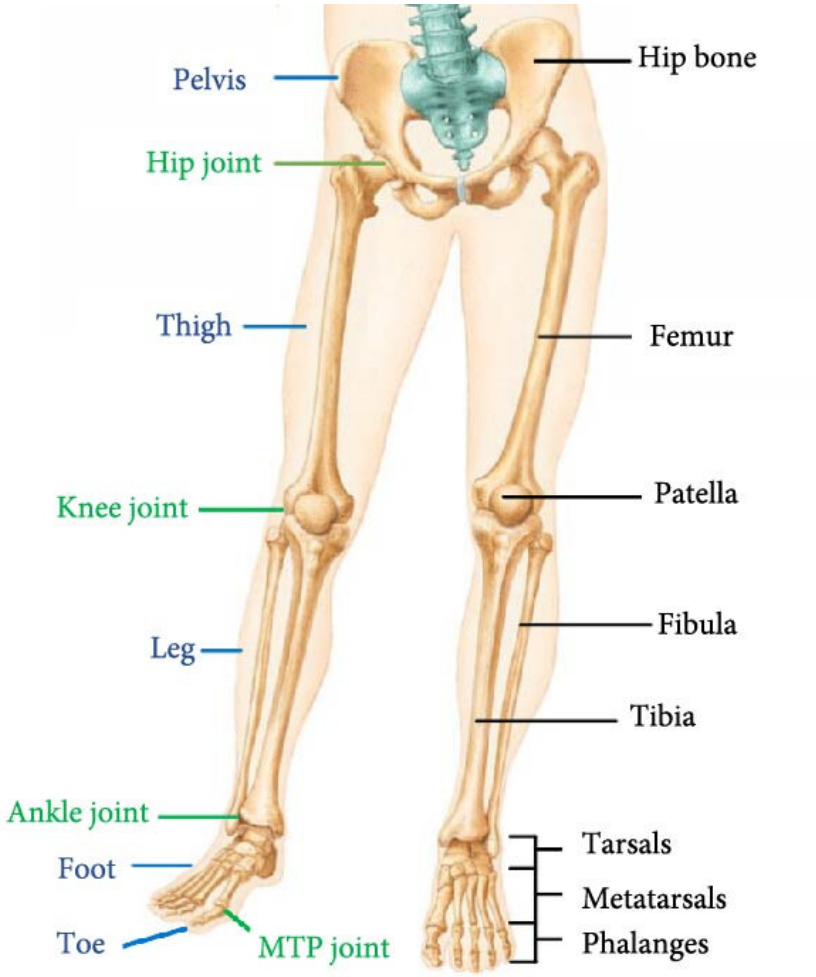


Figure 2.3: Main anatomical parts of the lower limb (Luu and Nguyen 2026).

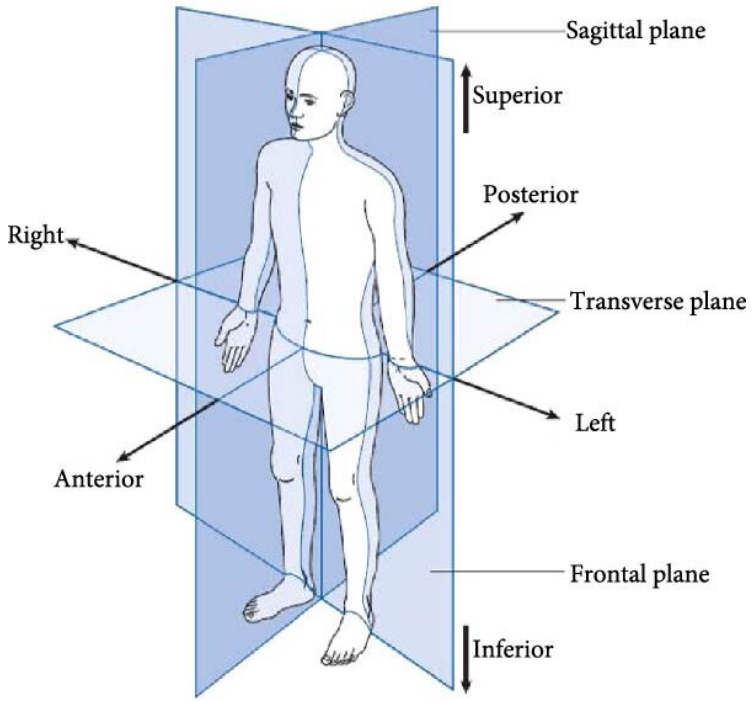


Figure 2.4: Anatomical reference planes (Luu and Nguyen 2026).

Nguyen 2026). The reference ROM values for the major movements of the hip, knee and ankle are described in Table 2.2. In rehabilitation robotics, these values are important for setting the rotational limits and workspace of robotic joints, since the system must not cause the patient's limb to move beyond a safe range (X. Wang et al. 2021; Luu and Nguyen 2026). Yet the reference values do not necessarily reflect the ROM available to all patients. The ROM differs among healthy people depending on factors such as age and sex (Soucie et al. 2011), and in the context of rehabilitation, the amount of movement available may also depend on the patient's functional state and the degree of their impairment. For that reason, the operating range of a rehabilitation robot should be determined for each individual patient rather than being based only on normative values (X. Wang et al. 2021; Luu and Nguyen 2026).

Table 2.2: Reference ranges of motion for the lower limb. Adapted from Luu and Nguyen (2026).

Joint	**Plane**	**Movement**	**ROM** (°)
Hip	Sagittal	Extension / Flexion	−30 to 120
	Frontal	Adduction / Abduction	−20 to 45
	Transverse	Medial / Lateral rotation	−50 to 40
Knee	Sagittal	Extension / Flexion	0 to 150
Ankle	Sagittal	Plantarflexion / Dorsiflexion	−40 to 20
	Transverse	Pronation / External rotation	−35 to 30
	Frontal	Inversion / Eversion	−35 to 20

The dimensions of the lower limb and its segments also show great variation from one individual to another. Anthropometric data are therefore important when defining the geometry of systems that physically interact with the human body. Large anthropometric databases can be used to characterise this variability and provide statistical distributions of different body measurements. An example is the ANSUR II database, which includes 93 anthropometric measurements taken from over 6,000 adult U.S. military personnel (Gordon et al. 2015). In addition to linear body dimensions, the database also includes body weight measurements. Among the measurements relevant to lower-limb design are trochanterion height, lateral femoral epicondyle height, lateral malleolus height, foot length and body weight. The relevant anatomical landmarks and linear measurements are illustrated in Figure 2.5. These measurements provide information not only about the position of relevant anatomical landmarks and the dimensions that a mechanical system may need to accommodate, but also about the body mass from which lower-limb segment masses can be estimated. However, it is important to clarify that the ANSUR II database is based on a U.S. military population and, as such, does not represent a general civilian or clinical population, which should be taken into account when applying these data to rehabilitation system design.

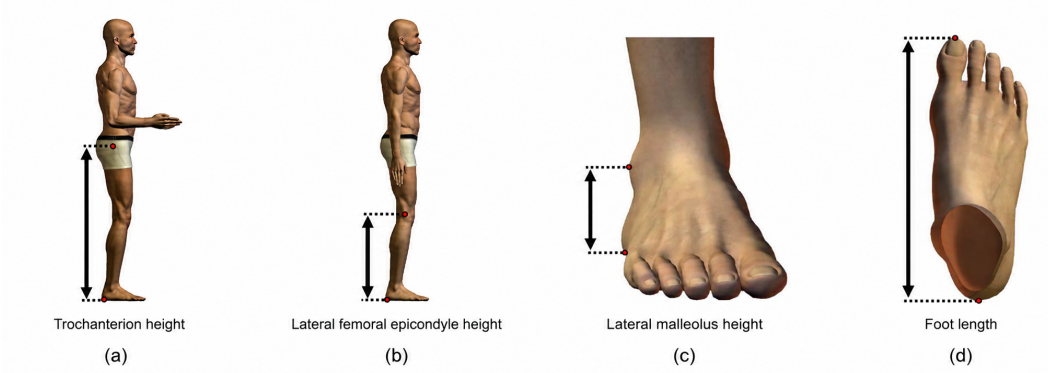


Figure 2.5: Relevant lower-limb anthropometric measurements from ANSUR II. Compiled from Gordon et al. (2015)

Other significant parameters, along with the geometric dimensions, are the mass of each segment and the location of its Centre of Mass (COM), since these properties are required to describe the mechanical behaviour of the lower limb. Anthropometric models can estimate these segment characteristics based on general body measurements. The coefficients reported by Winter (2009), based on classical anthropometric data from Dempster, express segment mass as a fraction of total body mass and the position of the COM relative to the corresponding segment length. These coefficients can therefore be combined with body-mass data, such as those available in ANSUR II, to estimate the mass and COM position of the lower-limb segments. The coefficients for the thigh, shank and foot used in this work are summarized in Table 2.3.

The biomechanical and anthropometric parameters have a direct bearing on the design of rehabilitation robots. The lengths of the segments and the positions of the anatomical joints affect the dimensions and the range of adjustment needed in the mechanical structure, while the segments' mass and the positions of their COMs have an impact on the mechanical loads and torques at the

Table 2.3: Anthropometric coefficients for the lower-limb segments, based on the data reported by Winter (Winter 2009).

Segment	**Mass / body mass**	**COM / segment length**
Thigh	0.1000	0.433
Leg (shank)	0.0465	0.433
Foot	0.0145	0.500

joints. These torques are especially important when setting actuator requirements in rehabilitation systems (Kavalieros et al. 2022). For this reason, these parameters must be considered together when defining both the geometry and the actuation requirements of the robotic system.

2.5 Mechanical architecture, adjustability and human-robot alignment

The way in which the mechanical structure of a lower-limb rehabilitation system is designed determines both how the robotic device follows the human limb and how movement or support is delivered to the patient. Lower-limb wearable systems can generally be divided into three types according to the degree of their structural flexibility: rigid, flexible, and soft architectures (Jiang et al. 2024). Rigid rehabilitation exoskeletons are commonly implemented using serial architectures, with the mechanical links being connected by robotic joints and placed along the relevant parts of the lower limb. This setup enables the forces produced by the actuators to be transmitted directly to the limb. On the other hand, flexible and soft systems include deformable components that can more easily adapt to the shape and motion of the body (Jiang et al. 2024; Falkowski et al. 2024).

Anthropometric adaptation can be achieved by altering the distances between the robot's joints, with adjustment mechanisms being employed for this purpose (Falkowski et al. 2024). A possible method is to make the mechanical links capable of having their length changed. In this arrangement, one section of the link moves in relation to another until the desired distance between two robotic joints has been reached, after which the structure is secured in place. Different rehabilitation systems have incorporated sliding mechanisms and other length-adjustment features to accommodate variations in lower-limb dimensions (Meng et al. 2023; Yu et al. 2023).

Adjustments may also be made to the position of the entire mechanical structure without changing the distances between the robotic joints. For example, the system developed by Yu et al. (2023) uses vertical guides to adjust the height of the mechanical leg according to the required rehabilitation configuration.

Joint alignment must also be considered when defining the geometry of the robotic structure. Geometric alignment aims to position the robotic joint so that its centre of rotation is as close as possible to that of the corresponding anatomical joint. The adjustment of the distances between the robot's joints, described above, can contribute to this alignment. Anatomical landmarks, measurements or biomechanical models can also be used as references. In the ankle rehabilitation

robot developed by Meng et al. (2023), anatomical information was employed to estimate the ankle rotation centre, and software simulation was used to compare the position of the centre with that of the mechanical mechanism in order to refine the robot's geometry.

A basic approach to the mechanical design of a robotic joint consists of using two mechanical links connected by a revolute joint, allowing relative rotation about a single axis. In knee exoskeletons, this is commonly implemented as a single degree of freedom joint that reproduces flexion and extension in the sagittal plane. By considering only this primary movement, both the mechanical structure and the corresponding dynamic model can be simplified (Z. Wu et al. 2023). Nevertheless, perfect alignment may not always be maintained over the whole range of movement, even after geometric adjustment. Small fitting errors and deformation of the soft tissues can cause relative movement between the limb and the robotic structure during use (Lim, Kim, and Suh 2025).

The mechanical structure also needs to be physically connected to the patient via interfaces that ensure a stable link while adjusting to the shape and size of the limb. Various methods are possible here, extending from flexible straps and cuffs to more rigid supports and moulded shells, as shown in Figure 2.6. Belts based on Velcro and bracket-type attachments are among the most commonly reported attachment methods in rigid lower-limb rehabilitation exoskeletons (Falkowski et al. 2024). Flexible straps and cuffs encircle the limb and can be tightened in accordance with its dimensions, offering a simple and adjustable connection, whereas more rigid supports can provide additional structural support and a more defined contact with the limb (Andrade et al. 2024). Moulded shells offer a greater surface area of contact that conforms to the geometry of the body segment and may also be combined with adjustable straps so as to fit different users (Sarkisian, Ishmael, and Lenzi 2021).



(a) Strap/cuff-based fixation **(b)** Rigid support with straps **(c)** Molded shell with straps

Figure 2.6: Examples of physical interfaces employed to attach lower-limb robotic systems to the user. (a) Fixation using straps and cuffs, (b) a rigid support together with straps, and (c) a moulded shell secured by straps. Panels (a) and (b) are adapted from Andrade et al. (2024); panel (c) is adapted from Sarkisian, Ishmael, and Lenzi (2021).

The main mechanical approaches mentioned in this section are summarized in Table 2.4. The

implementations described here are examples that have been reported in the literature and not a complete list of all possible solutions.

Table 2.4: Main mechanical methods for user adaptation and human-robot compatibility in lower-limb rehabilitation systems.

Design challenge	**Mechanical approach**	**Operating principle**	**References**
Different segment dimensions	Adjustable link length	The distance between robotic joints is modified by allowing relative movement between parts of the mechanical link.	(Falkowski et al. 2024; Meng et al. 2023; Yu et al. 2023)
Different rehabilitation configurations	Structural positioning adjustment	The complete limb mechanism is repositioned without changing the distances between the robotic joints.	(Yu et al. 2023)
Joint alignment	Geometric joint alignment	The robotic structure is designed or adjusted so that the robotic joint centre is as close as possible to the corresponding anatomical joint centre.	(Meng et al. 2023)
Physical attachment to the limb	Flexible and rigid body interfaces	Straps, cuffs, rigid supports and moulded shells provide different forms of fixation and adaptation to the limb.	(Falkowski et al. 2024; Andrade et al. 2024; Sarkisian, Ishmael, and Lenzi 2021; Squartecchia et al. 2026)

2.6 Actuation technologies for lower-limb rehabilitation systems

Actuators are the components responsible for transforming energy into mechanical motion and driving the joints of a robotic rehabilitation system. The choice of actuators has a significant effect on the overall performance of the device, including the torque and speed that can be achieved, the positioning accuracy and the portability (Aliman, Ramli, and Amiri 2024). Active actuation can be obtained through a variety of technologies. Among the main ones used in lower-limb rehabilitation systems are electric motors, pneumatic actuators and hydraulic actuators (Aliman, Ramli, and Amiri 2024). The various technologies differ in how energy is transformed into motion and as a result have different advantages and limitations.

Pneumatic actuators produce an output force by means of pressurised air. Examples of such actuators are pneumatic artificial muscles and pneumatic cylinders, typically producing linear motion which has to be converted into rotational motion in order to actuate a revolute robotic joint (Aliman, Ramli, and Amiri 2024). They are usually lightweight and naturally compliant, which

enables a softer interaction with the user while at the same time keeping a reasonable power-to-weight ratio. In contrast, pneumatic systems show nonlinear behaviour and generally offer less accurate control of position and force. Furthermore, their need for a compressed-air supply restricts their portability, especially in cases where the systems are intended to move with the user (Aliman, Ramli, and Amiri 2024).

Hydraulic actuators create mechanical motion by means of a pressurised fluid. Their key benefit is that they are able to generate large forces together with a high power-to-weight ratio at the actuator level (Aliman, Ramli, and Amiri 2024). For this reason, hydraulic actuation is suitable for applications that demand high mechanical power. It should be noted, though, that lower-limb rehabilitation systems generally do not need that level of power. Moreover, the entire hydraulic system can become both heavy and complex due to the cylinders, hoses and the auxiliary pressure-supply components. Another disadvantage of hydraulic actuators is that they have no inherent compliance and there is a potential risk of fluid leakage, which is an additional drawback in rehabilitation settings (Aliman, Ramli, and Amiri 2024).

Electric motors transform electrical energy into mechanical movement and are therefore commonly used in both immobile and ground-based lower-limb rehabilitation systems (Aliman, Ramli, and Amiri 2024). Their key benefits are high precision, reliability, a relatively simple method of control, quiet operation and a good power-to-weight ratio. They can also be easily combined with various mechanical transmission systems, which, however, are usually mandatory in order to achieve the torque and speed required at the robotic joint (Aliman, Ramli, and Amiri 2024).

The main characteristics, advantages and limitations of these actuation technologies are given in Table 2.5.

Table 2.5: Comparison of the main actuation technologies used in lower-limb rehabilitation systems, based on Aliman, Ramli, and Amiri (2024).

Actuation type	**Operating principle**	**Main advantages**	**Main limitations**
Electric	Electrical energy is transformed into mechanical motion.	High precision, reliability, a relatively simple method of control, quiet operation and a favourable power-to-weight ratio.	Often requires a transmission mechanism. Gearing may introduce backlash and reduce backdrivability.
Pneumatic	Pressurised air is used to generate force, generally resulting in linear motion.	Lightweight, naturally compliant, soft interaction and reasonable power-to-weight ratio.	Nonlinear behaviour, lower degree of precision in both position and force control, and dependence on a compressed-air supply.
Hydraulic	Pressurised fluid is converted into mechanical motion.	High force capability and high power-to-weight ratio.	Heavy auxiliary components, greater system complexity, low inherent compliance and potential fluid leakage.

Different types of electric motors have been used in lower-limb rehabilitation systems. Brushed

DC motors rely on mechanical commutation via brushes and a commutator, while Brushless DC (BLDC) motors use electronic commutation and as a result do not need brushes. BLDC motors are especially common due to their high efficiency, the fact that they have a quick response to changes in current and torque, and their good torque-to-weight ratio. Although brushed DC motors generally have lower manufacturing costs and simpler control, their shorter service life in comparison to that of BLDC motors has led to their less frequent use in recent systems (Falkowski et al. 2024). Another electric motor technology is that of stepper motors, which rotate in discrete angular steps depending on the control pulses applied to them (Falkowski et al. 2024).

Stepper motors thus offer a simple method of controlling the rotational position and speed through the number and frequency of the pulses. It is possible for them to function without the need for continuous position feedback. Nevertheless, if the torque needed to drive the load is greater than the torque the motor can provide, steps may be lost, and the actual position will then differ from the one commanded. Because of this, position sensing can be included whenever reliable knowledge of the actual joint position is required (Fang et al. 2023).

The actuator itself is only one component of the mechanism which is used to produce movement at the robotic joint. It is common to place a mechanical transmission between the actuator and the joint so that the motion produced by the actuator can be adapted to the needs of the rehabilitation task. A number of different solutions are available, such as direct-mounted transmission mechanisms, gear trains, tendon-driven systems, push-pull cables and chain-and-gear mechanisms, as shown in Figure 2.7 (Aliman, Ramli, and Amiri 2024). With electric actuation, reduction mechanisms are especially common because electric motors generally run at relatively high rotational speeds and provide lower torque than what is needed at the joint. A reduction mechanism reduces the output speed while increasing the torque that is available. Nevertheless, the transmission also has an effect on the dynamic behaviour of the system. For instance, gear mechanisms can cause backlash, which refers to a small amount of lost motion due to the mechanical clearance between parts, and can reduce backdrivability, meaning that it becomes harder for an external force applied to the joint to make the transmission and motor move in the opposite direction (Aliman, Ramli, and Amiri 2024). Such effects can lead to a decrease in positioning accuracy and increase the resistance that the user feels when interacting with the device.

2.7 Sensing technologies for lower-limb rehabilitation systems

Sensors are essential in lower-limb robotic rehabilitation systems, as they provide the information required to monitor both the device and the user and to support the control process (Tiboni et al. 2022). Depending on the information required, sensors may be used to characterize the mechanical state of the robotic system and its interaction with the user, or to monitor the patient's physiological activity.

Inertial sensors are generally used for gathering data concerning the movement and orientation of the robotic structure or of the user's limbs. Inertial Measurement Units (IMUs) usually include accelerometers and gyroscopes, and in some cases magnetometers as well. Accelerometers detect

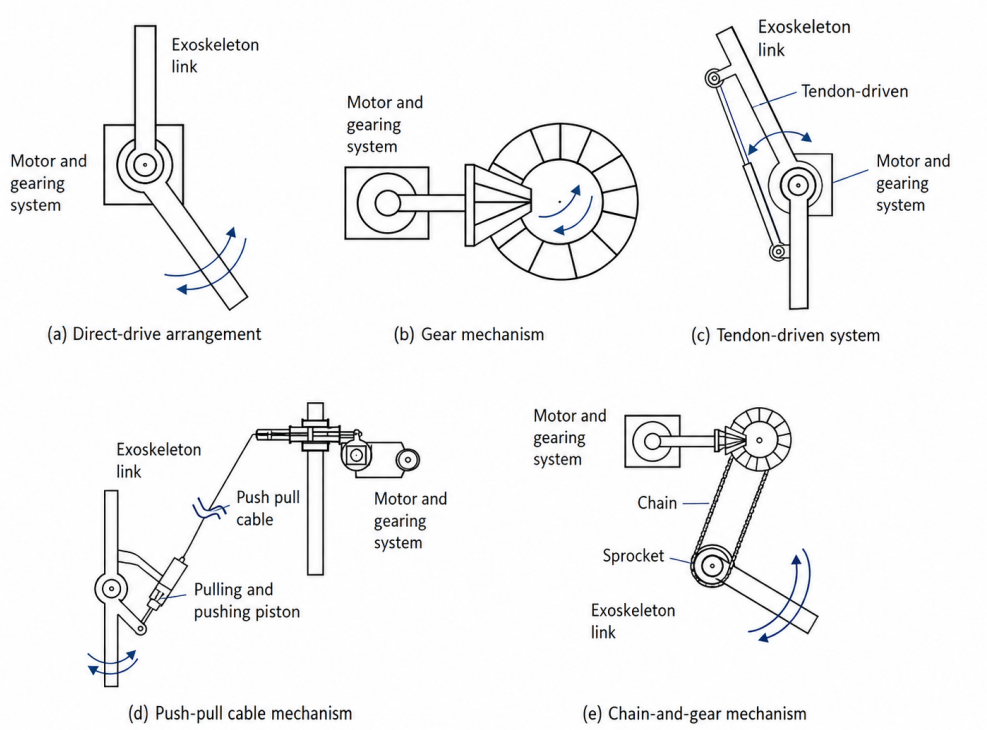


Figure 2.7: Examples of power transmission mechanisms used in lower-limb rehabilitation systems are shown: (a) direct-mounted transmission with a speed reducer, (b) gear mechanism, (c) tendon-driven system, (d) push–pull cable mechanism, and (e) chain-and-gear mechanism. Adapted from Aliman, Ramli, and Amiri (2024).

linear acceleration along various axes, while gyroscopes record angular velocity. From analysing these measurements, it is possible to estimate the movement and orientation of a body or of a robotic section in three-dimensional space. IMUs are especially appealing for motion monitoring since they allow multi-axis information to be obtained with relatively small and cost-effective devices. However, sensor noise can influence the measurements and errors may build up over time, causing a drift from the true motion (Yao et al. 2024).

Force and torque sensors offer data on the physical interaction between the robotic system and the user. Specifically, force sensors can directly measure the forces applied at the human-robot interface and may therefore be used for interaction monitoring, control, and safety (Tiboni et al. 2022).

Displacement sensors give details regarding the position and movement of the robotic structure by measuring either linear or angular displacements (Yao et al. 2024). With respect to rotational joints, both angular displacement and position are usually determined using rotary encoders. A rotary encoder transforms the angular position or motion of a rotating shaft into an electrical signal which can then be processed by the control system (Tiboni et al. 2022). Rotary encoders can be classified as absolute or incremental. An absolute encoder immediately indicates the angular position of the shaft at any given time, while an incremental encoder picks up changes in position as the shaft rotates, generally by producing a series of pulses. The pulses can be counted in order to find out how far the shaft has moved, and their frequency can be used to estimate the rotational speed (Tiboni et al. 2022).

Encoders may be positioned either near the motor or directly at the robotic joint. In the case where the encoder is located close to the motor, the joint position is calculated on the basis of the motor's rotation. This method is suitable when the transmission between the motor and the joint is sufficiently rigid. If the encoder is placed directly at the joint, then the motion of the joint can be measured directly (Tiboni et al. 2022).

Rotary encoders can be implemented using different physical technologies, such as mechanical, magnetic and optical solutions, as shown in Figure 2.8 (Tiboni et al. 2022):

- **Mechanical encoders** use a coded disc which rotates together with the shaft. An example of the coded disc is shown in Figure 2.8(a). This disc has a number of concentric conductive and non-conductive tracks which are detected by fixed electrical contacts. When the shaft rotates, the contact pattern changes and produces a particular combination that indicates the angular position.

- **Magnetic encoders** consist of a permanent magnet which rotates together with the shaft, as shown in Figure 2.8(b). As the magnet turns, the direction of the magnetic field changes and this change is picked up by a magnetic sensor, for example a Hall sensor. This variation is then used to find the angular position of the shaft.

- **Optical encoders** consist of a disc with alternating transparent and opaque areas, as shown in Figure 2.8(c). A light source is placed on one side of the disc and an optical detector

on the other. When the disc rotates, the light beam is alternatively transmitted and blocked, thereby producing electrical signals from which the angular displacement and rotational speed can be calculated.

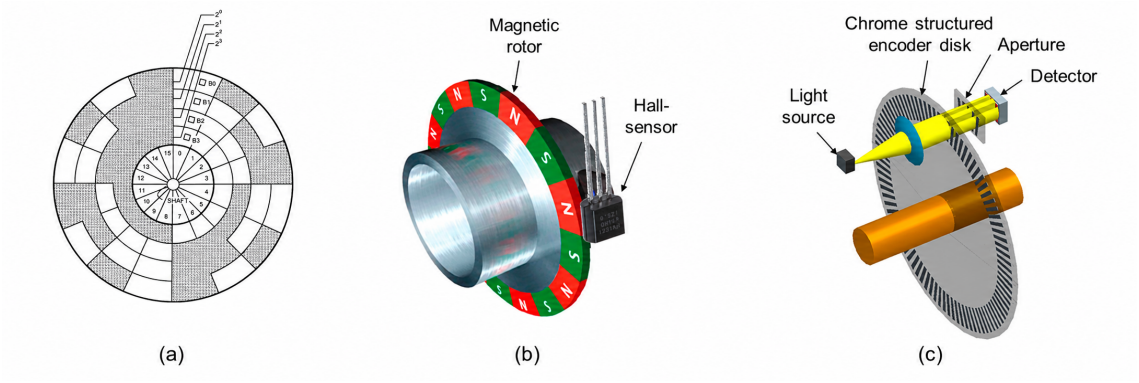


Figure 2.8: Examples of rotary encoder technologies: (a) coded disc used in a mechanical contact encoder, and operating principles of (b) a magnetic encoder and (c) an optical encoder. Adapted from Dynamics Research Corporation (1992) and Seybold et al. (2019).

In addition to the mechanical condition of the system, physiological signals can tell us something about the user's activity and their intention to move. A widely used method for monitoring muscle activity in exoskeleton applications is Surface Electromyography (sEMG) (Net'uková et al. 2022). sEMG sensors pick up the electrical activity linked to muscle activation by means of electrodes that are placed on the skin. As this electrical activity takes place before the actual mechanical movement is produced, EMG can offer information regarding an intended movement before that movement can be observed (Net'uková et al. 2022). In the context of robotic rehabilitation, EMG signals can therefore be used to characterize neuromuscular activity and may also be included in the control algorithms to estimate the intended forces or movements and to determine the level of assistance given by the robotic system.

Even though they have these advantages, sEMG measurements are affected by a number of factors. The signal obtained is influenced by the position of the electrode, the skin impedance, sweat, and the properties of the muscle being measured. As the electrical signal has to pass through various tissue layers before reaching the skin surface, it is also prone to noise, interference and cross-talk from adjacent muscles. As a result, surface electrodes do not fully isolate the activity of a single muscle, and therefore the number and position of the sensors become important when EMG is being used to estimate movement intention (Net'uková et al. 2022).

Brain activity also offers a physiological signal which may be employed in order to gain information about motor intention. Electroencephalography (EEG) involves the use of electrodes positioned on the scalp to record electrical brain activity (Net'uková et al. 2022). It is frequently used in brain–computer interfaces, and the advantage of this technique is that it provides high temporal resolution, enabling it to detect rapid changes in brain activity associated with motor intention. On the other hand, its spatial resolution is relatively low and the signals obtained can be

influenced by artefacts and external disturbances (Yao et al. 2024; Net'uková et al. 2022). Traditional EEG acquisition may also require the use of conductive gel or a saline solution in order to lower the impedance between the electrodes and the skin (Net'uková et al. 2022).

2.8 Control strategies for lower-limb rehabilitation systems

The control strategy establishes the way in which a lower-limb robotic rehabilitation system reacts to the user and how the assistance or resistance required during a rehabilitation task is produced. Control architectures can be divided into three levels: high-level, mid-level and low-level control (Miguel-Fernández et al. 2023). As shown in Figure 2.9, the high-level control establishes the control objective and estimates the state of the human-robot system based on the available signals. It is then upon this information that the mid-level control creates a reference command, before the low-level control transforms this command into signals for the actuators (Miguel-Fernández et al. 2023).

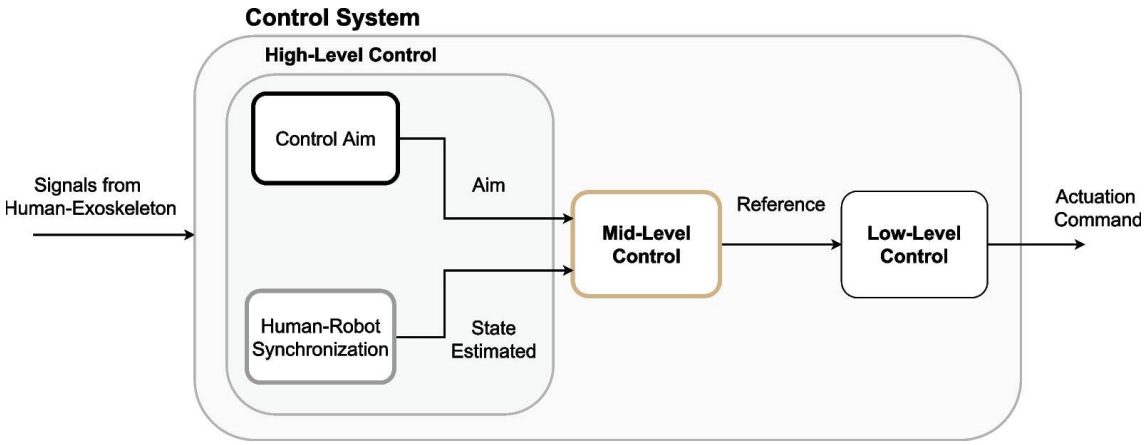


Figure 2.9: General hierarchical structure of an exoskeleton control system, consisting of high-level, mid-level and low-level control. Reproduced from Miguel-Fernández et al. (2023).

At the high level, different control objectives can be chosen depending on the rehabilitation task and the patient's abilities. As shown in Figure 2.10, these objectives can be divided into assistive, challenge-based and adaptive control (Miguel-Fernández et al. 2023):

- **Assistive control** aims to help the patient complete the rehabilitation task, as represented in Figure 2.10(I). Assistance can be given at various levels of patient involvement. In the case of *passive assistance*, the robotic system produces and guides the movement without needing any active input from the patient. In *active assistance*, the patient voluntarily starts or contributes to the movement, while the robotic system offers the extra support or correction necessary to finish the task. *Passive assistance* is especially appropriate when voluntary movement is greatly restricted, whereas *active assistance* encourages a higher level of patient participation (Miguel-Fernández et al. 2023).

- **Challenge-based control** deliberately makes the task more difficult, as illustrated in Figure 2.10(II). It is possible to do this by applying resistance to the patient's movement, augmenting movement errors in order to encourage their correction, or by introducing perturbations that require the patient to adapt the movement. These strategies are especially appropriate for the later stages of rehabilitation or when dealing with patients who have lighter impairments (Miguel-Fernández et al. 2023).

- **Adaptive control** adjusts the control parameters in accordance with the patient's needs or performance, as shown in Figure 2.10(III). Because motor abilities differ from patient to patient and may also change during the course of rehabilitation, modifying the control parameters can lead to a more personalized interaction. The control parameters can be established prior to training or adjusted automatically while using the system according to the patient's performance (Miguel-Fernández et al. 2023).

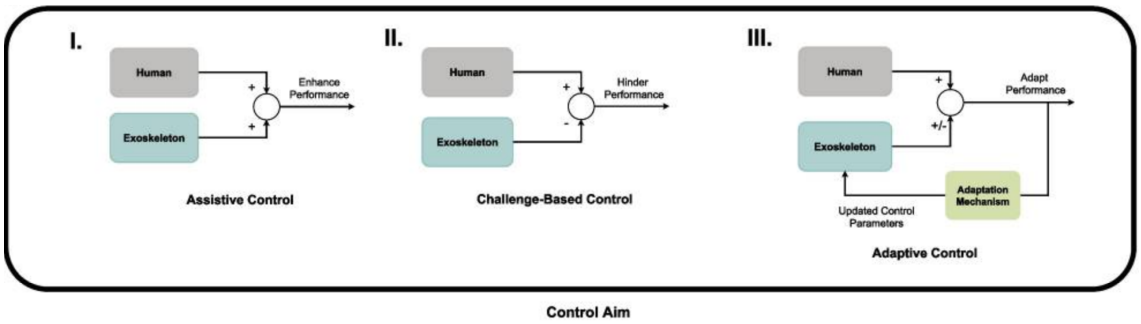


Figure 2.10: Main High-level control objectives: (I) assistive control, (II) challenge-based control, and (III) adaptive control. Reproduced from Miguel-Fernández et al. (2023).

At the Mid-level, there are three main families of control strategies: trajectory-tracking, neuromuscular and compliant control, as shown in Figure 2.11 (Miguel-Fernández et al. 2023).

- **Trajectory-tracking control** produces predefined position or force trajectories which are used as reference commands, as shown in Figure 2.11. Such trajectories may be derived from movements recorded in individuals without impairment, from the patient's unaffected limb, or from movements that were previously carried out under the guidance of a therapist. The robotic system then supplies the necessary actuation to follow the desired reference (Miguel-Fernández et al. 2023). While this offers a reliable method of reproducing rehabilitation movements, when implemented as rigid trajectory tracking, this approach can limit the patient's ability to influence the movement.

- **Neuromuscular control** produces the control reference by means of the physiological signals supplied by the patient, such as EMG and EEG, as illustrated in Figure 2.11. The resulting information is then employed to create position or torque references for the lower control level (Miguel-Fernández et al. 2023). With this approach, the robotic response becomes directly dependent on the patient's physiological activity.

- **Compliant control** does not strictly enforce a desired movement but instead regulates the physical interaction between the patient and the robotic system. As shown in Figure 2.11, the way the robot responds to the user's interaction can be defined using position or force measurements (Miguel-Fernández et al. 2023). The two main approaches are:
  - *Impedance control* adjusts the force or torque that the robotic system applies in accordance with the user's movement. For instance, if the joint moves away from the desired position, the controller can increase the corrective assistance supplied by the robot (Baud et al. 2021).
  - *Admittance control* operates in the opposite way: the force applied by the user to the robotic system is measured and then used to decide how the robot should move (Miguel-Fernández et al. 2023; Xu et al. 2023).

  Compliant control can also be combined with trajectory-tracking or neuromuscular control, allowing the system to maintain a desired movement objective while providing a more flexible interaction with the patient (Miguel-Fernández et al. 2023).

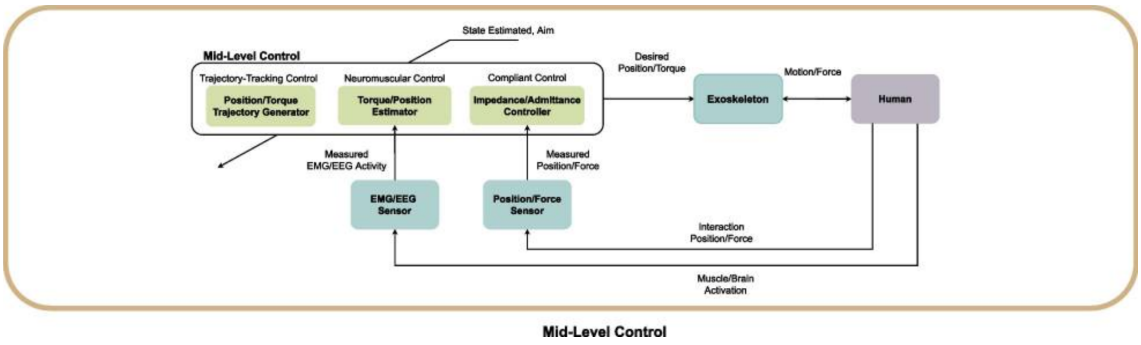


Figure 2.11: Main mid-level control strategies used in lower-limb rehabilitation systems: trajectory-tracking control, neuromuscular control and compliant control. Reproduced from Miguel-Fernández et al. (2023).

Compliant control is closely linked to the AAN rehabilitation approach. The aim of AAN is to offer only the degree of robotic assistance necessary for the patient to carry out the rehabilitation task, at the same time encouraging active participation (Xu et al. 2023). This is especially important for patients who still have some voluntary control, since too much assistance could decrease their level of involvement in the task and potentially limit the rehabilitation progress, as was mentioned previously in Section 2.1 (Miguel-Fernández et al. 2023). In practice, AAN can be implemented using compliant strategies such as impedance or admittance control (Xu et al. 2023).

At the low level, the reference signal generated by the higher control levels has to be transformed into commands for the actuators. Rigid position control is usually implemented using Proportional-Integral-Derivative (PID) controllers, which continuously compensate for the difference between the desired and the actual position (Baud et al. 2021). This method is relatively simple and is capable of providing accurate trajectory tracking. Yet, very rigid position tracking

is not always desirable in rehabilitation systems, as the user can influence the movement and the mechanical structure itself may have a certain degree of flexibility (Baud et al. 2021).

2.9 Research gap

Even though there has been technological advancement in lower-limb rehabilitation systems, their actual use is still subject to a number of limitations. Among the relevant concerns are safety, the use of a one-size-fits-all approach, ease of use, the weight and placement of the device, and cost (Morris et al. 2023).

One of the main limitations is the need to adapt rehabilitation devices to individual patients. Physiotherapists have stressed the importance of adjusting features such as joint configurations and segment lengths, although they also point out that customising the equipment for each patient can be time-consuming (Morris et al. 2023).

Weight, size and cost are also important practical limitations. Both patients and rehabilitation professionals have raised concerns about the weight and device placement, as well as about their affordability, with a high cost possibly restricting clinical adoption (Morris et al. 2023).

Apart from these practical limitations, the design requirements discussed in Section 2.3 must also be considered. These requirements are as follows: appropriate support of the lower limb, adaptation to both seated and lying rehabilitation positions, anthropometric adjustability, safe joint ranges of motion, correct alignment between human and robot, suitable physical interfaces, and various practical features such as compactness and ease of positioning.

2.10 Summary

This chapter presented the main clinical, biomechanical and technological aspects involved in lower-limb robotic rehabilitation. Since lower-limb motor disorders can have a significant impact on a patient's mobility and independence, rehabilitation should involve repetitive and progressive training which is tailored to the patient's abilities. Robotic systems can aid this process by offering controlled movements, keeping track of the patient's performance and modifying the level of assistance or resistance used during rehabilitation. In the case of patients who have limited mobility, rehabilitation might also have to be carried out while they are seated or lying down, which in turn brings about particular requirements concerning limb support, positioning, adjustment and safety.

The design of such systems is based on a number of closely related factors. The dimensions, ranges of motion and mechanical loads needed are determined by lower-limb biomechanics and variations in anthropometric data, and the robotic structure has to offer proper adjustment and alignment for the user. Various actuation and transmission technologies involve different trade-offs concerning torque, precision, compliance, weight and complexity. Moreover, mechanical and physiological sensors can supply data regarding the state of the robotic system and the patient's level of activity. This information can then be used by a variety of control strategies, including those based on predefined trajectory tracking as well as neuromuscular and compliant methods,

with adaptive and AAN strategies enabling the degree of robotic assistance to depend more closely on the patient's abilities and level of participation.

Despite the available technological solutions, important practical limitations remain. Problems relating to patient adaptation, ease of use, the weight and position of the device, and cost remain important. As a result, the creation of lower-limb rehabilitation systems needs to strike a balance between functionality, adaptability, safe interaction between humans and robots, and various practical factors such as mechanical complexity and accessibility.

Chapter 3

System Development and Implementation

3.1 System Overview

The system developed in this dissertation is a robotic lower-limb rehabilitation support system meant to be used when the user is seated or lying down. The prototype was built for one limb and includes three motor-driven joints, one for the hip, one for the knee and one for the ankle. As the system is not designed for gait rehabilitation, it does not need to support the user's full body weight. It only has to give adequate support to the lower limb during the rehabilitation exercises. Most of the custom mechanical components of the prototype were manufactured in Polylactic Acid (PLA) using 3D printing, while a stationary supporting structure was made from wood. The primary purpose of the system is to assist controlled lower-limb movements to support the rehabilitation process.

The mechanical structure supports the lower limb and provides the physical connection between the hip, knee and ankle joints, while the actuation system drives the corresponding joint movements. The position of the joints is monitored using joint position sensing, and information about the user's voluntary muscle activity is obtained through EMG sensing. The control system is implemented using two Arduino UNO boards, with one dedicated to physiological sensing and movement-intention detection and the other responsible for actuator control, joint-position monitoring and rehabilitation control. The two controllers communicate through a direct Universal Asynchronous Receiver-Transmitter (UART) connection. The system also includes various safety features which limit its operation to the prescribed limits and allow it to react to abnormal conditions. Figure 3.1 presents the overall architecture of the developed system and the interaction between its main components.

The physical implementation of the prototype in the two intended rehabilitation configurations is shown in Figure 3.2.

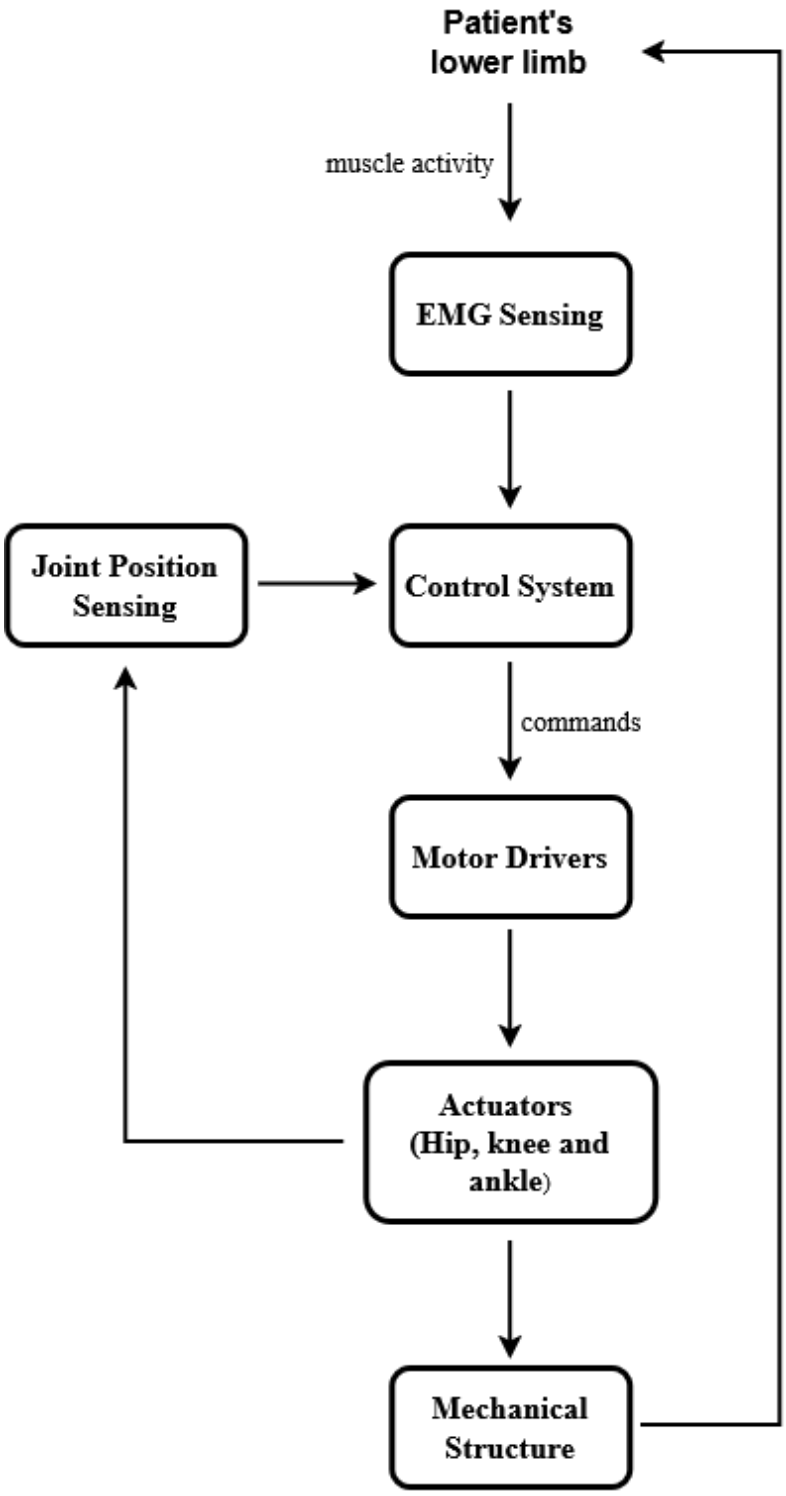
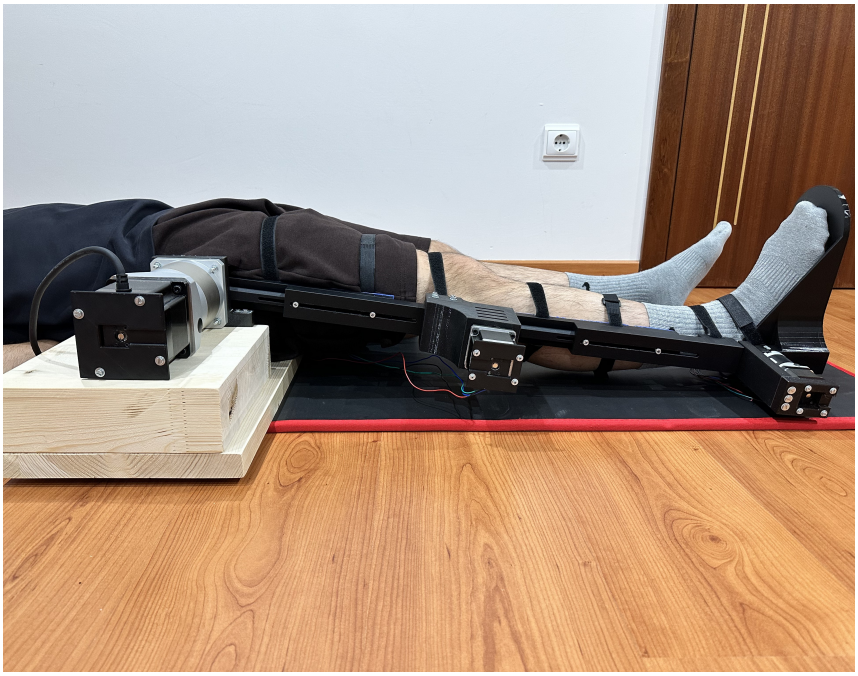


Figure 3.1: Overall architecture of the developed robotic lower-limb rehabilitation support system.



(a) Seated configuration.



(b) Lying configuration.

Figure 3.2: Developed robotic lower-limb rehabilitation support system in the two intended rehabilitation configurations.

3.2 Mechanical Structure

The design of the mechanical structure was guided by the biomechanical and anthropometric considerations discussed in Chapter 2, together with the practical constraints associated with the development of the prototype. The following subsections describe its mechanical architecture, anthropometric adjustability, joint design and alignment, human-robot interfaces, and manufacturing and assembly.

3.2.1 Overall Mechanical Architecture

The mechanical structure was designed for a single lower limb and is divided into three major structural parts, which correspond to the thigh, the shank and the foot. The sections for the thigh and shank follow the relevant anatomical parts along the lateral side of the limb, whereas the foot is supported by a dedicated platform. These components together make up the mechanical chain that links the hip, knee and ankle joints and enables the movements produced by the motors to be transmitted to the user's lower limb. All mechanical components were designed using SolidWorks. A view of the complete mechanical design is given in Figure 3.3.

The thigh and shank sections are each composed of two overlapping structural plates, one of which is called the *guide plate* and the other the *sliding plate*. These plates have complementary rail profiles through which they are mechanically connected to one another. The respective models are shown in Figure 3.4. A description of the design and operation of the connection between these parts is given in Section 3.2.2.

The foot section includes a rigid platform which is intended to support the plantar surface of the foot. Its shape is based on a simplified shoe-like configuration, consisting of a base that supports the foot and a raised area at the back which gives extra support to the heel and to the posterior part of the foot. This platform makes up the distal part of the mechanical chain and is attached to the ankle motor. The SolidWorks model of the platform is shown in Figure 3.5.

Mechanical supports have been designed to integrate the three actuators with the structure, as illustrated in Figure 3.6. The assemblies for the knee and ankle actuators are attached to the moving parts of the system and therefore move together with the lower-limb structure. On the other hand, the hip motor is mounted on a fixed supporting structure and stays in position relative to the base of the system, while its output shaft causes the thigh section to rotate. As a result, the mass of the hip motor is supported directly by the stationary structure, avoiding any additional load on both the moving mechanical assembly and the patient's lower limb.

The stationary support structure was designed to give a stable foundation for the proximal part of the system and for the hip motor. It is made up of two plates arranged in an L-shaped configuration. The horizontal plate supports the area under the user and the proximal part of the thigh, while the vertical plate offers back support. An additional mounting block is placed on this structure so that the motor can be positioned at the correct height and along the required length. The motor is then fixed to the block using its specific support. The main components of this stationary assembly are shown in Figure 3.7.

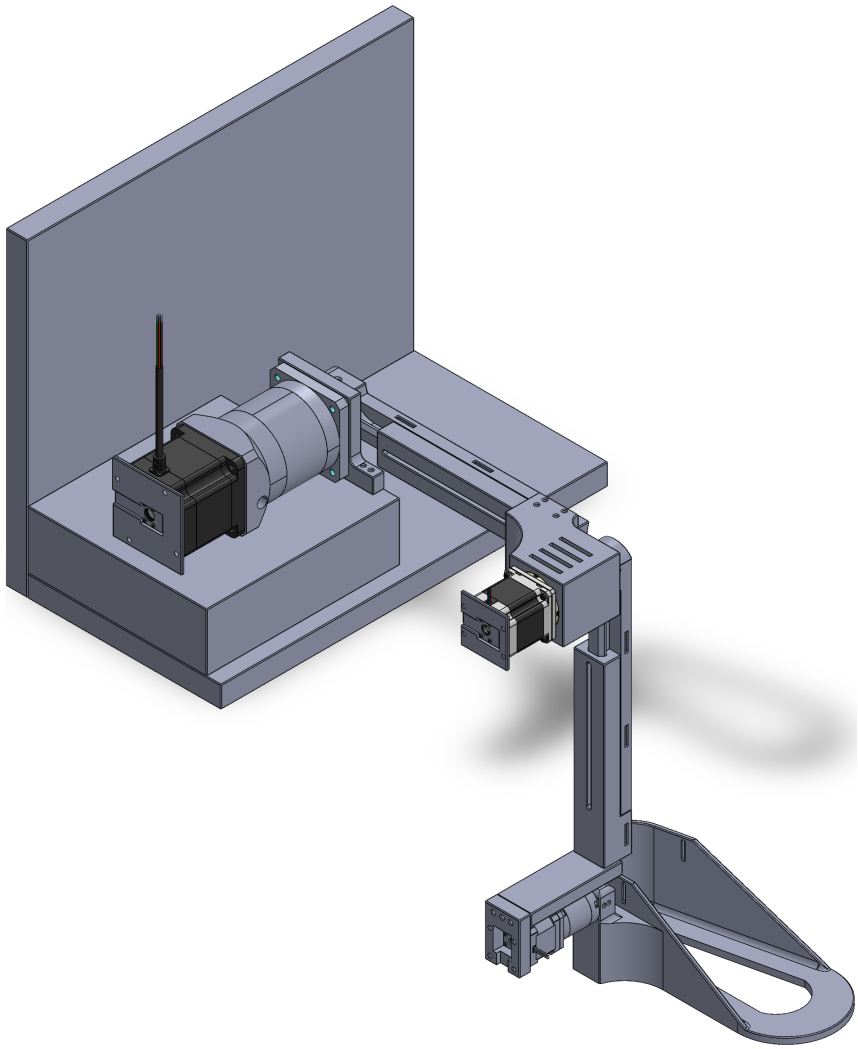
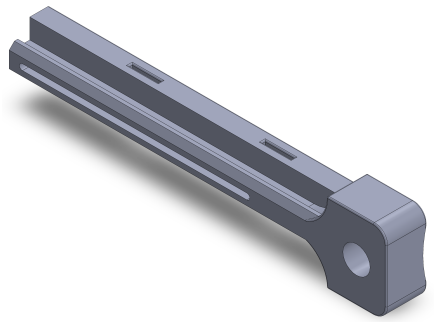
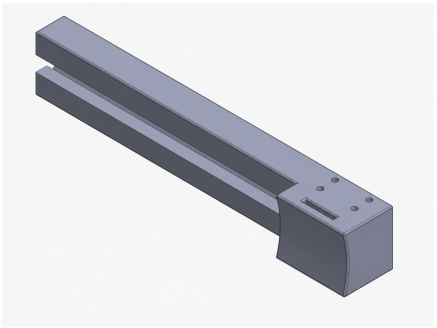


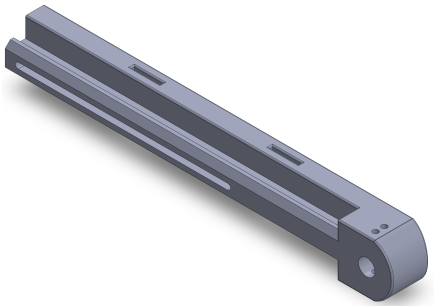
Figure 3.3: Overview of the mechanical design of the developed robotic lower-limb rehabilitation support system.



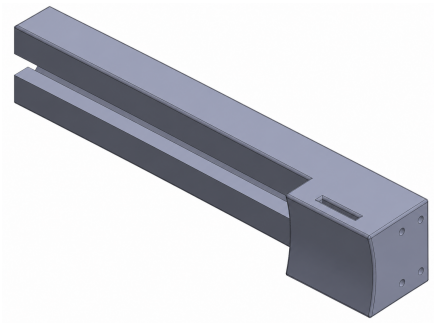
(a) Thigh guide plate.



(b) Thigh sliding plate.



(c) Shank guide plate.



(d) Shank sliding plate.

Figure 3.4: Models of the structural plates used in the thigh and shank sections.

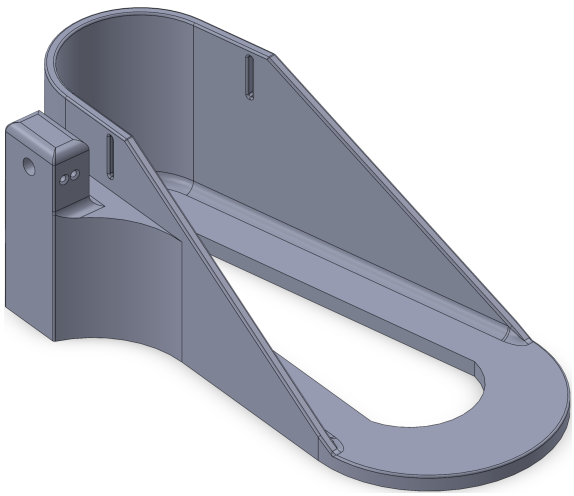
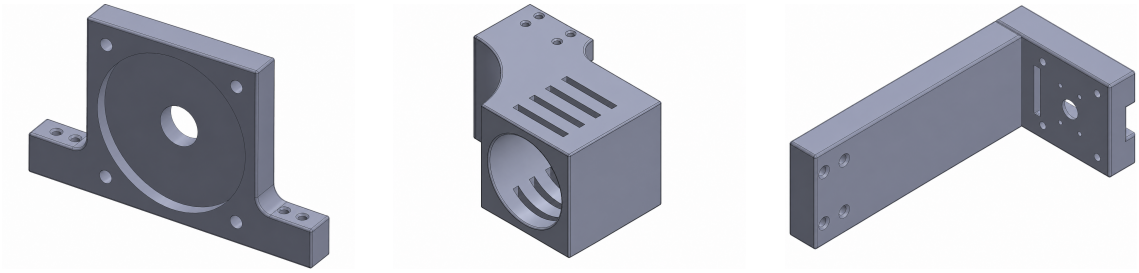
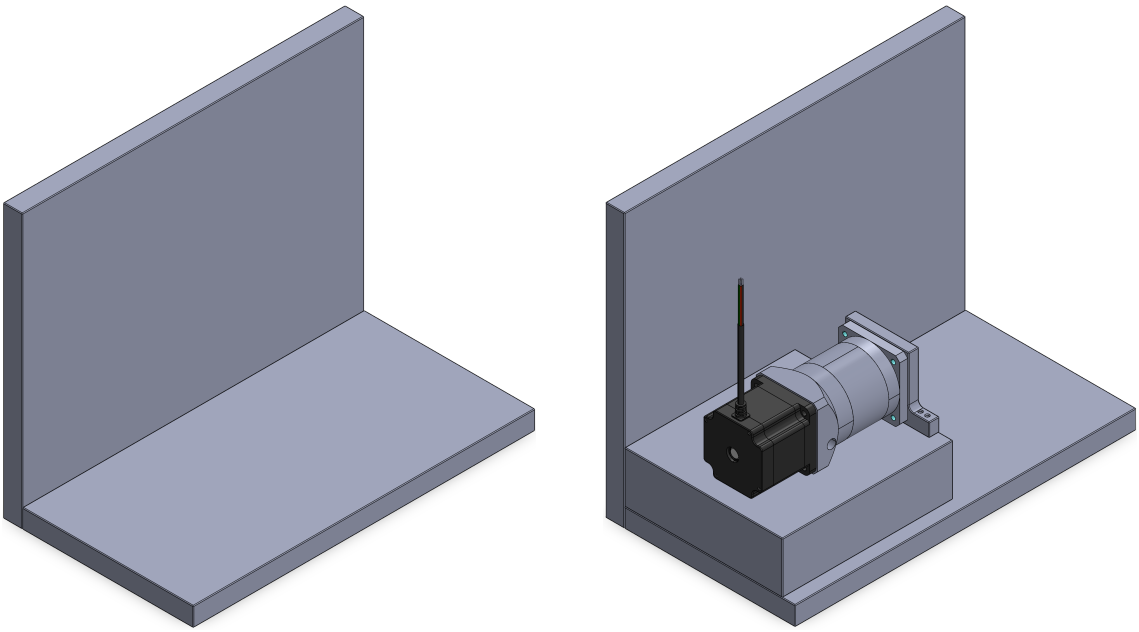


Figure 3.5: Model of the foot platform.



(a) Hip motor support. (b) Knee motor support. (c) Ankle motor support.

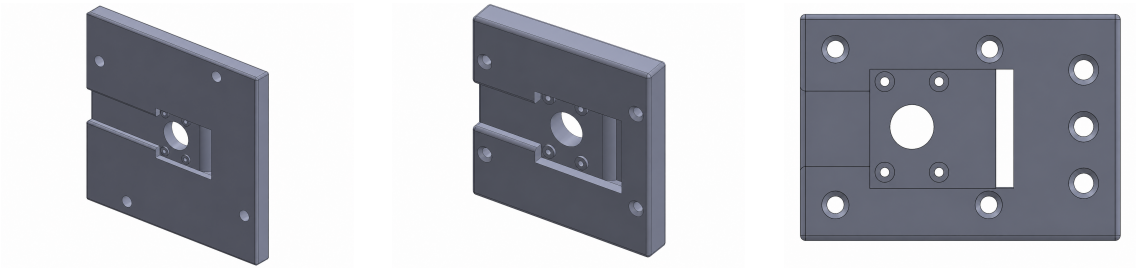
Figure 3.6: Models of the mechanical supports developed for the hip, knee and ankle motors.



(a) L-shaped stationary supporting structure. (b) Hip actuator assembly.

Figure 3.7: Models of the stationary supporting structure and the hip actuator mounting arrangement.

To deal with the joint-position sensors, further mounting parts were designed. At the hip and knee, individual rear supports are secured to the relevant motor assemblies to incorporate the encoder. At the ankle, a different arrangement was adopted because the motor support is attached to the rear end rather than to the front of the motor, as it is in the hip and knee assemblies. This allowed the encoder support to be integrated directly into the actuator support. The three mounting solutions are shown in Figure 3.8, and a detailed explanation of their mechanical integration with the encoders is given in Section 3.4.2.



(a) Hip encoder support.

(b) Knee encoder support.

(c) Ankle encoder support (integrated in the ankle motor support).

Figure 3.8: Models of the encoder mounting solutions developed for the hip, knee and ankle motor assemblies.

The manufacturing and assembly of the mechanical components, together with the main design iterations introduced during development, are described in Section 3.2.5. The technical drawings of the mechanical components developed in SolidWorks are provided in Appendix B.

3.2.2 Anthropometric Adjustability

The dimensions of the lower limb vary considerably between individuals, making anthropometric adaptation an important requirement for the mechanical structure. As discussed in Section 2.4, the anthropometric dimensions used in the design were based on the ANSUR II database (Gordon et al. 2015).

The ANSUR II datasets for men and women were each considered separately, in accordance with the guidelines linked to the database (Paquette and Parham 2017). The percentile values for the anatomical measurements relevant to the dimensional design of the thigh and shank sections are given in Table 3.1. For reference, the relevant anatomical landmarks are illustrated in Figure 2.5.

The dimensional limits of the prototype were determined by using the female 10th Percentile (P10) measurements as the lower design limit and the male 90th Percentile (P90) measurements as the upper design limit. For the measurements considered, these corresponded to the lower and upper anthropometric bounds, respectively. At first, a broader range, extending to more comprehensive percentiles, had been considered, but the necessary structural parts would have been too

Table 3.1: Anthropometric measurements from ANSUR II considered for the dimensional design of the thigh and shank sections (Gordon et al. 2015).

Measurement	**Female P10**	**Female P90**	**Male P10**	**Male P90**
Trochanterion height	790 mm	904 mm	840 mm	964 mm
Lateral femoral epicondyle height	434 mm	501 mm	458 mm	526 mm
Lateral malleolus height	57 mm	69 mm	66 mm	80 mm

long to fit on the available 3D-printer build plate. The selected limits therefore constitute a compromise between accommodating anthropometric requirements and the manufacturing limitations of the prototype.

The thigh and shank lengths are not directly given by ANSUR II. Instead, they were estimated from the vertical positions of the anatomical landmarks listed in Table 3.1. The corresponding calculations are provided in Appendix A, Section A.1. The resulting design estimates are summarised in Table 3.2.

Table 3.2: Estimated reference lengths of the thigh and shank used to establish the lower and upper design limits of the prototype.

Segment	**Lower design limit (from Female P10)**	**Upper design limit (from Male P90)**
Thigh	356 mm	438 mm
Shank	377 mm	446 mm

Adjustment of the thigh and shank sections is achieved through the relative displacement of the guide and sliding plates introduced in Section 3.2.1. This arrangement was inspired by the T-slot rail configuration typically present in Rexroth-type profiles. The matching profiles keep the two plates relative to one another in the transverse direction while allowing longitudinal sliding, as shown in Figure 3.9.

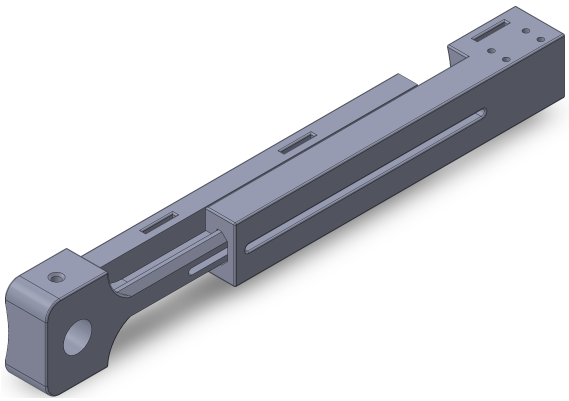
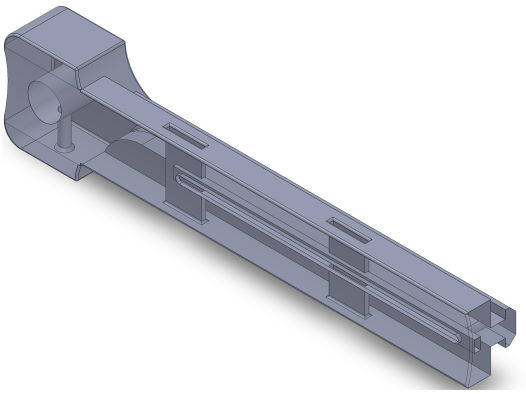


Figure 3.9: Assembly of the guide and sliding plates used for longitudinal adjustment.

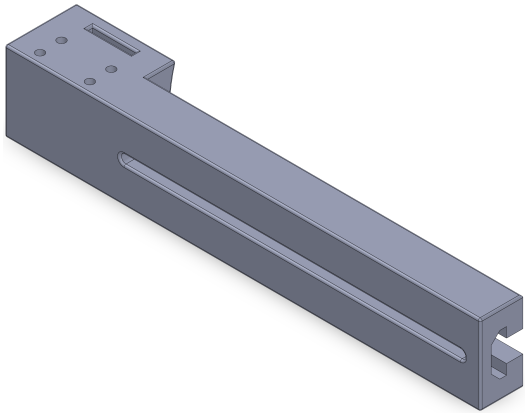
When the necessary segment length has been achieved, the relative position of the two plates

is held in place by two bolt-and-nut connections in each segment. Since both the guide and the sliding plates have a longitudinal through-slot, the bolts can move to different positions as the plates slide past one another. Each bolt is passed transversely through both plates from the lateral side of the sliding plate.

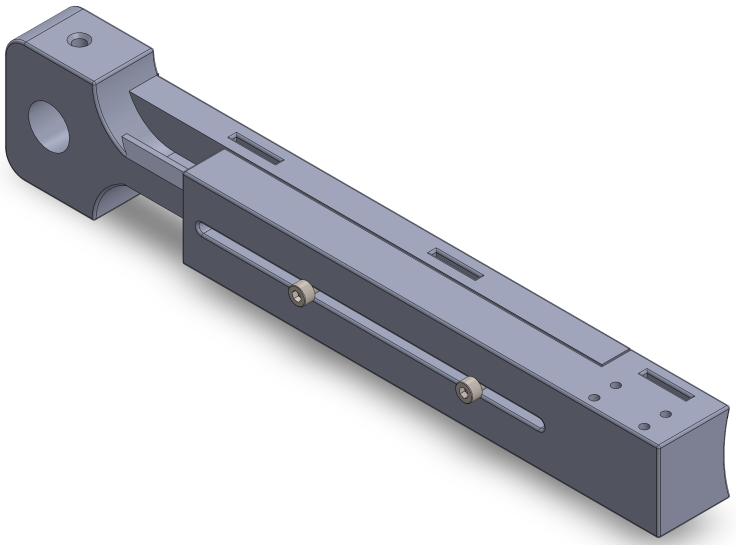
The guide plate additionally incorporates a longitudinal channel for retaining the nuts, which is open at the end of the plate. The nuts are put through this opening and stay within the channel while the adjustment is being made. Once the desired position has been reached, the bolts are screwed into the appropriate nuts, thereby clamping the guide and sliding plates together and stopping any further relative movement. Under each bolt head, a lock washer with external teeth is placed in order to increase the resistance against loosening of the connection. The main elements of the locking mechanism are illustrated in Figure 3.10.



(a) Guide plate with nut-retaining channel and longitudinal through-slot.



(b) Sliding plate with longitudinal through-slot.



(c) Assembled locking mechanism with the two bolts and lock washers.

Figure 3.10: Main elements of the locking mechanism to fix the relative position of the guide and sliding plates.

The anthropometric reference lengths could not be directly converted into the actual physical lengths of the guide and sliding plates. For dimensional purposes, the effective length of each segment was defined as the distance between the rotation axes of two adjacent robotic joints. When determining the plate dimensions, it was necessary to take into account the space occupied by the motor supports and their attachment to the structural plates. In addition, a minimum overlap of 100 mm between the guide and sliding plates was maintained to preserve engagement between the complementary profiles and provide adequate structural stability throughout the adjustment range. The resulting plate dimensions and effective adjustment ranges are summarised in Table 3.3, while the corresponding minimum and maximum configurations are illustrated in Figure 3.11. For both the thigh and shank sections, the achieved adjustment ranges cover the anthropometric design limits defined in Table 3.2.

Table 3.3: Plate dimensions and adjustment ranges of the thigh and shank sections.

Segment	**Guide plate**	**Sliding plate**	**Minimum system length**	**Maximum system length**
Thigh	283.75 mm	303.75 mm	349.25 mm	438 mm
Shank	294 mm	294 mm	367 mm	446 mm

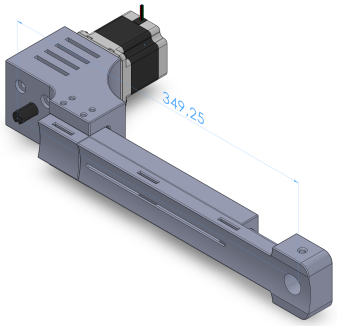
In the present prototype, anthropometric adjustment is applied only to the lengths of the thigh and shank sections. The dimensions of the foot platform were instead defined according to measurements taken from the author's right foot, which are summarised in Table 3.4. The positions of the hip and ankle joint axes are also fixed in the current prototype and are discussed in Section 3.2.3.

Table 3.4: Specific anthropometric measurements used to define the fixed dimensions of the foot platform.

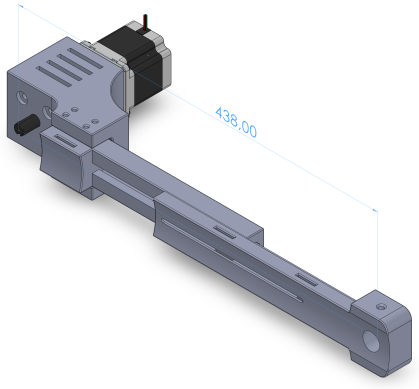
Measurement	**Value**
Foot length	261.5 mm
Heel width	65 mm
Forefoot width	105 mm

The dimensions of the foot platform were based on these measurements and are fixed in the current prototype. Moreover, the position of the ankle actuator towards the lateral side and its connection to one side of the foot platform cause the existing foot structure to be asymmetric. Therefore, the developed prototype is specifically designed for the right lower limb. Although the thigh and shank plates can themselves be reoriented in order to be used on either side, the present foot platform cannot.

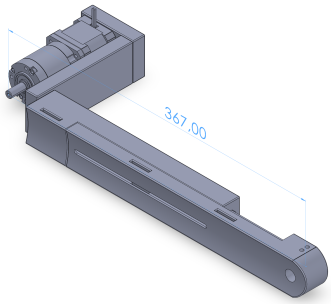
The anthropometric adaptability of the developed system is currently focused on the thigh and shank lengths, while the remaining dimensions are specific to the configuration used during prototype development.



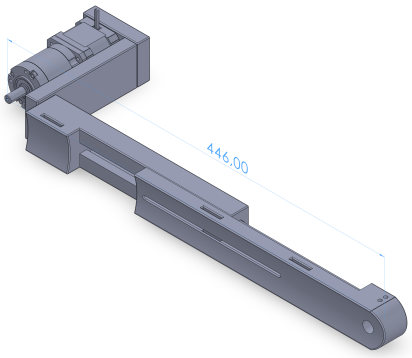
(a) Minimum thigh length.



(b) Maximum thigh length.



(c) Minimum shank length.



(d) Maximum shank length.

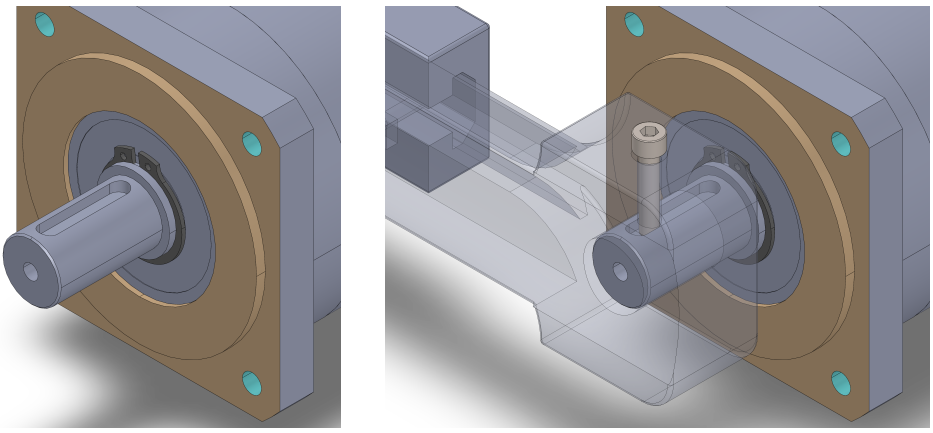
Figure 3.11: Minimum and maximum configurations of the adjustable thigh and shank sections. At maximum length, a 100 mm overlap between plates is observable.

3.2.3 Joint Design and Alignment

As mentioned in Section 2.4, the anatomical joints of the lower limb can produce movements in more than one anatomical plane. In the case of the developed prototype, however, the mechanical design was limited to movement in the sagittal plane, the hip, knee and ankle being represented by revolute joints each having a single rotational degree of freedom. Accordingly, the implemented joints allow for hip flexion–extension, knee flexion–extension and ankle dorsiflexion–plantarflexion, as previously outlined in Table 2.2.

At the three robotic joints, a direct-mounted transmission system was adopted. Each motor's output shaft is mechanically coupled directly to the respective moving structural component. Direct coupling was chosen mainly in order to reduce mechanical complexity. This setup also establishes a simple relationship between the rotation of the motor and the robotic joint and simplifies the mechanical assembly. Moreover, the direct coupling eliminates the need for extra gears, chains, cables or other transmission parts which could cause additional mechanical backlash between the actuator and the robotic joint.

The coupling was achieved by inserting the keyed output shaft of the motors into the appropriate opening in the structural plates. One or two screws (the number depending on the joint) pass radially through the plate and bear against the flat surface of the key shaft, as shown in Figure 3.12. As the shaft rotates, the contact between this flat surface and the screw transmits the torque directly to the robotic link. A conventional key was not used since its relatively small contact area would have concentrated the transmitted load over a small area, thus increasing the risk of local deformation of the PLA. The screw-based solution was therefore chosen in order to establish a more widely distributed mechanical connection within the printed component.



(a) Example of a keyed shaft.

(b) Detail of the screw-shaft connection used in the prototype, shown for the hip joint.

Figure 3.12: Keyed-shaft geometry and its use in the direct mechanical coupling.

Despite its simplicity, the coupling may still introduce some residual mechanical backlash due to relative movement at the screw-shaft contact. Additionally, since the motors are located directly at the robotic joints, the knee and ankle assemblies become part of the moving structure

and increase its mass. This effect is even more significant in the case of the distal motor at the ankle, since this component's mass must also be moved by the more proximal knee and hip joints. The consequent increase in the mass of the moving parts therefore contributes to the mechanical loads on the system and increases the mass moving together with the user's lower limb.

Having defined the joint kinematics and the transmission arrangement, the positioning of the robotic joint axes relative to the corresponding anatomical joints was considered. As explained in Section 2.5, proper geometric alignment is important in order to minimise the misalignment between the robotic and anatomical joints. The alignment of the prototype in question was therefore determined using anatomical landmarks together with direct measurements of the lower limb.

As was explained in Section 3.2.2, the only dimensions in the current prototype to which anthropometric adjustments have been applied are those of the thigh and shank. The other dimensions needed to determine the positions of the hip and ankle joint axes were set based on measurements taken from the author. These measurements are given in Table 3.5.

Table 3.5: Specific anthropometric measurements used to define the fixed positions of the hip and ankle joint axes.

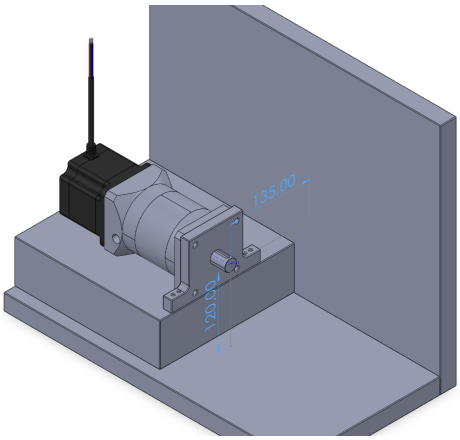
Measurement	**Value**
Hip joint	
Height	120 mm
Longitudinal distance from the back	135 mm
Ankle joint reference	
Lateral malleolus height	85 mm
Lateral malleolus longitudinal distance from the heel	60 mm

At the hip, a reference position for the joint axis was defined from measurements of its height relative to the supporting surface and its longitudinal distance from the author's back. These measurements were then used to establish the size of the mounting block and the associated motor support, with the aim of placing the motor's output shaft at the reference hip-joint position defined for the developed configuration.

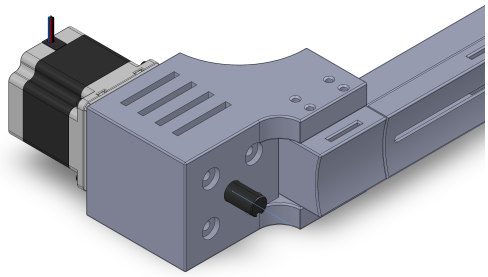
The lateral femoral epicondyle at the knee was taken as an external anatomical reference point for the placement of the robotic rotation axis. The position of the knee axis in relation to the hip can be adjusted by means of the adjustable thigh section described in Section 3.2.2.

At the ankle, the lateral malleolus was used as an external anatomical reference for the positioning of the sagittal-plane robotic rotation axis. Adjustment of the shank section enables the knee-ankle distance to be modified. However, the position of the ankle axis with respect to the foot platform is fixed and its vertical position as well as its longitudinal distance from the heel were determined from the author-specific measurements given in Table 3.5 and were used to define the position of the ankle actuator.

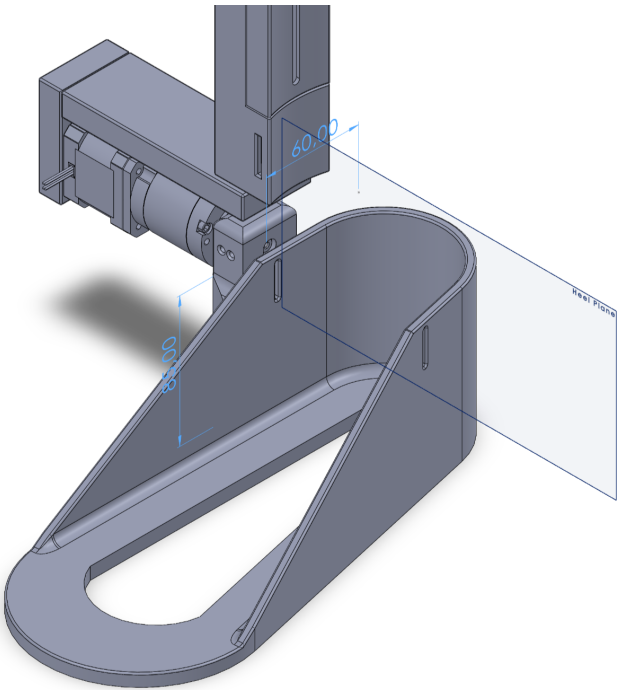
Figure 3.13 illustrates the implemented hip, knee and ankle joint arrangements and the corresponding motor rotation axes.



(a) Hip joint.



(b) Knee joint.



(c) Ankle joint.

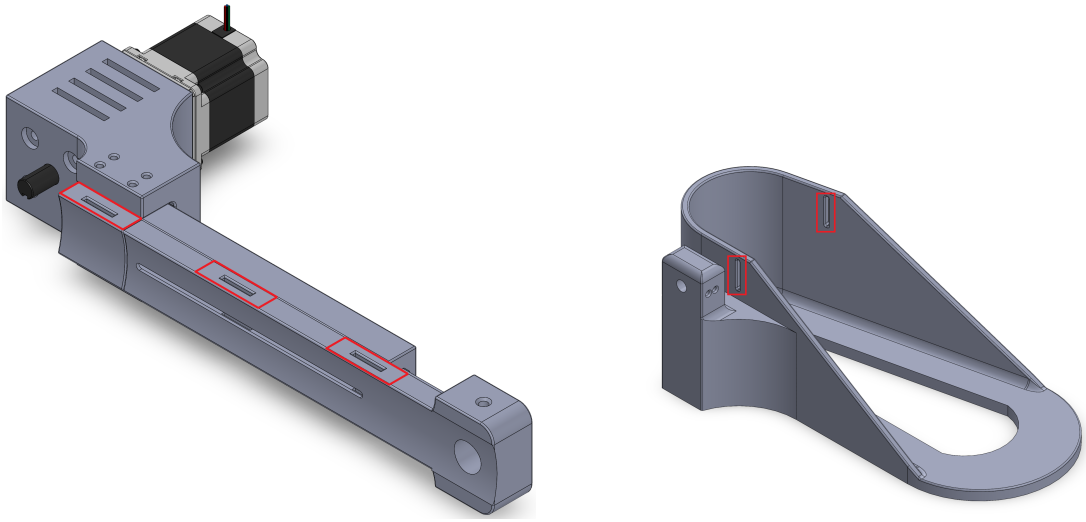
Figure 3.13: Geometric alignment of the robotic joint axes in the developed prototype.

3.2.4 Human-Robot Interfaces

The mechanical structure must be physically connected to the user's lower limb in order for the movements generated by the actuators to be transmitted to the corresponding body segments. As explained in Section 2.5, the human-robot interface should provide adequate fixation while at the same time limiting the relative movement between the limb and the robotic structure, without causing excessive pressure at the points of contact. In the prototype that was developed, this interface was implemented by using adjustable Velcro straps together with the structural thigh and shank plates and the foot platform.

In both the thigh and shank sections, three straps were used: two along the guide plate and a third on the sliding plate, positioned as far distally as possible before the corresponding motor assembly. A transverse slot was incorporated for each strap, allowing it to pass through the structural plate before wrapping around the user's limb. This arrangement provides a defined path for the straps and helps to keep them securely aligned with the corresponding limb segment during use.

The foot is fastened to the rigid platform by means of one Velcro strap which is placed across the dorsal region of the foot, near the ankle. This strap keeps the foot in place against the platform, while the platform itself supports the plantar surface and the heel of the foot. The implemented interfaces are illustrated in Figure 3.14.



(a) Strap arrangement used in the thigh and shank sections (example shown for the thigh).

(b) Strap arrangement used to secure the foot to the platform.

Figure 3.14: Interfaces implemented in the prototype using adjustable Velcro straps.

This arrangement was chosen because Velcro straps provide a simple, lightweight, low-cost and adjustable method of attaching the robotic structure to the limb. The use of multiple straps along the thigh and shank provides fixation at multiple locations, helping to limit relative movement between the limb and the structural plates and to maintain a more stable connection during joint motion.

To improve the physical interface with the user, the surfaces of both the guide and sliding plates that come into contact with the user were covered with an Ethylene-Vinyl Acetate (EVA) foam layer. This padding provides a softer interface between the user's limb and the rigid PLA structure, helping to improve comfort during use. Figure 3.15 shows the EVA foam padding applied to the structural plates, using the thigh section as an illustrative example.

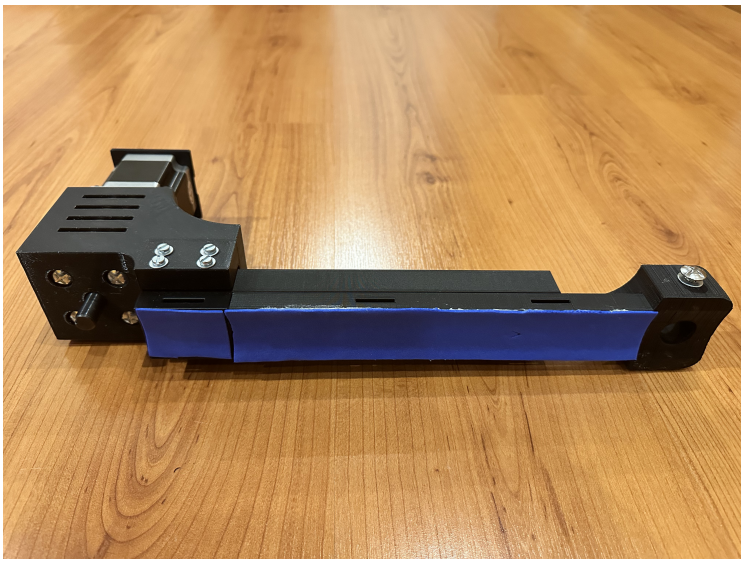


Figure 3.15: EVA foam lining applied to the contact surfaces of the thigh section.

3.2.5 Manufacturing and Assembly

Different manufacturing methods were used for the mechanical components according to their geometry, dimensions and structural function. The lower-limb structural plates and the motor and encoder supports were manufactured in PLA using 3D printing. This approach was selected because of its availability within the faculty facilities, relatively low cost and suitability for rapid prototyping. In particular, individual components could be redesigned and reprinted as the mechanical structure evolved throughout the development process. Additive manufacturing also allowed customised geometries, including the sliding guides and dedicated motor and sensor supports, to be produced without requiring complex machining.

The L-shaped supporting structure and the hip actuator mounting block were instead manufactured from wood. These components were required to support the user and the hip actuator assembly and therefore had different structural requirements from the remaining components. Their dimensions also exceeded the available 3D-printer build volume, while their relatively simple prismatic geometry made them straightforward to manufacture from wood.

The resulting mechanical architecture was assembled in a modular manner, with the main structural, motor support and sensor support components being manufactured separately and subsequently connected to form the complete structure. This arrangement facilitated the modification or replacement of individual components during the iterative development process.

Several mechanical components underwent multiple iterations before reaching their final configuration. Although different parts of the prototype were modified throughout development, some changes were particularly relevant. The support for the knee motor was initially based on the arrangement used for the ankle, but this configuration did not provide sufficient rigidity for the larger knee motor and was therefore redesigned. For the hip and knee assemblies, dedicated encoder-support components were developed because their mechanical layouts did not allow the encoder support to be incorporated directly into the actuator support, as was possible at the ankle. In addition, the region of the thigh guide plate surrounding the opening used to connect the plate to the hip motor shaft was reinforced after an earlier version fractured around this opening during testing. A reinforced geometry was therefore adopted around the shaft connection in the subsequent version.

3.3 Actuation System

The actuation system was dimensioned according to the mechanical loads expected at the hip, knee and ankle joints. As discussed in Section 2.4, these loads depend on the dimensions and masses of the lower-limb segments and on the positions of their COMs. This section describes the dimensioning and selection of the motors and gearboxes used to drive the three robotic joints, together with their associated drive electronics. An initial torque estimation was performed before selecting the motors and gearboxes. The resulting requirements were then used as a basis for their selection, after which the calculations were repeated, including both the mass of the selected motor-gearbox assemblies and the mass of the moving mechanical components, in order to verify the suitability of the final configuration.

3.3.1 Joint Torque Estimation

Before selecting the actuators, the torque required at each robotic joint was estimated in order to establish the initial actuation requirements. At this stage, the calculation took into account the gravitational load of the user's lower limb as well as a simplified estimate of the torque associated with its angular acceleration. The actuators and the mechanical components of the robotic structure had not yet been included because the final configuration had not been defined.

The calculations were performed for the same lower and upper anthropometric design cases previously considered in Section 3.2.2, corresponding to the female P10 and male P90, respectively. In each instance, the total body mass was needed in order to calculate the masses of the different lower-limb segments, and the segment lengths were required to find the positions of their COM relative to the joint axes. The estimates in question were made using the anthropometric coefficients given by Winter, as previously mentioned in Section 2.4.

The anthropometric values employed in these calculations are given in Table 3.6. The lengths of the thigh and shank are the same as those previously estimated from the ANSUR II anatomical landmarks, while the foot length and total body mass are directly taken from the ANSUR II data (Gordon et al. 2015). Even though the foot platform described in Section 3.2.2 was designed on

the basis of measurements made from the author's right foot, the foot length used for the torque estimation was based on the ANSUR II values, allowing the calculations to represent a broader range of users.

Table 3.6: Anthropometric values used for the lower and upper design cases in the torque estimations (Gordon et al. 2015).

Parameter	**Lower design case (Female P10)**	**Upper design case (Male P90)**
Body mass, M	54.6 kg	104.4 kg
Thigh length, L_t	356 mm	438 mm
Shank length, L_s	377 mm	446 mm
Foot length, L_f	230 mm	288 mm

The lower limb was represented using the rigid-link model described in Section 2.4, consisting of the thigh, shank and foot as separate rigid segments. Using the coefficients reported by Winter and presented in Table 2.3, the segment masses and COM positions were determined for each anthropometric case (Winter 2009). The segment mass was estimated from the total body mass, while the position of the COM was obtained from the corresponding segment length.

The gravitational contribution was first estimated by considering the greatest possible gravitational moment arm for the lower-limb segments that have an effect on each joint. This condition was approximated by the relevant segments being completely extended and positioned horizontally. At the ankle, only the foot contributed to the calculation; at the knee, the shank and foot were considered; and at the hip, the thigh, shank and foot were included.

In addition to the gravitational component, a simplified inertial contribution was considered, since the aim was to obtain a practical preliminary estimate for actuator sizing rather than to develop a complete dynamic model. In order to obtain a representative value of the maximum angular acceleration for this estimate, rather than assuming an arbitrary constant acceleration, a cubic polynomial trajectory was adopted. This type of trajectory was used by Z. Wang et al. (2024) for lower-limb rehabilitation motion planning. The same trajectory profile and movement duration of 2 s were therefore considered in the present work, while the angular displacement was adapted to the complete sagittal-plane ROM of each joint presented in Section 2.4.

Each lower-limb segment was represented by its mass concentrated at the corresponding COM. The equivalent rotational inertia about each joint was estimated from the masses of the segments moved by that joint and their distances from its axis of rotation. The inertial torque was then obtained from the equivalent inertia and the maximum angular acceleration.

The complete expressions and intermediate calculations used to determine the segment masses and COM positions, the maximum angular accelerations, and the gravitational and inertial torque contributions are provided in Appendix A, Section A.2.

The maximum gravitational and inertial contributions were added to obtain a conservative preliminary torque requirement. These two maximum contributions do not necessarily occur at the

same instant during an actual movement. Their direct addition therefore represents a conservative upper-bound estimate with respect to these two contributions rather than a prediction of the actual maximum torque occurring along a specific trajectory.

The resulting gravitational, inertial and combined torque estimates are presented in Table 3.7. As expected, the required torque increases towards the more proximal joints, since these joints are responsible for moving a larger proportion of the lower limb.

Table 3.7: Preliminary joint torque estimates used for actuator selection.

Joint	**Lower design case**			**Upper design case**		
	τ_g **(N m)**	τ_{in} **(N m)**	τ_{prelim} **(N m)**	τ_g **(N m)**	τ_{in} **(N m)**	τ_{prelim} **(N m)**
Ankle	0.89	0.02	0.91	2.14	0.05	2.19
Knee	7.89	1.02	8.91	17.96	2.78	20.74
Hip	27.78	5.43	33.21	64.75	15.35	80.10

These preliminary values were used to guide the selection of the actuators and their reduction mechanisms. At this stage, the masses of the mechanical structure and motor assemblies were still unknown, so configurations with additional torque capacity were preferred where possible. Once the actuators and main mechanical components had been selected, the torque calculations were repeated, including the masses of the moving robotic components, in order to check whether the final configuration remained suitable.

3.3.2 Motor and Gearbox Selection

The actuators were chosen on the basis of the torque requirements set out in Section 3.3.1, as well as taking into account some practical aspects concerning the implementation of the prototype. As stated in Section 2.6, pneumatic, hydraulic and electric actuation are three of the main technologies employed in lower-limb rehabilitation systems. Pneumatic actuators were found to be less appropriate for the system in question because of their need for a compressed air supply and their lower precision in both position and force control. Although hydraulic actuators are capable of producing high forces, this feature was not necessary for the application in mind, and the requirement for a hydraulic supply together with the need for additional components and the risk of fluid leakage would have introduced further practical constraints. Electric motors were therefore selected because they provide high positioning precision, relatively simple control and straightforward integration with the mechanical and electronic architecture of the prototype.

Of the various electric motor technologies mentioned in Section 2.6, stepper motors were selected. This was because the simple way of controlling position and speed via command pulses suited the prototype under development, since such pulses can be produced directly by an Arduino-based control system. The relatively low cost of stepper motors also matched the aim of creating an accessible prototype. Furthermore, independent sensing of the joint positions was included in the system, as explained in Section 3.4.

The preliminary torque requirements obtained in Section 3.3.1, which included both gravitational and simplified inertial contributions, could not be provided directly by compact stepper motors without mechanical reduction. Gearboxes were therefore used to increase the torque available at the joint while reducing the output speed. The theoretical output torque for each motor-gearbox combination was calculated using the motor torque, the gear ratio, and the gearbox efficiency. The corresponding expression is provided in Appendix A, Section A.3. The theoretical value on its own does not determine the usable output torque, since the maximum torque permitted for the gearbox must also be observed.

Different actuator sizes were required since, as indicated in Section 3.2.1, the torque demand increases significantly from the ankle to the hip. The final actuator and gearbox combinations are given in Table 3.8 (StepperOnline 2026a, 2026b, 2026d, 2026c).

Table 3.8: Specifications of the actuators and gearboxes selected for the three robotic joints. Underlined values indicate the torque considered available for each actuator assembly.

Parameter	**Hip**	**Knee**	**Ankle**
Motor size	NEMA 34	NEMA 23	NEMA 17
Motor model	34HE31-6004S	23HS22-2804S	17HS15-1584S
Gearbox	EG34-G50	PG47	MG20
Motor holding torque	4.80 N m	1.25 N m	0.36 N m
Gear ratio	50:1	46.656:1	20:1
Gearbox efficiency	94%	73%	90%
Theoretical static output torque	225.60 N m	42.57 N m	<u>6.48 N m</u>
Maximum permissible gearbox torque	<u>100 N m</u>	<u>30 N m</u>	10 N m
Actuator assembly mass	6.02 kg	1.70 kg	0.68 kg

Regarding the hip and knee assemblies, the theoretical torque calculated from Equation A.21 is greater than the maximum allowable torque of the respective gearbox. As a result, 100 N m and 30 N m were taken as the maximum static output torques for these two joints. In the case of the ankle assembly, the calculated output torque of 6.48 N m is less than the 10 N m maximum permissible torque of the gearbox and therefore serves as the relevant static torque estimate. These values are underlined in Table 3.8 to indicate the torque considered available for each actuator assembly. The relatively high reduction ratios were regarded as suitable for the slow movements intended for the rehabilitation system.

Following the motor and gearbox selection, the torque calculations were repeated to take into account the masses added by the robotic structure. As in the preliminary estimation, both the gravitational and simplified inertial contributions were considered. The masses regarded in this verification are given in Table 3.9. The masses listed for the thigh and shank refer to the combined structural plates of each section.

The hip motor assembly is held in place by the stationary structure described in Section 3.2.1 and therefore does not contribute to the gravitational or inertial loads of the moving lower-limb structure. In contrast, the knee and ankle motor assemblies are part of the moving mechanical

Table 3.9: Masses of the actuator assemblies and moving mechanical components considered in the final torque verification.

Component	Symbol	Mass
Actuator assemblies		
Hip actuator assembly	m_{ha}	6.02 kg
Knee actuator assembly	m_{ka}	1.70 kg
Ankle actuator assembly	m_{aa}	0.68 kg
Mechanical components		
Thigh structural plates	m_{th}	0.30 kg
Shank structural plates	m_{sh}	0.30 kg
Foot platform	m_{fp}	0.40 kg

chain and were therefore included in the calculations for the proximal joints.

For the gravitational contribution, the same worst-case condition considered in Section 3.3.1 was used. The masses of the thigh and shank structural plates were assumed to act at the same COM distances as the respective anatomical segments, while the mass of the foot platform was taken as acting at the same COM distance as the foot. The knee and ankle actuator assemblies were regarded as being located at their respective robotic joint axes.

For the inertial contribution, the same cubic trajectory, movement duration and joint angular displacements used in the preliminary estimation were considered. The additional moving components were represented using the same concentrated-mass approximation adopted for the lower-limb segments.

At the ankle, the foot platform was added to the load of the foot. At the knee, in addition to that, the shank structural plates, the ankle actuator assembly and the foot platform were taken into account. At the hip, the thigh and shank structural plates, the knee and ankle actuator assemblies, as well as the foot platform, were included. These moving components were considered in both the gravitational and inertial calculations, according to their respective positions relative to each joint. The full set of expressions employed for this final verification is provided in Appendix A, Section A.4. The resulting torque estimates for both anthropometric design cases are presented in Table 3.10.

Table 3.10: Final joint torque estimates including gravitational and inertial contributions.

Joint	Design case	τ_g (N m)	τ_{in} (N m)	τ_{final} (N m)	Available torque (N m)	Margin (%)
Hip	P10	43.91	9.18	53.09	100	88.4
	P90	84.40	20.89	105.29	100	-5.0
Knee	P10	12.81	1.81	14.62	30	105.2
	P90	23.82	3.90	27.72	30	8.2
Ankle	P10	1.34	0.02	1.36	6.48	376.5
	P90	2.70	0.06	2.77	6.48	134.3

The final estimates show that the available torque is well above the calculated requirements for all three joints in the lower design case. For the upper design case, the knee and ankle actuator configurations also remain above the calculated upper-bound torque requirements after the moving robotic components are included. For the hip, however, the combined gravitational and inertial estimate reaches approximately 105.29 N m, slightly above the 100 N m torque limit considered for the selected gearbox.

As in the preliminary estimation, the maximum gravitational and inertial contributions were added directly, even though these maxima do not occur at the same instant during the considered movement. The resulting value therefore represents an upper-bound estimate and is expected to be higher than the maximum torque actually required along the trajectory. Consequently, although the estimated value for the hip slightly exceeds the 100 N m torque limit of the selected gearbox, this does not necessarily indicate that the actuator assembly is insufficient. Given the small difference and the conservative nature of the calculation, it was considered reasonable to retain the selected hip actuator for the prototype.

3.3.3 Motor Drivers and Power Electronics

The stepper motors could not be connected directly either to the Arduino or to the external power supply. The Arduino only provides low-power control signals, while direct connection to the power supply would not provide the electrical control required to operate the motors correctly. A dedicated motor driver was therefore used between the controller, the power supply and each actuator.

Each driver receives STEP, DIR and ENABLE signals from the Arduino. The STEP signal commands the motor movement, the DIR signal defines the direction of rotation, and the ENABLE signal allows the motor to be enabled or disabled. The driver then interprets these control signals and operates the motor accordingly.

Different drivers were selected for the three joints because the motors have different electrical requirements. The DM860T was used for the hip actuator, which has the highest current requirements, while the DM542T was used for the knee actuator. The smaller ankle motor was controlled using a DRV8825. In each case, the driver settings were selected according to the requirements of the corresponding motor. The main electrical configurations are given in Table 3.11.

Table 3.11: Driver configurations used for the three robotic joints.

Parameter	**Hip**	**Knee**	**Ankle**
Driver	DM860T	DM542T	DRV8825
Supply voltage	24 V DC	24 V DC	24 V DC
Current setting	3.14 A RMS	2.03 A RMS	1.00 A current limit
Microstepping	1/16	1/16	1/16

The motor drivers were supplied from a single 24 V DC external power supply, while the Arduino board was powered separately through its USB connection. In this arrangement, the Arduino was responsible for generating the control signals, while the external power supply provided the electrical power required by the motors through their respective drivers.

3.4 Joint Position Sensing

The system was designed to include independent measurements of joint position in order to obtain information about the real position of the hip, knee and ankle joints. This is especially important since the stepper motors are controlled by a series of STEP pulses, meaning that the position estimated from the number of commanded steps does not in itself ensure that the actuator has reached the desired position. As explained in Section 2.6, stepper motors can lose steps when the available torque is insufficient, resulting in a discrepancy between the commanded and actual positions.

For this reason, each of the three actuator assemblies included one rotary encoder. The measured position provides independent feedback on the state of the robotic joints and is used by the system's control and safety logic.

3.4.1 Encoder Selection

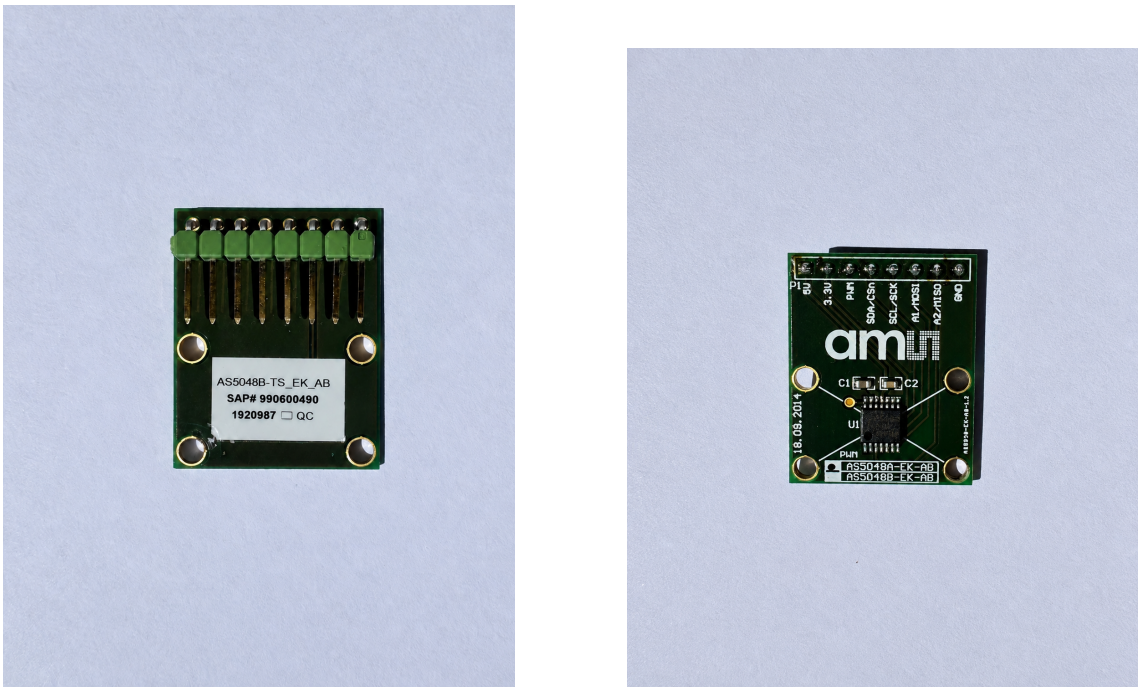
As stated in Section 2.7, rotary encoders can be implemented with different sensing technologies and are capable of providing either incremental or absolute position information. For the system under development, absolute magnetic encoders were chosen.

In the case of the system in question, an absolute encoder was chosen since it gives a direct measurement of the angular position of the motor shaft, enabling the actual movement to be determined independently of the step commands issued to the stepper motors. The magnetic sensing principle was adopted because it allows angular position to be measured without contact by using a permanent magnet attached to the rotating shaft, which in turn results in a compact design with relatively easy mechanical integration. Apart from these technical benefits, magnetic encoders were available at the time the prototype was developed, which also made this option a practical one to implement.

The selected sensor was the AS5048B magnetic rotary encoder, used in the AS5048B Adapter Board configuration. It offers absolute angular measurement over a full 360° rotation with a resolution of 14 bits and sends data via an Inter-Integrated Circuit (I^2C) interface (ams AG 2018). The same encoder model was used for the hip, knee and ankle, providing a common sensing principle and allowing the three sensors to share the same communication bus.

3.4.2 Mechanical Integration

The encoders were mechanically attached to the rear of the respective motor, with the encoder board staying in place while a permanent magnet rotated together with the rear end of the motor



(a) Front view. (b) Rear view.

Figure 3.16: AS5048B Adapter Board used for joint-position sensing.

shaft. This setup enabled the angular position of each motor to be determined separately. The fact that the encoder is situated before the gearbox means that the angle measured relates to the rotation of the motor and not directly to the angle of the robotic joint. The method employed to convert this measurement into the corresponding joint position is given in Section 3.4.3.

A disc-shaped permanent magnet, 6 mm in diameter and 2.5 mm thick, was used with each encoder. The magnet was made of neodymium and was diametrically magnetised, the latter being required for angular sensing with the AS5048B (ams AG 2018). It was positioned on the rear metallic shaft of the motor, where it remained fixed by magnetic attraction.

As was explained in Section 3.2.1, special supports were created in order to place the encoder boards at the back end of the three actuators. Separate rear supports were employed at the hip and at the knee, while at the ankle the encoder support was built into the actuator support itself (see Figure 3.8). These supports were designed specifically for the AS5048B Adapter Board, with the sensing element being positioned towards the magnet at the correct location relative to the motor shaft. An example of the encoder mounting setup is given in Figure 3.17.

3.4.3 Encoder Acquisition and Calibration

The encoder measurements are acquired by the actuation Arduino UNO through the I^2C interface. The three AS5048B encoders share the same SDA and SCL communication lines. Each encoder is identified by a different I^2C address, with `0x40`, `0x41` and `0x42` assigned to the hip, knee and ankle encoders, respectively. This allows the Arduino to acquire the three encoder measurements

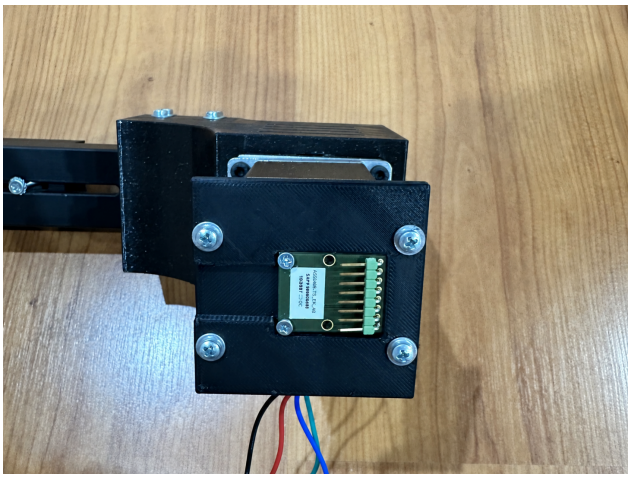


Figure 3.17: Example of an AS5048B encoder mounting arrangement.

independently while using the same communication bus. The software then converts each 14-bit raw value into an angle between 0° and 360° (ams AG 2018).

As explained in Section 3.4.2, the encoder records the rotation of the motor shaft prior to the gearbox. Due to the gearbox reduction, the motor can make several complete turns while the robotic joint moves through a much smaller angular range. The encoder, however, only gives the angular position within one single revolution, from 0° to 360°. For this reason, the software detects transitions across the 0°/360° boundary and accumulates the successive angular changes, allowing the motor position to be tracked continuously over multiple revolutions.

The corresponding joint displacement is calculated by dividing the total motor rotation by the gearbox ratio of the respective actuator. Since the positive rotation direction of the motor does not necessarily correspond to the positive rotation direction defined for the robotic joint, a direction factor is also taken into account:

$$\Delta\theta_{\text{meas}} = s_e \frac{\Delta\theta_m}{G}, \tag{3.1}$$

where $\Delta\theta_{\text{meas}}$ represents the measured joint angular displacement, $\Delta\theta_m$ the accumulated motor angular displacement, G is the gearbox ratio, and $s_e \in \{-1, +1\}$ is the encoder direction factor.

Because the encoder is located before the gearbox and provides an absolute position only within one revolution of the motor, the system has to establish an initial joint reference when it is started. The robotic joint is first put into a known angular position, which is given to the software as part of the initialization process. The encoder reading at that position is then used to determine the angular offset between the total motor position and the corresponding joint angle. The subsequent joint positions are calculated according to

$$\theta_{\text{meas}} = \theta_{\text{offset}} + s_e \frac{\theta_m}{G}, \tag{3.2}$$

where θ_m represents the accumulated motor angle and θ_{offset} is the offset established during initialization.

The validity of the encoder measurements is also monitored by the acquisition software. I^2C communication errors and diagnostic conditions reported by the AS5048B, including problems associated with the magnetic field, are used to identify invalid encoder operation before the measured joint position is accepted by the control system.

3.5 EMG Acquisition and Processing

The sEMG was included in the system in order to get information on the user's voluntary muscle activity as part of active-assisted rehabilitation. As explained in Section 2.7, physiological sensing can provide information concerning movement intention, and both EMG and EEG are possible methods for this. For this prototype, sEMG was chosen since it provides information that is directly linked to the activation of the lower-limb muscles involved in the rehabilitation movements, and it has a simpler and more practical method of acquisition setup than EEG. As discussed in Section 2.7, EEG requires electrodes to be positioned on the scalp, may involve additional preparation to obtain adequate electrode-skin contact, and its measurements can be affected by artefacts and external disturbances.

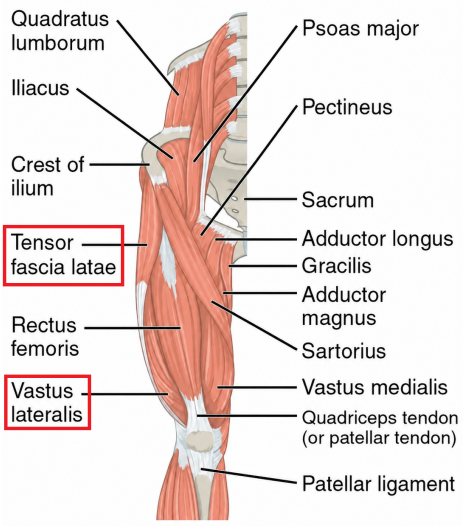
The EMG measurements were considered for the flexion and extension of the hip, knee, and ankle. The following subsections explain the muscles and sensor positions that were selected, the procedures followed for signal acquisition and calibration, and the method employed to detect movement intention.

3.5.1 Sensor Placement

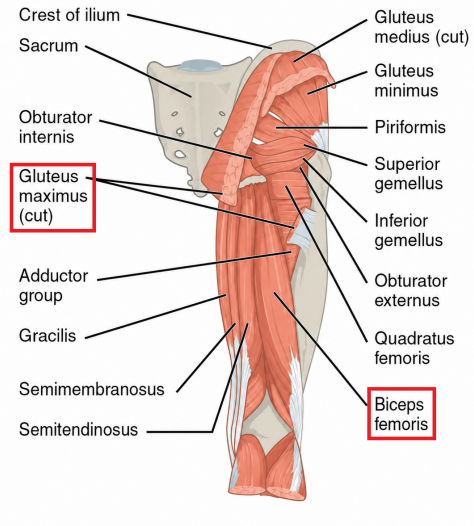
For each of the three robotic joints, two muscles associated with opposite sagittal-plane movements were selected for surface EMG acquisition. At the hip these were the tensor fasciae latae and the gluteus maximus, at the knee the biceps femoris and the vastus lateralis, and at the ankle the tibialis anterior and the gastrocnemius lateralis. The anatomical positions of these muscles are shown in Figure 3.18.

The tensor fasciae latae is involved in hip flexion, and the gluteus maximus takes part in hip extension. At the knee, the biceps femoris contributes to knee flexion, while the vastus lateralis, as part of the quadriceps group, contributes to knee extension. Lastly, the tibialis anterior has a role in ankle dorsiflexion and the gastrocnemius contributes to plantarflexion (Betts et al. 2022). The muscle pairs were used to represent the opposing movements at each of the three actuated joints.

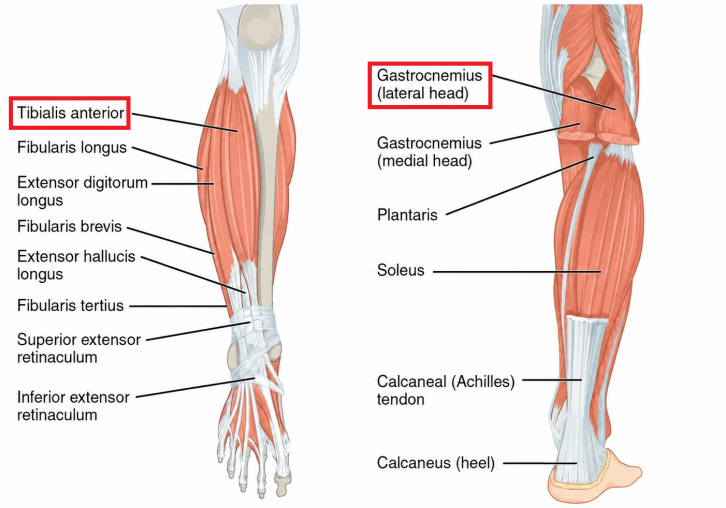
The sensor positions were defined according to SENIAM-based electrode-placement recommendations reported by Cutler and Hodson-Tole (2022) and Santuz et al. (2018). The resulting positions for the six muscles considered are given in Table 3.12. The electrodes were oriented according to the main direction of the muscle fibres, following the same general recommendations.



(a) Anterior view of the hip and thigh.



(b) Posterior view of the hip and thigh.



(c) Anterior and posterior views of the lower leg.

Figure 3.18: Anatomical locations of the lower-limb muscles. Adapted from Betts et al. (2022).

Table 3.12: sEMG sensor locations.

Joint	Movement	Muscle	Sensor location
Hip	Flexion	Tensor fasciae latae	Proximal 1/6 of the line between the anterior superior iliac spine and the lateral femoral condyle (Santuz et al. 2018).
	Extension	Gluteus maximus	50% of the line between the sacral vertebrae and the greater trochanter (Cutler and Hodson-Tole 2022).
Knee	Flexion	Biceps femoris	50% of the line between the ischial tuberosity and the lateral epicondyle of the tibia (Cutler and Hodson-Tole 2022).
	Extension	Vastus lateralis	2/3 of the line between the anterior superior iliac spine and the lateral side of the patella (Cutler and Hodson-Tole 2022).
Ankle	Dorsiflexion	Tibialis anterior	1/3 of the line between the tip of the fibula and the medial malleolus (Cutler and Hodson-Tole 2022).
	Plantarflexion	Gastrocnemius lateralis	1/3 of the line between the head of the fibula and the heel (Cutler and Hodson-Tole 2022).

3.5.2 Signal Acquisition

The MyoWare 2.0 Muscle Sensor was chosen in order to acquire the sEMG signals. In the system that was developed, six sensors were employed, one for each of the muscles mentioned in Section 3.5.1, which gave rise to two EMG channels for each robotic joint. These channels correspond to the opposing movements considered at the hip, knee and ankle. The MyoWare 2.0 was selected because of its simple integration with the Arduino, its relatively low cost, and its suitability for the signal-acquisition needs of the present prototype. Amanov and Ibrayev (2024) similarly used the MyoWare 2.0 for lower-limb EMG acquisition, also highlighting its ease of use and compatibility with Arduino.

The MyoWare 2.0 is a wearable device which is intended for sEMG acquisition and for integration with microcontrollers. It is powered by a single power supply, usually being in the range of 3.3 to 5 V, and includes analogue signal-conditioning circuitry that allows the EMG signal to be accessed at three different stages of processing (SparkFun Electronics). The *RAW* output provides the signal in its least processed form, showing the fast positive and negative variations produced by muscle activity. The *RECT* output is the rectified version of this signal, where the negative parts are converted to positive values. The *ENV* output smooths this rectified signal, producing a slower-changing envelope that gives a clearer indication of the muscle activation level.

For the developed system, the *ENV* output was selected. This output provides a smoothed analogue signal whose amplitude varies with the detected muscle activity. Since the objective of the present implementation is to determine the level of muscle activation for movement-intention detection rather than to analyse the detailed frequency content or waveform of the raw EMG signal,

the *ENV* output reduces the amount of additional signal processing that has to be performed by the microcontroller.



Figure 3.19: MyoWare 2.0 Muscle Sensor (SparkFun Electronics).

The *ENV* output of each MyoWare sensor was connected to a separate analogue input of the Arduino used for EMG acquisition, so that the activity of the six selected muscles could be acquired independently. Each sensor produces an analogue voltage that varies according to the measured muscle activity. The Arduino's analogue-to-digital converter samples this voltage and converts it into a numerical value that can be processed by the software. During each acquisition cycle, the six analogue inputs are read sequentially, resulting in an individual EMG measurement for each muscle.

The absolute amplitude derived from sEMG cannot be interpreted in the same manner for all muscles or in all cases of acquisition, since the signal measured can differ depending on factors such as the muscle itself and the position of the electrodes, as mentioned in Section 2.7. The values obtained are not employed directly for the purpose of detecting movement intention. Instead, each channel is calibrated and normalised individually before being used by the control system.

3.5.3 EMG Calibration and Normalisation

Each EMG channel was calibrated individually before movement-intention detection. The reason for this calibration was to set up a lower and an upper reference level for each muscle, so that the signals obtained could be given a normalised form instead of using the absolute values supplied by the sensors. A summary of the calibration and normalisation procedure is given in Figure 3.20.

The calibration procedure has two stages. In the first stage, a resting reference is obtained with the user keeping the muscle relaxed. When the user has been told to stay at rest, an *ENV* signal is collected for 3 s. The resting reference, x_{rest}, is calculated as the average of all the samples gathered during this time interval. An average is used rather than a single measurement in order to obtain a reference that is representative of the baseline signal throughout the calibration period.

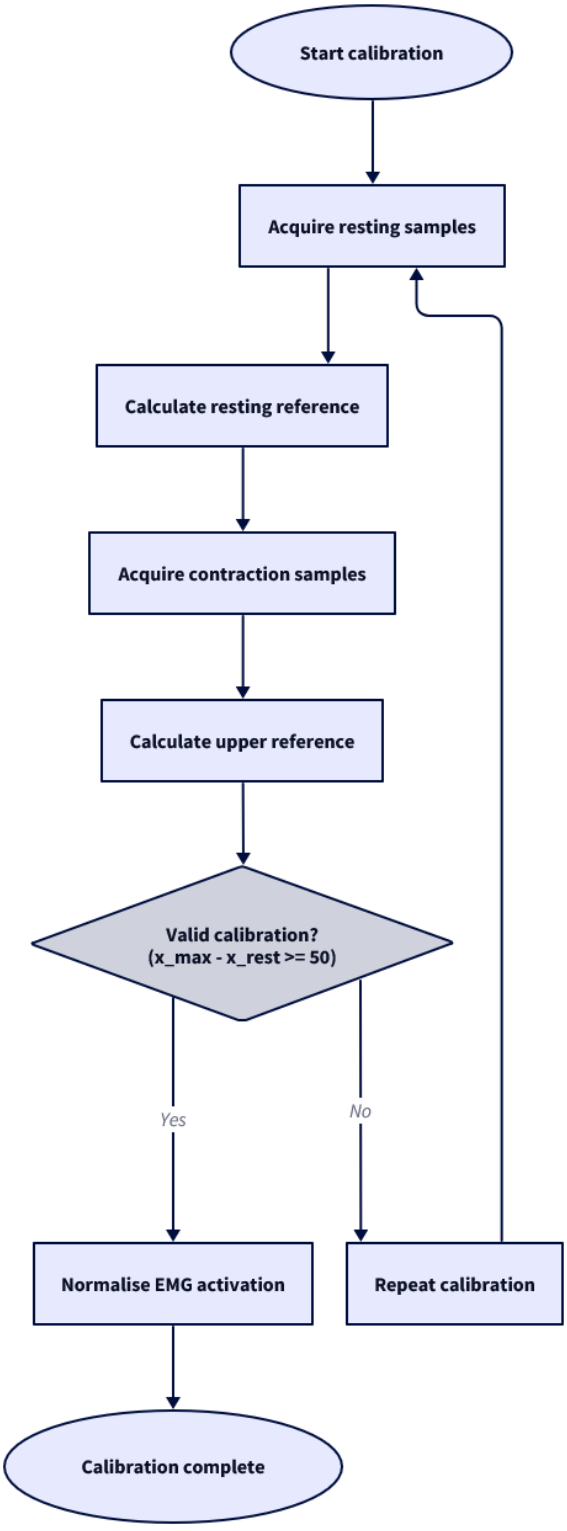


Figure 3.20: EMG calibration and normalisation procedure.

In the second stage the upper reference level is set by asking the user to carry out a strong voluntary contraction of the muscle and then recording the signal again for 3 seconds. Rather

than taking the single highest sample value that was recorded during the contraction, the software keeps the ten highest values measured over this period and calculates their average. This average is then used as the upper calibration reference, $x_{\max}$, in order to ensure that the upper reference is not determined by a single isolated peak in the recorded signal.

Once the two reference values have been found, the calibration is verified before it is accepted. The upper reference is required to exceed the resting reference by more than 50 digital units. If this condition is not met, the measured range is regarded as inadequate and the calibration must be repeated. This check is important since a very small difference between the resting and contraction reference levels would make the normalised activation more sensitive to small fluctuations in the acquired signal.

Once the calibration has been accepted, the acquired EMG values are normalised using the two reference values:

$$a = \frac{x - x_{\text{rest}}}{x_{\max} - x_{\text{rest}}}, \tag{3.3}$$

where x is the current EMG value, x_{rest} is the resting reference, $x_{\max}$ is the upper reference obtained during voluntary contraction, and a is the resulting normalised muscle activation. The resulting activation is limited to the interval from 0 to 1, with values close to 0 corresponding to the calibrated resting level and values approaching 1 corresponding to activity near or above the upper calibration reference.

3.5.4 Movement Intention Detection

The activation values obtained by normalisation from the two opposing muscles at each joint are used to judge the user's intention to move. Instead of looking at the activation of each muscle separately, the algorithm compares the activation levels of the muscles involved in order to identify which movement direction is dominant.

For each muscle pair, a net activation value is calculated as

$$a_{\text{net}} = a_{\text{ext}} - a_{\text{flex}}, \tag{3.4}$$

where a_{ext} and a_{flex} denote the normalised activation levels of the muscles associated with extension and flexion, respectively. As both are limited to the range from 0 to 1, a_{net} varies between -1 and 1. Positive values indicate the extensor muscles are more actively engaged, whereas negative values indicate flexor predominance. Values near zero indicate that neither muscle clearly dominates.

A threshold-based method is used to distinguish directional movement intention from small variations around the resting condition. Extension is detected when the net activation exceeds 0.15, whereas flexion is detected when it falls below -0.15.

Hysteresis is used to avoid quick switching between movement states when the activation level is near the detection threshold. In order to enter a flexion or extension state, the net activation

magnitude must exceed 0.15. Once such a state has been detected, it is kept until the activation drops below a lower threshold of 0.10. Because separate entry and exit thresholds are used, there is a small range around the point at which state changes occur and this makes the detected intention less sensitive to small variations in the EMG signals.

The main conditions employed for classifying movement intention are given in Table 3.13.

Table 3.13: Conditions used for movement-intention classification.

Condition	**Detected state**
$a_{\text{net}} > 0.15$	Extension
$a_{\text{net}} < -0.15$	Flexion
$\lvert a_{\text{net}} \rvert \leq 0.15$ when no directional state is active; $\lvert a_{\text{net}} \rvert < 0.10$ to leave flexion or extension	Relaxed

Together with the detected state, the algorithm also calculates a movement intensity between 0 and 1. In the case of flexion and extension, this intensity is obtained from the magnitude of the net activation rather than being directly taken from the activation of the main muscle. This enables the intensity to show the degree to which one muscle outperforms its antagonist. For instance, if both of the opposing muscles are highly activated but there is only a small difference between them, the resulting directional intensity will still be low, even though the level of activation of the dominant muscle is high.

The intensity is calculated according to

$$I = \frac{\lvert a_{\text{net}} \rvert - T_{\text{exit}}}{1 - T_{\text{exit}}}, \tag{3.5}$$

where T_{exit} is the hysteresis exit threshold, set to 0.10. This threshold is subtracted so that an activation equal to the minimum level required to maintain a directional intention corresponds to an intensity of 0. The remaining range, from T_{exit} to 1, is then rescaled to the interval from 0 to 1. Consequently, the intensity increases as the directional predominance between the opposing muscles becomes stronger. For a directional state, the intensity approaches 0 as $\lvert a_{\text{net}} \rvert$ approaches the exit threshold and reaches 1 as the net activation approaches its theoretical maximum.

3.6 Control System

The control system coordinates the data gathered from the sensors with the commands sent to the actuators. As stated in Section 2.8, the control architecture can be divided into high-level, mid-level and low-level functions, extending from the interpretation of the user's state or the definition of the rehabilitation objective to the generation of reference commands and their execution by the actuators. In the developed system, two rehabilitation modes were implemented in order to accommodate different levels of voluntary motor ability. Passive rehabilitation provides externally generated movement when the user is unable to contribute sufficiently to the exercise,

whereas active-assisted rehabilitation is intended for users who retain voluntary muscle activity and can therefore participate actively in the movement. During passive rehabilitation, movement is generated by a dedicated trajectory generator that moves the selected joint repeatedly along a predefined angular trajectory. During active-assisted rehabilitation, the control functions instead include movement intention derived from the EMG signals, reference generation, AAN control and joint-position feedback. In both modes, the resulting angular commands are processed by the safety functions and then executed by the low-level control of the stepper motors.

3.6.1 Control Architecture

The implemented architecture keeps the physiological sensing and the detection of movement intention separate from the control of the actuators. Two individual Arduino Uno boards are used for these functions: one handles the acquisition and processing of the EMG signals, and the other carries out the rehabilitation control functions, monitors the joint positions, and controls the stepper motors. The two boards communicate directly with each other through a serial UART connection.

On the sensing side, the EMG signals are processed in order to determine the movement intention and the corresponding intensity for each joint, as described in Section 3.5. This information is then sent to the actuation Arduino and used when active-assisted rehabilitation is selected.

The control path depends on the selected rehabilitation mode. In the case of passive rehabilitation, the movement is defined from prescribed exercise parameters by a dedicated trajectory generator. In active-assisted rehabilitation, the movement intention and intensity are first used to generate the desired angular reference. This reference is then combined with the measured joint position and the user's voluntary contribution by the AAN controller to determine the assisted angular target.

These functions may be arranged in accordance with the three-level control architecture explained in Section 2.8. At the high level, the rehabilitation mode is selected and, during active-assisted rehabilitation, the user's intended movement is determined from the EMG-derived intention and intensity. At the mid level, the selected mode determines whether the angular command is produced by the passive trajectory generator or through the active-assisted control path, in which the generated reference is processed by the AAN controller. At the low level, the resulting safe angular command is converted into the signals required to operate the stepper motors.

The measured joint positions described in Section 3.4 are fed back to the control system and are used by the AAN and safety functions. Before any angular command is passed on to the low-level controller, it is processed by the safety layer to ensure that the movement remains within the specified operating limits and that the system can respond to any abnormalities.

A system state machine controls the operation of the actuation controller and decides, according to the current system state, whether movement generation and motor operation are allowed, whether the current position should be maintained, or whether motor operation should be disabled. The control architecture and the interaction between its main functional levels are shown in Figure 3.21.

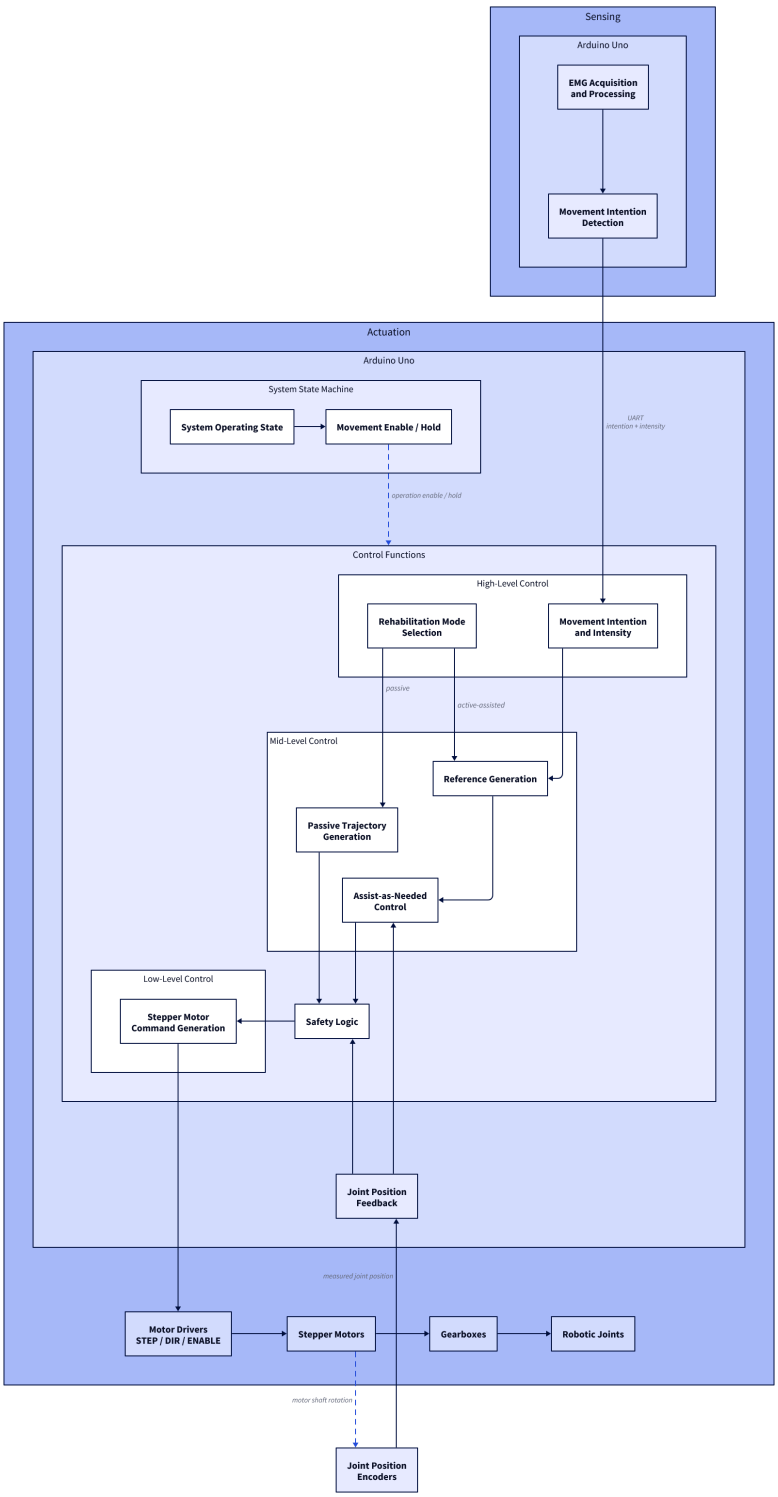


Figure 3.21: Control architecture of the developed system and organisation of the high, mid and low-level control functions.

3.6.2 High-Level Control

The high-level control is responsible for selecting the rehabilitation mode and, during active-assisted rehabilitation, interpreting the information obtained from the user to determine the intended direction of movement. As described in Section 3.5.4, the sensing Arduino classifies the muscle activity associated with each joint as flexion, extension or relaxed and assigns a corresponding intensity value.

After this information is received by the actuation Arduino, flexion and extension are treated as commands for movement in the corresponding direction. Their intensity value, ranging from 0 to 1, is then passed to the mid-level controller to influence the generated reference. By contrast, relaxation does not produce a directional command. The high-level interpretation of the three movement states is summarised in Table 3.14.

Table 3.14: High-level interpretation of the detected movement states.

Movement state	**High-level interpretation**
Flexion	Directional intention towards joint flexion.
Extension	Directional intention towards joint extension.
Relaxed	No directional movement intention.

Only flexion and extension lead to the generation of a changing movement reference. When the relaxed state is detected, the joint is instead kept at the position reached when the previous movement ended. The direction and intensity accepted at this level are subsequently used by the mid-level control to generate the angular reference and determine the robotic assistance.

3.6.3 Mid-Level Control

The mid-level control is responsible for generating the joint-angle commands used by the actuation system. Both rehabilitation modes rely on an angular reference that is updated continuously during operation, but they differ in the way its evolution is determined. In passive rehabilitation, the reference follows a prescribed exercise defined by set parameters. In active-assisted rehabilitation, the reference is instead driven by the user's detected movement direction and intensity.

3.6.3.1 Passive Rehabilitation

In passive rehabilitation, the robotic system repeatedly moves a single joint along a predefined angular trajectory. This mode is intended to provide the prescribed movement when the user's voluntary contribution is insufficient to drive the exercise. Only one robotic joint is operated at a time, and for each exercise the hip, knee or ankle can be chosen. Before an exercise starts, the trajectory is set by specifying the minimum and maximum angles, the speed of movement, the number of repetitions and the duration of the pause at the endpoints of the trajectory. A different joint can be selected once the current exercise has been completed or stopped.

Before the movement begins, the exercise configuration is checked to make sure that it is valid. The angular range chosen must stay within the allowed ROM of the joint, with the minimum angle below the maximum, and the requested movement speed must not exceed the allowed maximum.

The overall operation of the passive rehabilitation mode is summarised in Figure 3.22.

The commanded joint position is represented by an angular reference whose evolution is determined by the prescribed exercise parameters, including the movement range, speed, number of repetitions and endpoint pause duration. During each movement phase, the passive trajectory generator updates this reference at each control cycle so that it progresses at the configured constant speed in the current movement direction:

$$\theta_{\text{pass}}(k+1) = \theta_{\text{pass}}(k) + d_{\text{pass}}\, v_{\text{pass}}\, \Delta t, \tag{3.6}$$

where θ_{pass} is the passive angular reference, v_{pass} is the defined movement speed, $d_{\text{pass}} \in \{-1, +1\}$ sets the current direction of movement, and Δt represents the time between consecutive control updates.

The generated reference is limited to the specified angular range. At the start of the exercise, the chosen joint is first moved to the minimum angle before the cyclic movement begins. The reference then progresses to the maximum angle, remains there for the configured pause duration, and subsequently reverses direction to return to the minimum angle, where the same pause is applied before the next cycle starts. One repetition corresponds to a complete movement from the minimum to the maximum angle and back again. This sequence is repeated until the requested number of repetitions has been completed.

The angular reference produced by the passive trajectory generator is processed by the safety functions before being forwarded to the low-level motor controller.

3.6.3.2 Active-Assisted Rehabilitation

Active-assisted rehabilitation also relies on an angular reference that is continuously updated at each control cycle. Unlike the passive mode, however, its evolution is not determined by a prescribed exercise sequence, but by the user's detected movement intention. The active-assisted control path is divided into two main stages. First, the detected movement direction and intensity are used to generate the angular reference for the corresponding joint. The movement direction determines whether the reference increases or decreases, while the intensity determines how quickly it changes. The reference therefore continues to progress for as long as a flexion or extension intention is maintained.

The second stage corresponds to the AAN controller. Instead of sending the generated reference directly to the motor, the controller compares it with the joint position measured by the encoder and also considers the user's EMG intensity and the intended movement direction. This allows the controller to distinguish between a user who is falling behind the generated reference

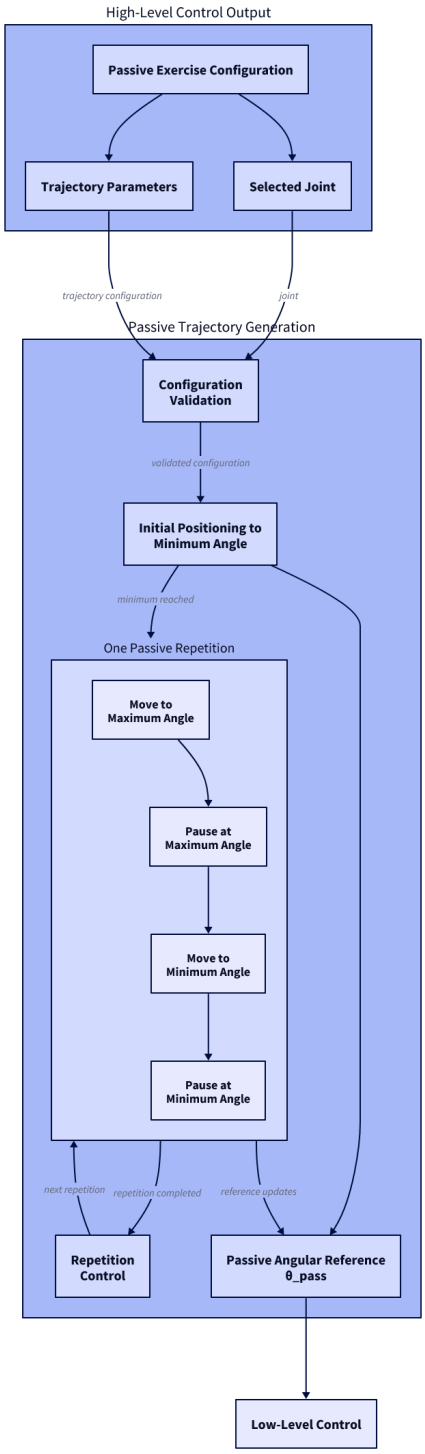


Figure 3.22: Implemented passive rehabilitation trajectory-generation algorithm.

and one who has already reached or moved beyond it in the intended direction. From this information, it determines how much robotic assistance should be provided and generates the final assisted angular target that is passed to the lower control level.

The overall operation of the active-assisted mid-level control, from reference generation to the calculation of the assisted angular target, is summarised in Figure 3.23.

When a flexion or extension intention is present, the reference speed is defined from the corresponding intensity according to

$$\dot{\theta}_{\text{ref}} = d\, I\, \dot{\theta}_{\max}, \tag{3.7}$$

where I is the movement intensity determined from the EMG signals, $\dot{\theta}_{\max}$ is a fixed maximum reference speed defined for the controller, and d defines the direction of movement. The sign assigned to d depends on the angular convention adopted for each joint. The reference speed is therefore obtained by scaling this predefined maximum value according to the detected movement intensity. Consequently, stronger movement intention causes the angular reference to change more rapidly, while weaker activation results in a slower progression.

The reference angle is updated at each control cycle according to

$$\theta_{\text{ref}}(k+1) = \theta_{\text{ref}}(k) + \dot{\theta}_{\text{ref}} \Delta t, \tag{3.8}$$

where Δt represents the time between consecutive control updates. In this way, the controller does not define a single final position when an intention is detected. Instead, the desired joint position progresses continuously in the corresponding direction for as long as the intention is maintained. The reference angle is limited to the allowed ROM of the corresponding joint.

The AAN calculation first considers the difference between the generated reference and the position measured by the joint encoder. The resulting tracking error is defined as

$$e = \theta_{\text{ref}} - \theta_{\text{meas}}, \tag{3.9}$$

where θ_{meas} is the measured joint angle.

Since the same signed tracking error can have a different meaning depending on the intended direction of movement, the controller also considers the direction associated with the current flexion or extension intention. A directional tracking error is therefore defined as

$$e_{\text{dir}} = d\, e, \tag{3.10}$$

where $d \in \{-1, +1\}$ is the movement-direction factor already used for reference generation. A positive value of e_{dir} indicates that the measured joint position is behind the generated reference in the intended movement direction. Conversely, $e_{\text{dir}} \leq 0$ indicates that the user has reached or moved beyond the reference in that direction.

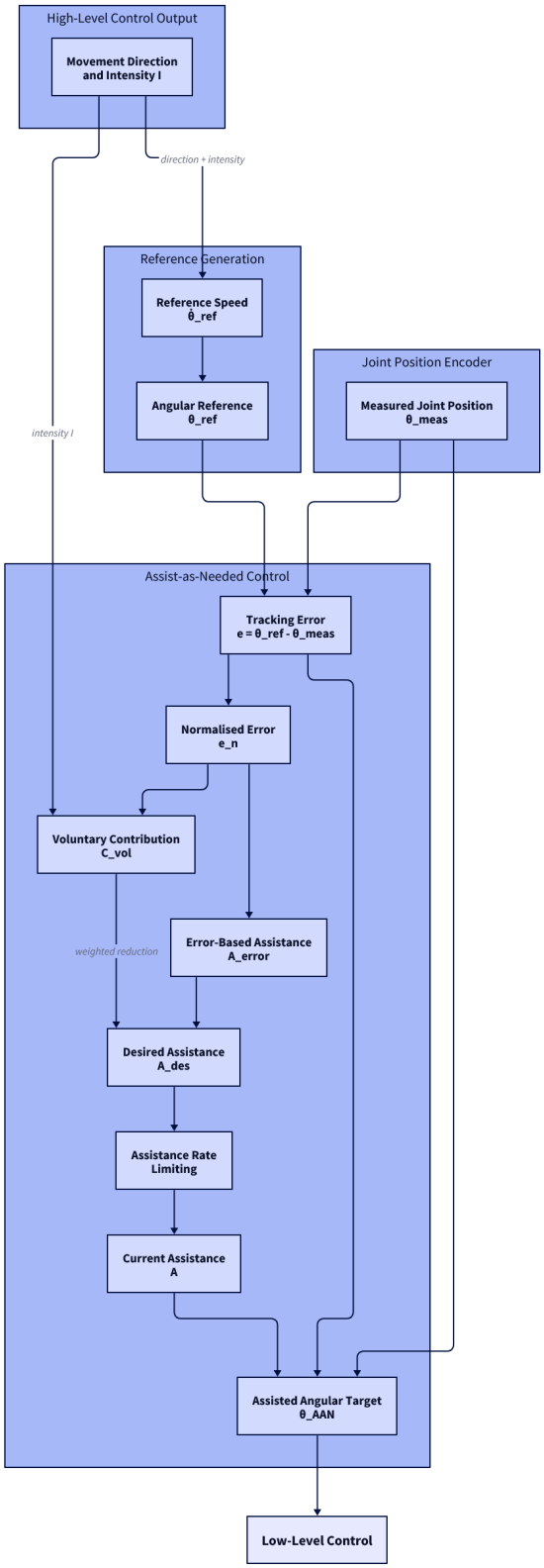


Figure 3.23: Implemented active-assisted mid-level control structure.

Only the portion of the tracking error for which the measured position remains behind the reference is used to determine the assistance demand. The normalised directional error is calculated as

$$e_{\mathrm{n}} = \min\left(\frac{\max(e_{\mathrm{dir}}, 0)}{e_{\mathrm{full}}}, 1\right), \tag{3.11}$$

where e_{full} is the predefined directional tracking-error value at which maximum error-related assistance is required. When $0 < e_{\mathrm{dir}} < e_{\mathrm{full}}$, the normalised error increases proportionally with the amount by which the measured position lags behind the reference. Once e_{dir} reaches or exceeds e_{full}, e_{n} is limited to 1. When $e_{\mathrm{dir}} \leq 0$, the normalised error is zero and no corrective assistance is requested to return the joint towards the reference.

An initial assistance demand is calculated from the tracking error:

$$A_{\mathrm{error}} = A_{\mathrm{min}} + (A_{\mathrm{max}} - A_{\mathrm{min}})\, e_{\mathrm{n}}, \tag{3.12}$$

where A_{min} and A_{max} are the minimum and maximum assistance levels used while assistance is required. With this formulation, the assistance demand increases progressively as the measured position falls further behind the generated reference in the intended movement direction.

The user's voluntary contribution, denoted by C_{vol}, is also considered through the EMG intensity. Its effect is weighted according to the tracking error:

$$C_{\mathrm{vol}} = I\,(1 - e_{\mathrm{n}}), \tag{3.13}$$

When the measured joint position is close to the generated reference, e_{n} is small and the voluntary contribution is mainly determined by the EMG intensity. Therefore, a high activation level indicates that the user is actively contributing to the movement and can justify a reduction in robotic assistance. As the directional tracking error increases, however, the factor $(1 - e_{\mathrm{n}})$ decreases, reducing the influence of the EMG intensity. This prevents a high muscle activation from reducing the assistance when the user is nevertheless unable to follow the desired reference. When $e_{\mathrm{n}} = 1$, the voluntary contribution becomes zero and the desired assistance is determined entirely by the directional tracking error, reaching A_{max}.

The voluntary contribution is therefore used to reduce the assistance initially determined from the tracking error. The desired assistance level is calculated as

$$A_{\mathrm{des}} = \begin{cases} A_{\mathrm{error}} - w_{\mathrm{EMG}} C_{\mathrm{vol}}, & e_{\mathrm{dir}} > 0, \\ 0, & e_{\mathrm{dir}} \leq 0. \end{cases} \tag{3.14}$$

where w_{EMG} is a weighting parameter that determines how strongly the voluntary contribution reduces the robotic assistance. A higher value gives greater importance to the user's contribution, whereas a lower value makes the assistance depend more strongly on the directional tracking error. When $e_{\mathrm{dir}} > 0$, the resulting assistance demand is limited to the interval between A_{min} and A_{max}.

When $e_{\text{dir}} \leq 0$, the desired assistance is instead set to zero, since the user has reached or moved beyond the generated reference in the intended direction.

The two sources of information therefore influence the assistance calculation in different ways. Joint-position feedback indicates how successfully the generated reference is being followed, while the EMG intensity provides information on the user's voluntary contribution to the movement. Their respective roles in the AAN controller are summarised in Table 3.15.

Table 3.15: Effect of the AAN input variables on assistance.

Input variable	**Variable change**	**Effect on assistance**
Directional tracking error	$e_{\text{dir}} \uparrow$, $e_{\text{dir}} > 0$	$A \uparrow$
	$e_{\text{dir}} \downarrow$ towards 0	$A \downarrow$
	$e_{\text{dir}} \leq 0$	No corrective assistance
EMG intensity	$I \uparrow$	$A \downarrow$ when e_{n} is small and $e_{\text{dir}} > 0$
	$I \downarrow$	$A \uparrow$ when e_{n} is small and $e_{\text{dir}} > 0$

After the desired assistance level has been determined, its variation between consecutive control cycles is limited in order to avoid abrupt changes in actuator behaviour. Separate rate limits are defined for increasing and decreasing assistance, allowing the controller to control independently how quickly additional assistance is introduced and how quickly it is withdrawn. When the user reaches or exceeds the generated reference in the intended movement direction, the desired assistance is set to zero and the internal assistance level is progressively reduced according to the configured decrease-rate limit.

Finally, the assistance level is used to determine how much of the difference between the measured joint position and the generated reference should be compensated by the actuator. The assisted angular target is calculated as

$$\theta_{\text{AAN}} = \begin{cases} \theta_{\text{meas}} + Ae, & e_{\text{dir}} > 0, \\ \theta_{\text{meas}}, & e_{\text{dir}} \leq 0. \end{cases} \tag{3.15}$$

where A is the current assistance level. While $e_{\text{dir}} > 0$, the measured position remains behind the reference in the intended movement direction and the assistance level determines how much of this difference is compensated. If $A = 0$, the assisted target is equal to the measured joint position, whereas if $A = 1$, it is equal to the generated reference. Intermediate values place the target between these two positions. When $e_{\text{dir}} \leq 0$, the measured position has reached or exceeded the reference in the intended movement direction, and the assisted target is therefore kept equal to the measured position. In this situation, the controller does not command the joint to return towards the generated reference, allowing voluntary movement beyond the reference to be tolerated.

The angular target produced by the AAN controller is subsequently passed through the safety functions before being sent to the low-level motor controller.

3.6.4 Low-Level Motor Control

The low-level controller converts the angular command produced by the selected rehabilitation mode into the signals needed to drive the stepper motors, as explained in Section 3.6.3. Before being applied to the actuator, the corresponding target is processed by the safety functions, producing the safe angular target, θ_{safe}. This safe target is then forwarded to the respective motor-control module.

As the actuators are stepper motors, θ_{safe} must be converted into the corresponding number of motor steps. The number of steps per degree of joint rotation is determined from the motor step resolution, the microstepping setting chosen and the gearbox ratio:

$$N_{\text{deg}} = \frac{N_{\text{motor}}\,\mu\,G}{360}, \tag{3.16}$$

where N_{motor} is the number of full motor steps per revolution, μ is the microstepping factor, G is the gearbox ratio, and N_{deg} is the resulting number of steps per degree of joint rotation.

The safe angular target is then converted into an absolute step position according to

$$N_{\text{target}} = s_{\text{m}}\,\theta_{\text{safe}}\,N_{\text{deg}}, \tag{3.17}$$

where $s_{\text{m}} \in \{-1,+1\}$ accounts for the physical rotation direction of the corresponding motor assembly. The resulting value is rounded to the nearest complete microstep before being used as the motor target.

The motor's movement towards the target position is achieved by using the AccelStepper library in driver mode. This library generates the STEP and DIR signals required by the motor drivers mentioned in Section 3.3.3. For each actuator, maximum speed and acceleration values are set so that the motor can move progressively towards the desired position while respecting the established motion limits.

The low-level motor control implemented is different from a conventional closed-loop position controller such as a PID. When using a PID controller, the measured joint position is continuously compared with the desired position and the resulting error is used to modify the actuator command. In the current implementation, the safe angular target, θ_{safe}, is converted into the commanded step position, N_{target}, and the motor is driven towards this position by means of the STEP pulses produced by AccelStepper. The encoder measurement, θ_{meas}, is therefore not used to directly correct the motor command at this level.

This approach keeps the actuator control consistent with the step-based positioning principle of the selected motors and avoids the need to introduce and tune an additional position-control loop for each actuator. The independent encoder measurements are nevertheless retained in the overall control architecture and are used by the AAN and safety functions. As a consequence, the low-level controller assumes that the commanded STEP pulses result in the corresponding motor displacement. If a discrepancy develops between the commanded and measured positions, for

example because of lost steps or an external disturbance, it is not corrected directly by the low-level controller, although the measured joint position remains independently available to the AAN and safety functions.

3.6.5 Communication Architecture

As explained in Section 3.6.1, the sensing and actuation functions are implemented on separate Arduino UNO boards. The sensing Arduino determines the user's movement intention and corresponding intensity from the EMG signals and transmits this information to the actuation Arduino, where it is combined with the joint-position measurements for control of the robotic joints.

A direct serial UART connection was used for communication between the two controllers. The connection is used both to transfer movement-intention information and to forward system commands required by the actuation controller. Once a movement intention has been detected, the sensing Arduino periodically transmits the corresponding movement-intention message using the following structure:

```
J,<joint>,<intention>,<intensity>
```

The meaning of each message field is summarised in Table 3.16.

Table 3.16: Structure of the movement-intention message transmitted through the UART connection.

Field	Information
`J`	Fixed identifier used to recognise a joint movement message.
`joint`	Identifies the robotic joint (hip, knee or ankle) associated with the message.
`intention`	Indicates the detected movement state (flexion, extension or relaxed).
`intensity`	Contains the normalised movement-intensity value associated with the detected state.

On the actuation side, the received movement-intention messages are decoded and associated with the corresponding joint. The resulting intention and its intensity are then passed on to the high-level and mid-level control functions described in Sections 3.6.2 and 3.6.3. In this way, the communication link transfers the processed movement information rather than the individual EMG measurements.

During active-assisted rehabilitation, the communication is monitored so that it can be determined whether valid movement information is still being received from the sensing controller. If no valid message has been received within the specified communication timeout, the connection is considered lost. This situation is passed to the system state machine, which then stops normal active-assisted operation until communication has been reestablished.

3.7 Safety Implementation

The operation of the robotic system is supervised by a number of software safety mechanisms designed to prevent actuator commands from being applied outside the established operating conditions and to respond to abnormal system behaviour. These mechanisms work together with the system state machine described in Section 3.6.1 and use information from the control system, the joint-position encoders and the communication link.

Before being sent to the low-level motor controller, the angular command produced by either rehabilitation mode is processed by the safety functions. In addition, before a passive rehabilitation exercise begins, its trajectory configuration is checked to ensure that the selected angular range remains within the permitted joint range, the requested movement speed does not exceed the allowed maximum, the number of repetitions is valid, and the pause duration is not negative.

During operation, the desired target angle is restricted to the angular range permitted for the relevant robotic joint, producing the safe angular target, θ_{safe}, which was introduced in Section 3.6.4. Likewise, the rate of change of the commanded target is limited to the predetermined maximum value. These restrictions prevent the control system from commanding joint positions or movements outside the configured operating limits.

Joint-position sensing is also used to determine if the actuator is moving as it should. While the motor is operating, the controller monitors the position that should have been reached based on the number of STEP pulses ordered for the motor. The estimated joint position is represented by θ_{step} and corresponds to the position that would be reached if all of the commanded motor steps had been successfully executed.

At the same time, the encoder gives an independent reading of the joint position, θ_{meas}, as explained in Section 3.4. By comparing these two values, the controller can detect cases in which the actual movement of the actuator no longer matches the commanded motion, for instance, if the motor loses steps. The resulting monitoring error is defined as

$$e_{\text{step}} = \theta_{\text{step}} - \theta_{\text{meas}}, \tag{3.18}$$

where θ_{step} is the joint position estimated from the commanded motor steps and θ_{meas} is the joint position obtained from the encoder. When the two positions stay approximately the same, it is concluded that the motor is following the commanded movement. If the difference increases, the commanded and measured motions are no longer in agreement.

A tracking fault occurs when the magnitude of e_{step} consistently stays above a predefined threshold. It is necessary for this condition to continue for a certain period of time so that short, temporary differences are not wrongly taken to indicate faults. The encoder is also kept under observation, and if valid position information consistently has not been received, an encoder fault is generated. Both of these conditions are regarded as system errors and result in the normal operation of the actuator being prevented.

During active-assisted rehabilitation, the interaction between the sensing and actuation controllers is also supervised. As explained in Section 3.6.5, when valid movement data are not

received within the communication timeout, the system goes into a communication-loss state and normal active-assisted movement is stopped. An emergency-stop condition is additionally available to immediately prevent further actuator operation when required.

The main software safety mechanisms and their corresponding system responses are summarised in Table 3.17.

Table 3.17: Implemented software safety mechanisms.

Safety mechanism	**Monitored condition**	**Safety response**	**System action**
Joint-position limits	Angular target outside the permitted joint range.	Target limited to the allowed range.	–
Command-speed limit	Rate of change of the commanded target above the predefined maximum value.	Target motion limited to the allowed speed.	–
Tracking monitoring	$\lvert e_{\text{step}} \rvert$ remains above the permitted threshold.	Tracking fault generated.	Operation is interrupted.
Encoder monitoring	Valid encoder data are not received.	Encoder fault generated.	Operation is interrupted.
Communication monitoring	Valid UART movement messages are not received during active-assisted operation.	Communication-loss condition activated.	Movement is stopped; after communication is restored, a new start command is required.
Emergency stop	Emergency-stop condition is activated.	Emergency-stop state activated.	Motor operation is disabled.

These conditions are coordinated by the system state machine. The main operating states are system startup, idle operation and active movement, as well as special states corresponding to communication loss, emergency stop and system errors. Based on the current state, the controller determines whether movement generation is permitted, whether the current position should be maintained, and whether the motor drivers may remain enabled. In fault or emergency conditions, normal actuator commands are therefore prevented from reaching the motors.

Before operation can resume after a fault, the corresponding abnormal condition has to be cleared and the system must be reset. During this process, the encoder measurement is verified and the internal motor-position estimate can be synchronised again with the measured joint position before normal control is re-enabled.

3.8 Desktop Application

A desktop application was created as a central interface for configuring, operating and monitoring the rehabilitation system. The application communicates with the sensing Arduino through the

USB serial connection. Commands intended for the actuation controller are subsequently transferred through the UART communication architecture described in Section 3.6.5. In this way, the application provides a clearer and more practical interface for interacting with the system, allowing the main functions to be accessed and monitored without requiring direct interaction with the Arduino controllers.

The system's operation is divided among six primary pages: Overview, Patient, Calibration, Rehabilitation, Settings and Advanced. The Overview page functions as the main operating interface and includes the controls needed to start, pause, resume or end a rehabilitation session. It also shows the current state of the system, the selected rehabilitation configuration and the real-time data from the three robotic joints. The Overview page is shown in Figure 3.24.

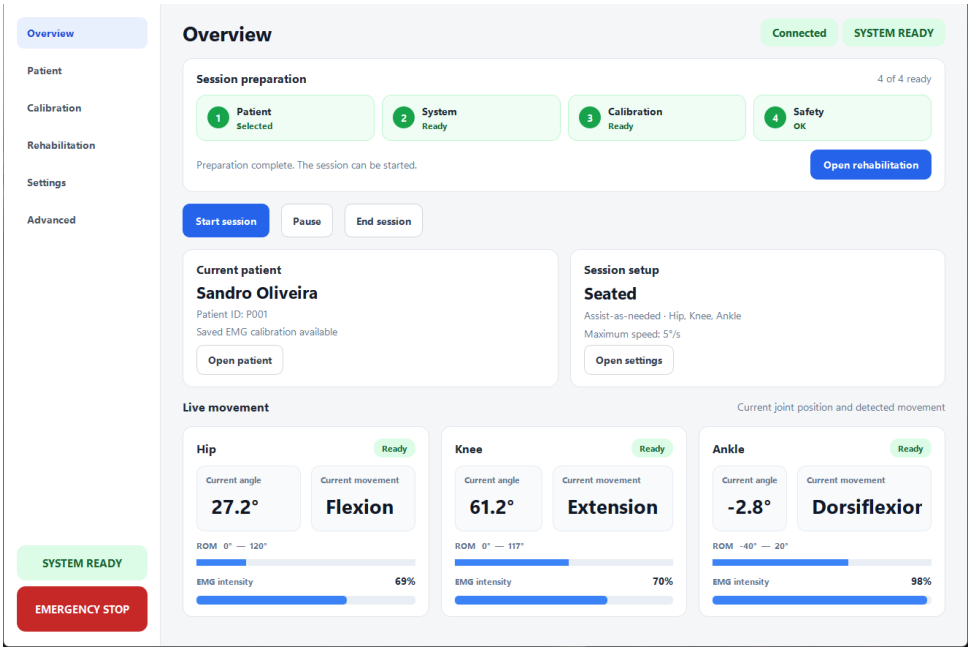


Figure 3.24: Overview page of the desktop application.

The Patient page enables patient profiles to be created or loaded and associates the relevant EMG calibration data to each profile. As the application was developed for experimental use within the scope of the present prototype, patient information is stored locally, and the application is not connected to an external database. The Patient page is shown in Figure 3.25.

The Calibration page guides the user through the calibration procedure for the six EMG channels. Calibration can be performed before a new session, or previously stored values associated with the selected patient can be reused. This means that there is no need to go through the full calibration procedure again if the earlier obtained values are still applicable. Furthermore, the page gives a visual indication of the progress being made during the calibration sequence, as illustrated in Figure 3.26.

The Rehabilitation page is used to select and configure the operating mode of the system. When using active-assisted rehabilitation, one or more of the hip, knee and ankle joints can be selected, as described in Section 3.6. In passive rehabilitation, a single joint is selected for each

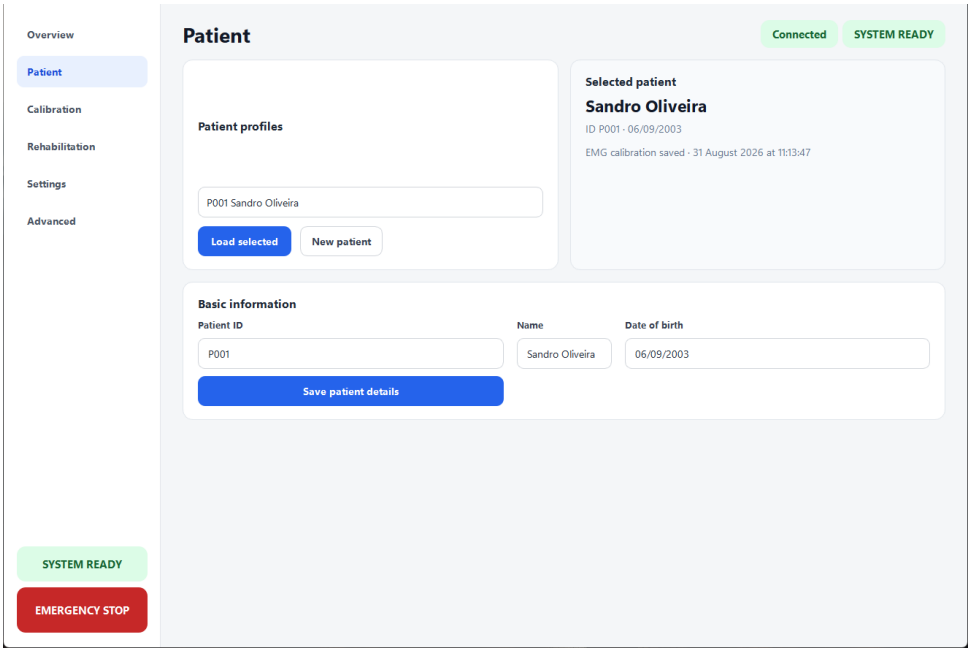


Figure 3.25: Patient-management page of the desktop application.

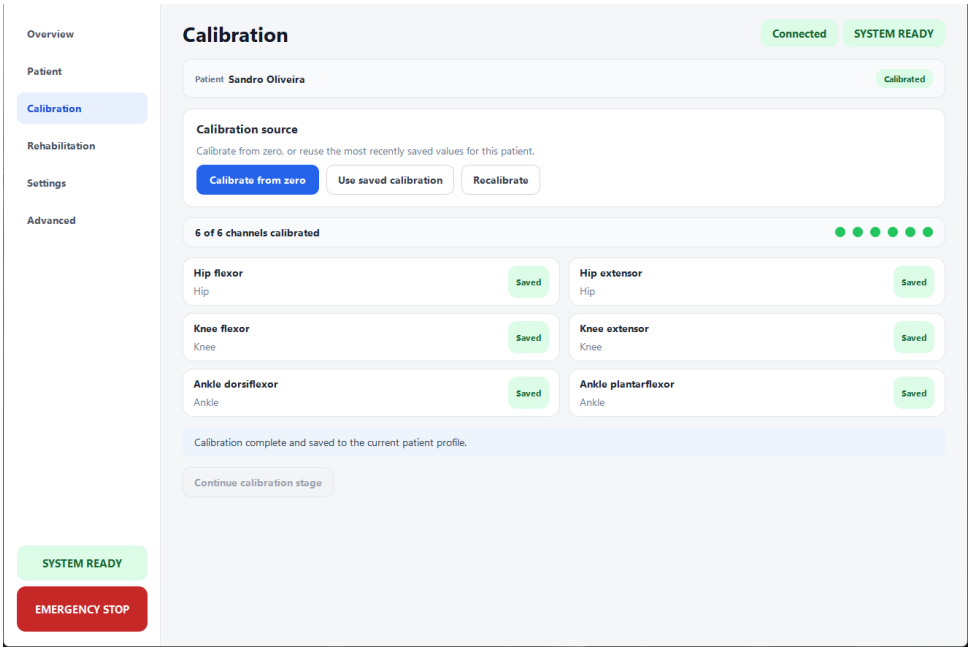


Figure 3.26: EMG calibration page of the desktop application.

rehabilitation sequence, with its movement interval, speed and number of repetitions defined before the exercise begins. The two rehabilitation modes available through the application are shown in Figure 3.27.

The Settings page has the general rehabilitation configuration parameters, enabling the user to choose between a seated or supine position and providing the joint ROM limits and the maximum system speed employed during operation. These settings are transmitted to the embedded control system so that the configuration used by the application remains consistent with the limits applied by the actuation controller. The Settings page is shown in Figure 3.28.

The Advanced page was included mainly for development, testing and diagnostic purposes. It provides access to lower-level communication and system information that is not required during normal rehabilitation operation. The Advanced page is shown in Figure 3.29.

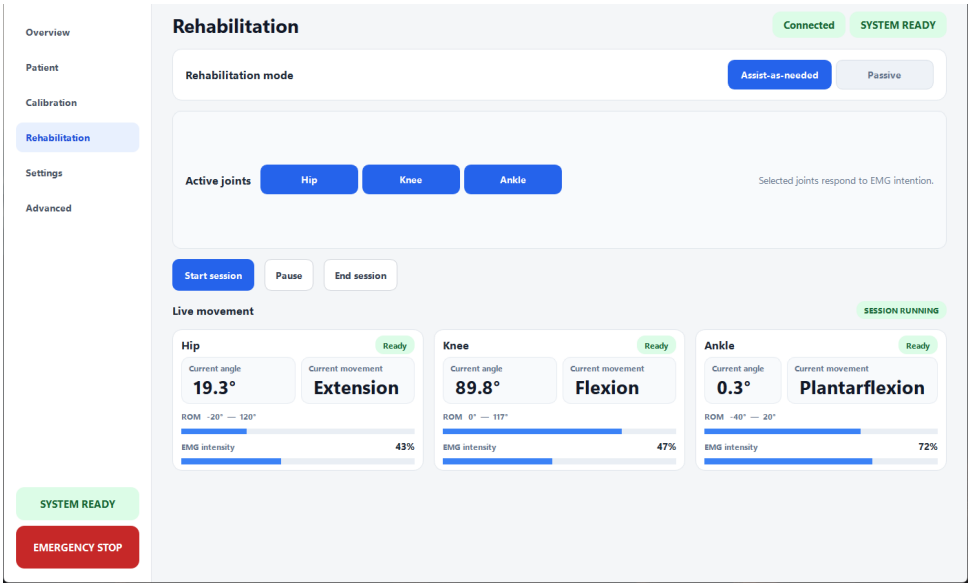
The application also implements several checks before a rehabilitation session can be started. Communication with the embedded system must be available, and the selected rehabilitation parameters must satisfy the configured limits. A valid EMG calibration is additionally required when active-assisted rehabilitation is selected, whereas passive rehabilitation can be started without EMG calibration. A session will not be allowed to start if an emergency-stop, communication-loss or system-fault condition is in effect. When a session is in progress, the important configuration parameters are locked in order to prevent accidental changes, although the session can still be paused, resumed or terminated.

During operation, the application continuously receives system information and updates the displayed joint and session status. If communication is lost or a safety condition is reported by the embedded controller, the active rehabilitation session is interrupted. At the end of the session, the application stores the main session information, including the selected rehabilitation mode and configuration, active joints, session duration and any warnings or faults reported during operation.

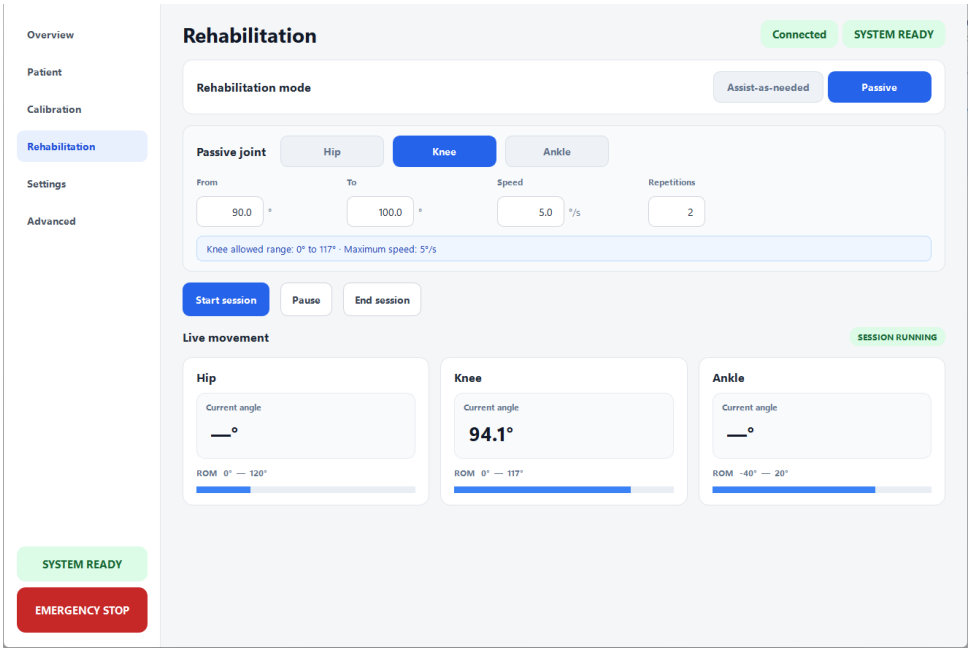
3.9 Final System Integration

After the individual subsystems had been developed, they were put together to form the complete robotic lower-limb rehabilitation support system. The final prototype includes the following main elements:

- an adjustable mechanical structure for the thigh and shank, together with the foot platform and the corresponding human-robot interfaces;
- three motor assemblies connected to the hip, knee and ankle joints;
- three joint-position encoders mounted at the rear of the actuators;
- six EMG sensors used to determine movement intention and intensity for the three robotic joints;
- two Arduino UNO boards, with separate sensing and actuation functions connected through UART communication;



(a) Active-assisted rehabilitation.



(b) Passive rehabilitation.

Figure 3.27: Configuration of the active-assisted and passive rehabilitation modes through the desktop application.

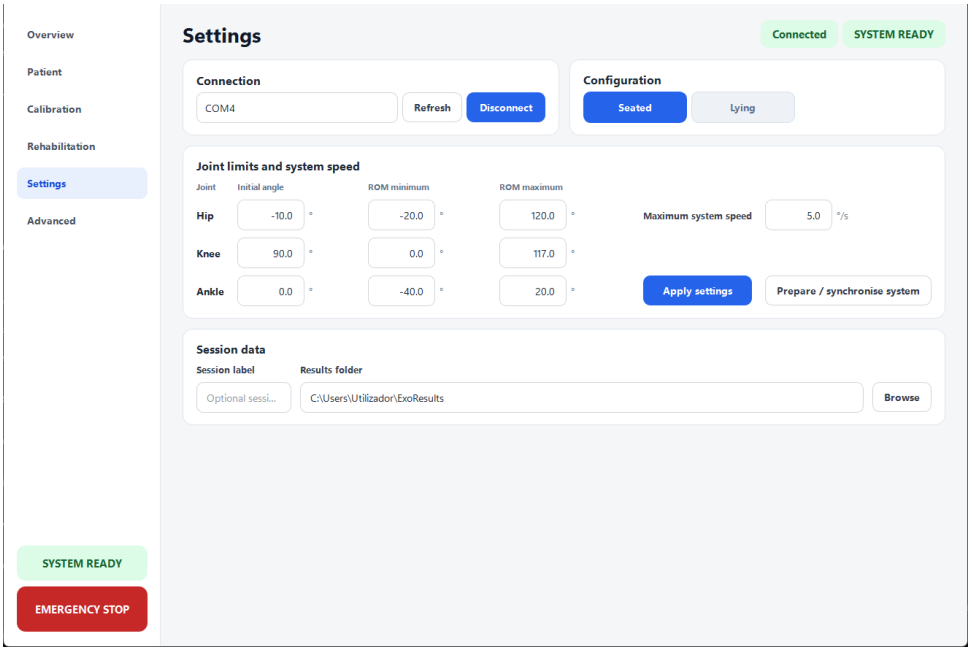


Figure 3.28: System-settings page of the desktop application.

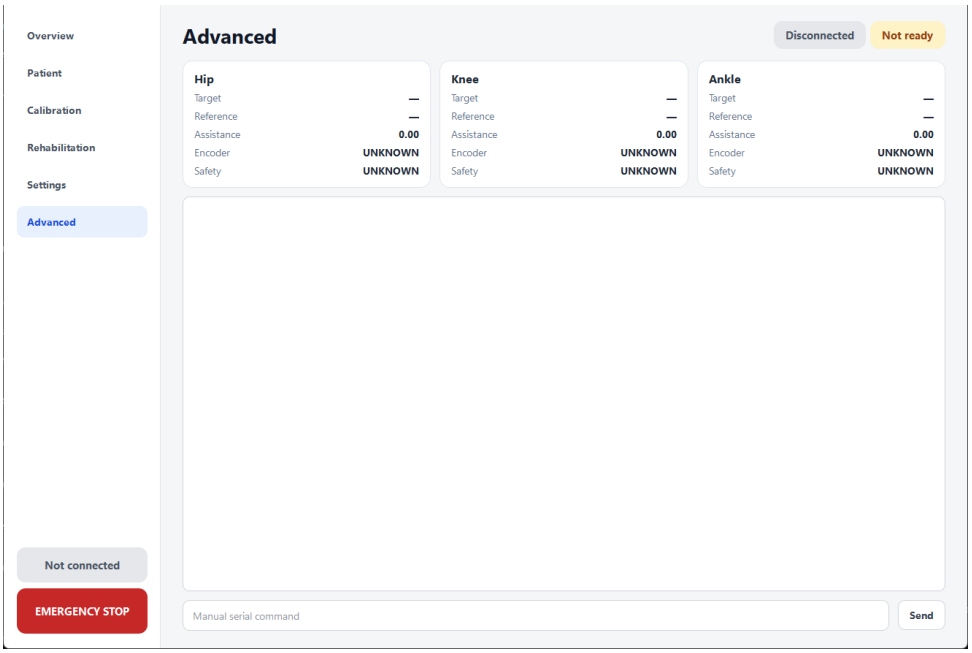


Figure 3.29: Advanced diagnostic page of the desktop application.

- the high-level, mid-level, and low-level control functions, including the passive and active-assisted rehabilitation modes, together with the implemented software safety mechanisms.
- a desktop application for EMG calibration, rehabilitation configuration, session control and system monitoring;

The complete information and actuation flow depends on the selected rehabilitation mode. During active-assisted rehabilitation, it can be represented as

$$\text{EMG} \rightarrow \text{movement intention and intensity} \rightarrow \text{reference generation} \rightarrow \text{AAN control} \rightarrow \text{safety} \rightarrow \text{motor command}$$

During passive rehabilitation, the corresponding flow is

$$\text{exercise configuration} \rightarrow \text{passive trajectory generation} \rightarrow \text{safety} \rightarrow \text{motor command}$$

To further characterise the final prototype, the mass of the main components associated with the moving part of the system was determined. The stationary support structure for the hip actuator assembly, as well as the components mounted on this stationary part, were not taken into account in the mass assessment since these elements are supported independently and do not add to the mass that is carried by the user's lower limb during rehabilitation. The relevant values are given in Table 3.18.

The cost of the main components used in the final prototype was also determined. The resulting values are presented in Table 3.19.

Mass and cost were considered throughout the development of the prototype and were reduced whenever possible while maintaining the required mechanical, sensing, actuation and control functions. The reported values therefore reflect the trade-off between limiting the physical and financial requirements of the system and maintaining the functionality needed for the intended rehabilitation tasks.

3.10 Summary

This chapter outlined the development and implementation of the robotic lower-limb rehabilitation support system. The mechanical structure was designed for a single lower limb and included three actuated joints at the hip, knee and ankle. Adjustable thigh and shank sections were introduced to accommodate the chosen anthropometric range. Fixed-axis joints and direct actuator coupling were adopted for the mechanical structure, while adjustable straps provided the physical interface between the system and the user's lower limb. The actuator assemblies were selected based on the estimated joint torque requirements and were then checked after taking into account the masses of the robotic components.

The system used magnetic absolute encoders mounted at the rear of the actuators to achieve independent sensing of joint position, with the measured motor rotation being converted into the

Table 3.18: Mass of the main components associated with the moving part of the final prototype.

Component	Mass (kg)
Motor-gearbox assemblies	
Knee motor-gearbox assembly	1.700
Ankle motor-gearbox assembly	0.680
Structural components	
Thigh structural plates	0.300
Shank structural plates	0.300
Foot platform	0.400
Supports	
Knee motor support	0.170
Knee encoder support	0.140
Ankle motor-encoder support	0.047
Motor drivers	
Knee motor driver	0.390
Ankle motor driver	0.003
Joint-position encoders	
Knee encoder	0.002
Ankle encoder	0.002
EMG sensing components	
6x MyoWare 2.0 sensors	0.066
Arduino Shield	0.102
6x Link Shields	0.036
Straps	0.029
Total	**4.367**

Table 3.19: Cost of the main components used in the final prototype.

Component	Quantity	Cost (€)
Hip motor-gearbox assembly	1	124.17
Knee motor-gearbox assembly	1	60.08
Ankle motor-gearbox assembly	1	30.87
Motor drivers	3	67.25
Joint-position encoders	3	49.83
MyoWare 2.0 sensors	6	226.26
Arduino Shields	1	11.85
Link Shields	6	54.00
Mechanical structure and supports	–	50.43
Straps	7	10.98
Total		**685.72**

corresponding joint position. The user's intention to move was derived from six EMG channels that were linked to the opposing muscle pairs at the three joints. After calibration and normalisation, the muscle activations were used to classify the flexion, extension and relaxed states, as well as to determine the corresponding level of movement intensity.

The control system was organised into high-level, mid-level and low-level functions which were distributed across two separate Arduino UNO boards responsible for sensing and actuation. Two rehabilitation operating modes were implemented. During passive rehabilitation, a selected joint followed a configurable cyclic trajectory defined by predefined angular limits, movement speed, number of repetitions and pause durations. During active-assisted rehabilitation, an angular reference was generated from the user's movement intention and intensity, and the AAN controller determined the degree of robotic assistance by combining EMG information with joint-position feedback. In both modes, the resulting angular command was converted into stepper-motor commands after the corresponding safety checks. Further software safety mechanisms were implemented to monitor joint and speed limits, actuator tracking, encoder operation, communication between the controllers, and emergency-stop situations. Finally, the mechanical, sensing, actuation and control subsystems were integrated into the complete prototype. The main components associated with the moving part of the system had a combined mass of 4.367 kg, while the main components included in the cost assessment had a combined cost of 685.72 €.

Chapter 4

Experimental Validation and Results

4.1 Validation Methodology

The experimental validation was organised to evaluate the main functions of the robotic lower-limb rehabilitation support system. The validation was carried out progressively, starting with the evaluation of each individual subsystem before moving to combined system testing. The validation covered the mechanical structure, the operation of the actuators, joint-position sensing, movement-intention detection, the control system and the implemented safety features.

For the integrated actuation tests, the robotic structure was first evaluated under unloaded conditions, without the user's lower limb mechanically coupled to the prototype. During active-assisted rehabilitation tests at this stage, the operator remained beside the system and performed the voluntary muscle contractions required to generate the EMG inputs, while the resulting commands produced movement of the unloaded robotic joints. A subsequent loaded evaluation was then initiated with the user's lower limb mechanically coupled to the prototype.

The purpose of this validation was to check the functional operation of the developed proof-of-concept prototype, rather than to assess its clinical effectiveness as a rehabilitation device. The tests were therefore concerned with determining whether the implemented functions behaved as expected and whether they could operate together as a complete system.

All experimental evaluations involving the user were performed with a healthy operator. No participants with motor impairments were included in the present validation.

4.2 Mechanical and Functional Validation

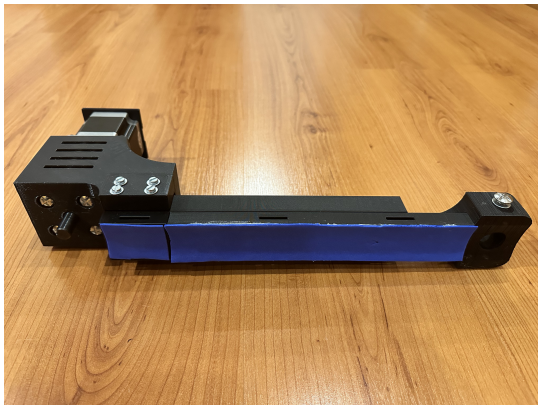
The mechanical and functional testing was carried out to assess the physical behaviour of the prototype and to verify whether the mechanical features worked as intended. The evaluation focused on the anthropometric adjustment of the thigh and shank sections, the ROM that could be achieved by the robotic joints, and the mechanical stability of the assembled structure.

4.2.1 Anthropometric Adjustment

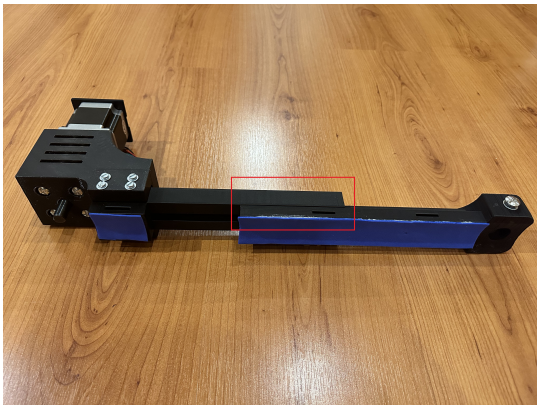
The anthropometric adjustment of the thigh and shank sections was evaluated by measuring the minimum and maximum lengths physically achieved by the prototype. These lengths were defined as the distances between the rotation axes of the adjacent robotic joints, as specified in Section 3.2.2.

For each section, the guide and sliding plates were first placed at the minimum allowable length and secured with the bolt-and-nut locking mechanism. The distance between the relevant joint axes was then measured using a tape measure graduated in millimetres. The procedure was repeated with the section adjusted to its maximum length, accounting for the required 100 mm overlap mentioned in Section 3.2.2. Each measurement was taken three times and the mean value was used for comparison with the corresponding design value.

The minimum and maximum configurations of the thigh section used during the evaluation are shown in Figure 4.1 as a representative example. The same adjustment procedure was applied to the shank section. The results are presented in Table 4.1.



(a) Minimum thigh configuration.



(b) Maximum thigh configuration. The red rectangle denotes the 100 mm overlap between plates.

Figure 4.1: Minimum and maximum adjustment configurations of the thigh section.

Table 4.1: Designed and measured adjustment dimensions of the thigh and shank sections.

Segment	**Position**	**Design**	**M1**	**M2**	**M3**	**Mean**	**Error**
Thigh	Minimum	349.25	350	349	350	349.67	0.42
	Maximum	438	437	437	436	436.67	-1.33
Shank	Minimum	367	366	367	367	366.67	-0.33
	Maximum	446	445	444	444	444.33	-1.67

All dimensions and errors are expressed in mm.

In addition to the dimensional measurements, the locking mechanism was examined at both the minimum and maximum configurations and at an intermediate point within the adjustment range. After the bolts had been tightened, a longitudinal force was manually applied to see whether any

visible slipping happened. During the manual assessment, the locking mechanism stayed stable and no noticeable longitudinal slipping of the guide and sliding plates was seen in any of the configurations.

The measured adjustment dimensions agreed well with the relevant design values for both structural sections. In the case of the maximum configurations, slightly greater errors were observed, since the measurement method also had to take into account the 100 mm overlap between the plates, adding another source of measurement uncertainty. Even so, the deviations were still small, the maximum absolute error being 1.67 mm, which indicates that the physical prototype reproduced the intended adjustment dimensions without compromising the necessary anthropometric range. The remaining differences are attributed to minor dimensional variations caused during the 3D printing process.

4.2.2 Joint Range of Motion

The hip, knee and ankle joint movements were assessed using the final mechanical assembly in SolidWorks, with the aim of determining whether the joint geometry allowed the required angular positions to be reached and of identifying possible mechanical limitations on the system's movement.

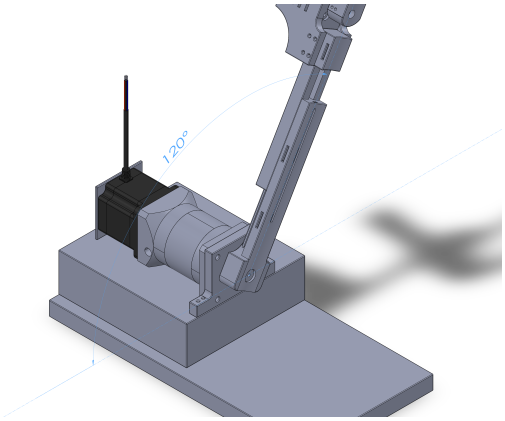
The hip was treated differently due to the intended operating positions of the system. In both seated and lying configurations, the posterior part of the thigh is supported by the surrounding surface, making substantial hip extension beyond the neutral position irrelevant for the intended rehabilitation tasks. Even so, deformation of the soft tissues between the limb and the supporting surfaces can still allow negative hip angles to occur. Nevertheless, the main rehabilitation workspace remains concentrated on the positive side of the hip ROM.

The SolidWorks configurations used to obtain the angular measurements for the three joints are shown in Figure 4.2, illustrating the reference lines and angular definitions used during the evaluation.

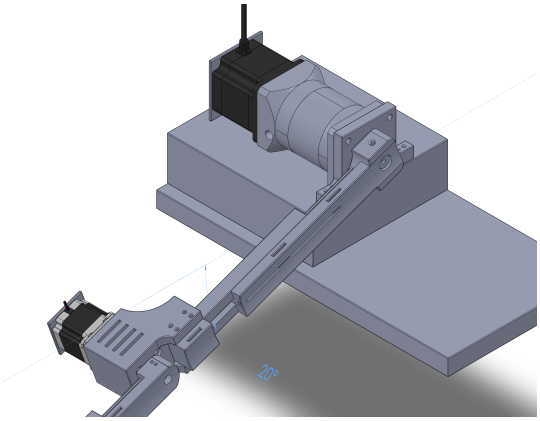
The angular limits obtained are summarised in Table 4.2. Even though SolidWorks shows the magnitude of the measured angle, the signs listed in the table are in accordance with the joint angle convention used throughout this work.

Table 4.2: Comparison between the designed and practical ROM values.

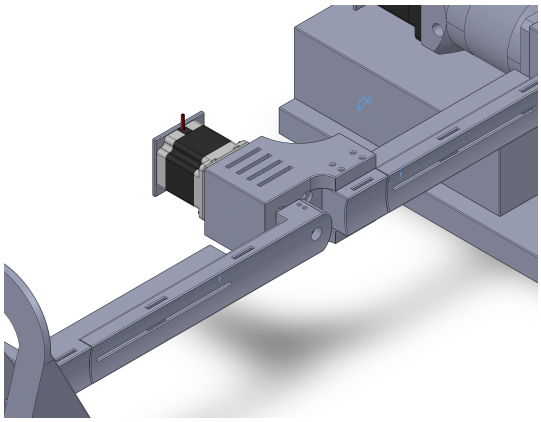
Joint	Movement	Design	SolidWorks	Error
Hip	Extension	-30°	-20°	10°
	Flexion	120°	120°	0°
Knee	Extension	0°	0°	0°
	Flexion	150°	117°	-33°
Ankle	Plantarflexion	-40°	-40°	0°
	Dorsiflexion	20°	20°	0°



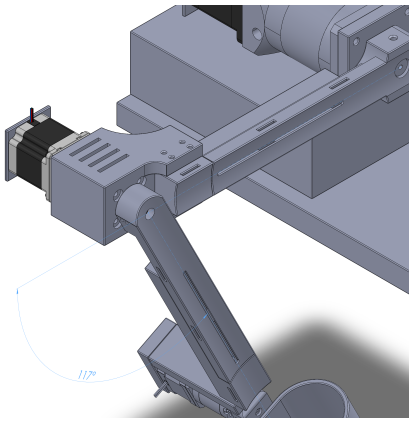
(a) Hip flexion.



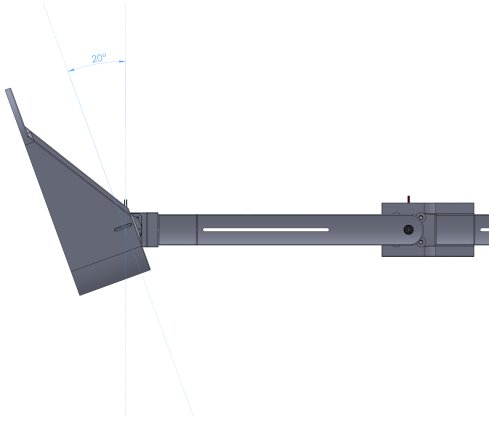
(b) Hip extension.



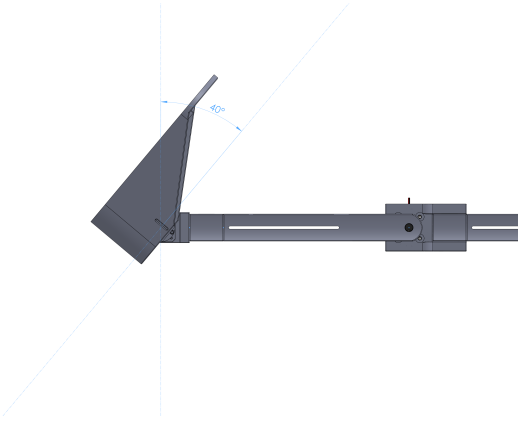
(c) Knee extension.



(d) Knee flexion.



(e) Ankle plantarflexion.



(f) Ankle dorsiflexion.

Figure 4.2: SolidWorks configurations showing the reference geometry and angular measurements used to evaluate the joint ROM limits.

The geometric evaluation showed that the intended angular positions were achieved at the ankle, for hip flexion and for knee extension. Hip extension was limited to approximately $-20°$, rather than the $-30°$ considered during the design stage. However, this limitation does not significantly affect the intended use of the system. Since hip extension beyond the neutral position is not a primary rehabilitation movement in the seated and lying configurations, the available range still allows the user's lower limb to assume a comfortable position while supported by the system. The hip joint was therefore considered to fulfil the functional requirements defined for the prototype.

The main limitation was found in knee flexion. The maximum flexion was $33°$ below the design value, showing that the present mechanical arrangement restricts the joint before the intended maximum flexion is achieved. Even so, the joint still allows a large flexion movement, which may be sufficient for the seated and lying rehabilitation exercises considered in this work.

Apart from the angular measurements, both the SolidWorks assembly and the physical prototype were examined throughout the movement of each joint to identify possible collisions or mechanical obstructions involving the structural components, actuator supports and other parts of the system. No additional interference or obstruction was observed during this assessment.

4.2.3 Structural and Assembly Assessment

A qualitative evaluation of the assembled prototype was conducted in order to investigate the stability and practical behaviour of its main mechanical parts. This assessment looked at the structural connections, the adjustable sections, the printed components, the actuator supports and the human-robot interfaces, while the dimensional adjustment and the joint ROM were examined separately in Sections 4.2.1 and 4.2.2.

The structure remained stable during handling and during the actuator tests performed with the mechanical plates coupled to the corresponding actuators and moved through their intended joint motion. No unintended relative movement of the various components was observed. Particular attention was given to the connection between the guide and sliding plates of the thigh and shank sections. In the final configuration, the clearance between the matching profiles was small enough to prevent noticeable lateral movement of the plates without preventing them from sliding relative to one another during adjustment. A small amount of mechanical backlash was observed only at the connection between the knee actuator shaft and the corresponding structural plate. No comparable backlash was observed at the hip or ankle connections.

The bolted connections stayed secure throughout the evaluation, with no signs of loosening or need for retightening. During these evaluations, the final 3D-printed components also exhibited no visible cracking, permanent deformation or structural failure. The actuator supports remained stable under the weight of the respective motor and gearbox assemblies, with no noticeable deformation.

As explained in Section 3.2.4, the contact surfaces of the thigh and shank guide and sliding plates were covered with EVA foam, which provided a softer interface between the rigid PLA components and the user's limb. In order to evaluate the physical interface, the lower limb was briefly placed and secured into the system. During this assessment, the Velcro straps could be

positioned and tightened without difficulty and stayed firmly in place, while the EVA padding ensured a softer contact between the limb and the structure. No discomfort was noticed during this evaluation. However, since the periods of use were relatively short, these observations cannot be extrapolated to prolonged use and do not constitute an assessment of long-term comfort.

Overall, the final mechanical assembly provided sufficient stability and rigidity under the conditions considered at this stage of the validation. Nevertheless, this assessment was qualitative and did not include structural load or fatigue testing, and therefore does not constitute a quantitative validation of the mechanical strength of the system.

4.3 Actuation and Joint-Position Validation

The actuation and joint-position sensing subsystems were tested in order to check the movement of the actuators and the accuracy of the measured joint positions. The tests included actuator movement, encoder operation and position tracking.

4.3.1 Actuator Movement Tests

The aim of these tests was to visually check whether each actuator was able to execute predetermined angular displacements repeatedly in a consistent way. For this reason, the same reference positions were applied to the hip, knee and ankle actuators. Since this was an isolated actuator test, the mechanical limitations and the joint ROM of the final assembled system were not taken into account.

Each test started from 0°. The actuator was first ordered to move in the positive direction to 45° and then to 90°, before returning progressively to its starting position, after which the same procedure was repeated in the negative direction. The entire movement pattern was repeated ten times for each actuator. These reference positions were selected because they provided simple and easily identifiable angular positions, which made it easier to visually confirm the actuator's motion during the tests.

During the tests, the movement of each actuator was monitored in order to detect any possible irregular motion, excessive vibration, or changes in behaviour between successive cycles. The observations obtained for each actuator were recorded and are summarised in Table 4.3.

Table 4.3: Summary of the actuator movement tests.

Joint	Tested positions	Main observation
Hip	0°, $\pm45^\circ$, $\pm90^\circ$	Commanded positions reached; smooth and consistent movement
Knee	0°, $\pm45^\circ$, $\pm90^\circ$	Commanded positions reached; smooth and consistent movement
Ankle	0°, $\pm45^\circ$, $\pm90^\circ$	Commanded positions reached; smooth and consistent movement

All three actuators completed the 10 movement cycles and reached the commanded positions consistently, with no degradation in their behaviour. During operation, all three motors produced the normal mechanical noise associated with their movement. No unusual sounds or changes in

actuator behaviour were observed, and the movement remained smooth and consistent throughout the tests.

4.3.2 Encoder Operation

The encoder-processing chain was evaluated to verify the acquisition of angular measurements and rotation unwrapping.

To evaluate the rotation-unwrapping function, the knee actuator was used as a representative case. The corresponding hip and ankle results are provided in Appendix C, Section C.1. The actuator was rotated through multiple full motor revolutions in both the positive and negative directions. The angle directly obtained from the encoder readings and the accumulated motor angle were recorded at the same time, enabling a comparison of the two signals. Particular attention was given to transitions across the $0^\circ/360^\circ$ boundary, since at these points the single-turn measurement goes back to the start of its range. The accumulated angle was checked to see if the motor rotation stayed continuous through these transitions, without showing any abnormal jumps. The results are presented in Figure 4.3.

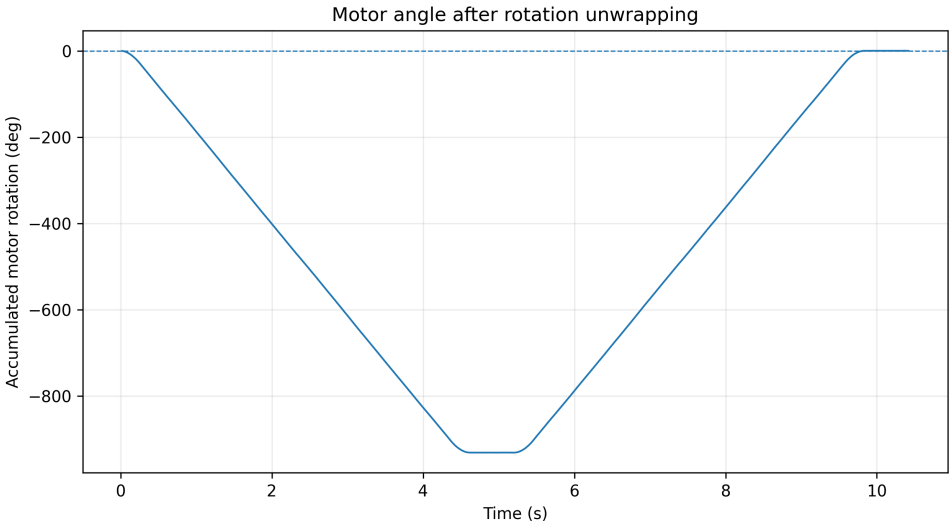
The main quantitative results obtained for the three actuator assemblies are summarised in Table 4.4.

Table 4.4: Results of the encoder rotation-unwrapping tests.

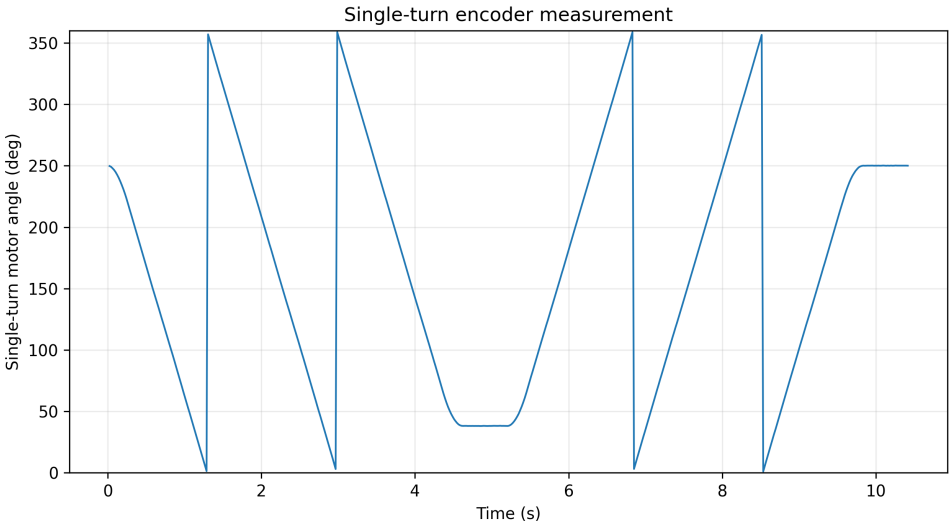
Joint	**Wraps out/return**	**Closure error** (°)	**Joint-equivalent error** (°)
Hip	3/3	0.483	0.0097
Knee	2/2	0.286	0.0061
Ankle	3/3	0.198	0.0099

From Figure 4.3, it is possible to see that the single-turn measurement showed the expected transitions between values near 360° and 0° each time a full revolution of the motor was completed. On the other hand, the accumulated motor angle stayed continuous during these transitions in either direction, which showed that the unwrapping process correctly preserved the successive motor revolutions. The span of the accumulated motor angle was approximately 932.12°, as compared with the theoretical value of 933.12° corresponding to a 20° displacement of the knee joint and the corresponding gearbox ratio. The difference between these values was therefore approximately 1.00° at the motor shaft, corresponding to approximately 0.02° when expressed at the joint. The quantitative results in Table 4.4 also show a final closure error of 0.286° at the motor shaft for the knee, corresponding to approximately 0.0061° at the joint.

Similarly, small closure errors were obtained for the hip and ankle actuators. As shown in Table 4.4, the final motor-angle closure errors were 0.483°, 0.286° and 0.198° for the hip, knee and ankle, respectively. When expressed at the corresponding robotic joints, all three errors were below 0.01°. No discontinuities associated with the encoder wrap-around were observed.



(a) Accumulated motor angle after unwrapping.



(b) Single-turn motor angle.

Figure 4.3: Evaluation of the rotation-unwrapping function using the knee actuator.

During the tests, no invalid encoder measurements, communication faults or diagnostic faults were observed, and the encoder health status remained *OK*.

4.3.3 Joint-Position Tracking

The agreement between the step-based and encoder-derived joint positions was determined by comparing the joint position commanded from the motor steps with the position obtained from the corresponding encoder. The encoder readings were converted into joint angle by accounting for the gearbox ratio, in order for both position estimates to be given in the same reference frame.

All three actuator assemblies were evaluated using the same procedures. For conciseness, the figures presented in this subsection show the knee results as a representative example, while the corresponding hip and ankle plots are provided in Appendix C, Section C.2.

The evaluation was divided into three tests. The first was a multi-position tracking test designed to examine the agreement between the positions calculated from the motor steps and those derived from the encoder at various commanded angles. For the hip and knee, beginning at 0°, the actuator was moved progressively through several intermediate positions up to 45° and was then returned to the starting position through the same intermediate angles. For the ankle, positions between -20° and $+20^\circ$ were used. The maximum difference between the step-based and encoder-derived positions and the final error after returning to 0° were used to characterise the tracking performance. The results obtained from the multi-position tests are summarised in Table 4.5, while the corresponding knee tracking trajectories are shown in Figure 4.4.

Table 4.5: Results of the multi-position joint tracking tests.

Joint	Max. error (°)	Final error (°)
Hip	0.015	-0.001
Knee	0.059	0.000
Ankle	0.091	0.016

A second test was conducted in order to assess repeatability when the same movements were performed multiple times. For the hip and knee, the two movement ranges taken into account were 0° to 20° and 0° to 45°. For the ankle, the corresponding ranges were 0° to $+20^\circ$ and 0° to -20°. For each of these ranges, five full cycles were carried out. The maximum tracking error, the remaining error after the final return to 0°, and the presence of progressive drift between the cycles were recorded. The results are given in Table 4.6. The errors recorded after each return to the initial position during the knee tests are shown in Figure 4.5.

The third test assessed the stability of the joint position calculated by the encoder when the actuator was not moving. Each actuator was kept at a fixed position, and its measured joint angle was recorded for 30 s without any movement. The range, meaning the difference between the maximum and minimum recorded values, and the standard deviation were used to describe the fluctuations in the measured position. The results are summarised in Table 4.7, while the stationary knee measurement is shown in Figure 4.6.

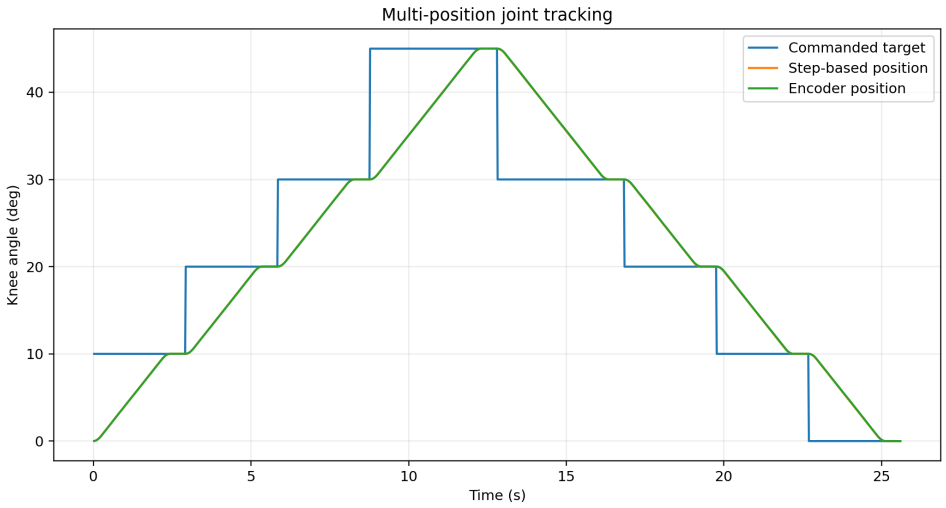
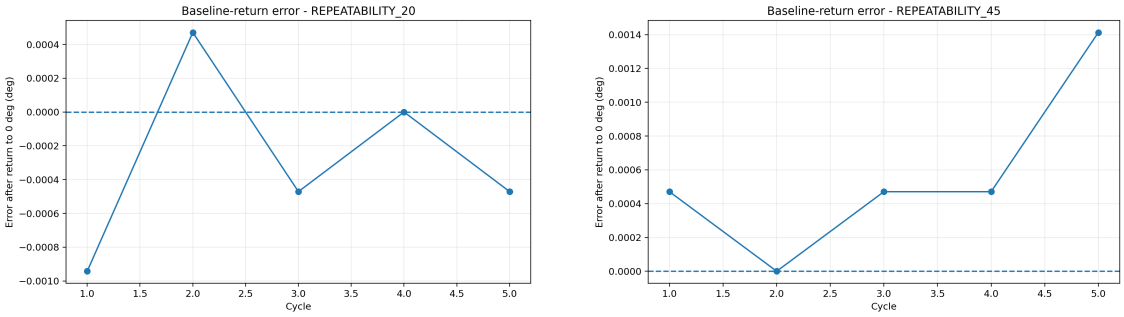


Figure 4.4: Step-based and encoder-derived knee joint positions during the multi-position tracking test.

Table 4.6: Results of the joint repeatability tests.

Joint	Range	Max. error (°)	Final error (°)	Drift (°/cycle)
Hip	0°–20°	0.016	-0.001	0.00000
	0°–45°	0.016	-0.000	0.00035
Knee	0°–20°	0.059	-0.000	0.00005
	0°–45°	0.059	0.001	0.00024
Ankle	0°–+20°	0.092	0.008	0.00055
	0°–−20°	0.093	0.014	-0.00011



(a) 0° - 20° movement range.

(b) 0° - 45° movement range.

Figure 4.5: Error after each return to the initial position during the knee joint repeatability tests.

Table 4.7: Stationary stability of the encoder joint-position measurements.

Joint	**Range (°)**	**Standard deviation (°)**
Hip	0.0040	0.0006
Knee	0.0047	0.0008
Ankle	0.0110	0.0018

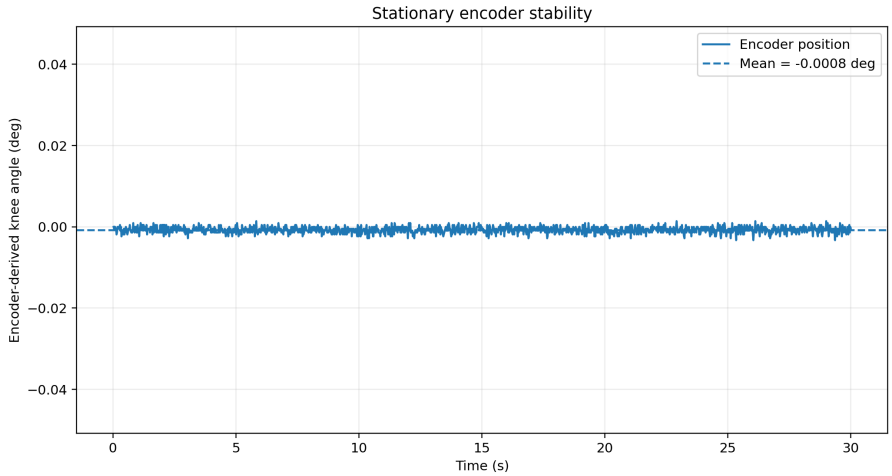


Figure 4.6: Stationary stability of the encoder-derived knee joint-position measurement.

The multi-position tracking test showed close agreement between the step-based and encoder-derived joint positions over the different commanded angles. For all three actuator assemblies, the maximum errors remained small, with the highest value being 0.091° for the ankle. The final errors after returning to 0° were also small, indicating that no relevant position offset had accumulated during the movement sequence. This behaviour was confirmed by the repeatability tests, in which the direction of movement was changed repeatedly. The maximum errors remained low and no progressive drift was observed, as also illustrated by the return errors in Figure 4.5.

The stationary test also showed only minor fluctuations in the joint positions. The measured ranges and standard deviations remained low for the hip, knee, and ankle, as indicated in Table 4.7. The greatest range observed was 0.0110°, and the highest standard deviation was 0.0018°. The small fluctuations observed for the knee can also be seen in Figure 4.6. These variations were small when compared to the angular movements considered in the tracking tests and indicate that the encoder-derived joint positions remained stable when the actuators were stationary.

Overall, the results show that the encoder system provided stable and consistent joint measurements during the performed tests. The encoder health status remained *OK* throughout all completed movements, with no diagnostic faults being detected.

4.4 EMG and Movement-Intention Validation

The EMG-based movement-intention processing was evaluated by considering the calibration and normalisation of the acquired signals, movement-state classification, and movement-intensity estimation. The validation procedure was applied independently to the muscle pairs associated with the three robotic joints. For conciseness, the knee muscle pair is used as a representative example throughout the following sections, while the corresponding additional joint-specific results are provided in Appendix C, Section C.3.

4.4.1 Calibration Evaluation

The calibration and normalisation procedure was examined using signals acquired during rest and during strong flexion and extension contractions. Figure 4.7 shows the acquired signals together with the corresponding calibration reference values.

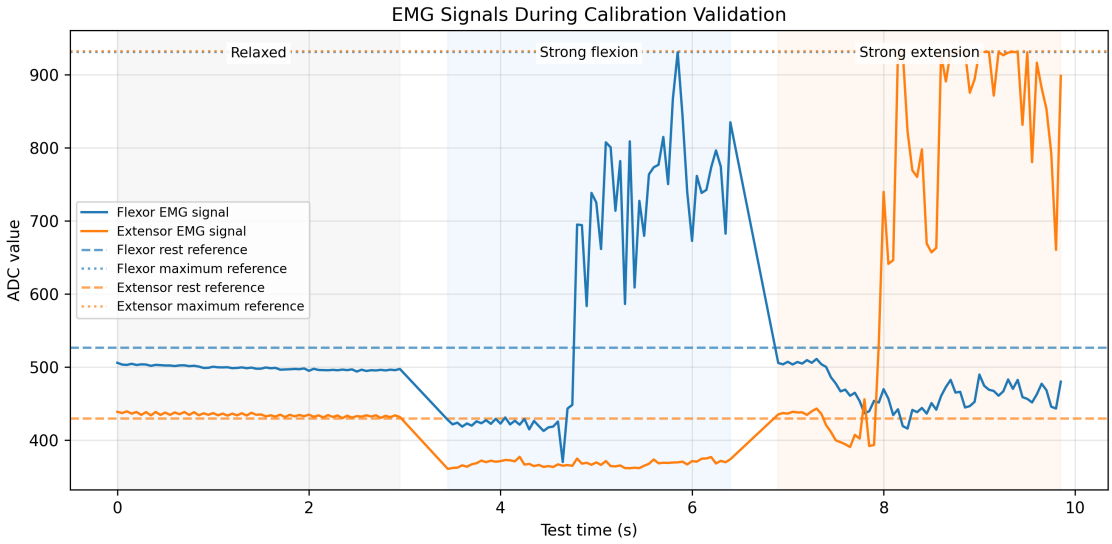


Figure 4.7: EMG signals and calibration reference values during rest, flexion and extension.

While in the relaxed state both EMG signals were near their respective resting values, upon a strong flexion contraction the flexor signal showed a clear rise whereas the extensor signal stayed comparatively low. During a strong extension the opposite behaviour was seen.

The corresponding normalised activation values are shown in Figure 4.8. When the muscles were relaxed, the activation level of both channels stayed near zero. In the case of strong flexion, the activation of the flexor muscles increased considerably and reached values close to 1, while the activation of the extensor muscles remained near zero. Conversely, during strong extension, the activation of the extensor muscles approached 1 while the flexor activation remained low.

These representative results show that the implemented calibration and normalisation procedure was successful, mapping the measured EMG signals to the normalised range from 0 to 1. Moreover, the activation of the muscle involved in the movement could be clearly seen as being different from that of the antagonist muscle, supplying the necessary input for the later calculation of net activation and for the detection of movement intention.

4.4.2 Movement-State Classification

The state classification was evaluated for the three movement states used in the final movement-intention detection: relaxed, flexion and extension. For each state, five trials were conducted, during which the instructed state was compared with the one detected by the algorithm.

Figure 4.9 compares the expected and detected movement states throughout the repeated trials.

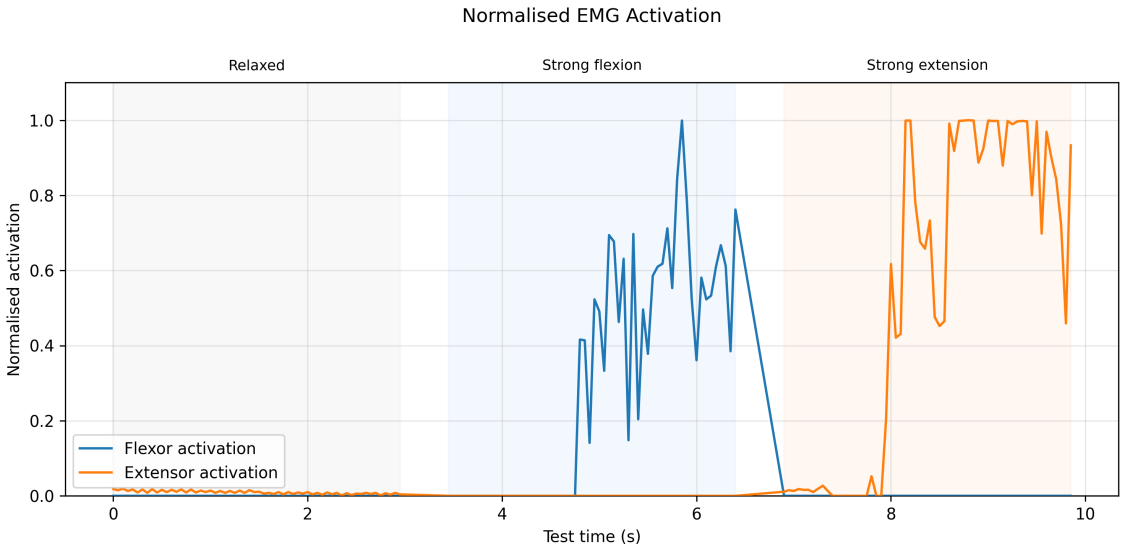


Figure 4.8: Normalised flexor and extensor EMG activation.

A short delay can be observed between the commanded state and the corresponding detected state. This delay is primarily due to the user's reaction time before initiating the requested contraction, rather than to the classification algorithm itself. That is why the classification performance was determined during the last second of each recording, when the desired movement state had already been achieved. The classification percentages obtained are given in Table 4.8.

Table 4.8: Classification performance for the tested movement states.

State	Correctly classified samples (%)
Relaxed	100.0
Flexion	97.1
Extension	100.0

For all the samples included in the analysis window, both the relaxed and extension states were correctly classified, whereas flexion achieved a classification rate of 97.1%. The slightly reduced value for flexion is consistent with the small spike returns to the relaxed state seen in Figure 4.9. These isolated spikes may be linked to temporary measurement disturbances or to brief fluctuations in the acquired EMG signal.

Overall, the results indicate that the implemented classification method was capable of consistently distinguishing between the relaxed, flexion and extension states under the conditions tested. There was no ongoing confusion between flexion and extension and the only classification differences were limited to brief transient events. The threshold and hysteresis used therefore supplied appropriate movement-state information for the following control stages.

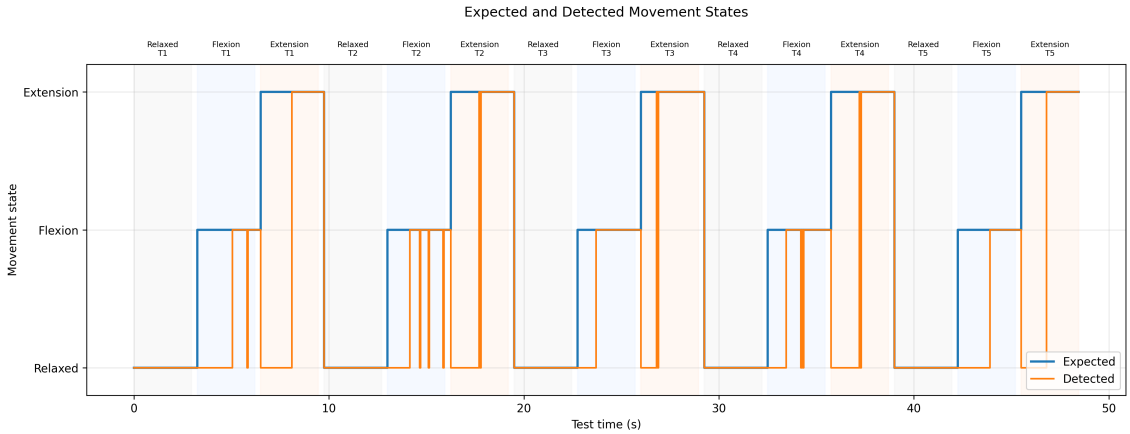


Figure 4.9: Comparison between instructed and detected movement states across repeated relaxed, flexion and extension trials.

4.4.3 Movement-Intensity Estimation

The movement-intensity variable was assessed during flexion and extension contractions performed at three voluntary levels: low, medium and high. Five repetitions were performed for each direction and intensity level, and for each repetition the maximum intensity reached during the contraction was recorded. The mean of the five maximum values obtained was used to represent each condition.

The resulting values are given in Figure 4.10. In the cases of both flexion and extension, the estimated intensity of the movement increased progressively from low to medium to high contraction levels. The high-intensity contractions reached the upper limit of the normalised range in both directions of movement.

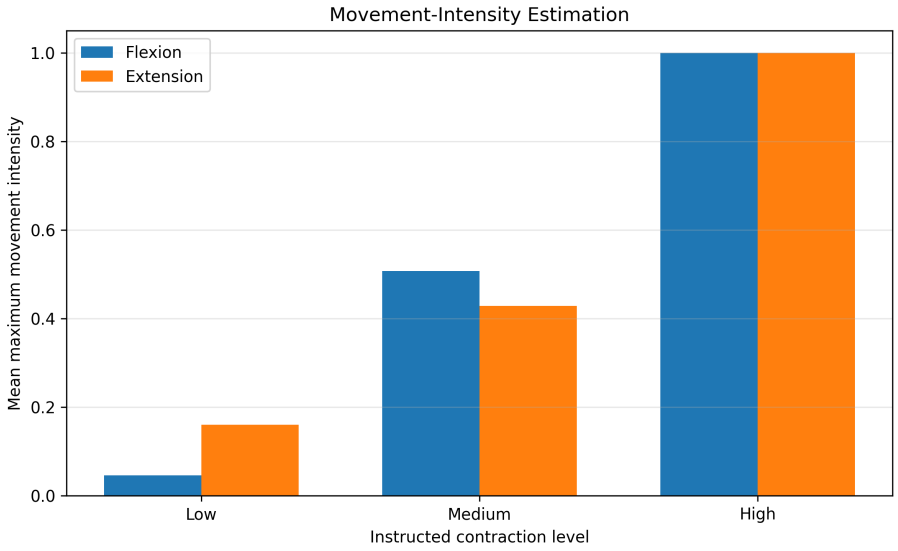


Figure 4.10: Mean maximum estimated movement intensity for low, medium and high voluntary flexion and extension efforts.

The differences observed between flexion and extension at the same instructed effort level are expected, since the movement-intensity variable is based on the normalised EMG response of each muscle and the user is not able to reproduce exactly the same voluntary effort from one contraction to another. There is therefore a natural variation between the two directions of movement. Nevertheless, the estimated intensity increased consistently as the instructed effort level increased, which shows that the method implemented was capable of detecting the relative changes in muscle activation.

One practical limitation was also observed during the EMG tests. For some movements, weaker voluntary contractions did not produce a relevant increase in the acquired EMG signal, whereas stronger contractions generated a clear and detectable response. This behaviour was already present at the signal-acquisition stage and was therefore not caused by the subsequent intention-detection algorithm. In practice, this means that strong muscle activation was sometimes required before a meaningful EMG response could be obtained from the sensor. This observation is particularly relevant because the present experiments were performed with a healthy operator. Since the tested movements required relatively little muscular effort for a healthy individual, performing them naturally did not always produce a sufficiently pronounced EMG response. During the tests, the operator therefore had to contract the corresponding muscles more strongly to obtain a clear signal.

Nevertheless, this limitation does not necessarily prevent the proposed approach from being applied to users with motor impairments. Surface EMG has been shown to detect muscle activity in individuals after stroke even when no corresponding activity is observable during clinical examination (Papazian et al. 2021). Lower-limb rehabilitation systems have also been developed in which EMG activity is used to contribute to the selection of robotic assistance in post-stroke users (Leerskov et al. 2024). In the present system, the calibration is performed individually for each muscle and user, meaning that the control method does not depend on reaching the same absolute EMG amplitude observed in a healthy individual. Instead, it requires voluntary muscle activity that can be reliably distinguished from the user's own resting condition. These findings support the potential applicability of the proposed approach to users with motor impairments, although this must still be confirmed experimentally in the target population.

4.5 Control-System Validation

The purpose of this section was to evaluate the implemented rehabilitation control functions under controlled conditions. The passive and active-assisted rehabilitation paths were assessed separately, according to the different ways in which they generate and process the movement reference.

The active-assisted control functions were evaluated using predefined inputs so that the reference-generation and AAN algorithms could be assessed independently under known conditions. Their operation with the physical encoder, actuator and EMG sensing chain is subsequently examined as part of the integrated system validation in Section 4.7.

4.5.1 Passive Rehabilitation

The passive rehabilitation mode was evaluated in order to determine if the implemented trajectory generator produced the prescribed cyclic movements and whether these trajectories could be consistently followed by the physical actuator. The knee was used as a representative joint, with its encoder position providing an independent measurement of the movement. This evaluation was performed under unloaded conditions, without the user's lower limb mechanically coupled to the prototype.

In order to examine different movement speeds, numbers of repetitions, and durations of endpoint pauses, three different exercise configurations were considered. All selected angular ranges remained within the prescribed knee ROM, and the speeds requested did not exceed the maximum passive rehabilitation speed. The configurations used during the evaluation are given in Table 4.9.

Table 4.9: Passive rehabilitation configurations used during validation.

Test	**Movement range (°)**	**Speed (°/s)**	**Repetitions**	**Endpoint pause (s)**
1	5–15	1.0	1	1.0
2	10–20	5.0	2	0.5
3	5–10	0.5	1	0.0

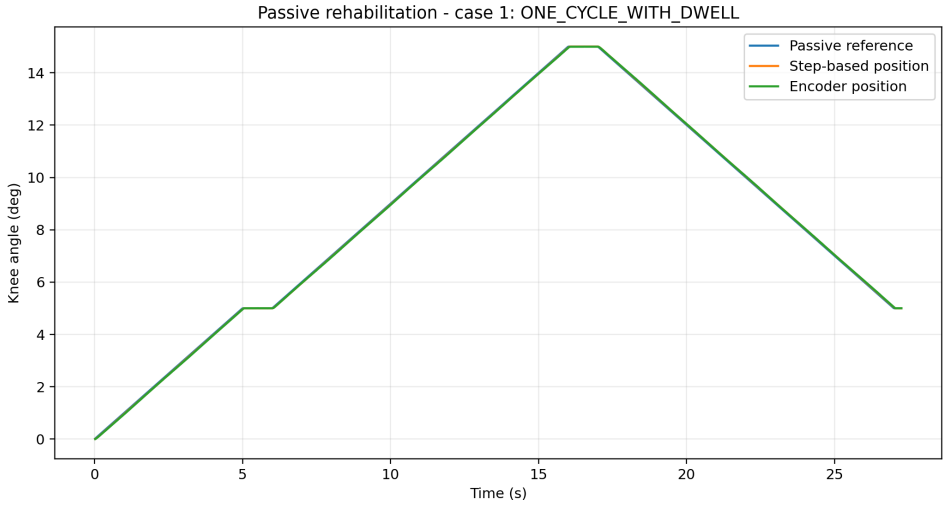
For every configuration, the passive reference, the step-based position and the encoder position were recorded during the test. The trajectory-generator state and the number of completed repetitions were also monitored to verify the specified movement range, repetition count and endpoint-pause behaviour. The trajectories for the three configurations are given in Figure 4.11. The corresponding quantitative position-tracking metrics are summarised in Table 4.10.

Table 4.10: Quantitative position-tracking results for the three passive rehabilitation test configurations.

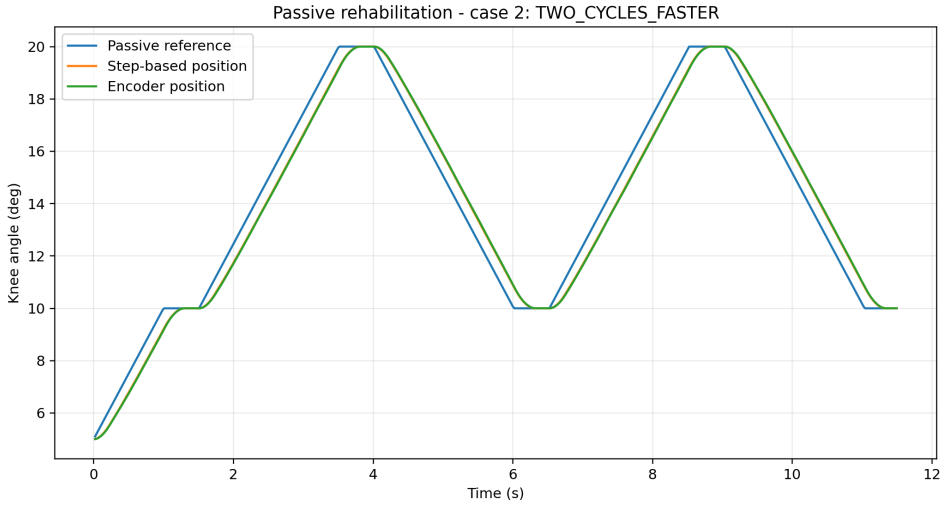
Test	**Max. ref.–encoder error (°)**	**Max. step–encoder error (°)**
1	0.0516	0.0190
2	0.8626	0.0479
3	0.0244	0.0160

In Test 1, the actuator closely followed the generated trajectory throughout the exercise. The greatest difference between the passive reference and the encoder-derived position was 0.052°. The required movement from 5° to 15° and back was completed successfully. The reference progressed at the configured rate of 1°/s and remained at the end points during the 1 s pauses that were prescribed before changing direction.

The largest reference-tracking errors occurred in Test 2, in which the speed of the passive movement was set to its maximum value of 5°/s. The maximum difference between the passive



(a) Test 1



(b) Test 2



(c) Test 3

Figure 4.11: Passive rehabilitation validation results, showing the generated reference and the corresponding step-based and encoder-derived knee positions for the three tested configurations.

reference and the encoder-derived position was approximately 0.863°. The increased tracking error can be attributed to the controller dynamics. The passive reference moves continuously toward the endpoint, while the motor velocity changes gradually in accordance with the specified acceleration limit. At this higher reference speed, the target advances more rapidly than the actuator can follow during acceleration and direction reversals, resulting in a larger tracking lag. This effect also occurs when the direction of the movement is reversed, since the actuator has to decelerate before accelerating in the opposite direction. Nevertheless, both of the prescribed repetitions were completed successfully, including the 0.5 s pauses at the end points.

Test 3 was performed at the lowest tested movement speed of 0.5°/s and, as expected from the slower variation of the reference, produced the smallest tracking errors. The maximum difference between the passive reference and the encoder-derived position was approximately 0.024°. The actuator consequently remained very close to the generated trajectory throughout the exercise. Since no endpoint pause was configured, the reference reversed direction immediately upon reaching each movement limit, and the single prescribed cycle was completed successfully.

During the tests, no invalid encoder measurements or diagnostic faults were observed, and the encoder health status remained *OK*. The exercises were therefore completed without interruptions related to joint-position sensing. In addition, the step-based and encoder-derived positions remained in close agreement across all three tests, with differences consistent with the joint-position tracking results presented in Section 4.3.3.

Overall, the passive rehabilitation mode behaved as intended, generating the prescribed trajectories and allowing the actuator to follow them consistently across the tested conditions.

4.5.2 Active-Assisted Rehabilitation

The active-assisted control path was evaluated in two stages. First, the generation of the angular reference from movement intention and intensity was assessed. The subsequent AAN stage was then evaluated to determine how this reference, together with the measured joint position and voluntary contribution, was used to generate the assisted angular target.

4.5.2.1 Reference Generation

The reference-generation stage of the active-assisted control path was evaluated to check how movement intention and intensity were converted into an angular reference. The tests looked at whether the reference moved in the direction intended, whether its rate of change depended on the intensity of the movement, and whether it stayed constant in the absence of any directional intention. The module was also assessed to see if the generated reference remained within the specified joint limits.

The knee was used as a representative joint. The final reference-generation parameters were used, while the applied movement state and intensity, together with the resulting reference speed and reference angle, were recorded during the tests.

The first test examined the effect of movement direction and intensity. Flexion and extension commands were given at normalised intensity levels of 0.25, 0.50 and 1.00. In each case, the condition was kept for 5 s, with the reference initialised at 60°, allowing the movement to be assessed without reaching the angular limits. The expected reference speed was determined by using Equation 3.7, and the actual rate of change was calculated from the recorded reference angles and the timestamps. These two values were then compared in order to evaluate the impact of intensity and movement direction on the generated reference. The evolution of the reference angle is presented in Figure 4.12. The expected and observed reference speeds are summarised in Table 4.11.

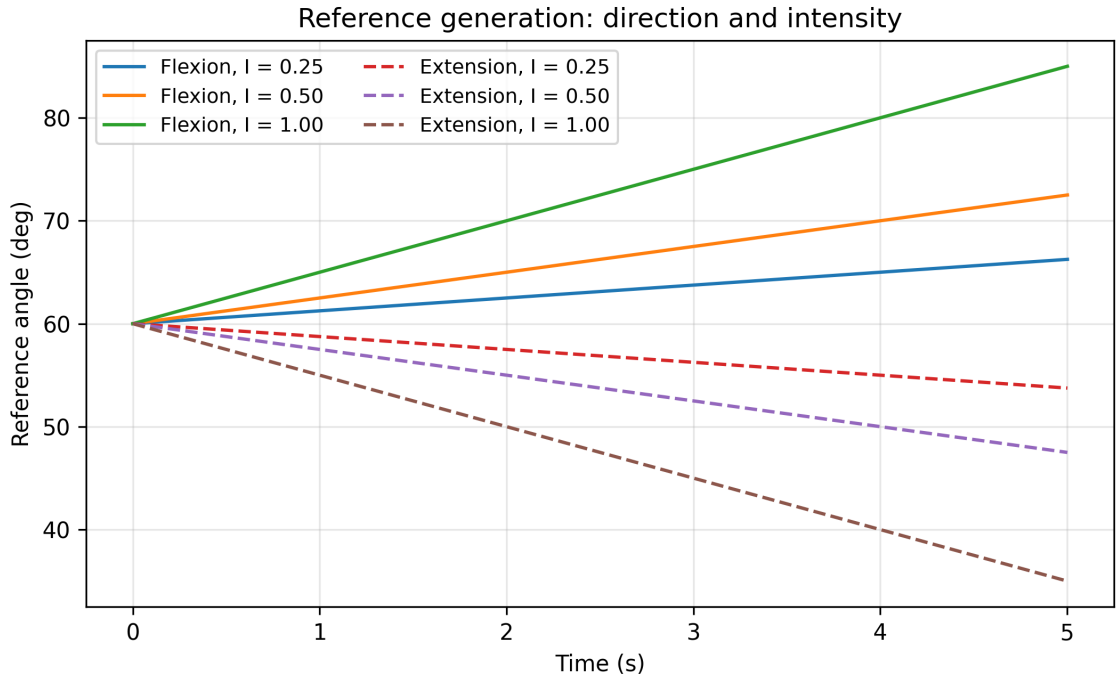


Figure 4.12: Angular reference trajectories for the different movement directions and intensity levels.

Table 4.11: Comparison between expected and observed reference speeds for different movement intensities.

Movement	**Intensity**	**Expected speed (°/s)**	**Observed speed (°/s)**	**Error (°/s)**
Flexion	0.25	1.25000	1.24997	-0.00003
	0.50	2.50000	2.49997	-0.00003
	1.00	5.00000	4.99998	-0.00002
Extension	0.25	-1.25000	-1.24998	0.00002
	0.50	-2.50000	-2.49998	0.00002
	1.00	-5.00000	-4.99987	0.00013

The behaviour in the absence of directional intention was subsequently evaluated. The reference was initialised at 60°, after which the relaxed state was applied to verify whether it remained stationary. The results obtained are shown in Figure 4.13.

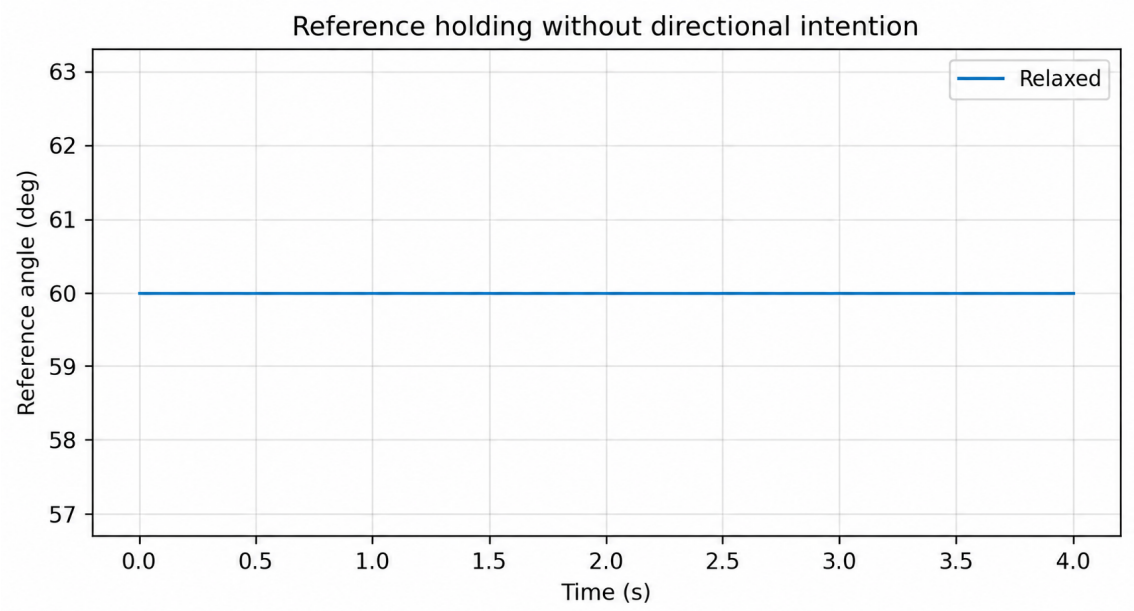


Figure 4.13: Reference behaviour in the absence of directional movement intention.

The last test examined the limits set by the reference-generation module, with the reference being initialised close to both the upper and lower angular limits and then movement commands being applied in the direction of each respective boundary. The angle that was generated was recorded in order to check whether it stayed within the specified range. The results are given in Figure 4.14. The safety restrictions imposed on the final actuator commands are examined separately in Section 4.6.1.

As shown in Figure 4.12, the generated reference changed in the expected way both during flexion and extension, and its rate of change increased with movement intensity. For intensity levels of 0.25, 0.50 and 1.00, the expected magnitudes of reference speed were 1.25, 2.50 and 5.00 °/s, respectively. The values observed in Table 4.11 were very close to these theoretical values. The greatest absolute difference recorded was 0.00013°/s, which occurred during extension at an intensity of 1.00. These discrepancies are negligible in relation to the commanded speeds and can be associated with the discrete implementation of the reference generator and the calculation of the observed speed from the recorded data.

The test carried out without any directional movement intention also resulted in the expected behaviour. As illustrated in Figure 4.13, the reference remained at 60° throughout the relaxed condition, with no measurable drift.

The results of the joint-limit tests are given in Figure 4.14. Starting at 116° and giving a flexion command at maximum intensity, the reference value increased until the upper limit of 117° was reached. Analogously, when starting at 1° and applying an extension command, the reference

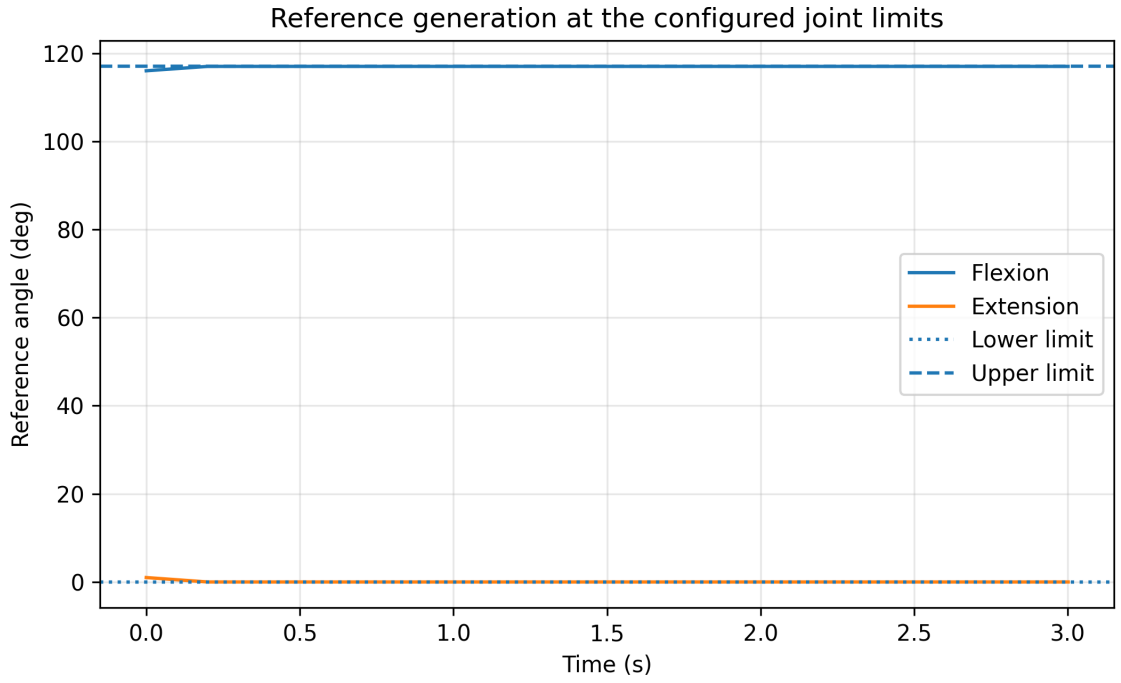


Figure 4.14: Generated angular reference behaviour at the configured joint limits.

decreased until the lower limit of 0°. In each case, the limit was reached after approximately 0.20 s, which is consistent with the initial distance of 1° from the limit and the configured maximum reference speed of 5°/s. After the relevant limit had been reached, the reference remained at that value and its speed dropped to zero.

In summary, the results show that the reference-generation module worked as intended.

4.5.2.2 Assist-As-Needed Behaviour

Following the evaluation of the generated reference, the AAN controller was assessed to determine how the level of assistance changed with the joint-position tracking error and the user's contribution. The tests also examined whether the calculated assistance produced the expected assisted angular target and whether changes in assistance respected the configured increase and decrease rate limits.

The knee was used as a representative joint. A reference angle of 60° and an e_{full} value of 10° were applied during the entire evaluation. The tracking error, desired and current assistance levels, and assisted angular target were recorded.

The assistance level was evaluated for different combinations of tracking error and EMG intensity. Positive tracking-error levels of $0.25e_{\text{full}}$ and e_{full} were paired with intensity values of 0.20 and 0.80, which gave a total of four conditions. A further condition was added in which the error was $-0.25e_{\text{full}}$, representing a situation in which the user had moved beyond the reference in the intended movement direction. This condition was used to verify that no corrective assistance was

applied to move the joint back towards the reference. All of the angular values provided remained within the joint range.

Each condition was maintained until the assistance level had stabilised, with $|A - A_{\text{des}}|$ remaining below 0.001 for 0.20 s. The actual level of assistance was then compared to the value predicted by the equations described in Section 3.6.3. The assisted angular target was also compared with the one obtained from Equation 3.15. This analysis offered a direct quantitative check on whether the implemented controller had reached the expected final values. The results are presented in Table 4.12.

Table 4.12: Comparison of expected and observed AAN outputs under different input conditions.

Condition	e	θ_{meas}	I	**Expected** A	**Observed** A	**Expected** θ_{AAN}	**Observed** θ_{AAN}
Small error, weak contribution	$+0.25e_{\text{full}}$	57.5	0.20	0.3550	0.3550	58.3875	58.3875
Small error, strong contribution	$+0.25e_{\text{full}}$	57.5	0.80	0.2200	0.2200	58.0500	58.0500
Large error, weak contribution	$+e_{\text{full}}$	50.0	0.20	1.0000	1.0000	60.0000	60.0000
Large error, strong contribution	$+e_{\text{full}}$	50.0	0.80	1.0000	1.0000	60.0000	60.0000
User ahead of reference	$-0.25e_{\text{full}}$	62.5	0.20	0.0000	0.0000	62.5000	62.5000

Assistance values are dimensionless. Angles are expressed in degrees. The reference angle was fixed at 60° for all conditions.

The evolution of the assistance level over time was also examined. A series of pre-determined inputs were used in order to produce changes in tracking error and voluntary contribution. For the first 4 seconds the effect of tracking error was studied with the EMG intensity held at 0.80. In the remaining 2 seconds the normalised tracking error was kept at 0.25 while the EMG intensity was varied. The operating conditions employed in this sequence therefore matched the conditions that were also assessed in Table 4.12.

The rates of assistance increase and decrease were calculated from the recorded assistance values and the timestamps and were then compared with the limits configured in the final implementation. Furthermore, the recorded signals were checked to see if the current level of assistance moved progressively towards the desired value without any sudden changes. The results are given in Figure 4.15.

During the same input sequence, the assisted angular target was also looked at. In order to evaluate how the level of assistance affected the resulting position command, the generated reference, the measured position and the assisted target were recorded. The results corresponding to this are given in Figure 4.16.

With a small positive tracking error and an EMG intensity of 0.80, Table 4.12 indicates a final assistance level of 0.220 and an assisted angular target of 58.0500°. The same operating condition was applied over the interval $[0, 1]$ s in Figures 4.15 and 4.16. During this interval, the level of assistance rose from its initial value until it reached the desired level of 0.220, and at the same time

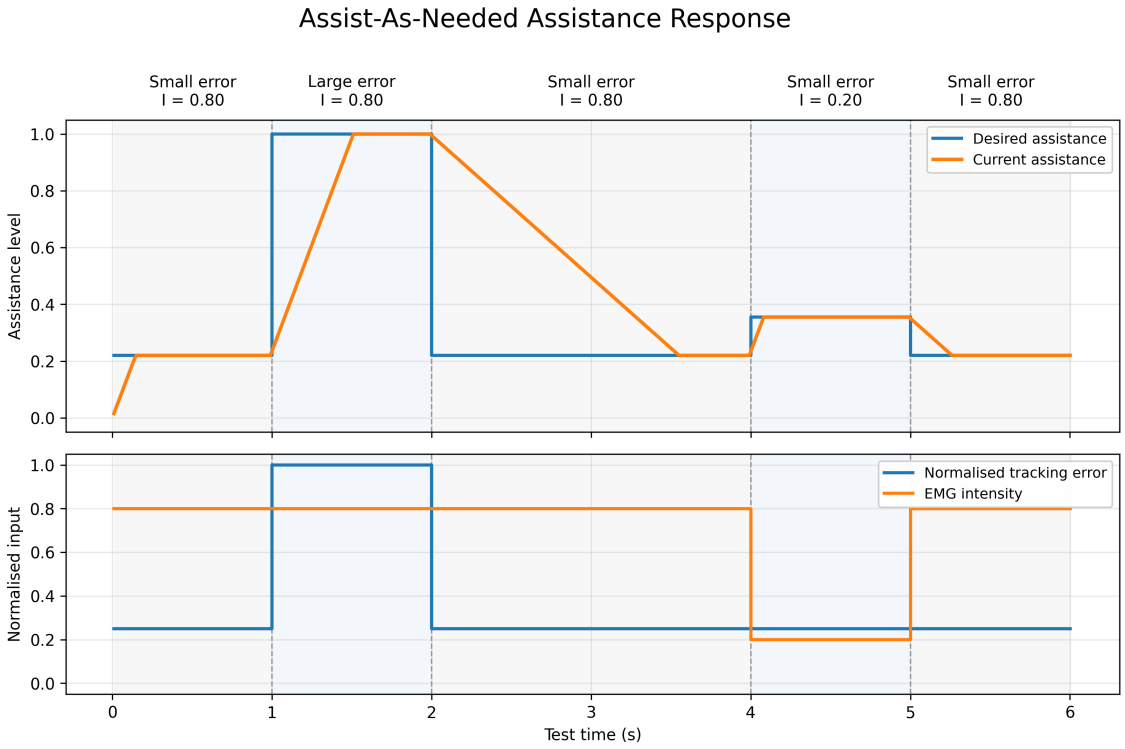


Figure 4.15: Assistance response to changes in tracking error and movement intensity.

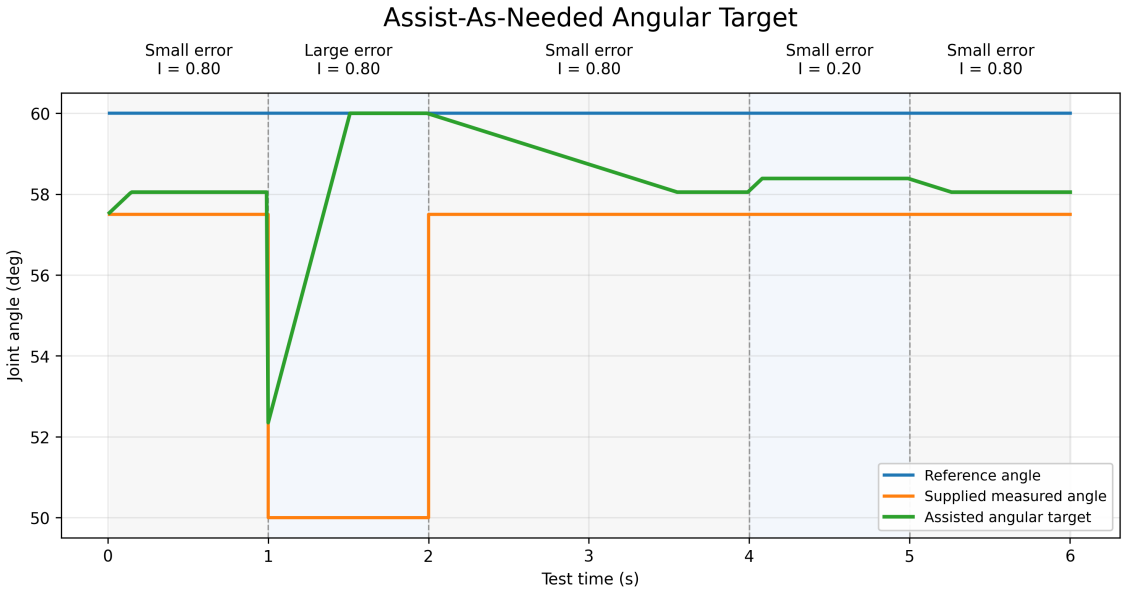


Figure 4.16: Assisted angular target during the AAN evaluation.

the assisted angular target gradually changed from the measured position supplied to its respective final value.

Between 1 and 2 s, the normalised tracking error rose from 0.25 to 1.00 while the EMG intensity stayed at 0.80. As the corresponding case in Table 4.12 also shows, the desired assistance increased to its maximum level of 1.00, which caused the assisted angular target to move towards and eventually match the 60° reference. In this situation, the EMG intensity no longer affects the assistance calculation since the tracking error has reached e_{full}. The current assistance approached the new desired value progressively rather than changing abruptly.

During the $[2,4]$ s interval, the normalised tracking error returned to 0.25 while the intensity remained unchanged. The desired level of assistance therefore returned to 0.220 and the assisted target moved once again towards the value from the small-error condition. The current level of assistance decreased more gradually towards the desired value. The observed rates of increase and decrease of assistance were approximately 1.50 s^{-1} and -0.50 s^{-1}, respectively, matching the corresponding limits set in the controller. Since the rates were different, additional assistance was introduced more quickly and withdrawal of assistance was slower, avoiding abrupt changes between consecutive control cycles.

The effect of voluntary contribution can be seen during the final part of the sequence. From 4 to 5 s, the normalised tracking error stayed at 0.25 while the EMG intensity dropped from 0.80 to 0.20. As the values in Table 4.12 show, this caused the desired assistance to rise from 0.220 to 0.355 and shifted the assisted angular target further towards the reference, from 58.0500° to 58.3875°. When the intensity was brought back up to 0.80 between 5 and 6 s, the desired assistance fell once more to 0.220 and the assisted target moved back to 58.0500°. This behaviour is consistent with the intended operation of the controller, since for the same tracking error a smaller voluntary contribution leads to a greater degree of robotic assistance.

Overall, these results illustrate the intended AAN behaviour. When the measured position remains behind the generated reference in the intended movement direction, a larger tracking error leads to a higher level of assistance, while a greater voluntary contribution, represented by a higher EMG intensity, reduces it. Once this directional tracking error reaches e_{full}, the assistance saturates and the EMG intensity no longer affects the result.

The additional negative-error condition shown in Table 4.12 represented the situation in which the measured position had moved beyond the reference in the intended movement direction. In this case, both the expected and observed assistance levels were zero, and the assisted angular target remained equal to the measured position at 62.5°. The controller therefore did not command a return towards the 60° reference. This behaviour allows voluntary movement beyond the generated reference to be tolerated.

Under the evaluated conditions, the AAN controller behaved as intended.

4.6 Safety and Fault-Handling Validation

The purpose of this section was to check that the implemented safety and fault-handling mechanisms worked correctly. The tests included the joint and speed limits, communication loss, encoder and tracking faults, and recovery from an emergency stop. The assessment focused on whether the implemented safety logic produced the expected response to known operating and fault conditions, including its interaction with the system state machine described in Section 3.7.

As in Section 4.5, where appropriate, predefined inputs were supplied directly to the relevant safety or monitoring functions. This made it possible to reproduce specific conditions and verify the corresponding safety responses in a controlled and repeatable way. The aim was to isolate the behaviour of the implemented safety logic from the rest of the system so that each mechanism could be evaluated independently.

The knee was used as the representative joint where a joint-specific configuration was required. Tests that involved a different procedure, such as communication loss or the emergency-stop function, are described separately in the corresponding subsections.

4.6.1 Joint and Speed Limits

The command-limiting functions were evaluated to check whether the angular targets forwarded to the motor controller stayed within the joint limits and whether their rate of change did not exceed the maximum allowed. Although the passive trajectory generator and the active-assisted control functions are responsible for generating the movement targets, these targets must still go through the safety functions before being transformed into motor commands. The tests therefore examined whether the safety manager correctly restricted angular targets that violated the configured position or speed limits. This evaluation was done separately from the movement-generation and AAN functions, whose behaviour was assessed in Section 4.5.

The requested target, safe target, returned safety status and motor-enable command were recorded. For the knee, the configured angular range was from 0° to 117°, while the maximum permitted rate of change of the safe target was 5°/s.

The first test examined the joint limits. Two separate targets were fed to the module: one angle below the minimum allowed and the other above the maximum. The safe target that resulted was then compared with the appropriate joint limit to ensure that the requested position had been restricted. Additionally, a target within the permitted range was provided to verify that valid commands were accepted without any angular limitation. The results are summarised in Table 4.13.

The following test examined the speed limitation. The safety manager was placed at a position within the operating range, and target changes which exceeded the defined maximum rate were applied in each direction. During successive control cycles, the requested and safe targets were recorded. The rate at which the change was observed was calculated from the safe-target values and the timestamps and then compared with the predetermined limit. The results are given in Figure 4.17 and Table 4.14.

Table 4.13: Results of the joint-position limiting tests.

Condition	**Requested target**	**Expected behaviour**	**Observed result**
Below minimum	-10.0°	Target restricted to the configured minimum.	0.0° (`ANGLE_LIMITED`)
Above maximum	127.0°	Target restricted to the configured maximum.	117.0° (`ANGLE_LIMITED`)
Within limits	60.0°	Target accepted without angular limitation.	60.0° (`OK`)

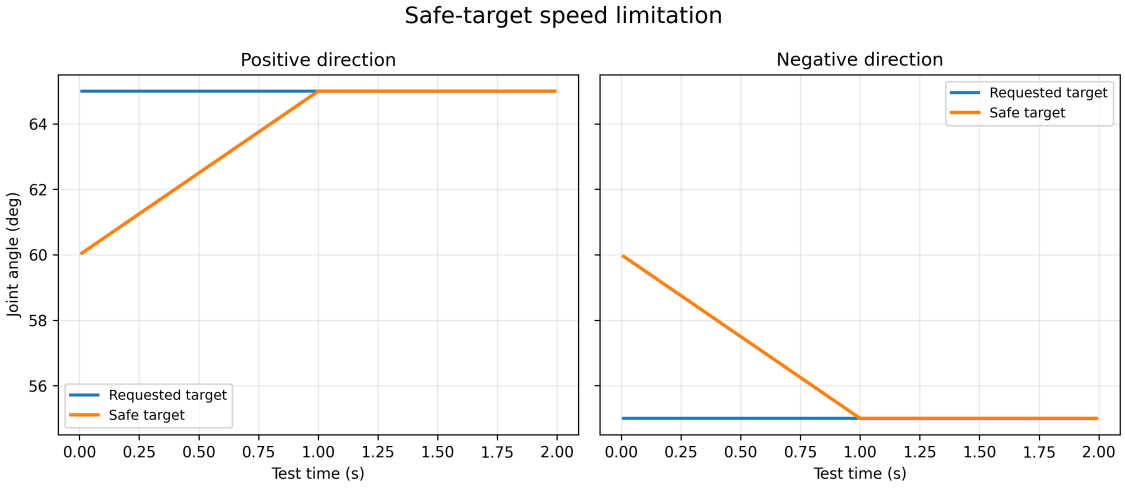


Figure 4.17: Requested and safe angular targets during the speed-limiting test.

Table 4.14: Comparison of configured and observed safe-target speed limits.

Direction	**Configured limit (°/s)**	**Observed rate (°/s)**	**Result**
Positive	5.0000	4.9998	Pass
Negative	-5.0000	-4.9999	Pass

The joint limiting results presented in Table 4.13 exhibited the expected behaviour in all three cases. When a target of -10° was requested, it was restricted to the lower joint limit of 0°, and, similarly, the 127° target was limited to the upper limit of 117°. In both instances, the safety status returned was `ANGLE_LIMITED`. The target of 60°, since it was within the allowed range, was accepted without modification and the `OK` status was returned. In all three cases the motor-enable command stayed active, which shows that angular limitation restricted the requested command without treating it as a fault that would require the motor to be disabled.

Regarding the speed-limiting behaviour, in the positive direction the safety manager began at 60° with a requested target of 65°. Rather than immediately moving the safe target to the requested value, it increased progressively at the configured maximum rate and reached the requested target after approximately 1 s, as shown in Figure 4.17. In the negative direction, the same initial position was used with a requested target of 55°, and the safe target similarly decreased at the limited rate until the requested value was reached after approximately 1 s.

Table 4.14 shows that the observed rates were approximately $+4.9998^\circ$/s and -4.9999°/s, respectively, which closely matched the configured limits of $\pm 5^\circ$/s. During the respective limiting conditions, the safety status returned was `SPEED_LIMITED`, and the motor-enable command stayed active.

The results indicate that the safety manager properly restricted the angular targets to the allowed joint range and limited their rate of change without unnecessarily disabling motor operation. The returned safety statuses were consistent with the applied conditions, and the observed rates matched the configured speed limits. Overall, the joint-position and speed-limiting functions behaved as intended under the evaluated conditions.

4.6.2 Communication Loss

The communication-loss response was evaluated to verify if the actuation controller detected the absence of valid movement messages and stopped the normal reference generation. The test also examined the transition to position holding and the conditions required for resuming operation.

The experiment was performed using the physical sensing and actuation controllers, the UART link, and the knee actuator assembly. The sensing and actuation controllers were connected through the UART link as described in Section 3.6.5. The sensing controller sent predefined messages indicating knee flexion at an intensity level of 1.0 using the standard communication protocol. These messages were then processed by the reference-generation, AAN, safety and motor-control functions that had been implemented. Once the actuation controller reached its active state and was receiving valid movement commands, transmission of the movement messages was stopped. This interruption was maintained for 1.5 s before normal communication was reestablished.

The encoder-derived joint position was used as the position input during this evaluation. The interval between the last valid message and the detection of communication loss was compared

with the configured timeout. The position-holding response was then checked to ensure that normal reference generation was stopped and that the joint position measured at the instant that communication loss was detected was stored as the holding target. This value was also used to reset the movement reference when the system reached the holding condition.

Once communication was restored, the system's state and the motor's behaviour were recorded to check that the movement did not begin automatically. A new start command was issued in order to see whether normal operation could be restarted. The results are shown in Figure 4.18.

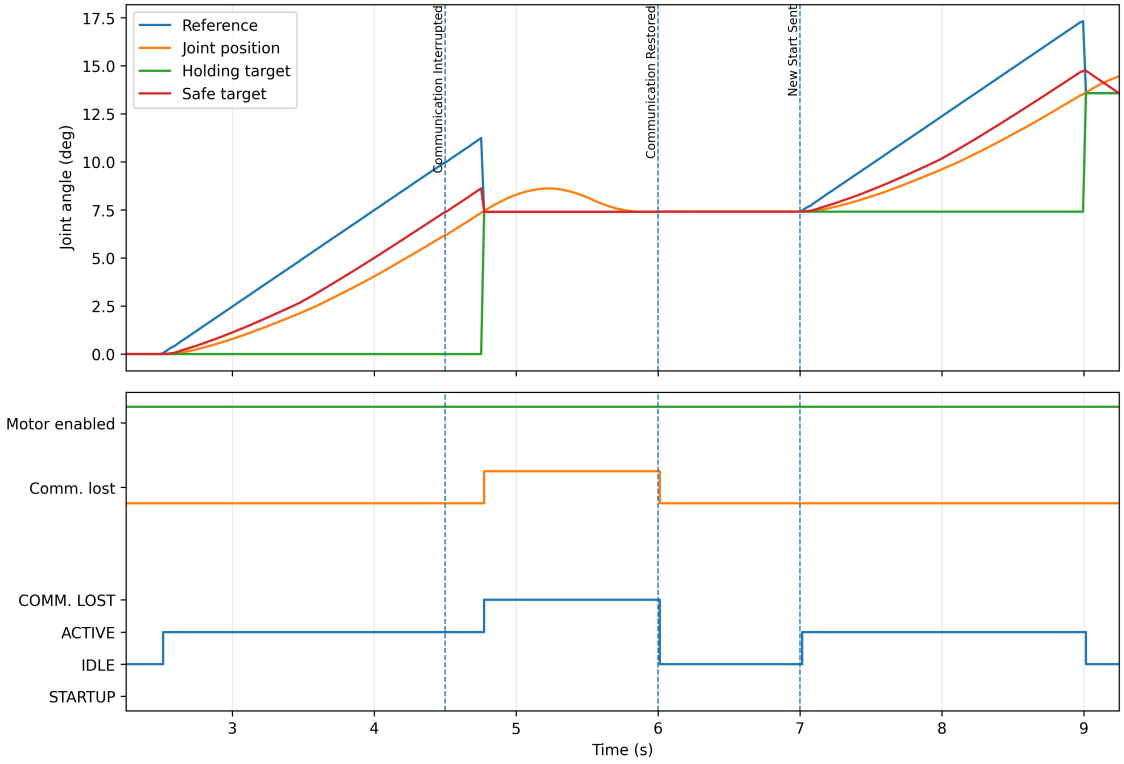


Figure 4.18: Control response to communication loss and restoration.

During normal operation, the reference angle and the safe target did not necessarily coincide, as illustrated in Figure 4.18. The reference was initially handled by the AAN controller and then passed on to the safety manager before the resulting target was forwarded to the motor controller. The safe target thus reflected the final angular target allowed by the control and safety system rather than a direct copy of the generated reference.

The communication loss was detected 314 ms after the last valid movement message, which was close to the configured timeout of 300 ms. At this point, the system changed from the `ACTIVE` state to `COMMUNICATION_LOST`, as shown in Figure 4.18. The 14 ms difference results from the fact that the timeout condition is verified once in each control-loop iteration, so the communication loss can only be detected in the first cycle that follows the moment the 300 ms threshold has been surpassed.

On detection of the communication loss, normal reference generation was stopped and the

encoder-derived joint position of approximately 7.396° was stored as the holding target. The reference angle was simultaneously set to this value and remained constant throughout the communication-loss interval. The safe target was also maintained at the same stored position.

The motor remained enabled while the system was in the `COMMUNICATION_LOST` state. Although the holding target, reference and safe target remained fixed at approximately 7.396°, the actuator continued to move briefly because it was still decelerating from the preceding movement. The encoder-derived position reached a maximum of approximately 8.613°, after which the actuator reversed direction and returned towards the stored holding position. By the end of the communication-loss interval, the measured position was approximately 7.402°, corresponding to a difference of approximately 0.006° from the holding target. This shows that the commanded position remained fixed during the communication loss while allowing the actuator to return to the position stored when the interruption was detected.

Once valid communication was restored, the system returned to the `IDLE` state and the movement did not automatically restart. Upon entering this state, the holding target was updated to the current encoder-derived joint position of approximately 7.402°, causing the reference and safe target to coincide with the measured position. The motor therefore remained enabled without continuing the previous movement command. Only after a new start command was given did the system return to the `ACTIVE` state and normal movement resumed.

The findings indicate that the communication-loss mechanism behaved as intended. After the configured timeout had elapsed, the absence of valid movement messages was detected and normal reference generation was interrupted. The joint position measured at that instant was stored as a fixed holding target and maintained as the reference and safe target. Although the actuator briefly continued moving while decelerating, it subsequently returned to the stored holding position. Restoring communication alone was not sufficient to restart movement, since the system returned to `IDLE` and a new start command was required before normal operation could resume.

4.6.3 Encoder Fault

The encoder-fault mechanism was evaluated to verify how the system responded when valid joint-position information was no longer available. The test checked whether the monitoring function detected the absence of valid measurements, whether the fault was reported after the prescribed timeout, and whether the system reached the appropriate error state and stopped motor operation. Normal encoder acquisition and rotation-unwrapping behaviour were separately assessed in Section 4.3.2.

The encoder-fault mechanism was assessed by intentionally interrupting the acquisition of encoder measurements for controlled periods, so that the behaviour of the monitoring and fault-handling mechanisms could be examined using the real encoder acquisition chain.

Three encoder fault situations were examined. In the first case, encoder acquisition was interrupted for about 150 milliseconds, a duration less than the set timeout of 250 milliseconds, after which normal acquisition was resumed. In the second case, the interruption continued past

the configured timeout. Lastly, the system was started while valid encoder information was not available in order to check whether normal operation was prevented from beginning.

The encoder-validity condition, time since the last valid measurement, encoder-fault signal, system state and motor-enable status were recorded throughout the tests. The results for the three evaluated conditions are presented in Figures 4.19, 4.20, and 4.21.

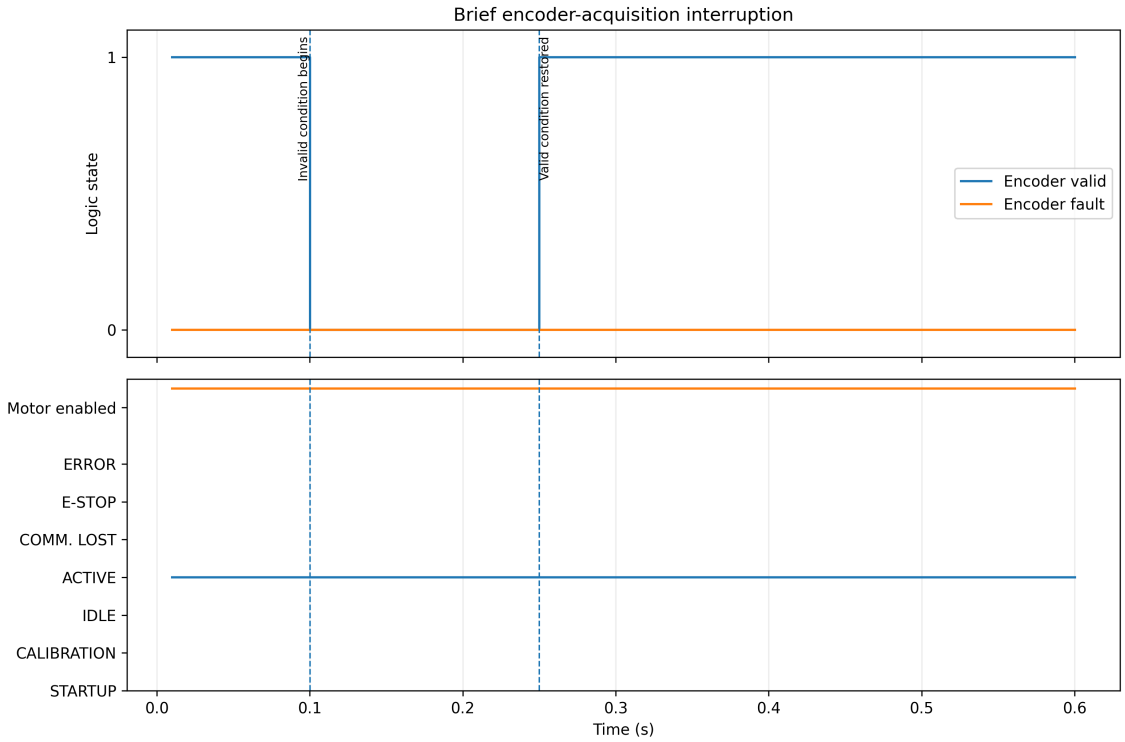


Figure 4.19: System response to a brief interruption of encoder acquisition.

As shown in Figure 4.19, the brief period during which the encoder acquisition was interrupted lasted about 150 ms and did not result in an encoder fault. As valid measurements became available again before the 250 ms timeout period expired, the system stayed in the `ACTIVE` state and motor operation remained enabled. This demonstrates that a short interruption in joint-position acquisition does not immediately lead to a system fault.

For the sustained acquisition interruption, the fault was detected when the time since the last valid measurement reached 250 ms, matching the configured timeout. As illustrated in Figure 4.20, the system then went into the `ERROR` state and motor operation was stopped. The response therefore occurred only after valid position information had remained unavailable for the required period.

At the initialisation check (Figure 4.21), the invalid encoder condition stopped the system from reaching normal operation and the motor stayed disabled. Since the invalid condition continued for 250 ms, an encoder fault was detected and the system then entered the `ERROR` state. This shows that valid position information was necessary before normal operation could begin.

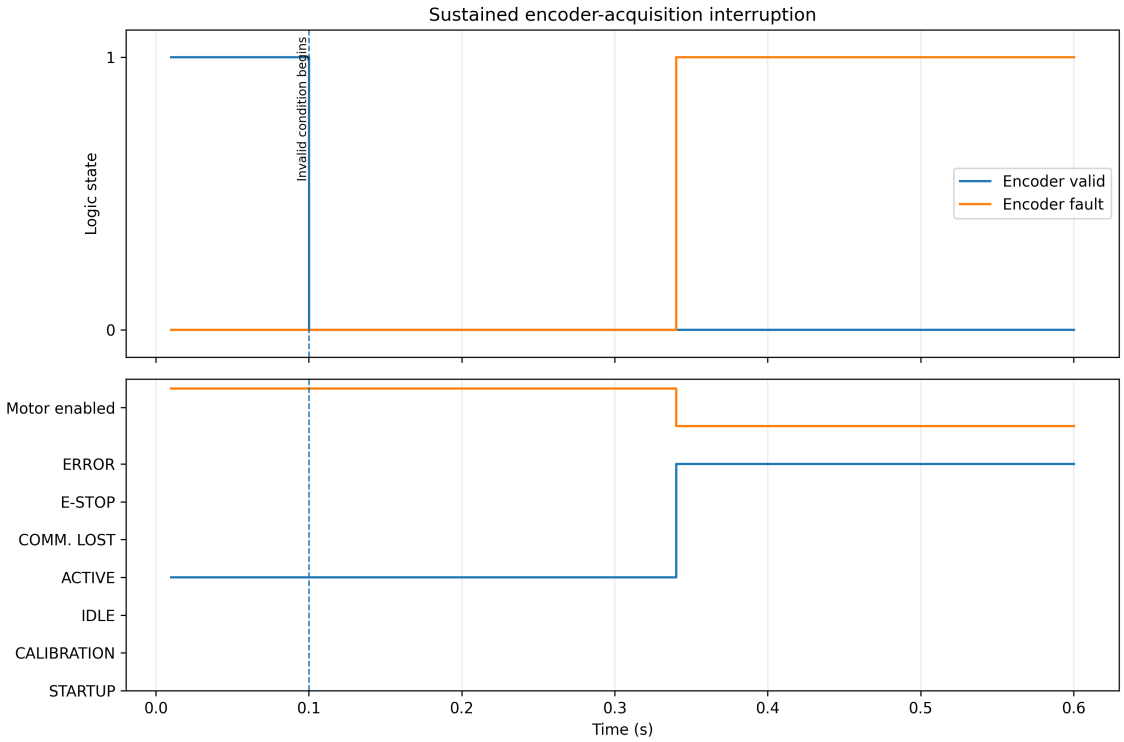


Figure 4.20: System response to a sustained interruption of encoder acquisition.

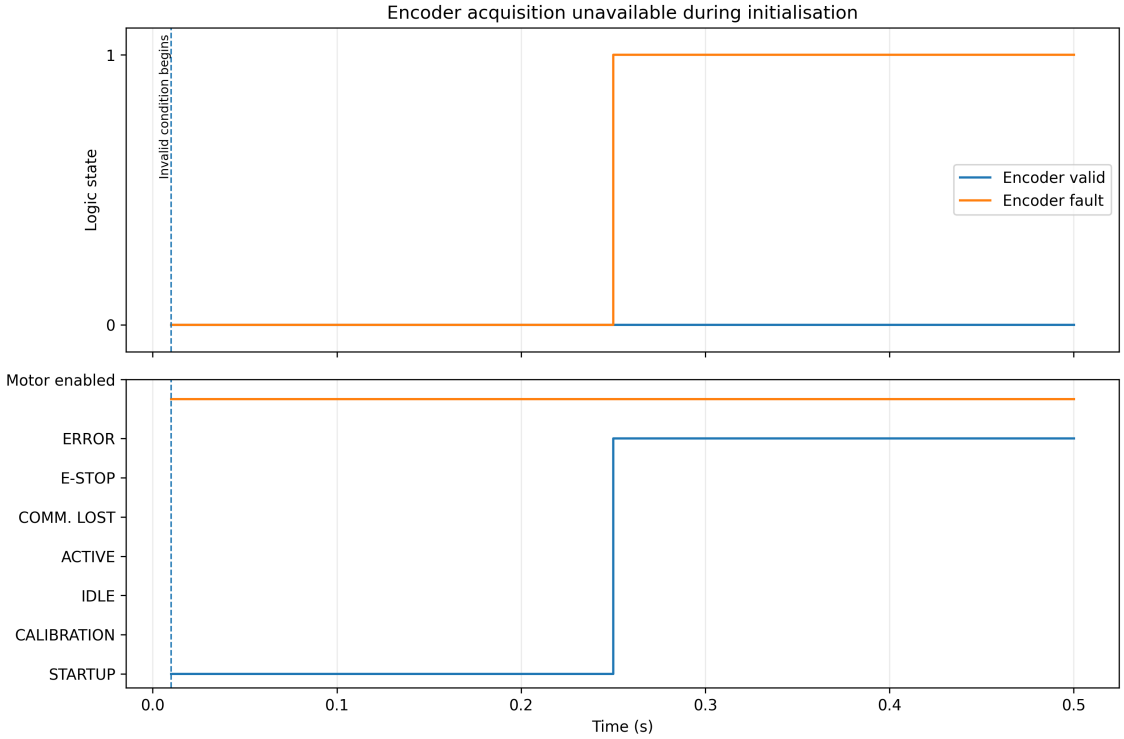


Figure 4.21: System response when encoder acquisition was unavailable during initialisation.

The results show that the encoder-fault mechanism worked as expected. Brief interruptions in encoder acquisition were tolerated but continuous interruptions caused a fault after the configured timeout and then stopped motor operation. Furthermore, failure to obtain valid encoder information during initialisation also stopped normal operation from starting.

4.6.4 Actuator Tracking Fault

The tracking-fault mechanism was evaluated using the step-based and encoder-derived joint positions available during normal system operation. In order to introduce known and repeatable discrepancies without requiring the actuator to physically lose steps, a predetermined angular offset was applied to the encoder-derived position fed into the tracking-fault monitoring logic. The unmodified encoder position was recorded separately so that the introduced discrepancy could be distinguished from the actual difference between the step-based and encoder-derived joint positions.

Three tracking-error conditions were evaluated by applying controlled offsets to the encoder-derived position supplied to the monitoring logic. In the first instance, a discrepancy of 1.5° was introduced, this being below the set threshold of 2°. In the second case, a discrepancy of 3° was introduced above the threshold for approximately 150 ms, which was shorter than the configured persistence time of 250 ms, after which the offset was removed. For the last condition, the same excessive discrepancy was maintained beyond the persistence period.

The step-based position, unmodified encoder-derived position, position supplied to the tracking-fault monitor, tracking error, fault signal, system state and motor-enable status were recorded throughout the tests. This made it possible to verify both the encoder acquisition and the response of the monitoring logic to the controlled discrepancy. The results are presented in Figure 4.22 and Table 4.15.

Table 4.15: Results of the actuator tracking-fault tests.

Condition	**Expected response**	**Observed result**
Error below threshold	No tracking fault.	No fault; `ACTIVE`; motor enabled.
Brief excessive error	No fault is triggered if the error returns below the threshold before the persistence period expires.	No fault; `ACTIVE`; motor enabled.
Sustained excessive error	Tracking fault detected; system enters `ERROR` and motor operation is disabled.	Fault detected; `ERROR`; motor disabled.

The error below the configured threshold did not produce a tracking fault. Since the discrepancy was 1.5°, the fault signal stayed inactive, the system remained in the `ACTIVE` state and motor operation continued to be enabled. This demonstrates that differences less than 2° were accepted without activating the fault-handling mechanism.

When the tracking error was raised to 3° for about 150 ms, as illustrated in Figure 4.22, no fault was triggered. Since the excessive error decreased below the threshold before the 250 ms

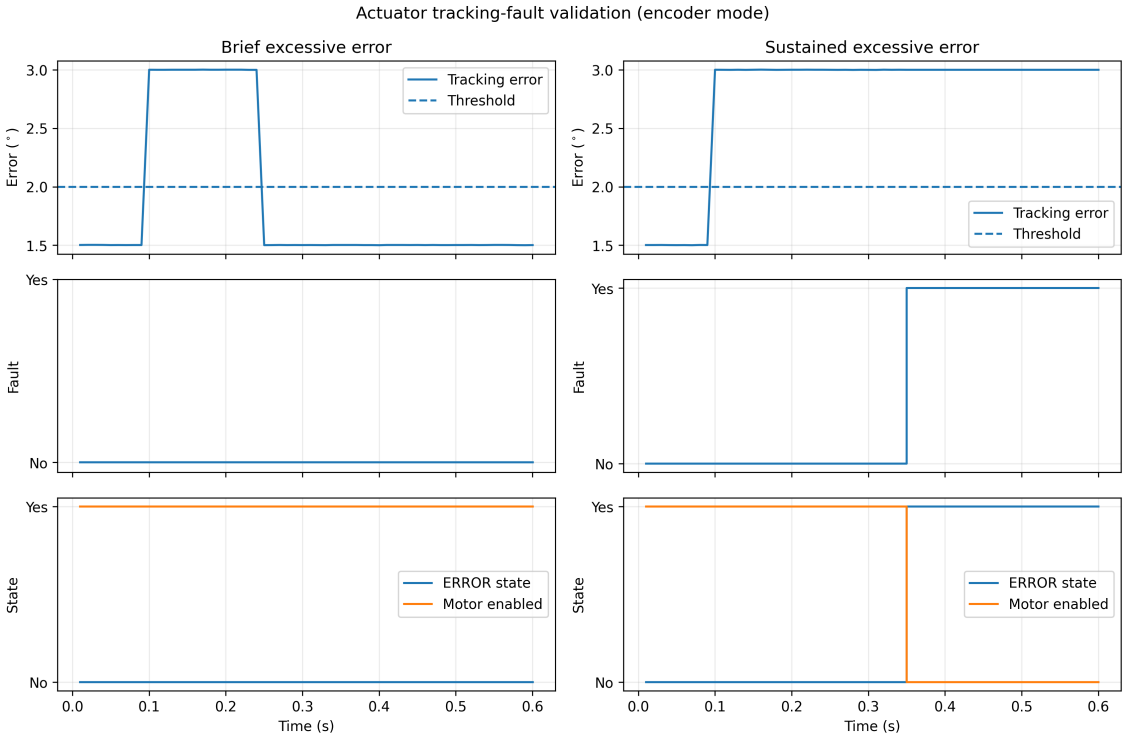


Figure 4.22: System response to brief and sustained tracking errors.

persistence period had ended, the system remained in the `ACTIVE` state with the motor enabled. This behaviour prevents short tracking discrepancies from immediately causing a system fault.

In the sustained-error condition, the 3° discrepancy remained beyond the specified persistence period. The tracking fault was detected after about 250.07 ms, which was very close to the configured value of 250 ms. The system then moved into the `ERROR` state, and motor operation was stopped. The response therefore occurred only after the tracking error had remained above the configured threshold for the required persistence period.

The results indicate that the actuator tracking-fault mechanism behaved as intended. A fault was generated only when the tracking error persisted above the configured threshold for the specified period, after which the system switched to the `ERROR` state and stopped motor operation.

4.6.5 Emergency Stop and Recovery

The emergency-stop function and the recovery behaviour were checked to see whether the actuator's operation would be interrupted when an emergency-stop condition was triggered and whether normal operation could only resume after the required reset procedure. The test also looked at the system's recovery from an error state without repeating the fault-detection tests mentioned in the previous subsections.

Unlike the isolated logic tests used in the preceding subsections, the emergency-stop test was carried out through the actuation controller using the implemented software command. The system was first put into its active state and was then ordered to move within the allowed range. During

the test, the system state, motor-enable status, emergency-stop signal and reset command were recorded. The following sequence was then carried out:

1. The emergency-stop command was activated to verify that the system entered the `EMERGENCY_STOP` state and that motor operation was disabled.
2. The emergency-stop signal was cleared without resetting the system to determine whether the system remained in the `EMERGENCY_STOP` state.
3. The emergency-stop signal was activated again, and a reset was attempted while the signal was active to check whether the reset was rejected.
4. The emergency-stop signal was cleared, and a new reset was performed to verify whether the reset was accepted.
5. After a valid reset, the startup and start commands were applied in the required sequence to make sure that movement did not resume automatically before operation was re-enabled.

System error recovery was similarly evaluated through the normal state-machine behaviour using an encoder fault. Encoder acquisition was interrupted until the system detected the fault and entered the `ERROR` state. A reset was first attempted while valid encoder measurements were still unavailable, in order to verify that recovery was rejected while the fault condition remained active. Encoder acquisition was then restored and a new reset was performed to verify the normal recovery procedure.

The temporal evolution of the measured joint position, system state and motor-enable status during the emergency-stop and fault-recovery sequences is presented in Figures 4.23 and 4.24. The individual conditions and corresponding responses are summarised in Table 4.16.

As shown in Figure 4.23, the emergency-stop sequence resulted in the expected state transitions. When the emergency-stop command was activated, the system immediately moved into the `EMERGENCY_STOP` state and motor operation was stopped. Simply clearing the emergency-stop signal was not sufficient for the system to leave this state, which demonstrated that the stop condition could not be eliminated by merely releasing the command.

When a reset was attempted while the emergency-stop signal was still active, the reset was rejected and the system remained in `EMERGENCY_STOP`. Once the signal had been cleared, the reset was accepted and the system returned to the `STARTUP` state. Motor operation remained disabled after this transition, and normal operation only resumed after the required startup and start commands had been applied. This confirms that movement could not restart automatically following an emergency-stop event.

As shown in Figure 4.24, a reset attempted while encoder acquisition remained invalid was rejected and the system stayed in the `ERROR` state. After encoder acquisition was restored, the system remained in `ERROR` until a valid reset was performed. The valid reset returned the system to `STARTUP`, with motor operation remaining disabled until the required startup and start commands were applied.

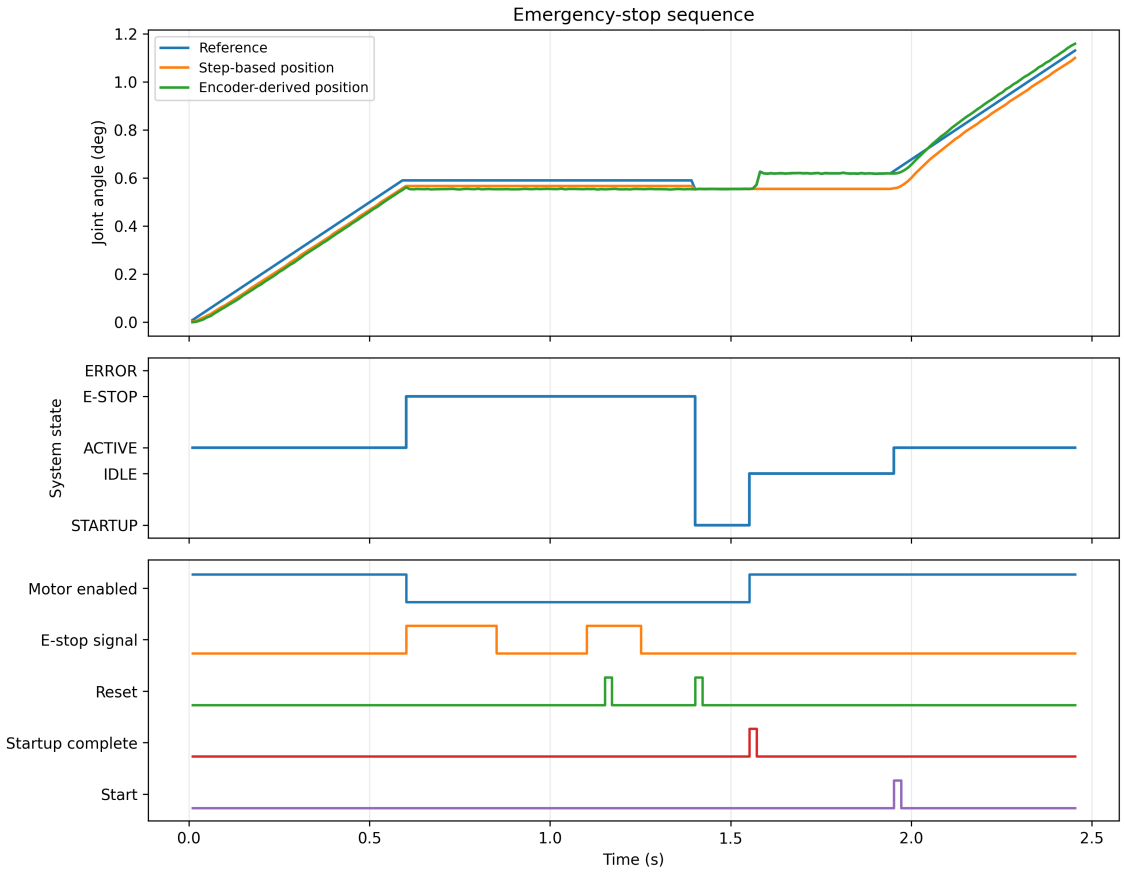


Figure 4.23: System response during the emergency-stop sequence.

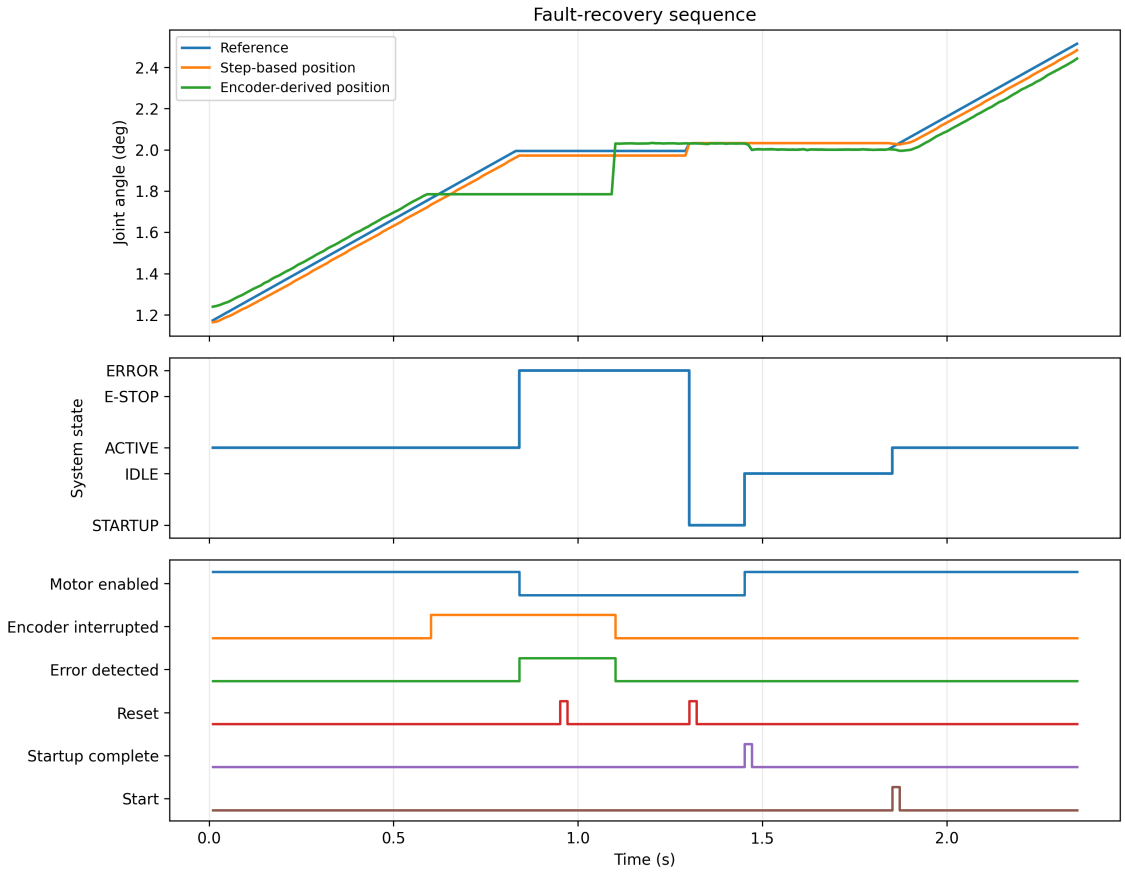


Figure 4.24: System response during the fault-recovery sequence.

Table 4.16: Results of the emergency-stop and fault-recovery tests.

Condition	Expected response	Result
Emergency-stop sequence		
Emergency stop activated	System enters `EMERGENCY_STOP` and motor operation is disabled.	PASS
Emergency-stop signal cleared	System remains in `EMERGENCY_STOP` until reset.	PASS
Reset with active emergency-stop signal	Reset rejected.	PASS
Valid reset	System returns to `STARTUP`; normal movement remains disabled.	PASS
Startup and start sequence	Normal operation resumes only after the required commands.	PASS
Fault-recovery sequence		
Reset while encoder acquisition remained invalid	Reset rejected.	PASS
Encoder acquisition restored	System remains in `ERROR` until reset.	PASS
Valid fault reset	System returns to `STARTUP`; normal movement remains disabled.	PASS
Startup and start sequence	Normal operation resumes only after the required commands.	PASS

As in the emergency-stop sequence, normal operation was not resumed until the necessary startup and start commands had been given. The results shown in Figures 4.23 and 4.24, together with Table 4.16, therefore demonstrate that both the emergency-stop and the fault-recovery mechanisms acted as intended, preventing automatic resumption of movement and requiring the defined recovery procedure before operation could continue.

4.7 Integrated System Validation

The integrated validation was performed to determine if the subsystems examined separately in the earlier sections would be able to operate together correctly. The evaluation progressed from unloaded integration of the complete sensing and control chain for a single joint to unloaded simultaneous operation of the three actuated joints. A subsequent stage then introduced mechanical loading by coupling the user's lower limb to the prototype.

The tests emphasised the interaction between the subsystems rather than repeating the individual performance evaluations. Validation involved only the functional assessment of the proof of concept and was not a clinical evaluation.

4.7.1 Single-Joint Integration

The single-joint integration test was performed to check if the entire sensing and control chain could function together to achieve the desired joint movement under unloaded conditions. The knee was chosen as an illustrative joint. The commands were applied to the knee actuator via the complete control architecture described in Section 3.6. The circuit used for this test is shown in Appendix D, Figure D.1.

The prototype was arranged in the seated configuration shown in Figure 3.2a, but the user's lower limb was not mechanically coupled to the robotic structure during this test. The operator remained beside the prototype with the EMG sensors attached to the corresponding muscle groups and carried out a series of flexion and extension contractions separated by relaxed periods. Three flexion-extension cycles were performed, giving a total of six trials. Each directional contraction was held for approximately 4 s and was followed by a 3 s relaxed period. The robotic knee joint was initially positioned at approximately 90°.

The detected movement state, intensity, generated reference, assistance level, assisted target, safe target and encoder-derived joint position were recorded together with their timestamps. The step-based position, system state and safety status were also monitored to identify any abnormal behaviour during the experiment.

The recorded signals were examined to see if the detected intentions to flex and extend caused movement in the respective directions and whether the controller reacted correctly to changes in the movement intention. Particular attention was given to position holding, the resumption of movement and direction reversal, as described in the state-handling behaviour in Section 3.6. The detected movement intention, reference, safe target and measured joint position are shown in Figure 4.25.

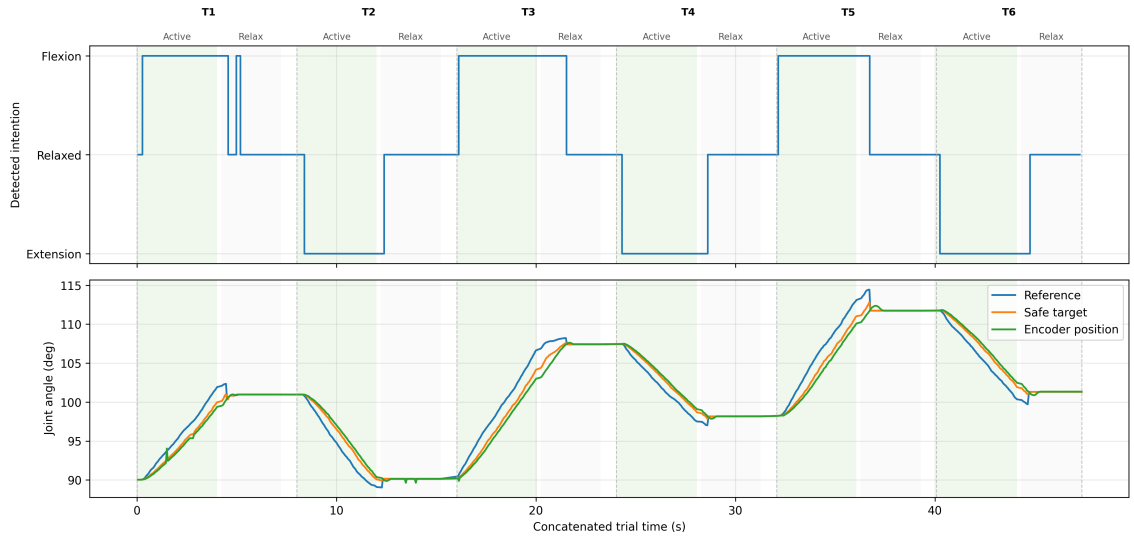


Figure 4.25: Knee movement during the integrated sensing and control test. T1, T3 and T5 correspond to knee flexion, whereas T2, T4 and T6 correspond to knee extension. Each active phase was followed by a relaxation period.

The response of the assistance level and the assisted angular target to the tracking error and to the intensity derived from the EMG during complete-chain operation was also investigated, with the results presented in Figure 4.26.

Position holding was evaluated during the final second of each relaxation period. The variation of the encoder-derived position during these intervals is shown in Figure 4.27. A maximum position variation of 0.10° was used as the acceptance criterion.

As illustrated in Figure 4.25, the detected intention alternated consistently between flexion, extension and relaxation over the three cycles, and all six active trials resulted in movement in the intended direction. The encoder-derived position increased during flexion and decreased during extension, as expected. Furthermore, the intention-detection stage clearly identified the flexion, extension and relaxed states throughout the experiment.

A small delay can be observed when transitioning between movement states, mainly due to the user's reaction time when initiating or terminating the requested muscle contraction. During the relaxation phase in T1, a brief flexion detection is also visible, corresponding to a flexion intention produced by the user outside the requested phase.

Once the directional intention was no longer detected, the controller established a holding position, which was maintained until a new directional intention was identified. Due to the delay during state transitions, position holding was assessed over the final second of each relaxation interval after this transition had settled. As illustrated in Figure 4.27, the greatest variation in encoder position observed across the six trials was merely 0.0047°. When a new directional intention was subsequently detected, reference generation resumed from the established holding position.

The results in Figure 4.26 show that the AAN controller remained active during the entire test. At the start of each active period, the level of assistance stayed at its set minimum value of

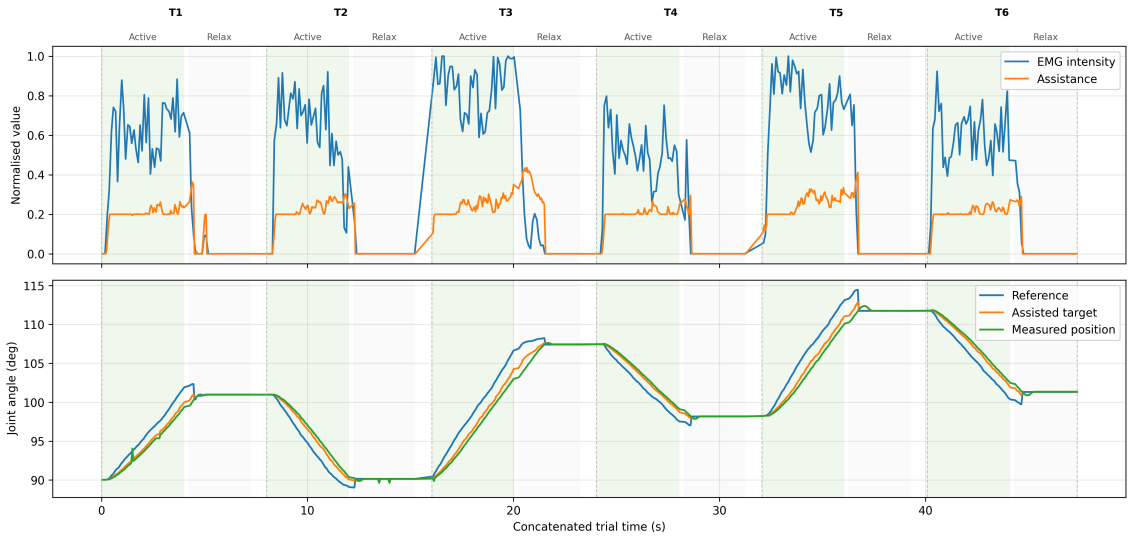


Figure 4.26: AAN behaviour during the integrated knee test. T1, T3 and T5 correspond to knee flexion, whereas T2, T4 and T6 correspond to knee extension.

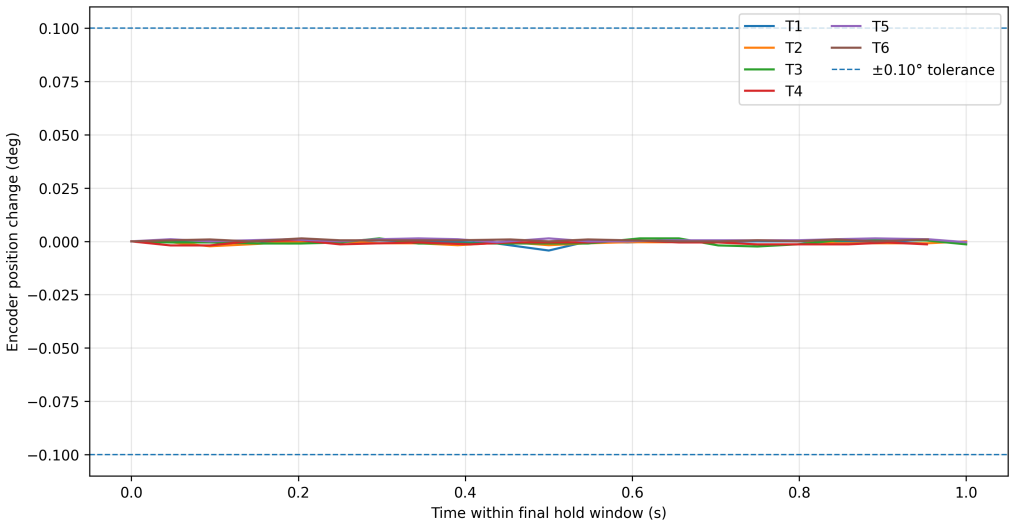


Figure 4.27: Encoder-derived knee-position variation during the final 1 s of the relaxation period following each single-joint trial.

0.20 since the tracking error was small, thus causing the initial plateau visible in the figure. As the reference position moved further away from the measured joint position, the tracking error increased and the assistance rose above this minimum, subsequently varying according to the combined effect of the tracking error and movement intensity. During relaxation, the assistance returned towards zero and the angular target converged to the holding position.

The entire sequence was carried out without errors, and the maximum absolute tracking error remained below 2°. Overall, the test confirmed that the complete single-joint control chain functioned properly and generated the desired knee movement, thus providing a foundation for the subsequent evaluation of multi-joint integration.

4.7.2 Multi-Joint Integration

The multi-joint integration test was performed in order to assess how the hip, knee and ankle joints functioned together. The prototype was arranged in the seated configuration shown in Figure 3.2a. The test checked whether the intended movements were correctly detected, whether they caused the expected robotic joint movements, and whether several joints could be operated at the same time through the complete sensing and control system.

The actuators, encoders, and EMG muscle pairs were connected in line with the architecture explained in Section 3.6.1. The full circuit employed for these tests is shown in Appendix D, Figure D.2. The prototype was operated under unloaded conditions, without the user's lower limb mechanically coupled to the robotic structure. The operator remained beside the system with the EMG sensors attached and generated the voluntary muscle contractions required for the corresponding movement intentions.

The experimental protocol consisted of nine trials. In the first six trials, the three joints were examined separately: hip flexion (T1), hip extension (T2), knee flexion (T3), knee extension (T4), ankle dorsiflexion (T5) and ankle plantarflexion (T6). In each trial, the operator was asked to generate the corresponding movement intention. Each active period lasted approximately 3 s and was followed by a 3 s relaxation period.

The final three trials evaluated simultaneous movement of multiple joints. Trial 7 combined hip flexion and knee extension, Trial 8 combined knee extension and ankle dorsiflexion, and Trial 9 combined hip flexion, knee extension and ankle dorsiflexion. These active periods lasted approximately 4 s and were followed by 4 s relaxation periods.

The detected movement intentions, movement intensities, generated references, assistance levels, assisted and safe targets, encoder-derived joint positions, system states and safety statuses were recorded throughout the session. The detected movement intentions are presented in Figure 4.28.

Figure 4.28 shows that the requested movement intentions were identified throughout the test, and all six individual trials produced movement of the intended joint in the expected direction. Some additional movement intentions were also detected throughout the protocol as a result of muscle activations produced by the operator outside the movement requested for the corresponding trial. In particular, additional ankle and knee intentions were observed in some trials.

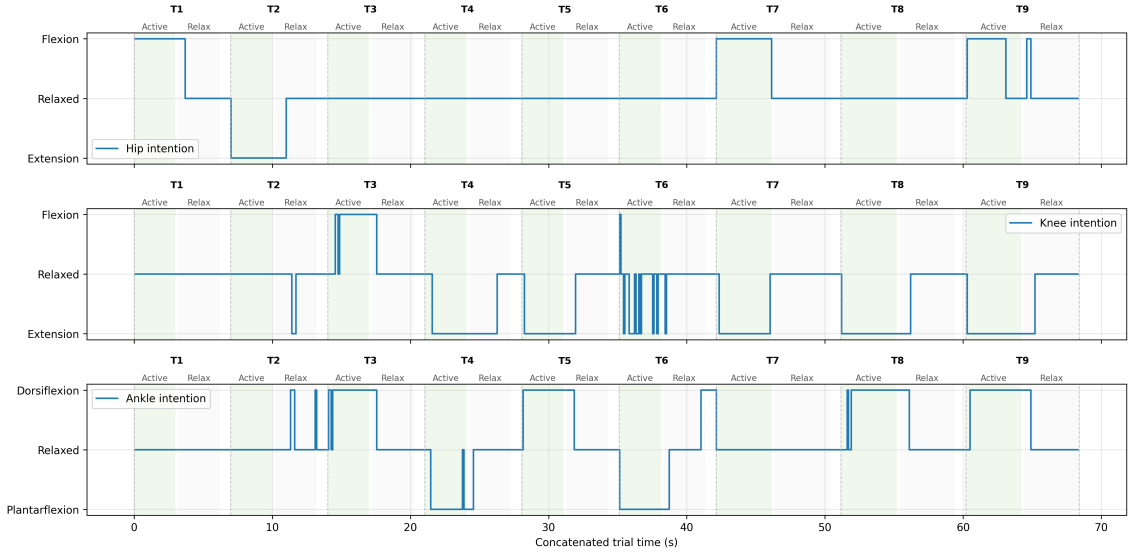


Figure 4.28: Detected movement intentions during the multi-joint integration test. T1-T6 correspond to the individual joint trials, whereas T7-T9 correspond to simultaneous multi-joint operation.

The final three trials were carried out to examine whether several actuators could respond at the same time to their individual movement intentions. Figure 4.29 shows the encoder-derived change in position of each joint relative to its position at the start of the corresponding active period.

All three of the simultaneous trials resulted in the expected patterns of movement. During T7, the hip flexed while the knee extended and the ankle remained approximately stationary. Trial 8 produced simultaneous knee extension and ankle dorsiflexion while the hip remained essentially unchanged. Lastly, Trial 9 demonstrated simultaneous movement of all three actuated joints, with hip flexion, knee extension and ankle dorsiflexion occurring during the same active period.

The performance of the AAN controller during the integrated session is shown in Figure 4.30. This evaluation was carried out with the aim of verifying that the assistance strategy continued to function when all three joint channels were integrated within the same system, rather than to repeat the isolated validation of the controller.

As shown in Figure 4.30, the generated references, assisted targets and measured joint positions followed the same general behaviour observed during the single-joint integration test. The assistance mechanism remained active for all three joints, and while the operator was producing the corresponding movement intentions, the measured positions followed the assisted movement targets.

Valid encoder feedback remained available from all three joints, and the session was completed without system faults. The test showed that the full sensing and control system could function with the three actuated joints incorporated, including cases where two or three joints moved at the same time. The additional intentions observed in some trials were associated with the operator's muscle activations rather than with incorrect channel association.

After the instrumented multi-joint evaluation in the seated configuration, a simpler functional

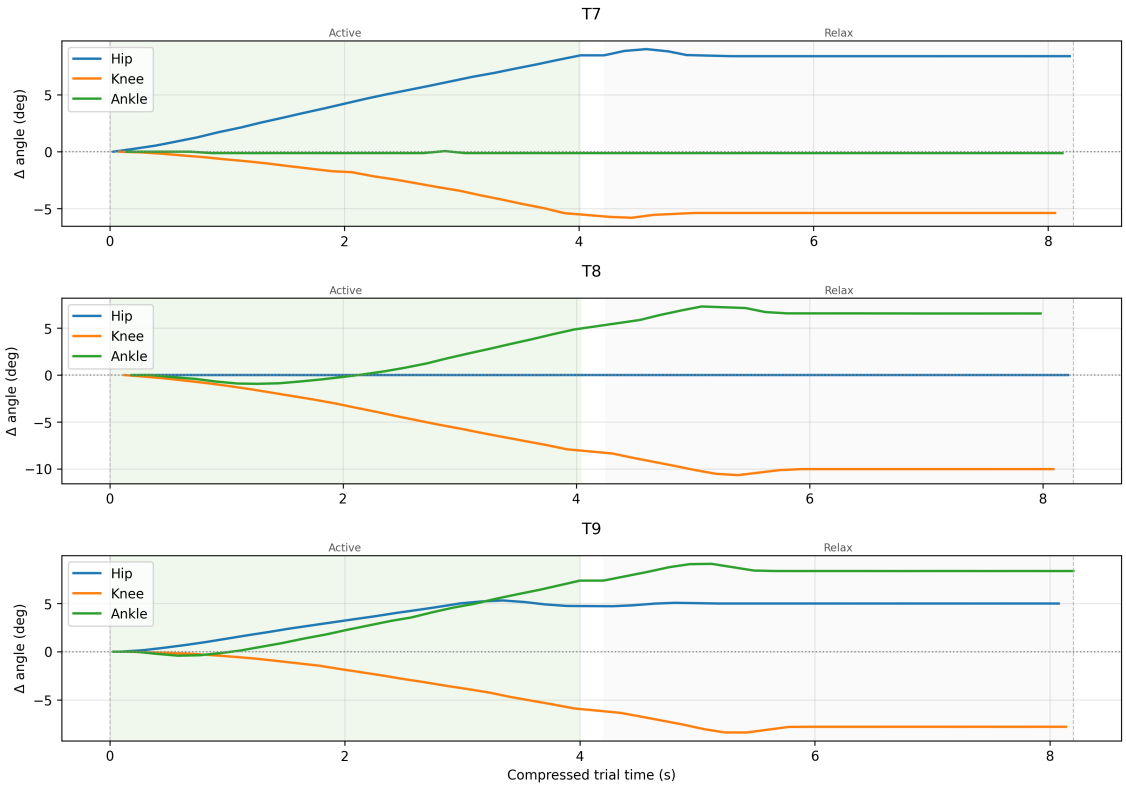


Figure 4.29: Joint-position changes during the simultaneous movement trials. T7 combined hip flexion and knee extension, T8 combined knee extension and ankle dorsiflexion, and T9 combined hip flexion, knee extension and ankle dorsiflexion.

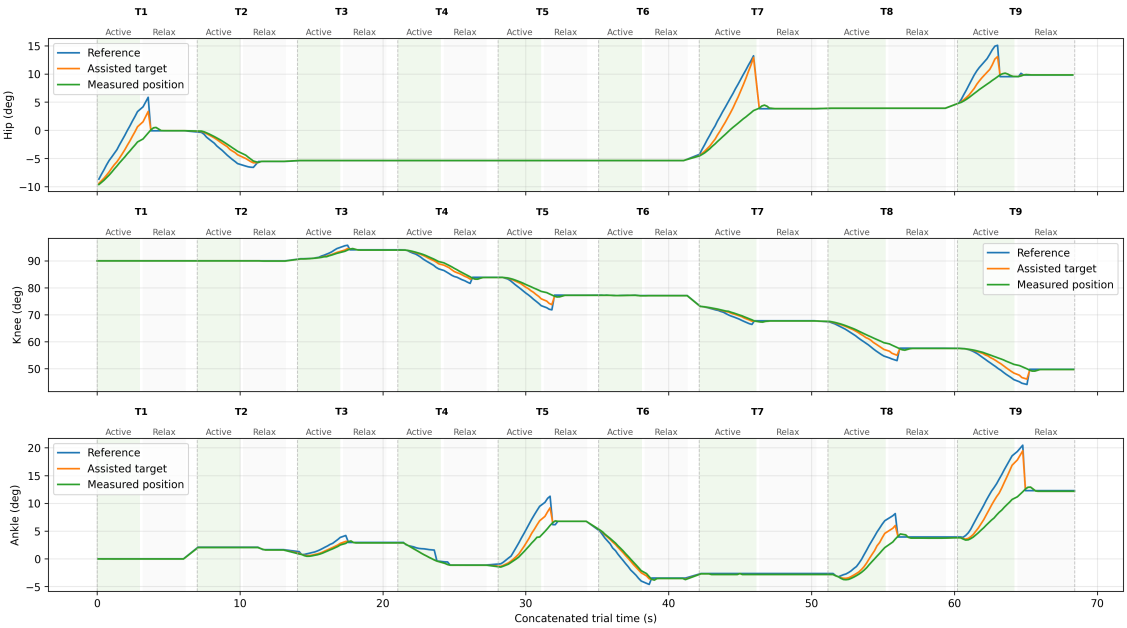


Figure 4.30: AAN behaviour during the multi-joint integration test.

check was carried out with the prototype arranged in the lying configuration shown in Figure 3.2b. Since the sensing, control and actuation functions had already been validated in detail, this additional check focused only on confirming that the change in physical arrangement did not affect the expected operation of the system. The intended joint movements were observed to be completed successfully, with no abnormal actuator behaviour or functional problems identified during this check.

4.7.3 System Evaluation Under Mechanical Loading

Following the unloaded integration tests, a final validation stage was initiated with the user's lower limb mechanically coupled to the prototype. Since the various subsystems and their integrated operation had already been validated under unloaded conditions, this stage was meant to look at how the system behaved under mechanical load and to reproduce more closely the conditions expected during actual use. The operator was positioned in the seated configuration shown in Figure 3.2a, and the lower limb was secured to the robotic structure using the implemented interfaces. The planned protocol first involved evaluating passive rehabilitation sequentially at the hip, knee and ankle, with one joint being tested at a time. After completion of these passive tests, active-assisted rehabilitation was also intended to be evaluated under the same loaded condition. The passive hip test was performed first.

During the test, structural failure occurred within the first few seconds of movement as the thigh began to be lifted from its supported resting position. Audible cracking was noted immediately before a fracture became apparent in the thigh guide plate, near the distal end of the reinforced region surrounding the hip motor shaft connection, as shown in Figure 4.31. No collision, voluntary resistance or other abnormal operating condition was observed before the failure.

No injury or other adverse consequence to the operator occurred. No software fault was triggered when the plate fractured, since the structural failure did not prevent the hip actuator from continuing its commanded rotation and the implemented monitoring mechanisms did not directly assess the structural integrity of the mechanical components. The hip motor therefore continued executing the commanded movement until the emergency-stop command was activated by the operator a few seconds later, stopping motor operation.

The failure occurred near the distal end of the reinforced region surrounding the hip motor shaft connection, in the part of the structure associated with the hip joint. As shown in Section 3.3.1, this joint has the highest estimated torque requirements of the three actuated joints. In addition, the guide plate was manufactured from 3D-printed PLA, and the fracture occurred close to the transition between the reinforced and non-reinforced regions of the component. The combination of these factors may therefore have contributed to the failure observed during the loaded test. Overall, the result showed that the thigh guide plate was not sufficiently robust for the evaluated loaded condition.

The loaded evaluation therefore identified an important mechanical limitation of the current prototype, as the structure did not demonstrate sufficient robustness under loading conditions. The failure of a load-bearing component showed that further mechanical development was required for

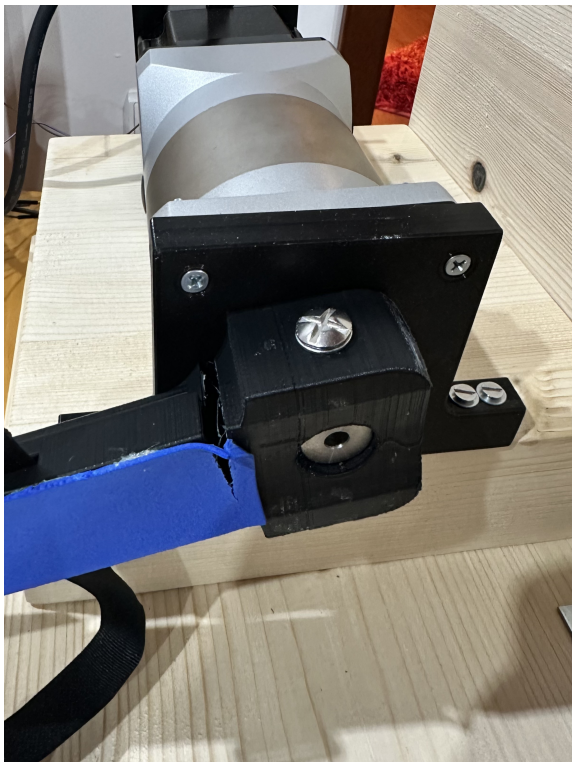


Figure 4.31: Thigh guide plate fracture observed during the loaded passive hip rehabilitation test.

the system to withstand the loads associated with its intended operation. The remaining passive tests of the knee and ankle, as well as the subsequent active-assisted evaluation, were therefore not performed.

4.8 Discussion

From a mechanical perspective, the adjustable thigh and shank sections matched the desired dimensions with only minor deviations from the design values. During the initial unloaded functional tests, the assembled structure also stayed stable. Most of the intended joint ROM was achieved, although two relevant geometric constraints were found. Hip extension was lower than the initial design value, but the negative range available was enough to hold the supported limb and was not regarded as critical for the rehabilitation tasks in question. Knee flexion was more obviously limited, reaching 117° rather than the intended 150°. This is the main geometric limitation of the final joint geometry, even though the range available still allows substantial knee movement for seated and lying exercises.

The actuation and joint-position results were consistent across the three joints. The actuators reached the requested positions, while the encoder-derived joint positions remained close to the step-based estimates, with only small tracking and stationary-position errors. This agreement indicates that the actuator operation and the implemented position-control method were able to drive the joints to the intended positions with good consistency. One practical limitation remains

at system start-up, since the joint position cannot be fully recovered after power-up unless the system is placed in a known initial position.

The rehabilitation control modes operated in accordance with their intended function. In passive rehabilitation, the prescribed trajectories and repetitions were carried out successfully, with low tracking lag even at the highest movement speed. For active-assisted rehabilitation, the EMG processing chain provided the information required by the controller. Calibration clearly distinguished resting from active muscle conditions, flexion and extension were consistently identified, and the estimated movement intensity increased with greater voluntary effort. The AAN controller increased the assistance as the directional tracking error rose and reduced it when a higher voluntary contribution was detected. The target position therefore varied between the measured position and the generated reference according to the user's contribution and the tracking condition.

The safety evaluation showed that the implemented software mechanisms responded correctly to the tested abnormal conditions. The limits on joint position and speed restricted commands that exceeded the configured limits, the loss of communication stopped the generation of the normal reference and enabled position holding, and persistent encoder or tracking faults stopped the system from continuing to operate. The tests involving emergency stop and recovery also revealed that movement could not be restarted automatically following a serious condition. These mechanisms provide several layers of protection within the control architecture, although they do not replace independent mechanical or hardware safety measures.

The integrated tests were particularly important because they examined how the previously validated subsystems interacted. In the single-joint experiment, which was performed under unloaded conditions, the complete chain from EMG acquisition and intention detection to reference generation, assistance, motor actuation and encoder feedback produced the expected knee movements. The subsequent three-joint test showed that the same architecture could operate with the hip, knee and ankle integrated, including simultaneous movement of two and three joints in the seated configuration. An additional unloaded functional check in the lying configuration also showed that the system could execute the intended joint movements in this arrangement, although this check was not subjected to the same instrumented analysis as the seated test. During these active-assisted tests, the operator remained beside the system and generated the required muscle activations, while the corresponding movements were produced by the unloaded robotic joints. Additional intentions were detected in some trials due to the operator's muscle activations outside the requested movement rather than incorrect measurements.

The subsequent loaded evaluation revealed an important mechanical limitation that had not been identified during the preceding unloaded tests. The fracture of the thigh guide plate during the first passive hip movement showed that the current structure did not provide sufficient robustness under loaded conditions. The high mechanical demands associated with the hip joint, the transition between the reinforced and non-reinforced regions of the guide plate, and the use of 3D-printed PLA may all have contributed to the observed failure. This result indicates that further mechanical development is required for the prototype to withstand the loads associated with its intended operation.

A practical limitation was observed in the acquisition of weaker EMG signals, since a sufficiently pronounced increase in the acquired EMG signal was sometimes only obtained when the healthy operator performed stronger voluntary contractions. However, this does not necessarily exclude the use of the proposed approach in users with motor impairments, particularly because the calibration is performed individually for each muscle. Further evaluation with the target population is still required to determine whether sufficiently distinguishable muscle activity can be acquired reliably.

Overall, the development and validation outcomes address the main objectives established in Section 1.3. The actuation, joint-position sensing, EMG-based intention detection, passive and active-assisted control strategies, safety mechanisms and their integration within the complete control architecture all operated as intended under the evaluated conditions. The unloaded integrated tests further showed that these functions could operate together across the three robotic joints, including simultaneous multi-joint movement. When mechanical loading was subsequently introduced, the limitation identified was associated with the structural robustness of the system rather than with the implemented sensing or control functions. The results therefore support the functional feasibility of the overall system architecture, while showing that further mechanical development and subsequent loaded validation are required before the prototype can operate as intended under rehabilitation loads.

4.9 Summary

This chapter presented the experimental validation of the developed robotic lower-limb rehabilitation support system. The evaluation adopted a step-by-step method, starting with the separate mechanical, actuation, sensing, control and safety functions before progressing to unloaded integrated system testing and, finally, to a loaded evaluation. The aim of the validation was to examine the functional behaviour of the proof-of-concept prototype and not to judge its clinical effectiveness.

The mechanical evaluation showed that the adjustable thigh and shank sections closely matched the intended dimensions and that the assembled structure remained stable during the initial unloaded testing. The required ankle and hip ROM and knee extension were achieved, although knee flexion was limited to 117°. The three actuator assemblies functioned consistently, and the encoder-processing system was able to accurately follow motor rotation over several revolutions. Step-based and encoder-derived joint positions also remained in close agreement.

The EMG-based processing successfully supported calibration, movement-state classification and movement-intensity estimation. The relaxed, flexed and extended states were consistently identified, and the estimated level of movement increased as voluntary effort increased. Under unloaded conditions, the desired behaviour was achieved in both rehabilitation modes: in the passive mode, the prescribed cyclic trajectories were generated, and in the active-assisted mode, the movement reference and the assistance were adjusted according to the detected intention, tracking

error and level of voluntary contribution. Also, the safety mechanisms reacted correctly when the tested operating limits and fault conditions were encountered.

Finally, the unloaded integrated tests showed that the complete sensing and control architecture could operate successfully across the three robotic joints, including simultaneous multi-joint movement. When the evaluation was subsequently extended to loaded operation, the test revealed an important structural limitation through the fracture of the thigh guide plate. The results therefore demonstrated the functional operation and integration of the implemented sensing, actuation and control functions, while showing that further mechanical development is required before the prototype can provide the structural robustness necessary for loaded rehabilitation.

Chapter 5

Conclusions and Future Work

5.1 General Conclusions

The main objective of this dissertation was to design, develop and experimentally evaluate an adjustable robotic lower-limb rehabilitation support system intended for rehabilitation in seated and lying positions. As a result, an integrated proof-of-concept prototype for one lower limb was obtained, the prototype having three actuated joints located at the hip, knee and ankle. The final system combined the mechanical structure, actuation, joint-position and EMG sensing, rehabilitation control, safety functions and a desktop application within a common architecture.

The mechanical development was guided by the biomechanical and anthropometric requirements identified during the initial stages of the work. In order to cover the chosen range of anthropometric measurements, adjustable parts were provided for both the thigh and the shank, and the three robotic joints allowed movement in the sagittal plane of the lower limb. The actuator assemblies were chosen on the basis of the estimated torque needs of the hip, knee and ankle joints, and independent sensing of joint position was achieved by means of magnetic absolute encoders.

Mass and cost were also considered throughout the development of the prototype. The main components associated with the moving part of the system had a combined mass of 4.367 kg, excluding the stationary hip-side structure and components that are independently supported and therefore do not contribute to the mass carried by the user's lower limb. The main components included in the cost assessment had a combined cost of 685.72 €. These values characterise the final proof-of-concept configuration and reflect the effort to limit the physical and financial requirements of the system while maintaining the functionality required for the intended rehabilitation tasks.

The sensing and control objectives were also addressed. Six EMG channels were used to obtain information from opposing muscle pairs associated with the three robotic joints. After individual calibration and normalisation, the obtained signals were processed to determine movement intention and estimate the level of voluntary muscle activation. Two types of rehabilitation modes were successfully introduced: in passive rehabilitation, the selected joint follows predetermined cyclic trajectories, while in active-assisted rehabilitation, the movement intention and intensity

together with the joint position information were used to generate the movement reference and to adjust the level of robotic assistance via the AAN controller.

The control architecture also incorporated software-based safety mechanisms to supervise joint and speed limits, communication between the controllers, encoder operation, actuator tracking and emergency-stop conditions. Moreover, a desktop application was created to offer a central interface for EMG calibration, rehabilitation configuration, session control and system monitoring. As a result, the main functions of the prototype could be operated via one interface rather than by interacting directly with the embedded controllers.

The experimental evaluation showed that the main sensing, actuation, control and safety functions developed throughout the dissertation could operate individually and as part of the complete system. The integrated tests further demonstrated the complete sensing and control chain from EMG acquisition and intention detection to reference generation, robotic assistance, actuator movement and encoder feedback. During these evaluations, the hip, knee and ankle joints were operated together, including simultaneous multi-joint movement. An additional unloaded functional check in the lying configuration also confirmed that the system continued to operate as expected in this arrangement, with the intended joint movements being successfully performed and no functional problems observed. When the evaluation was subsequently extended to loaded operation, the assessment revealed an important mechanical limitation, as the thigh guide plate fractured while the operator's lower limb was mechanically coupled to the prototype. This result showed that, although the implemented sensing and control functions had operated as intended during the preceding evaluations, further mechanical development is required for the system to provide the structural robustness needed for loaded rehabilitation.

Overall, the main development and functional-validation objectives established for this dissertation were achieved at the proof-of-concept level. The results demonstrate the functional feasibility of the proposed system architecture and support the continued development of the prototype. However, the structural limitation identified during loaded operation shows that further mechanical development and validation are required before the system can be used as intended with a user's lower limb mechanically coupled to the prototype.

5.2 Limitations

Although the main functions of the prototype were validated under the conditions described in Chapter 4, some limitations remain. These should be considered in the context of its proof-of-concept nature and its intended use in seated and lying rehabilitation.

The mechanical structure was developed for a single right lower limb and provides three actuated degrees of freedom in the sagittal plane, allowing hip and knee flexion-extension and ankle dorsiflexion-plantarflexion. The maximum knee flexion was also limited to 117°, below the initial design value of 150°, as reported in Section 4.2.2. Although this range may be enough for some of the intended rehabilitation exercises, it restricts the movements that can be performed with the prototype.

The structural components were mostly made of 3D-printed PLA, and the fixed supporting structure was made of wood. During loaded passive rehabilitation, the thigh guide plate fractured, showing that the current structural configuration did not provide sufficient robustness. No dedicated structural, fatigue or long-term strength analysis was performed, and the durability of the structure under repeated rehabilitation loads therefore remains unknown.

When the prototype is started, the joint-position sensing system needs an initial reference. As the AS5048B encoders are fitted ahead of the gearboxes and give absolute position information only for one revolution of each motor, it is not possible to recover the full joint position immediately after an unknown number of revolutions have taken place. It is therefore necessary to put the joints in known positions during the initialisation process in order to determine the corresponding angular offsets.

A limitation was also identified during the EMG tests, as weaker voluntary contractions did not always produce a sufficiently pronounced increase in the acquired EMG signal, and stronger contractions were sometimes required to obtain a clear response. This may partly be related to the relatively low muscular effort required from the healthy operator to perform the tested movements. Although the individual calibration procedure supports the use of user-specific activation ranges, the reliability of the acquired signals and the corresponding movement-intention detection has not yet been evaluated in users with motor impairments. Further evaluation in the target population is therefore required.

Finally, the implemented safety mechanisms are primarily software-based. The mechanical structure lacks physical joint stops capable of independently preventing movement beyond the permitted angular ranges. Furthermore, during the loaded evaluation, the structural failure did not trigger an automatic fault response because the hip actuator was still able to continue its commanded rotation and the monitoring mechanisms did not directly assess the structural integrity of the mechanical components. The movement therefore had to be stopped manually by the operator using the emergency-stop command.

5.3 Future Work

Future mechanical development should first address the structural limitation identified during the loaded evaluation. The use of higher-strength materials should be considered for components subjected to the greatest mechanical loads. Structural analysis and controlled load testing should then be carried out to evaluate the redesigned structure before further rehabilitation tests with the lower limb mechanically coupled to the prototype. Additional mechanical development should focus on increasing the knee flexion range, extending anthropometric adjustment to the hip and ankle joint positions, and adapting the foot platform to different users and both lower limbs.

Further evaluation of the EMG-based intention-detection method should be carried out with people presenting different degrees of motor impairment. Particular attention should be given to whether the acquired muscle activity can be reliably distinguished from the resting condition, as

well as to the reliability of the calibration, classification and intensity-estimation procedures in the target population.

Safety improvements should include physical joint stops, consideration of a dedicated hardware emergency-stop circuit, and additional measures for detecting or limiting abnormal mechanical loading or structural conditions that are not directly monitored by the current safety architecture.

Once the mechanical and safety limitations identified in this work have been addressed, the prototype should be evaluated with a broader range of healthy participants to assess adjustability, alignment, comfort, and usability under loaded conditions. Subsequent research involving the target population for rehabilitation could then be carried out.

References

Aliman, Norazam, Rizauddin Ramli, and Mohammad Soleimani Amiri. 2024. "Actuators and transmission mechanisms in rehabilitation lower limb exoskeletons: a review." *Biomedical Engineering / Biomedizinische Technik* 69 (4): 327–345. https://doi.org/10.1515/bmt-2022-0262. https://doi.org/10.1515/bmt-2022-0262.

Alt Murphy, Margit, Maria Munoz-Novoa, Charlotte Heremans, Meret Branscheidt, Rosa Cabanas-Valdés, Stefan T Engelter, Christina Kruuse, et al. 2025. "European Stroke Organisation (ESO) guideline on motor rehabilitation." *European Stroke Journal* 10 (4): 1160–1188. https://doi.org/10.1177/23969873251338142.

Amanov, Bekzat, and Sayat Ibrayev. 2024. "Enhancing Orthopedics and Sports Medicine with Lower Limb Exoskeleton Control in Rehabilitation Using Deep Learning Based Electromyography Signal Classification." *Retos* 61:616–625. https://doi.org/10.47197/retos.v61.109799. https://revistaretos.org/index.php/retos/article/view/109799.

ams AG. 2018. *AS5048A/AS5048B Magnetic Rotary Encoder (14-Bit Angular Position Sensor).* Datasheet, version 1-11. https://www.mouser.com/datasheet/2/588/AS5048_DS000298_4_00-2324531.pdf.

Andrade, Ricardo Luís, Joana Figueiredo, Pedro Fonseca, João P. Vilas-Boas, Miguel T. Silva, and Cristina P. Santos. 2024. "Human-Robot Joint Misalignment, Physical Interaction, and Gait Kinematic Assessment in Ankle-Foot Orthoses" [in en]. *Sensors* 24, no. 1 (January): 246. ISSN: 1424-8220. https://doi.org/10.3390/s24010246. https://www.mdpi.com/1424-8220/24/1/246.

Baud, Romain, Ali Reza Manzoori, Auke Ijspeert, and Mohamed Bouri. 2021. "Review of Control Strategies for Lower-Limb Exoskeletons to Assist Gait." *Journal of NeuroEngineering and Rehabilitation* 18 (1): 119. https://doi.org/10.1186/s12984-021-00906-3. https://doi.org/10.1186/s12984-021-00906-3.

Betts, J. Gordon, Kelly A. Young, James A. Wise, Eddie Johnson, Brandon Poe, Dean H. Kruse, Oksana Korol, Jody E. Johnson, Mark Womble, and Peter DeSaix. 2022. *Anatomy and Physiology 2e.* Houston, Texas: OpenStax. https://openstax.org/books/anatomy-and-physiology-2e/pages/11-6-appendicular-muscles-of-the-pelvic-girdle-and-lower-limbs.

Cieza, Alarcos, Kate Causey, Kaloyan Kamenov, Sarah Wulf Hanson, Somnath Chatterji, and Theo Vos. 2020. "Global estimates of the need for rehabilitation based on the Global Burden of Disease study 2019: a systematic analysis for the Global Burden of Disease Study 2019." *The Lancet* 396 (10267): 2006–2017. https://doi.org/10.1016/S0140-6736(20)32340-0. https://www.thelancet.com/journals/lancet/article/PIIS0140-6736(20)32340-0/fulltext.

Cutler, Hannah R., and Emma Hodson-Tole. 2022. "The Repeatability of Neuromuscular Activation Strategies Recorded in Recreationally Active Individuals During Cycling." *European Journal of Applied Physiology* 122 (4): 1045–1057. https://doi.org/10.1007/s00421-022-04899-2. https://pmc.ncbi.nlm.nih.gov/articles/PMC8927038/.

Dynamics Research Corporation. 1992. *Techniques for Digitizing Rotary and Linear Motion.* 4th ed. Wilmington, MA: Dynamics Research Corporation. https://irtfweb.ifa.hawaii.edu/~tcs3/tcs3/0306_conceptual_design/Docs/05_Encoders/encoder_primer.pdf.

Falkowski, Piotr, Krzysztof Zawalski, Jan Oleksiuk, Bazyli Leczkowski, Zbigniew Pilat, Mehmet Emin Aktan, Erhan Akdogan, et al. 2024. "Systematic Review of Mechanical Designs of Rehabilitation Exoskeletons for Lower-Extremity" [in en]. *Archive of Mechanical Engineering* 71 (4): 621–644. ISSN: 0004-0738. https://doi.org/10.24425/ame.2024.152944.

Fang, Yifan, Bingkai Hou, Xiuyuan Wu, Yuntian Wang, Keisuke Osawa, and Eiichiro Tanaka. 2023. "A Stepper Motor-Powered Lower Limb Exoskeleton with Multiple Assistance Functions for Daily Use by the Elderly." *Journal of Robotics and Mechatronics* 35 (3): 601–611. https://doi.org/10.20965/jrm.2023.p0601.

Feigin, Valery L, Michael Brainin, Bo Norrving, Sheila O Martins, Jeyaraj Pandian, Patrice Lindsay, Maria F Grupper, and Ilari Rautalin. 2025. "World Stroke Organization: Global Stroke Fact Sheet 2025." *International Journal of Stroke* 20 (2): 132–144. https://doi.org/10.1177/17474930241308142.

Gordon, Claire C., Cynthia L. Blackwell, Bruce Bradtmiller, Joseph L. Parham, Patricia Barrientos, Stephen P. Paquette, Bradley D. Corner, et al. 2015. *2012 Anthropometric Survey of U.S. Army Personnel: Methods and Summary Statistics.* Technical report NATICK/TR-15/007. Natick, MA: U.S. Army Natick Soldier Research, Development and Engineering Center. https://tools.openlab.psu.edu/publicData/ANSURII-TR15-007.pdf.

Jiang, Chunyu, Junlong Xiao, Haochen Wei, Michael Yu Wang, and Chao Chen. 2024. "Review on Portable-Powered Lower Limb Exoskeletons" [in en]. *Sensors* 24, no. 24 (December): 8090. ISSN: 1424-8220. https://doi.org/10.3390/s24248090. https://www.mdpi.com/1424-8220/24/24/8090.

Kavalieros, Dimitrios, Evangelos Kapothanasis, Athanasios Kakarountas, and Thanasis Loukopoulos. 2022. "Methodology for Selecting the Appropriate Electric Motor for Robotic Modular Systems for Lower Extremities." *Healthcare* 10 (10): 2054. https://doi.org/10.3390/healthcare10102054. https://www.mdpi.com/2227-9032/10/10/2054.

Leerskov, Kasper S., Cindy J. H. Rikhof, Erika G. Spaich, Strahinja Dosen, Gerdienke B. Prange-Lasonder, Erik C. Prinsen, Johan S. Rietman, and Lotte N. S. Andreasen Struijk. 2024. "A Robot-Based Hybrid Lower Limb System for Assist-As-Needed Rehabilitation of Stroke Patients: Technical Evaluation and Clinical Feasibility." *Computers in Biology and Medicine* 179:108839. https://doi.org/10.1016/j.compbiomed.2024.108839.

Li, Xiaohong, Yanjin He, Dawu Wang, and Mohammad J. Rezaei. 2024. "Stroke rehabilitation: from diagnosis to therapy." *Frontiers in Neurology* 15. https://doi.org/10.3389/fneur.2024.1402729.

Lim, Seungbum, Woojin Kim, and Jungwook Suh. 2025. "Method for Estimating Physical Interaction Forces Using Human–Exoskeleton Kinematic Modelling and Energy Optimization" [in en]. *Journal of Computational Design and Engineering* 12, no. 2 (February): 138–153. ISSN: 2288-5048. https://doi.org/10.1093/jcde/qwaf009. https://academic.oup.com/jcde/article/12/2/138/7994431.

Luu, Duc, and Trung Nguyen. 2026. "Knowledge Frameworks in Lower Limb Rehabilitation Robots." *Journal of Robotics* 2026 (1): 4628010. https://doi.org/10.1155/joro/4628010. https://onlinelibrary.wiley.com/doi/abs/10.1155/joro/4628010.

Meng, Qingyun, Guanxin Liu, Xin Xu, Qiaoling Meng, Liang Qin, and Hongliu Yu. 2023. "A multi-degree-of-freedom reconfigurable ankle rehabilitation robot with adjustable workspace for post-stroke lower limb ankle rehabilitation." *Frontiers in Bioengineering and Biotechnology* 11. https://doi.org/10.3389/fbioe.2023.1323645. https://www.frontiersin.org/journals/bioengineering-and-biotechnology/articles/10.3389/fbioe.2023.1323645/full.

Miguel-Fernández, Jesús de, Joan Lobo-Prat, Erik Prinsen, Josep M. Font-Llagunes, and Laura Marchal-Crespo. 2023. "Control strategies used in lower limb exoskeletons for gait rehabilitation after brain injury: a systematic review and analysis of clinical effectiveness." *Journal of NeuroEngineering and Rehabilitation* 20:23. https://doi.org/10.1186/s12984-023-01144-5.

Morris, Leah, Richard S. Diteesawat, Nahian Rahman, Ailie Turton, Mary Cramp, and Jonathan Rossiter. 2023. "The State of the Art of Soft Robotics to Assist Mobility: A Review of Physiotherapist and Patient Identified Limitations of Current Lower-Limb Exoskeletons and the Potential Soft-Robotic Solutions." *Journal of NeuroEngineering and Rehabilitation* 20 (1): 18. https://doi.org/10.1186/s12984-022-01122-3. https://doi.org/10.1186/s12984-022-01122-3.

Neťuková, Slávka, Martin Bejtic, Christiane Malá, Lucie Horáková, Patrik Kutílek, Jan Kauler, and Radim Krupička. 2022. "Lower Limb Exoskeleton Sensors: State-of-the-Art." *Sensors* 22 (23): 9091. https://doi.org/10.3390/s22239091. https://doi.org/10.3390/s22239091.

Papazian, Christina, Nick A. Baicoianu, Keshia M. Peters, Heather A. Feldner, and Katherine M. Steele. 2021. "Electromyography Recordings Detect Muscle Activity Before Observable Contractions in Acute Stroke Care." *Archives of Rehabilitation Research and Clinical Translation* 3 (3): 100136. https://doi.org/10.1016/j.arrct.2021.100136.

Paquette, Steven P., and Joseph L. Parham. 2017. *2012 U.S. Army Anthropometric Working Databases (ANSUR II).* Memorandum for Record. Natick, MA: U.S. Army Natick Soldier Research, Development and Engineering Center.

Rodríguez-Fernández, Antonio, Joan Lobo-Prat, and Josep M. Font-Llagunes. 2021. "Systematic review on wearable lower-limb exoskeletons for gait training in neuromuscular impairments." *Journal of NeuroEngineering and Rehabilitation* 18:22. https://doi.org/10.1186/s12984-021-00815-5. https://pmc.ncbi.nlm.nih.gov/articles/PMC7852187/.

Santuz, Alessandro, Antonis Ekizos, Lars Janshen, Falk Mersmann, Sebastian Bohm, Vasilios Baltzopoulos, and Adamantios Arampatzis. 2018. "Modular Control of Human Movement During Running: An Open Access Data Set." *Frontiers in Physiology* 9:1509. https://doi.org/10.3389/fphys.2018.01509. https://pmc.ncbi.nlm.nih.gov/articles/PMC6216155/.

Sarkisian, Sergei V., Marshall K. Ishmael, and Tommaso Lenzi. 2021. "Self-Aligning Mechanism Improves Comfort and Performance With a Powered Knee Exoskeleton." *IEEE Transactions on Neural Systems and Rehabilitation Engineering* 29:629–640. ISSN: 1558-0210. https://doi.org/10.1109/TNSRE.2021.3064463. https://ieeexplore.ieee.org/document/9371725.

Seybold, Jonathan, André Bülau, Karl-Peter Fritz, Alexander Frank, Cor Scherjon, Joachim Burghartz, and André Zimmermann. 2019. "Miniaturized Optical Encoder with Micro Structured Encoder Disc." *Applied Sciences* 9 (3): 452. https://doi.org/10.3390/app9030452. https://doi.org/10.3390/app9030452.

Soucie, J. M., C. Wang, A. Forsyth, S. Funk, M. Denny, K. E. Roach, D. Boone, and The Hemophilia Treatment Center Network. 2011. "Range of motion measurements: reference values and a database for comparison studies." *Haemophilia* 17 (3): 500–507. https://doi.org/10.1111/j.1365-2516.2010.02399.x. https://onlinelibrary.wiley.com/doi/abs/10.1111/j.1365-2516.2010.02399.x.

SparkFun Electronics. *MyoWare 2 Muscle Sensor.* https://www.sparkfun.com/myoware-2-muscle-sensor.html.

Squartecchia, Simona, Marco Rabuffetti, Tiziana Lencioni, Johanna Jonsdottir, Alberto Marzegan, Pietro Di Bello, Indya Ceroni, Marianna Semprini, and Maurizio Ferrarin. 2026. "Mechanical stability of the interaction between a lower-limb rehabilitation exoskeleton and the user's body during functional tasks." *Frontiers in Bioengineering and Biotechnology* 14. https://doi.org/10.3389/fbioe.2026.1733173. https://www.frontiersin.org/journals/bioengineering-and-biotechnology/articles/10.3389/fbioe.2026.1733173/full.

StepperOnline. 2026a. "E Series NEMA 34 Stepper Motor Bipolar 1.8deg 4.8 Nm 6.0 A 86x86x80 mm 4 Wires – 34HE31-6004S." Accessed September 1, 2026. https://www.omc-stepperonline.com/e-series-nema-34-stepper-motor-bipolar-1-8deg-4-8-nm-679-87oz-in-6-0a-86x86x80mm-4-wires-34he31-6004s.

StepperOnline. 2026b. "EG Series Planetary Gearbox Gear Ratio 50:1 for NEMA 34 Stepper Motor – EG34-G50." Accessed June 9, 2026. https://www.omc-stepperonline.com/eg-series-planetary-gearbox-gear-ratio-50-1-backlash-20-arc-min-for-nema-34-stepper-motor-eg34-g50.

StepperOnline. 2026c. "NEMA 17 Stepper Motor L=39 mm Gear Ratio 20:1 MG Series Planetary Gearbox – 17HS15-1584S-MG20." Accessed June 9, 2026. https://www.omc-stepperonline.com/nema-17-stepper-motor-1-40mm-gear-ratio-20-1-mg-series-planetary-gearbox-17hs15-1584s-mg20.

StepperOnline. 2026d. "NEMA 23 Stepper Motor Bipolar L=56 mm with Gear Ratio 47:1 Planetary Gearbox – 23HS22-2804S-PG47." Accessed June 9, 2026. https://www.omc-stepperonline.com/nema-23-stepper-motor-bipolar-l-56mm-w-gear-ratio-47-1-planetary-gearbox-23hs22-2804s-pg47.

Tiboni, Monica, Alberto Borboni, Fabien Vérité, Chiara Bregoli, and Cinzia Amici. 2022. "Sensors and Actuation Technologies in Exoskeletons: A Review." *Sensors* 22 (3): 884. https://doi.org/10.3390/s22030884. https://doi.org/10.3390/s22030884.

Wang, Daoyu, Jicai Li, Zhuo Jian, Hao Su, Hongbo Wang, and Fanfu Fang. 2023. "Modeling and control of a bedside cable-driven lower-limb rehabilitation robot for bedridden individuals." *Frontiers in Bioengineering and Biotechnology* 11. https://doi.org/10.3389/fbioe.2023.1321905. https://www.frontiersin.org/journals/bioengineering-and-biotechnology/articles/10.3389/fbioe.2023.1321905/full.

Wang, Hongyao, Haifei Shen, Yi Han, Wenlu Zhou, and Junjie Wang. 2025. "Effect of robot-assisted training for lower limb rehabilitation on lower limb function in stroke patients: a systematic review and meta-analysis." *Frontiers in Human Neuroscience* 19. https://doi.org/10.3389/fnhum.2025.1549379. https://www.frontiersin.org/journals/human-neuroscience/articles/10.3389/fnhum.2025.1549379/full.

Wang, Xusheng, Guowei Liu, Yongfei Feng, Wei Li, Jianye Niu, and Zhongxue Gan. 2021. "Measurement Method of Human Lower Limb Joint Range of Motion Through Human-Machine Interaction Based on Machine Vision." *Frontiers in Neurorobotics* 15. https://doi.org/10.3389/fnbot.2021.753924. https://www.frontiersin.org/journals/neurorobotics/articles/10.3389/fnbot.2021.753924/full.

Wang, Zhiqiang, Jianhai Han, Bingjing Guo, Xiangpan Li, and Ganqin Du. 2024. "Structural design and research of a novel lower limb rehabilitation robot for human–robot coupling." *International Journal of Advanced Robotic Systems* 21 (2). https://doi.org/10.1177/17298806241238992. https://doi.org/10.1177/17298806241238992.

Winter, David. 2009. "Biomechanics and Motor Control of Human Movement, Fourth Edition" (September). https://doi.org/10.1002/9780470549148.ch5.

Wu, Renxiang, Mingyang Luo, Jiaming Fan, Jingting Ma, Naiwen Zhang, Jianjun Li, Qiuyuan Li, Fei Gao, and Guo Dan. 2024. "A compact motorized end-effector for ankle rehabilitation training." *Frontiers in Robotics and AI* 11. https://doi.org/10.3389/frobt.2024.1453097. https://www.frontiersin.org/journals/robotics-and-ai/articles/10.3389/frobt.2024.1453097/full.

Wu, Zongpeng, Mingxing Yang, Yulei Xia, and Liwei Wang. 2023. "Mechanical Structural Design and Actuation Technologies of Powered Knee Exoskeletons: A Review" [in en]. *Applied Sciences* 13, no. 2 (January): 1064. ISSN: 2076-3417. https://doi.org/10.3390/app13021064. https://www.mdpi.com/2076-3417/13/2/1064.

Xu, Jiajun, Kaizhen Huang, Tianyi Zhang, Kai Cao, Aihong Ji, Linsen Xu, and Youfu Li. 2023. "A Rehabilitation Robot Control Framework with Adaptation of Training Tasks and Robotic Assistance." *Frontiers in Bioengineering and Biotechnology* 11. https://doi.org/10.3389/fbioe.2023.1244550. https://doi.org/10.3389/fbioe.2023.1244550.

Yao, Yumeng, Dongqing Shao, Marco Tarabini, Seyed Alireza Moezi, Kun Li, and Paola Saccomandi. 2024. "Advancements in Sensor Technologies and Control Strategies for Lower-Limb Rehabilitation Exoskeletons: A Comprehensive Review." *Micromachines* 15 (4): 489. https://doi.org/10.3390/mi15040489. https://doi.org/10.3390/mi15040489.

Yu, Hongfei, Siyuan Zheng, Jiantao Wu, Li Sun, Yongliang Chen, Shuo Zhang, and Zhongzhi Qin. 2023. "A New Single-Leg Lower-Limb Rehabilitation Robot: Design, Analysis and Experimental Evaluation." *Machines* 11 (4): 447. https://doi.org/10.3390/machines11040447. https://www.mdpi.com/2075-1702/11/4/447.

Zhang, Houqiang, Zhengwei Chen, Shufen Liu, Weihong Shi, Xingyu Cui, Wangshu Yuan, Runlin Shi, et al. 2026. "Trends of rehabilitation needs in 195 countries and regions from 1990 to 2021 and the impact of the COVID-19 pandemic on it: a systematic analysis of the Global Burden of Disease Study 2021." *International Journal of Surgery* 112 (1): 270–285. https://doi.org/10.1097/JS9.0000000000003486.

Appendix A

Calculation Details

A.1 Anthropometric Calculations

The reference thigh and shank lengths used in the mechanical design were estimated from the corresponding ANSUR II anatomical landmark heights according to

$$L_{\text{thigh}} = H_{\text{trochanterion}} - H_{\text{lateral femoral epicondyle}}, \tag{A.1}$$

$$L_{\text{shank}} = H_{\text{lateral femoral epicondyle}} - H_{\text{lateral malleolus}}. \tag{A.2}$$

A.2 Preliminary Joint Torque Calculations

For each lower-limb segment i, the segment mass and centre-of-mass distance were calculated using the anthropometric coefficients reported by Winter (2009) as

$$m_i = k_{m,i} M, \tag{A.3}$$

$$r_i = k_{r,i} L_i, \tag{A.4}$$

where M is the total body mass, L_i is the segment length, and $k_{m,i}$ and $k_{r,i}$ are the corresponding anthropometric coefficients.

Under the worst-case gravitational condition considered in Section 3.3.1, the torque produced by a mass m located at a perpendicular distance r from a joint axis is

$$\tau_g = mgr, \tag{A.5}$$

where $g = 9.81$ m/s^2.

The gravitational torque at the ankle was calculated as

$$\tau_{g,\text{ankle}} = m_f g r_f. \tag{A.6}$$

At the knee, the gravitational contributions of the shank and foot were considered:

$$\tau_{g,\text{knee}} = m_s g r_s + m_f g \left(L_s + r_f\right). \tag{A.7}$$

At the hip, the thigh, shank and foot were included:

$$\tau_{g,\text{hip}} = m_t g r_t + m_s g \left(L_t + r_s\right) + m_f g \left(L_t + L_s + r_f\right). \tag{A.8}$$

In addition to the gravitational contribution, an inertial contribution was estimated using the cubic trajectory described in Section 3.3.1. The trajectory profile was based on that adopted by Z. Wang et al. (2024) for hip and knee rehabilitation motion planning and was applied here to all three joints as a common basis for the preliminary torque estimation. For an angular displacement $\Delta\theta$ completed over a duration T, the trajectory was defined as

$$\theta(t) = \theta_0 + \Delta\theta \left[3\left(\frac{t}{T}\right)^2 - 2\left(\frac{t}{T}\right)^3\right]. \tag{A.9}$$

Differentiating twice with respect to time gives the angular acceleration:

$$\alpha(t) = \frac{6\Delta\theta}{T^2}\left(1 - \frac{2t}{T}\right). \tag{A.10}$$

The maximum absolute angular acceleration therefore occurs at the beginning and end of the trajectory and is given by

$$\alpha_{\max} = \frac{6|\Delta\theta|}{T^2}. \tag{A.11}$$

The complete sagittal-plane ranges of motion defined in Section 2.4 were used for the angular displacements. With a movement duration of $T = 2$ s, the values used were

$$\Delta\theta_{\text{hip}} = 150^\circ, \qquad \alpha_{\max,\text{hip}} = 3.927 \text{ rad/s}^2, \tag{A.12}$$

$$\Delta\theta_{\text{knee}} = 150^\circ, \qquad \alpha_{\max,\text{knee}} = 3.927 \text{ rad/s}^2, \tag{A.13}$$

$$\Delta\theta_{\text{ankle}} = 60^\circ, \qquad \alpha_{\max,\text{ankle}} = 1.571 \text{ rad/s}^2. \tag{A.14}$$

For the inertial estimate, each segment mass was considered to be concentrated at its corresponding centre of mass. The equivalent rotational inertia of a mass m_i located at a distance d_i from the joint axis was therefore approximated as

$$I_i = m_i d_i^2. \tag{A.15}$$

The equivalent inertia about the ankle was

$$I_{\text{eq,ankle}} = m_f r_f^2. \tag{A.16}$$

At the knee,

$$I_{\text{eq,knee}} = m_s r_s^2 + m_f \left(L_s + r_f\right)^2. \tag{A.17}$$

At the hip,

$$I_{\text{eq,hip}} = m_t r_t^2 + m_s \left(L_t + r_s\right)^2 + m_f \left(L_t + L_s + r_f\right)^2. \tag{A.18}$$

The maximum inertial torque for each joint was then estimated from

$$\tau_{\text{in},j} = I_{\text{eq},j} \alpha_{\text{max},j}, \tag{A.19}$$

where j represents the corresponding joint.

For the preliminary actuator sizing, the maximum gravitational and inertial contributions were added to obtain an upper-bound torque requirement:

$$\tau_{\text{prelim},j} = \tau_{g,j} + \tau_{\text{in},j}. \tag{A.20}$$

Since the maximum gravitational and inertial contributions do not necessarily occur at the same instant during an actual movement, this direct addition may overestimate the maximum torque occurring along a specific trajectory.

A.3 Gearbox Output Torque

The theoretical static output torque of each motor–gearbox assembly was estimated as

$$\tau_{\text{out}} = \tau_m i \eta, \tag{A.21}$$

where τ_m is the motor torque, i is the gear ratio and η is the gearbox efficiency.

A.4 Final Joint Torque Verification

After selection of the actuators and mechanical components, the torque calculations were repeated including the relevant masses of the robotic structure. The same gravitational and inertial calculation principles used in the preliminary estimation were retained, allowing the final actuator configuration to be evaluated using the masses of the actual moving components.

For the gravitational contribution, the masses of the thigh and shank structural plates were assumed to act at the same centre-of-mass distances as the respective anatomical segments. The foot-platform mass was considered to act at the same centre-of-mass distance as the foot. The

knee and ankle actuator assemblies were considered to be located at the corresponding robotic joint axes.

At the ankle, the gravitational torque was therefore calculated as

$$\tau^*_{g,\text{ankle}} = \left(m_f + m_{\text{fp}}\right) g r_f. \tag{A.22}$$

At the knee,

$$\tau^*_{g,\text{knee}} = \left(m_s + m_{\text{sh}}\right) g r_s + m_{\text{aa}} g L_s + \left(m_f + m_{\text{fp}}\right) g \left(L_s + r_f\right). \tag{A.23}$$

At the hip,

$$\begin{aligned} \tau^*_{g,\text{hip}} = {} & \left(m_t + m_{\text{th}}\right) g r_t + m_{\text{ka}} g L_t \\ & + \left(m_s + m_{\text{sh}}\right) g \left(L_t + r_s\right) + m_{\text{aa}} g \left(L_t + L_s\right) \\ & + \left(m_f + m_{\text{fp}}\right) g \left(L_t + L_s + r_f\right). \end{aligned} \tag{A.24}$$

The inertial contribution was recalculated using the same cubic trajectories and maximum angular accelerations defined in Section A.2. The additional moving robotic components were represented using the same concentrated-mass approximation.

At the ankle, the final equivalent inertia was

$$I^*_{\text{eq,ankle}} = \left(m_f + m_{\text{fp}}\right) r_f^2. \tag{A.25}$$

At the knee,

$$I^*_{\text{eq,knee}} = \left(m_s + m_{\text{sh}}\right) r_s^2 + m_{\text{aa}} L_s^2 + \left(m_f + m_{\text{fp}}\right) \left(L_s + r_f\right)^2. \tag{A.26}$$

At the hip,

$$\begin{aligned} I^*_{\text{eq,hip}} = {} & \left(m_t + m_{\text{th}}\right) r_t^2 + m_{\text{ka}} L_t^2 \\ & + \left(m_s + m_{\text{sh}}\right) \left(L_t + r_s\right)^2 + m_{\text{aa}} \left(L_t + L_s\right)^2 \\ & + \left(m_f + m_{\text{fp}}\right) \left(L_t + L_s + r_f\right)^2. \end{aligned} \tag{A.27}$$

The corresponding inertial torque was then calculated for each joint as

$$\tau^*_{\text{in},j} = I^*_{\text{eq},j} \alpha_{\text{max},j}. \tag{A.28}$$

Finally, the gravitational and inertial contributions were added to obtain the final upper-bound torque estimate:

$$\tau_{\text{final},j} = \tau^*_{g,j} + \tau^*_{\text{in},j}. \tag{A.29}$$

As in the preliminary calculation, this direct addition combines the maximum gravitational and inertial contributions even though they do not necessarily occur at the same instant. The resulting value therefore represents an upper-bound estimate for the simplified verification rather than the maximum torque expected along a specific movement trajectory.

Appendix B

Technical Drawings

This appendix presents the technical drawings of the main mechanical components developed in SolidWorks and used in the final prototype. The drawings are grouped according to the corresponding part of the mechanical structure.

B.1 Structural Plates and Foot Platform

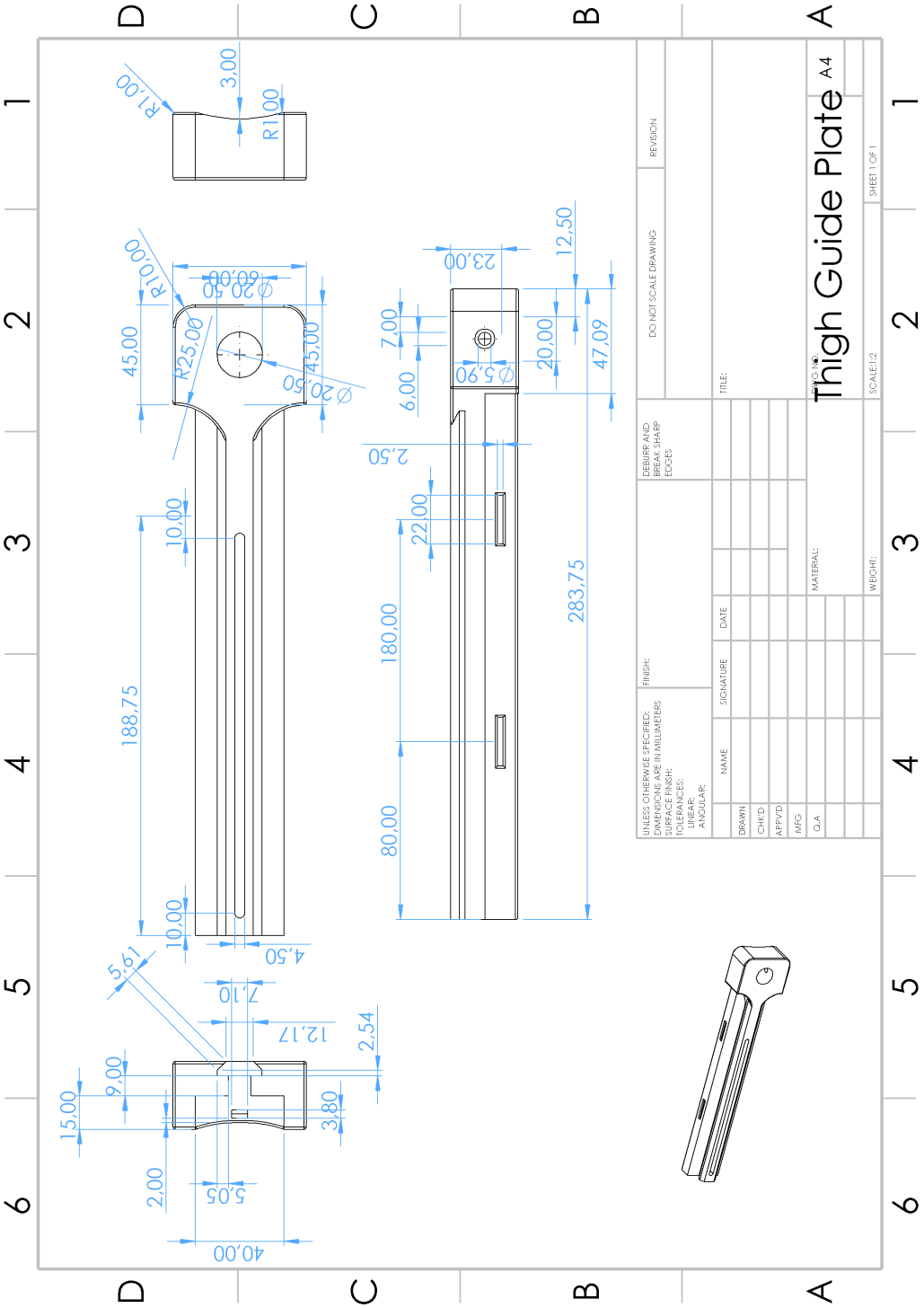


Figure B.1: Technical drawing of the thigh guide plate.

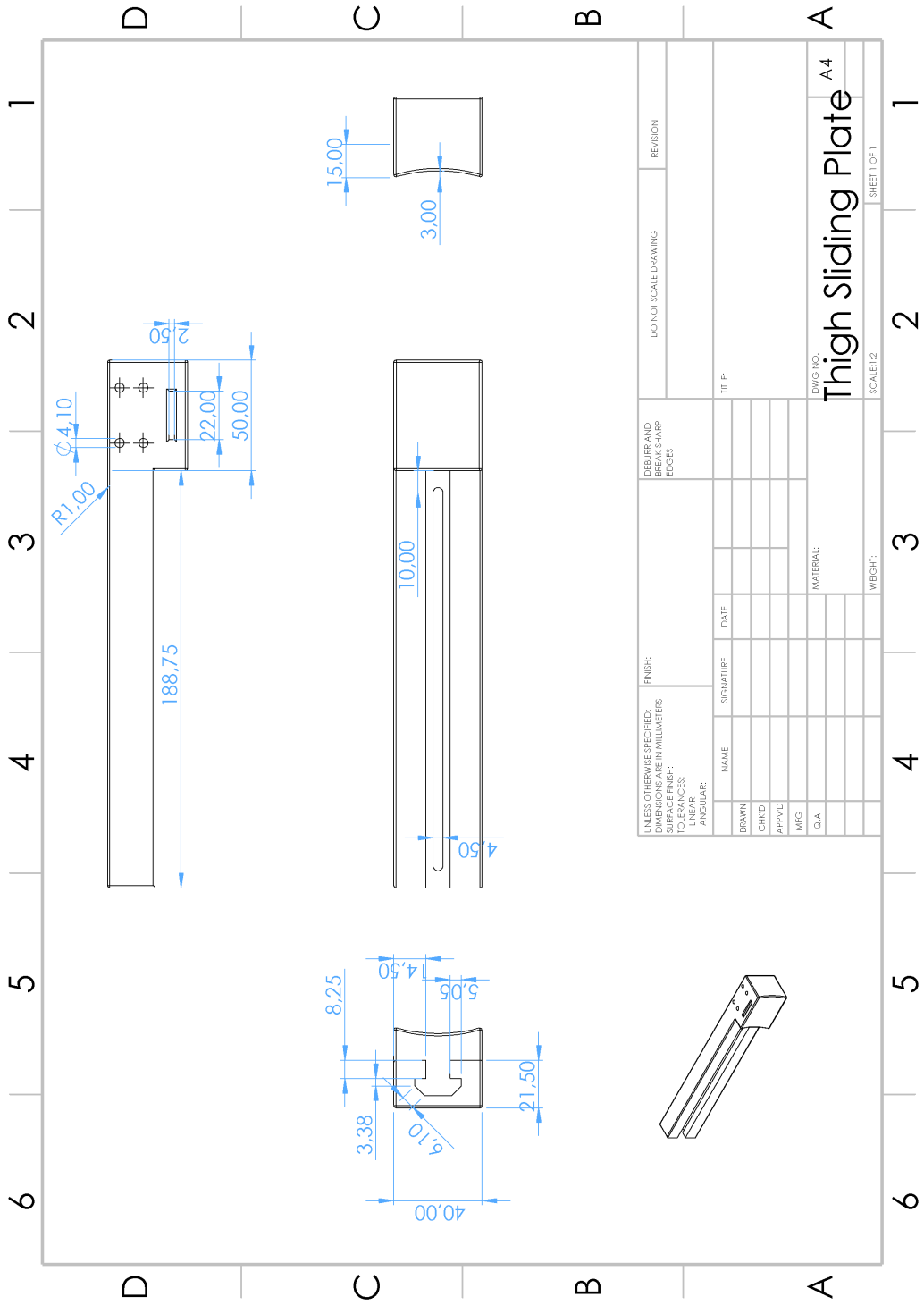


Figure B.2: Technical drawing of the thigh sliding plate.

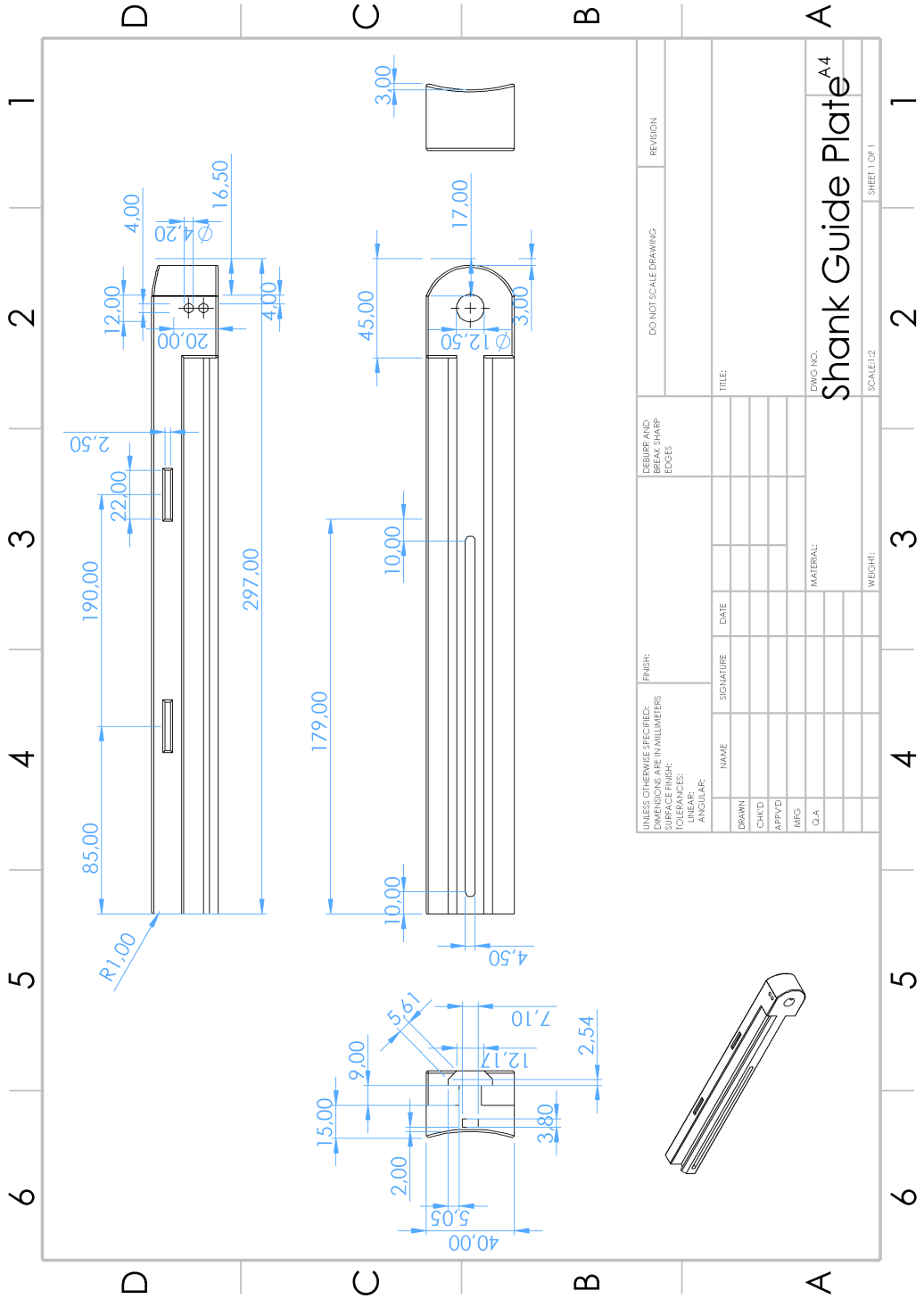


Figure B.3: Technical drawing of the shank guide plate.

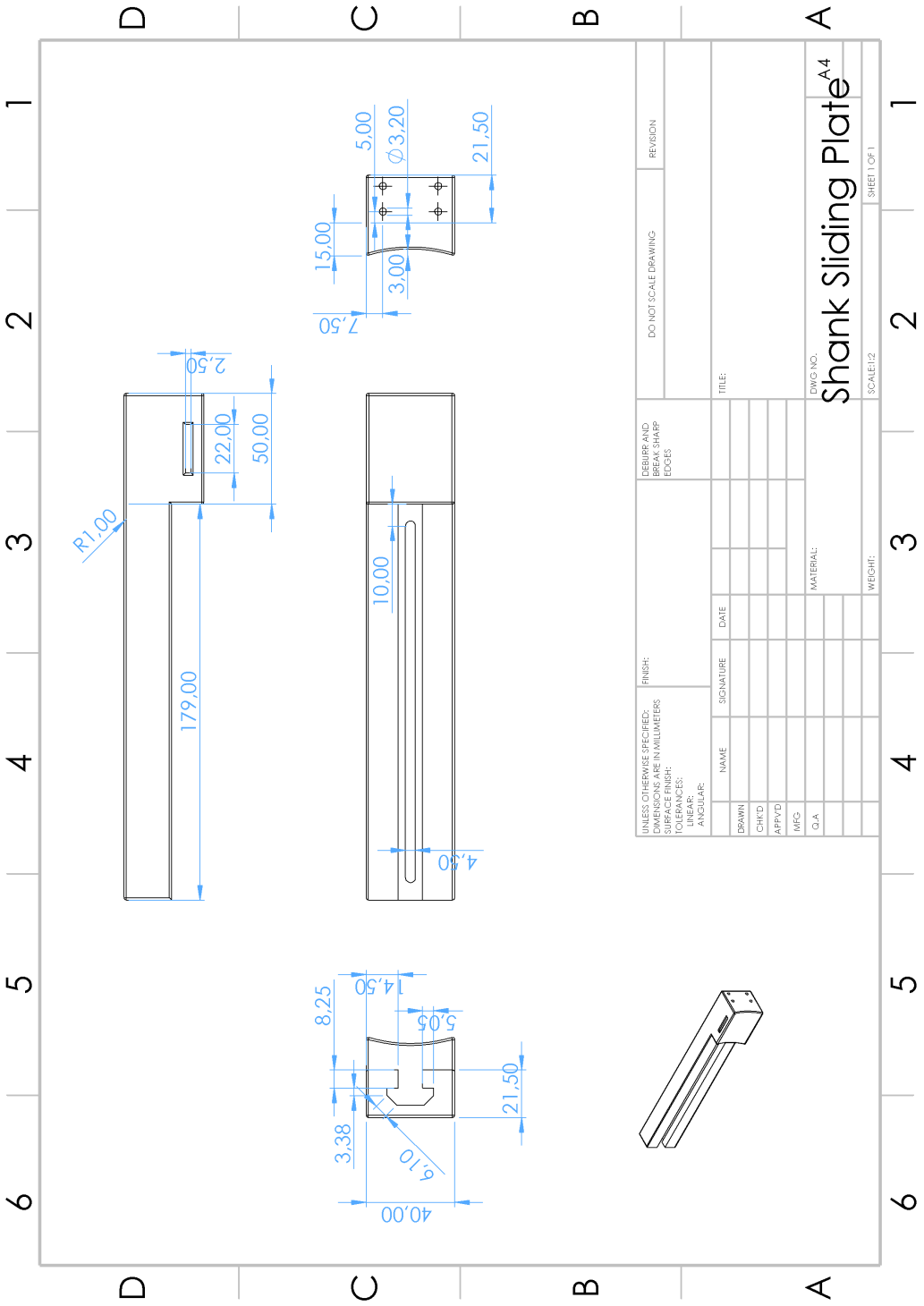


Figure B.4: Technical drawing of the shank sliding plate.

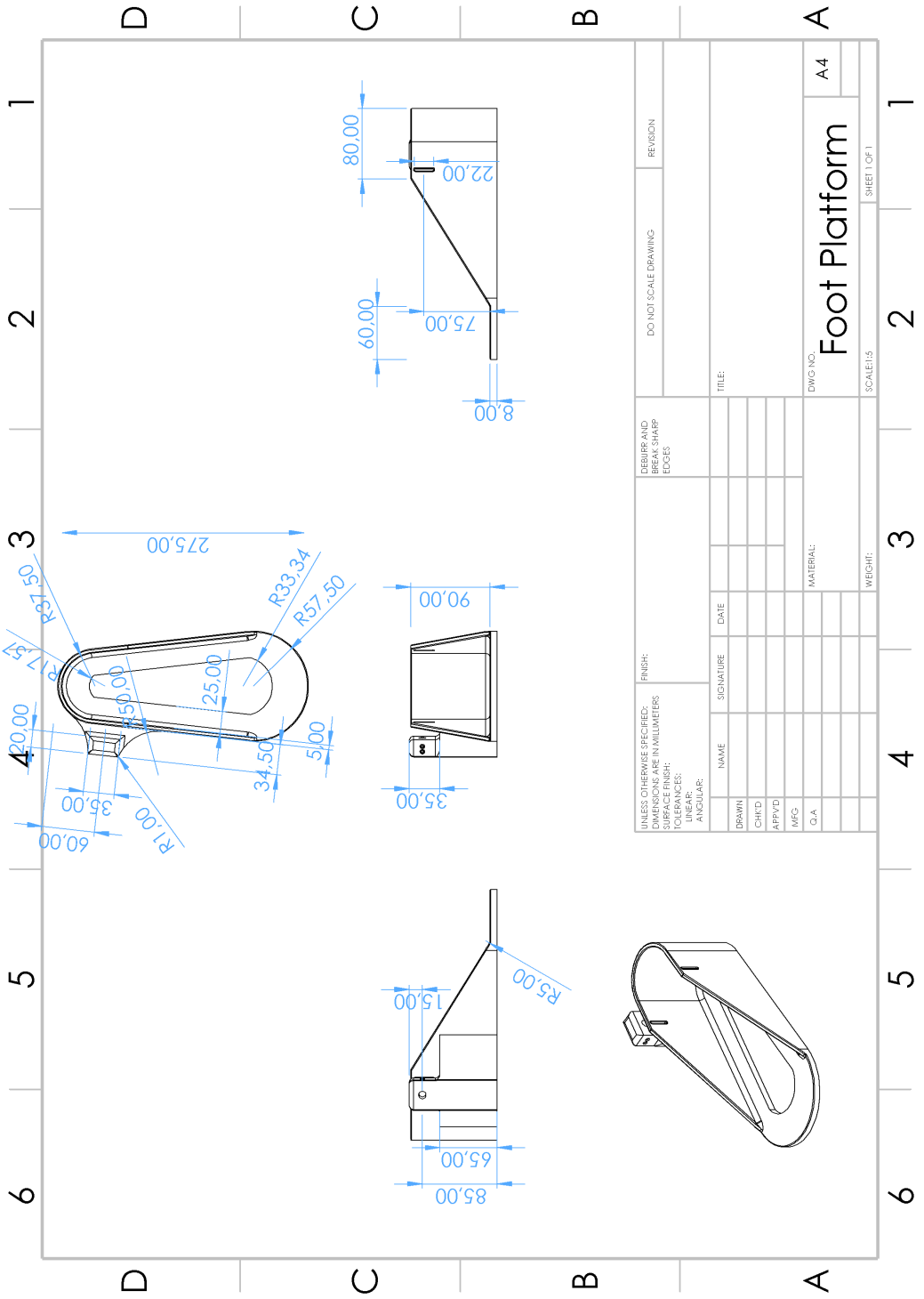


Figure B.5: Technical drawing of the foot platform.

B.2 Motor Supports

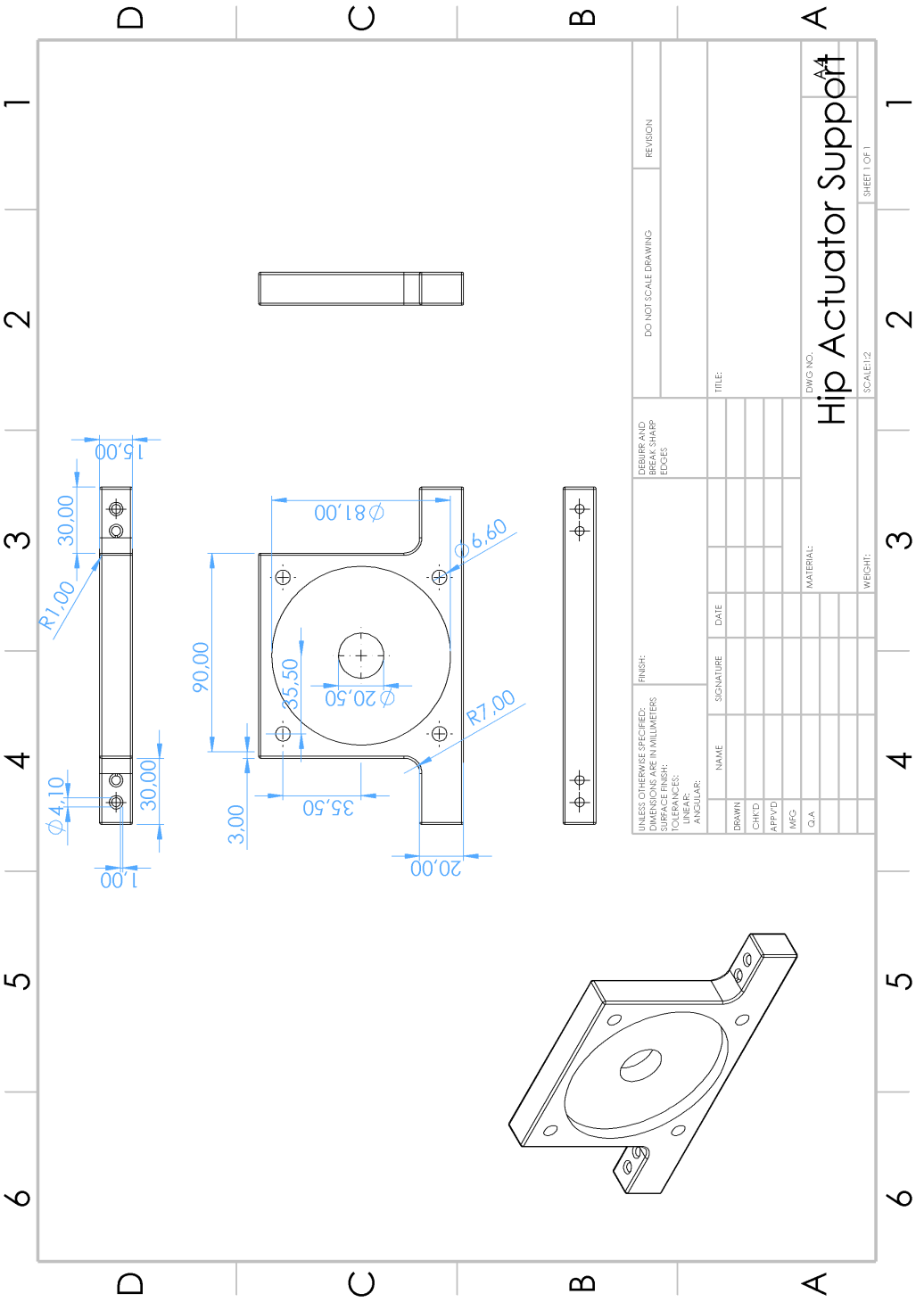


Figure B.6: Technical drawing of the hip motor support.

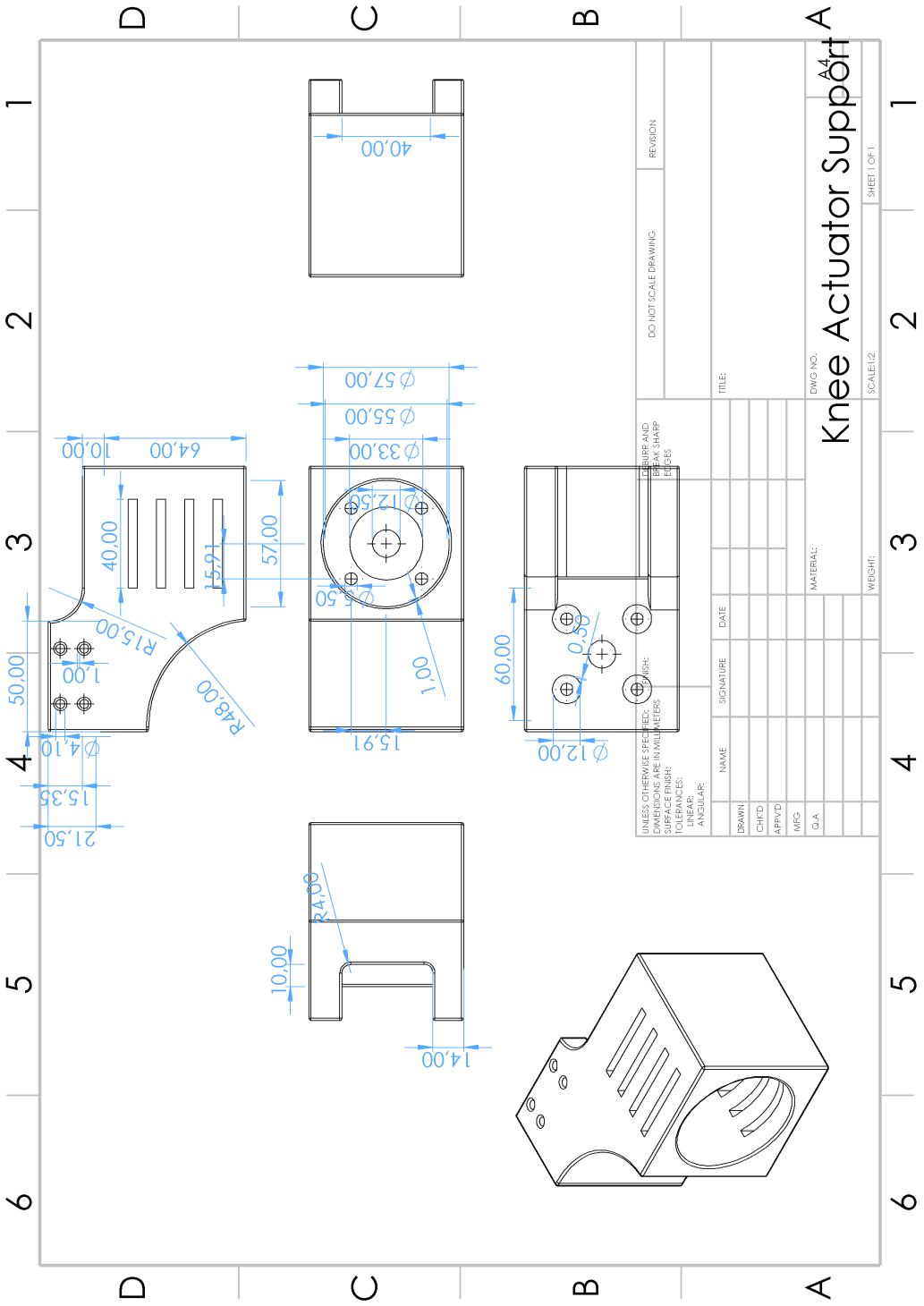


Figure B.7: Technical drawing of the knee motor support.

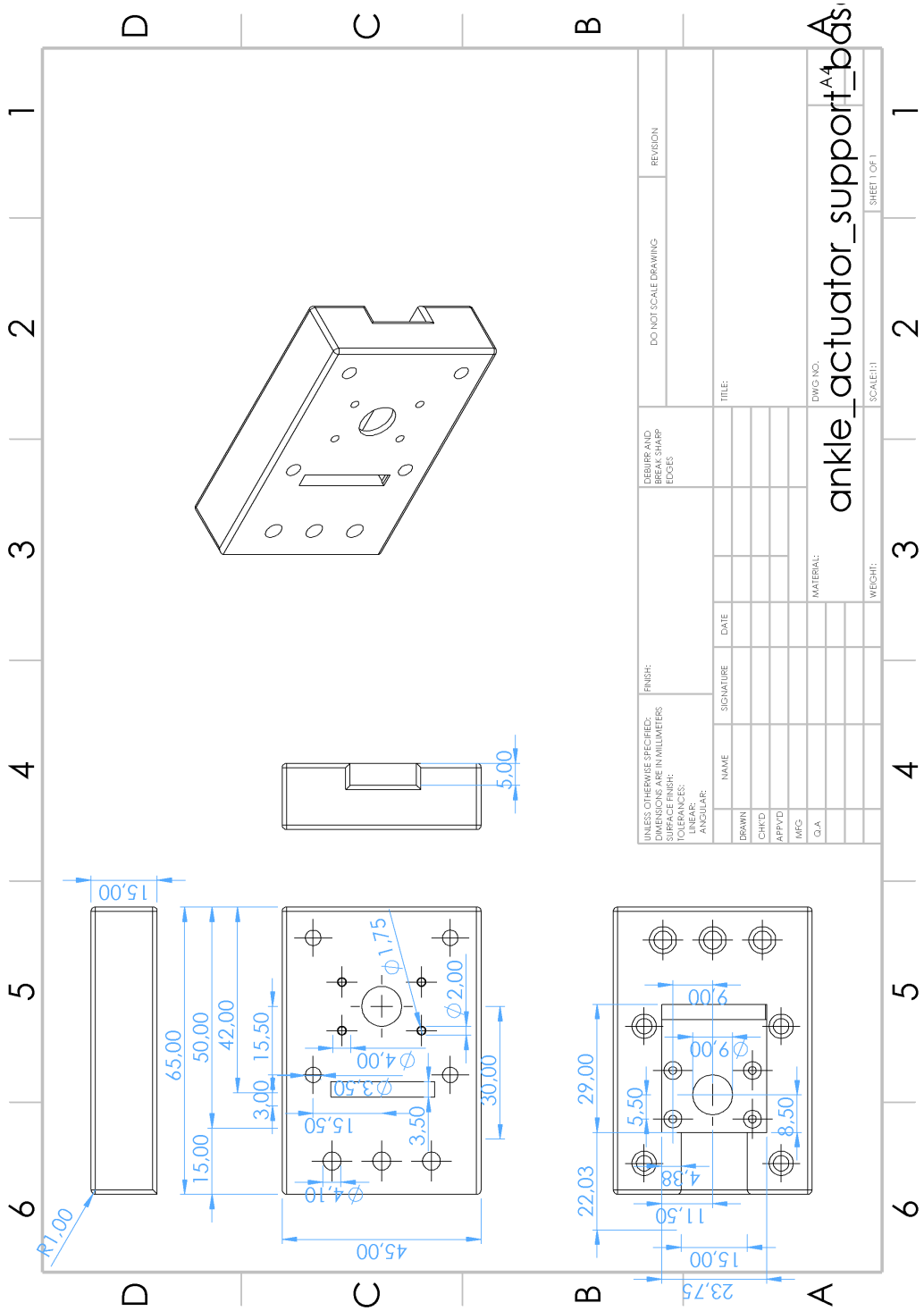


Figure B.8: Technical drawing of the ankle motor–encoder support base.

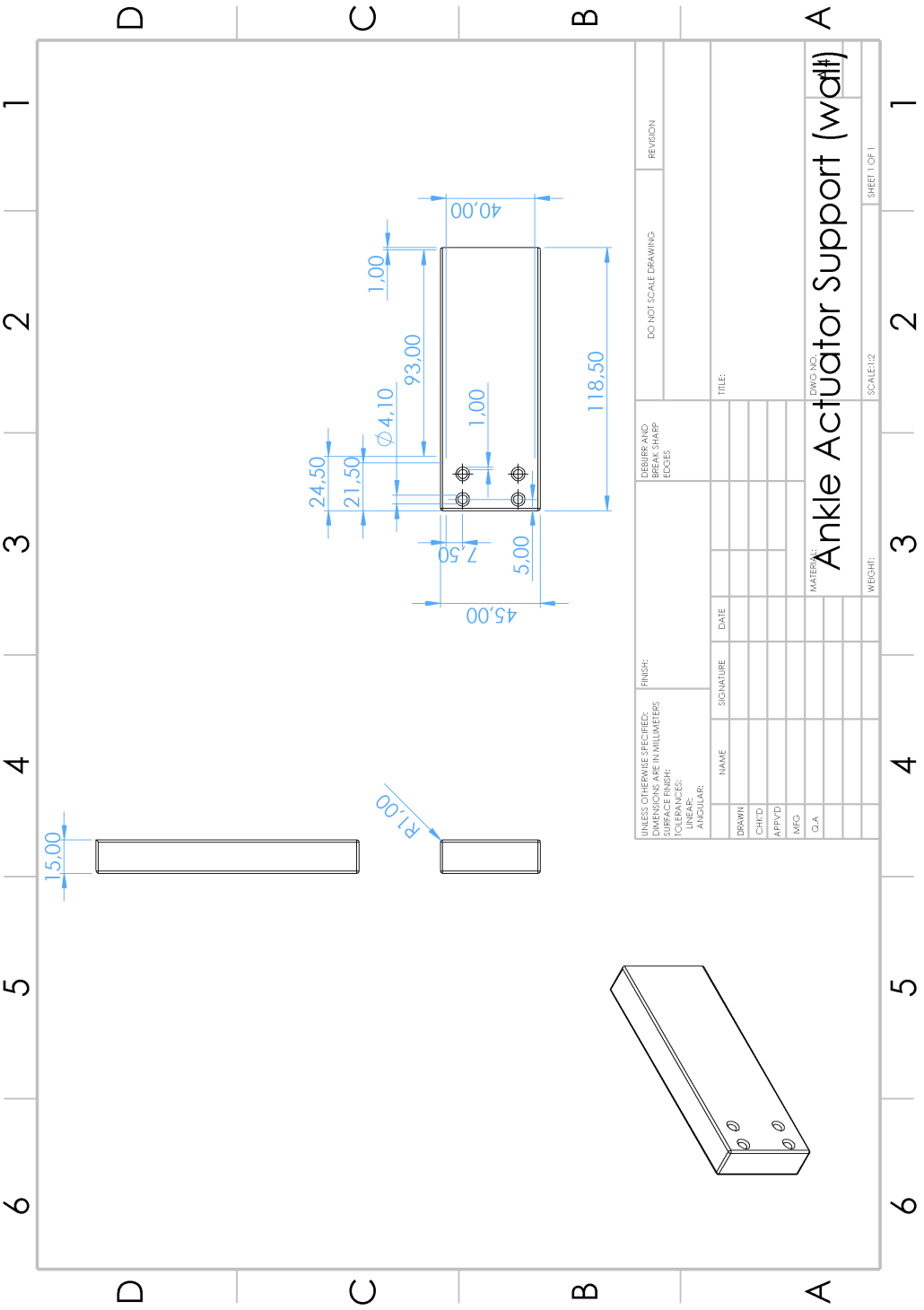


Figure B.9: Technical drawing of the ankle motor–encoder support wall.

B.3 Encoder Supports

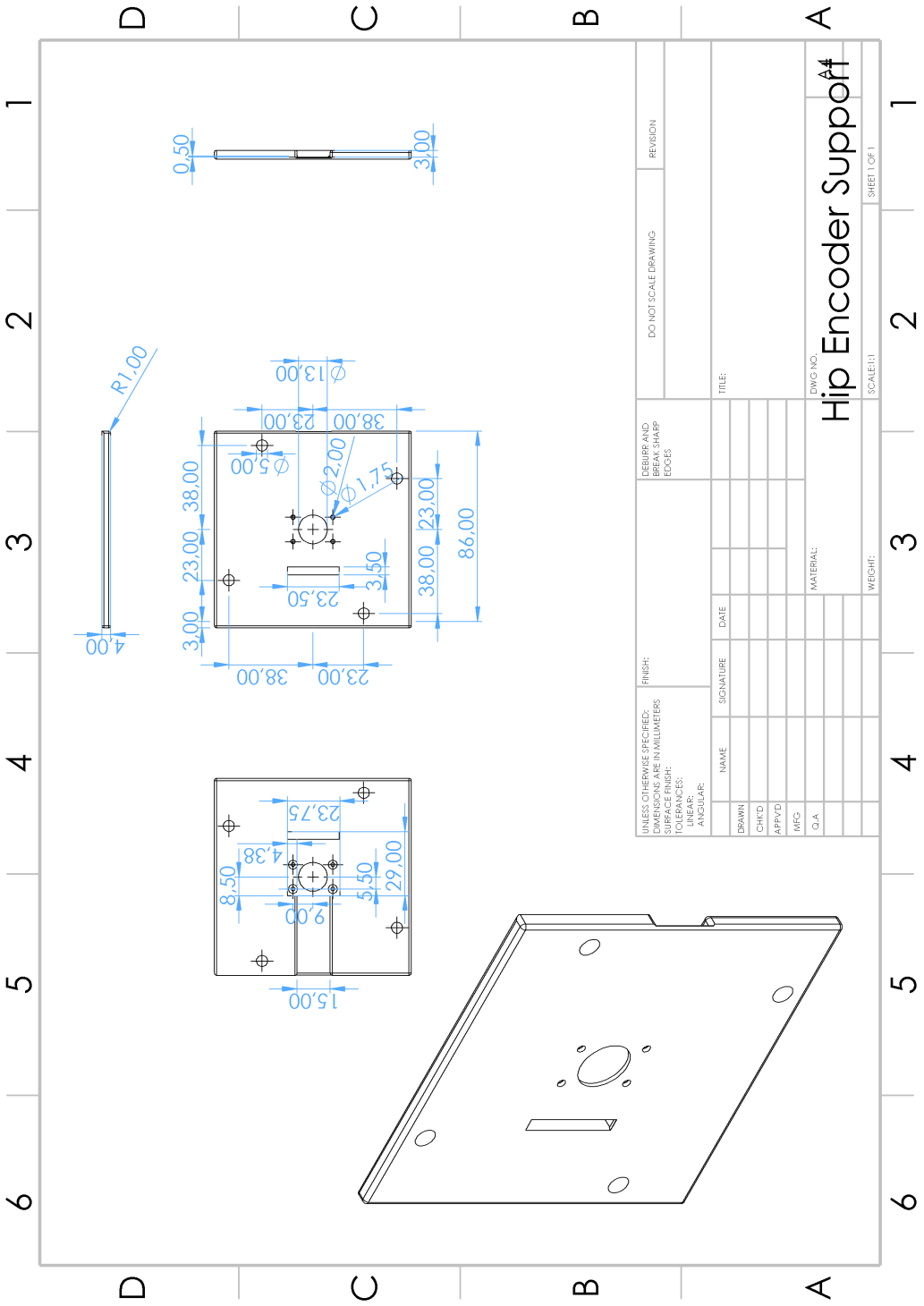


Figure B.10: Technical drawing of the hip encoder support.

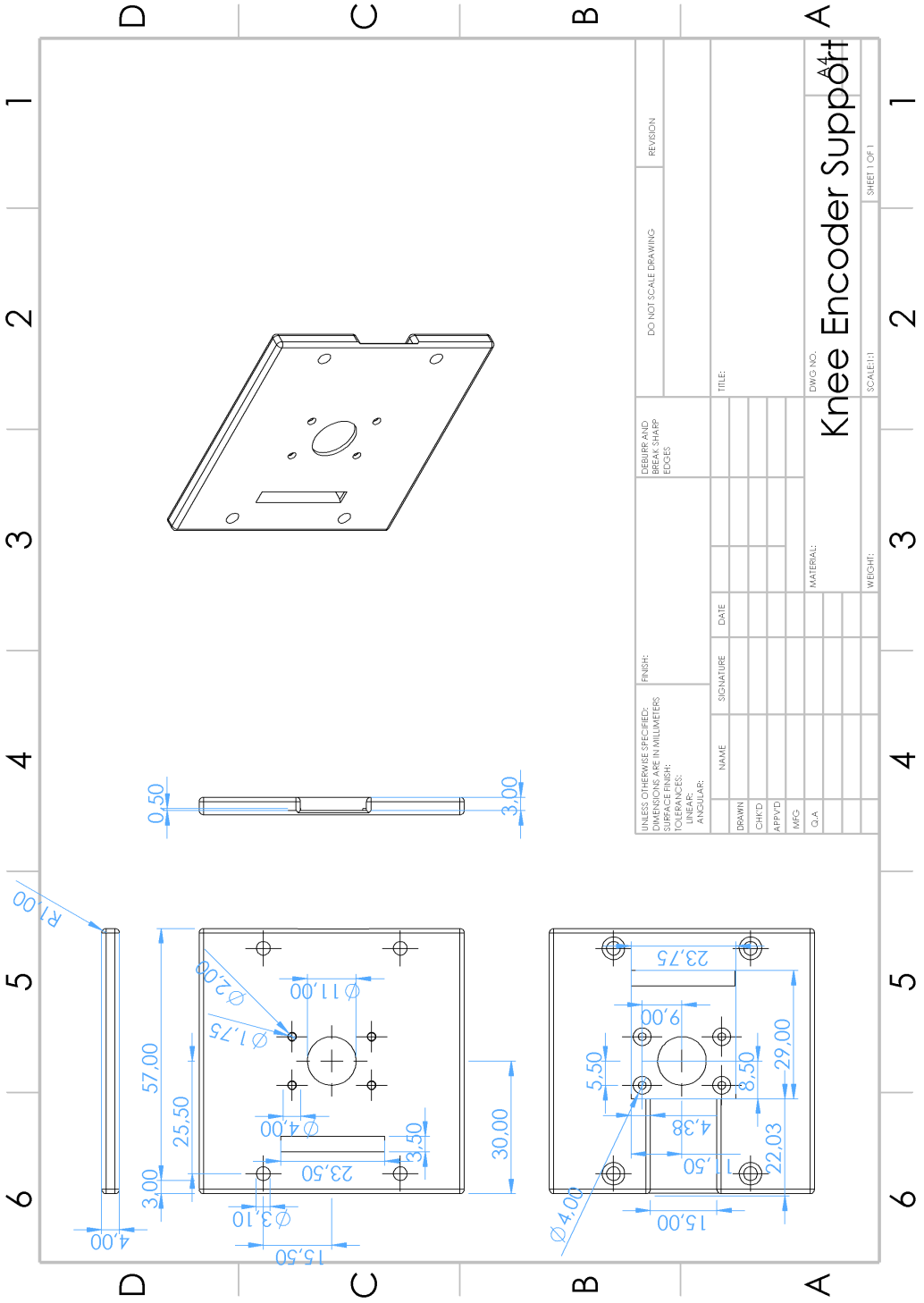


Figure B.11: Technical drawing of the knee encoder support.

B.4 Stationary Support Structure

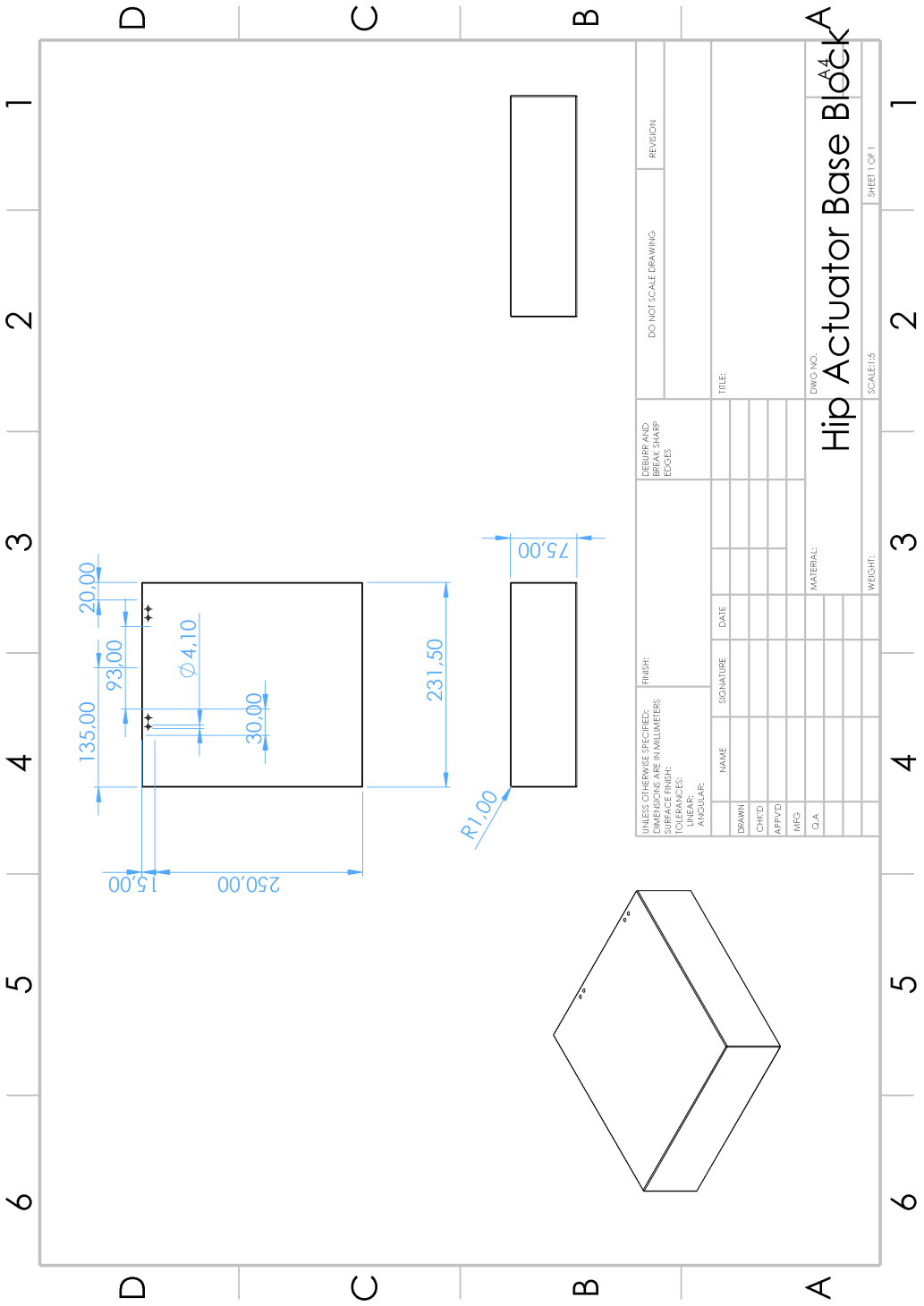


Figure B.12: Technical drawing of the hip motor mounting block.

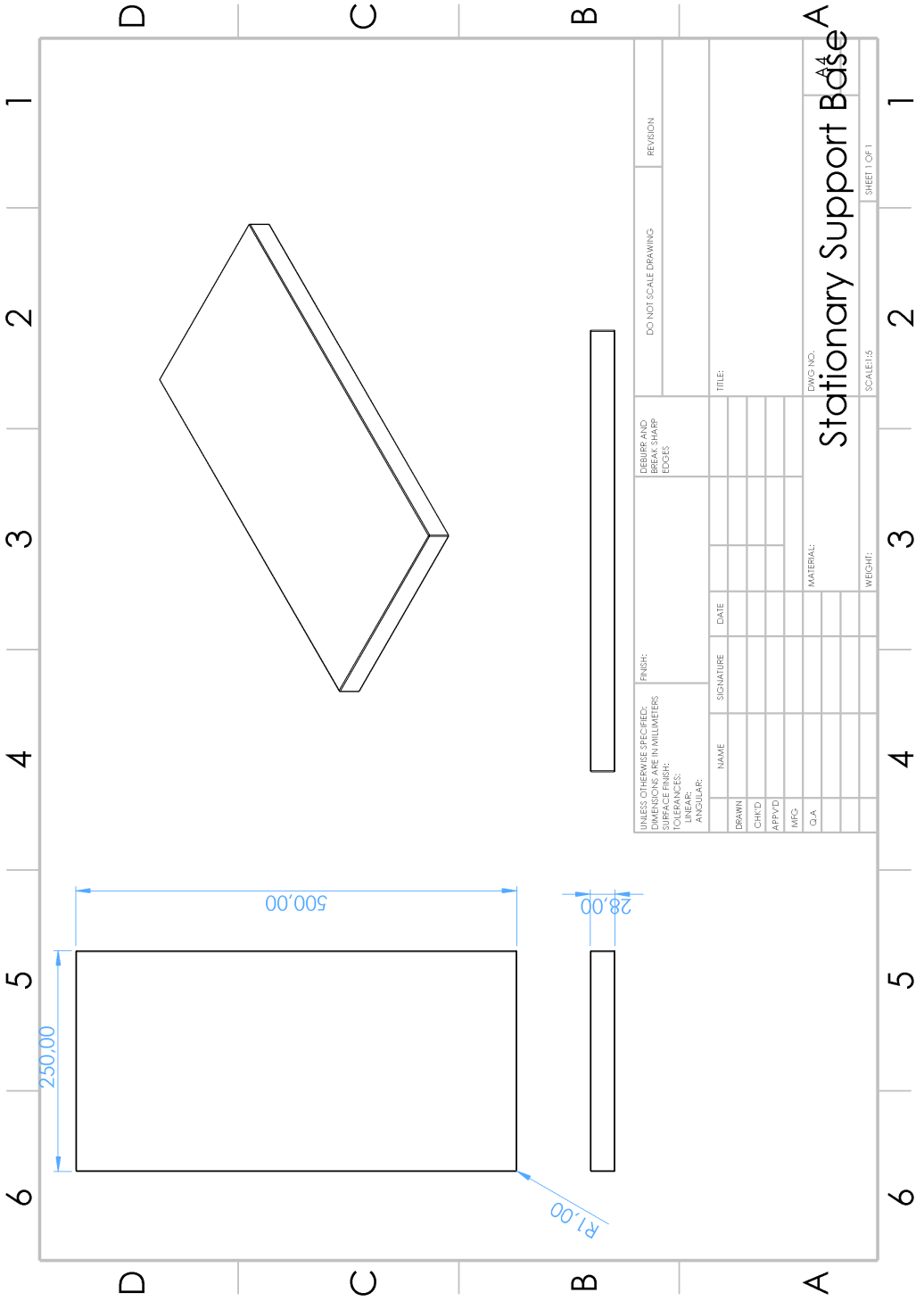


Figure B.13: Technical drawing of the stationary support base.

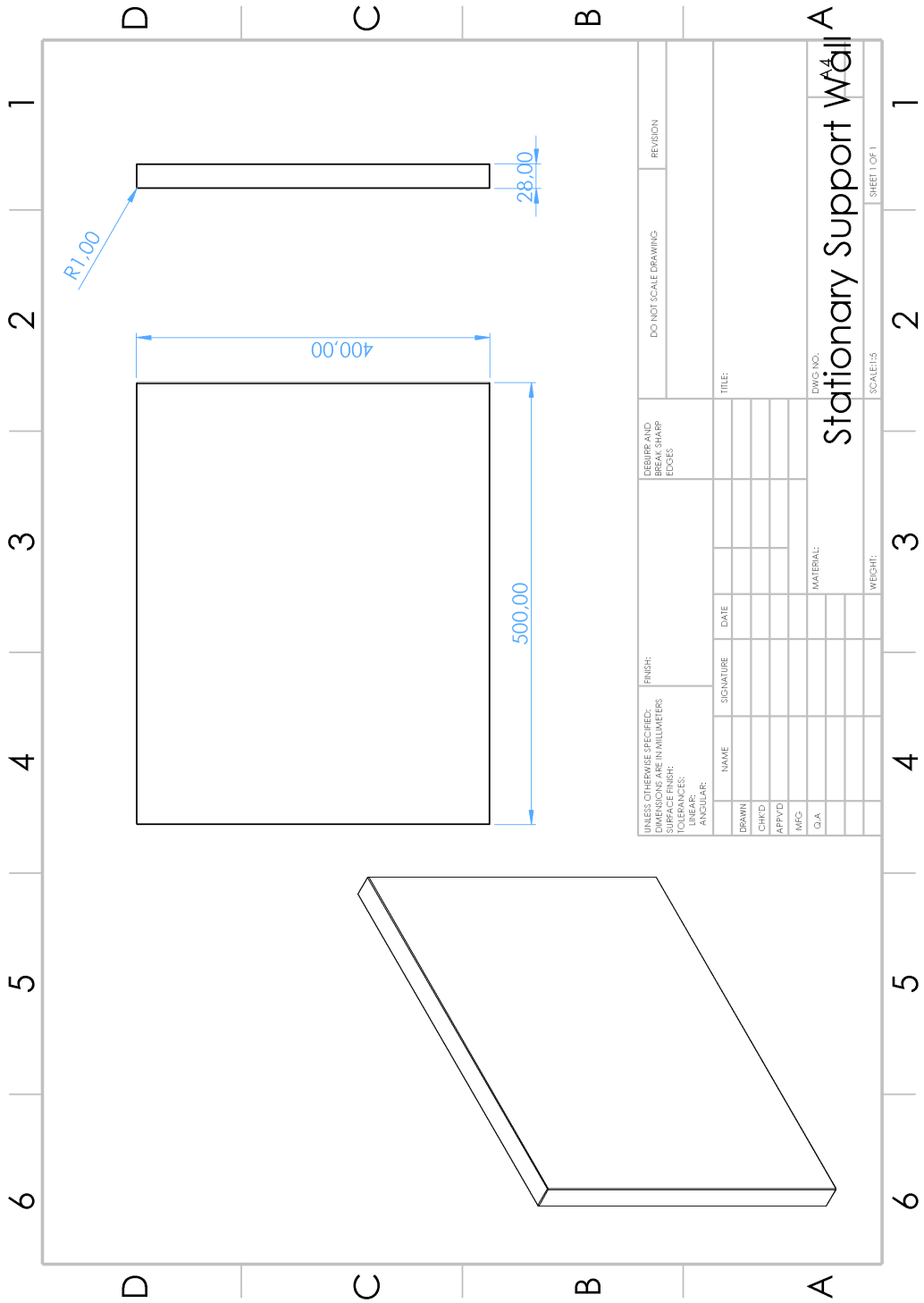


Figure B.14: Technical drawing of the stationary support wall.

Appendix C

Additional Validation Results

C.1 Encoder Operation

This section presents the additional encoder-operation results for the hip and ankle actuator assemblies. The same validation procedure described in Section 4.3.2 was applied to all three joints. The knee results are presented in the main text as a representative example, while the corresponding hip and ankle plots are included here for completeness.

C.1.1 Hip Joint

The accumulated and single-turn motor angles obtained during the hip rotation-unwrapping test are shown in Figure C.1.

C.1.2 Ankle Joint

The accumulated and single-turn motor angles obtained during the ankle rotation-unwrapping test are shown in Figure C.2.

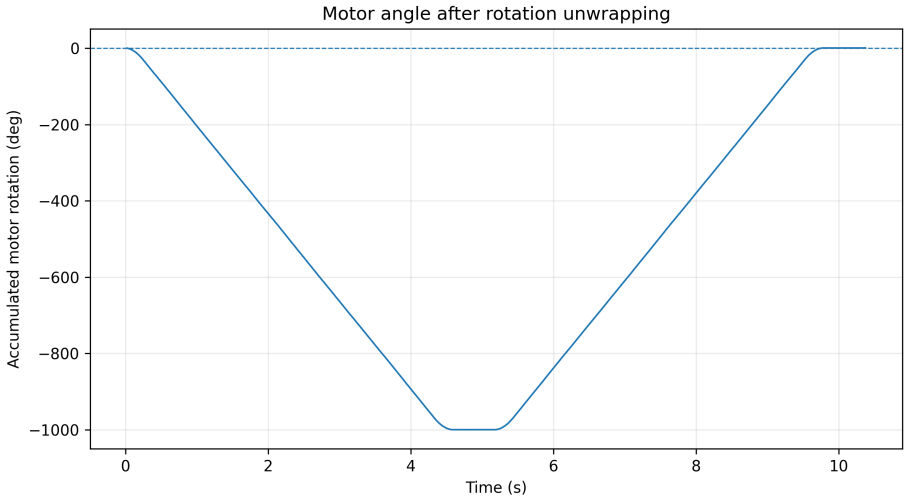
C.2 Joint-Position Tracking

This section presents the additional joint-position tracking plots for the hip and ankle actuator assemblies. The same validation procedures described in Section 4.3.3 were applied to all three joints. The knee results are presented in the main text as representative examples, while the corresponding hip and ankle plots are included here for completeness.

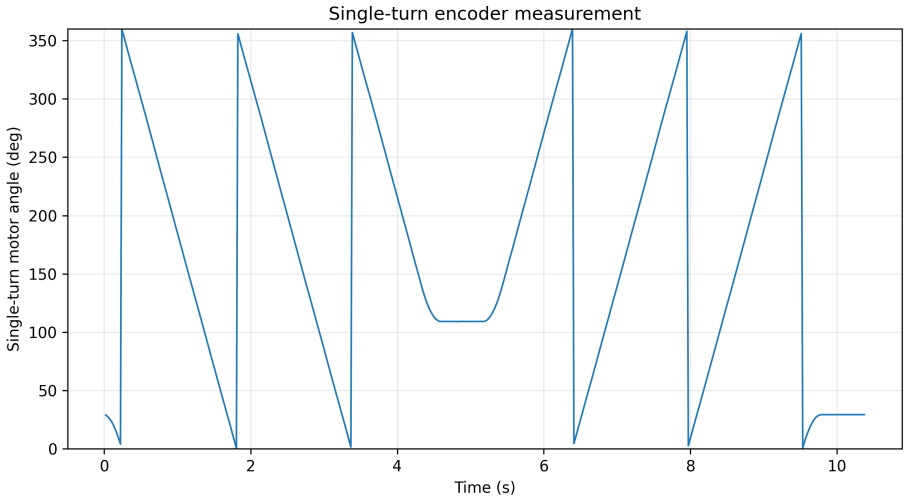
C.2.1 Hip Joint

Figure C.3 shows the comparison between the step-based and encoder-derived hip joint positions during the multi-position tracking test.

The errors recorded after each return to the initial position during the hip repeatability tests are shown in Figure C.4.

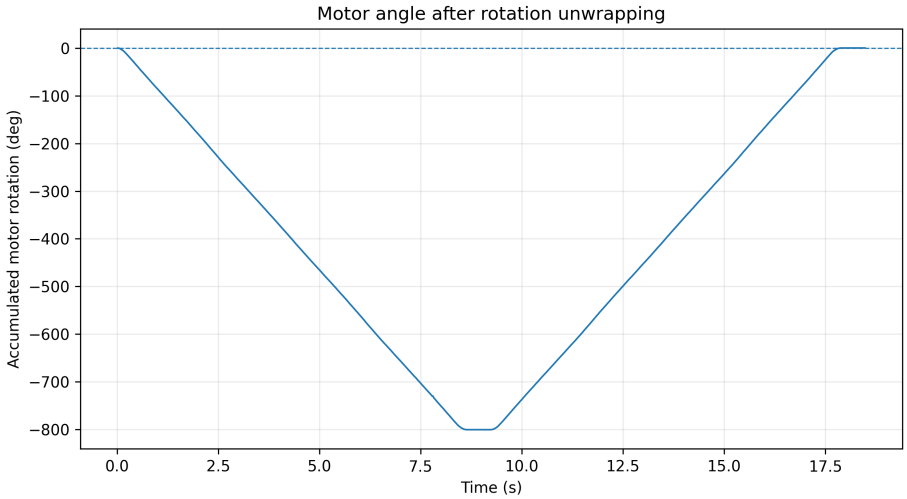


(a) Accumulated motor angle after unwrapping.

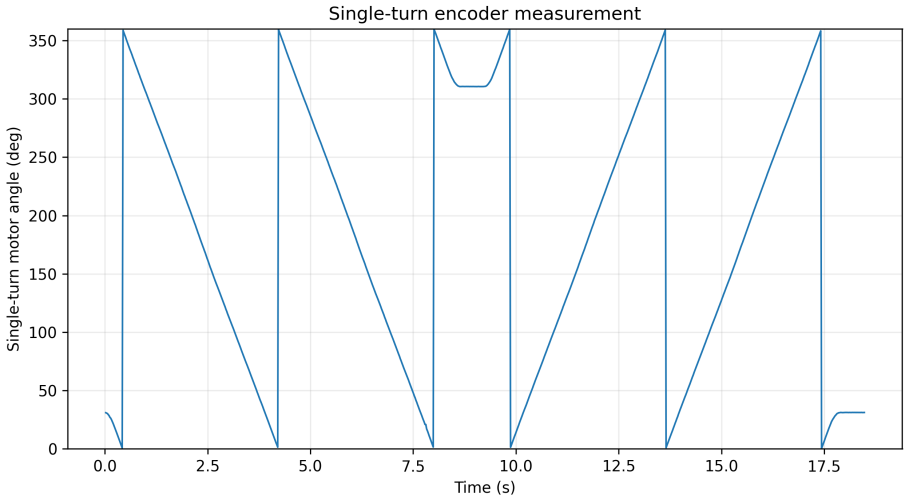


(b) Single-turn motor angle.

Figure C.1: Rotation-unwrapping results for the hip actuator.



(a) Accumulated motor angle after unwrapping.



(b) Single-turn motor angle.

Figure C.2: Rotation-unwrapping results for the ankle actuator.

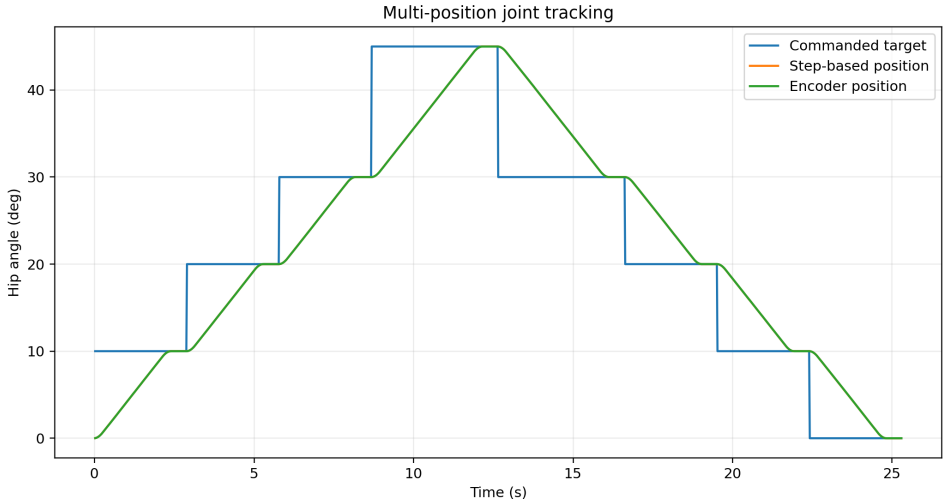
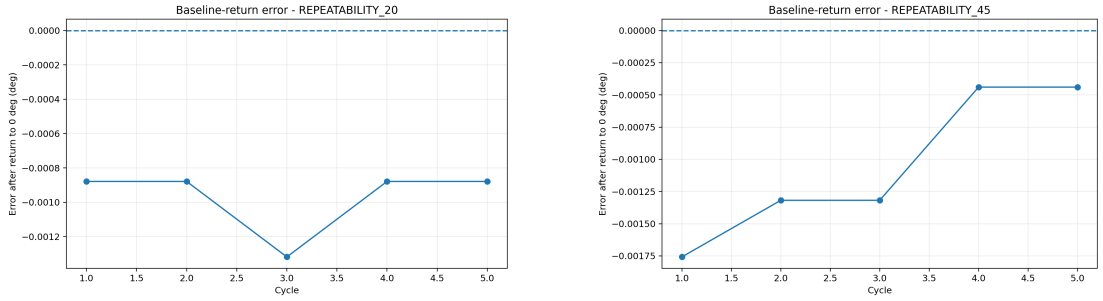


Figure C.3: Step-based and encoder-derived hip joint positions during the multi-position tracking test.



(a) 0°–20° movement range.

(b) 0°–45° movement range.

Figure C.4: Error after each return to the initial position during the hip joint repeatability tests.

The stationary encoder-derived hip joint-position measurement is shown in Figure C.5.

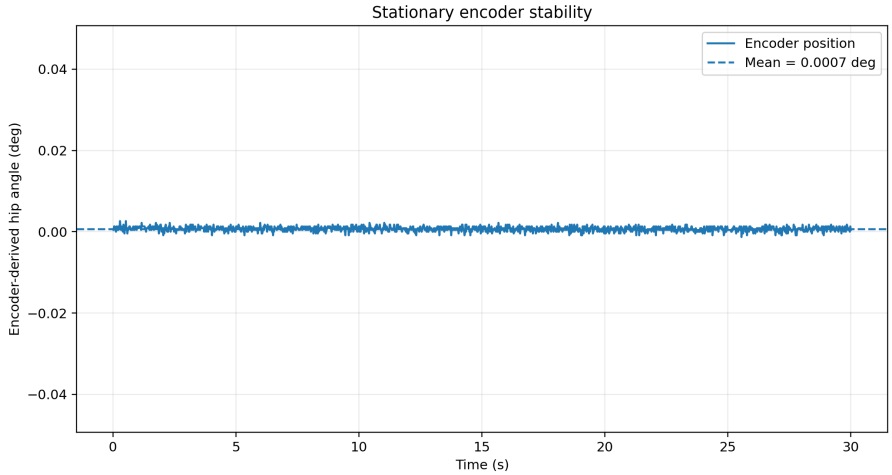


Figure C.5: Stationary stability of the encoder-derived hip joint-position measurement.

C.2.2 Ankle Joint

Figure C.6 shows the comparison between the step-based and encoder-derived ankle joint positions during the multi-position tracking test.

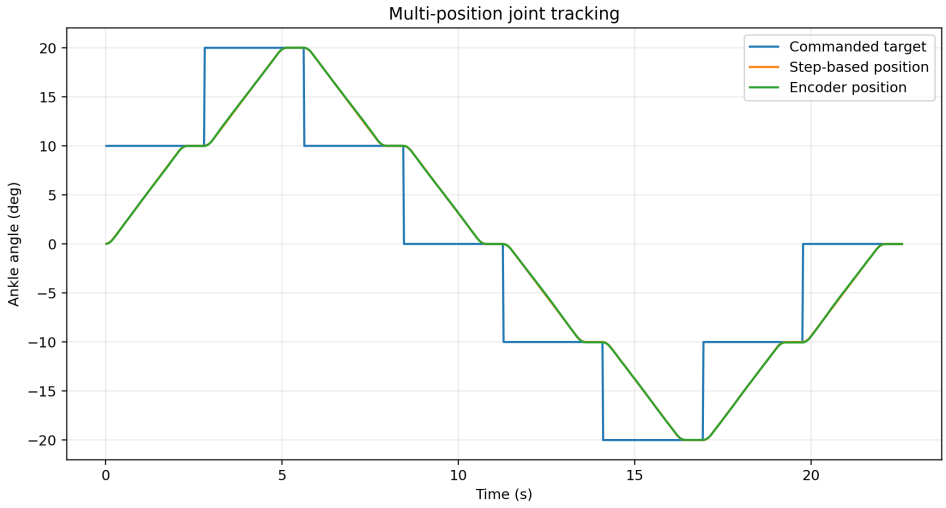
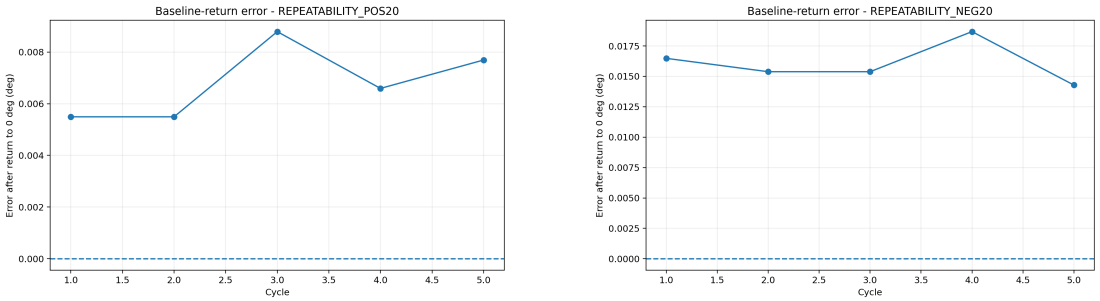


Figure C.6: Step-based and encoder-derived ankle joint positions during the multi-position tracking test.

The errors recorded after each return to the initial position during the ankle repeatability tests are shown in Figure C.7.

The stationary encoder-derived ankle joint-position measurement is shown in Figure C.8.



(a) 0°–+20° movement range.

(b) 0°–−20° movement range.

Figure C.7: Error after each return to the initial position during the ankle joint repeatability tests.

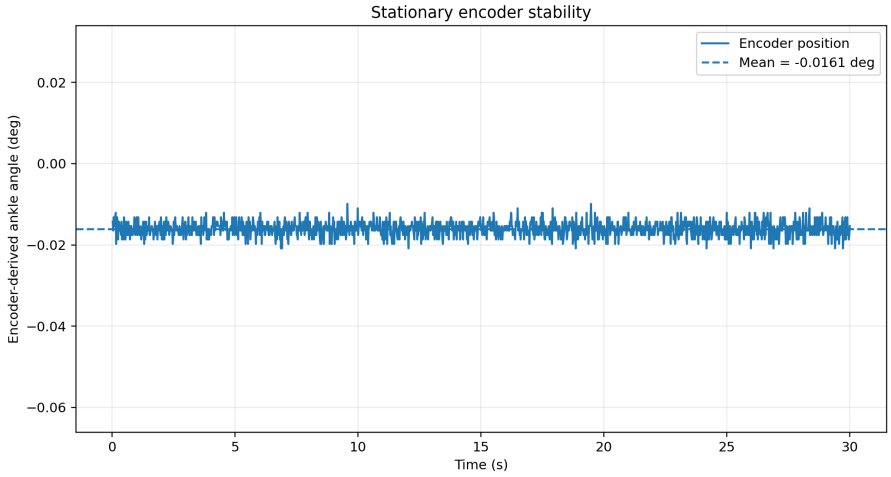


Figure C.8: Stationary stability of the encoder-derived ankle joint-position measurement.

C.3 EMG and Movement-Intention Validation

This section presents the additional EMG and movement-intention validation results for the hip and ankle muscle pairs. The same validation procedures described in Section 4.4 were applied to all three joints. The knee results are presented in the main text as representative examples, while the corresponding hip and ankle results are included here for completeness.

C.3.1 Hip Joint

Figure C.9 shows the acquired hip EMG signals and the corresponding calibration reference values.

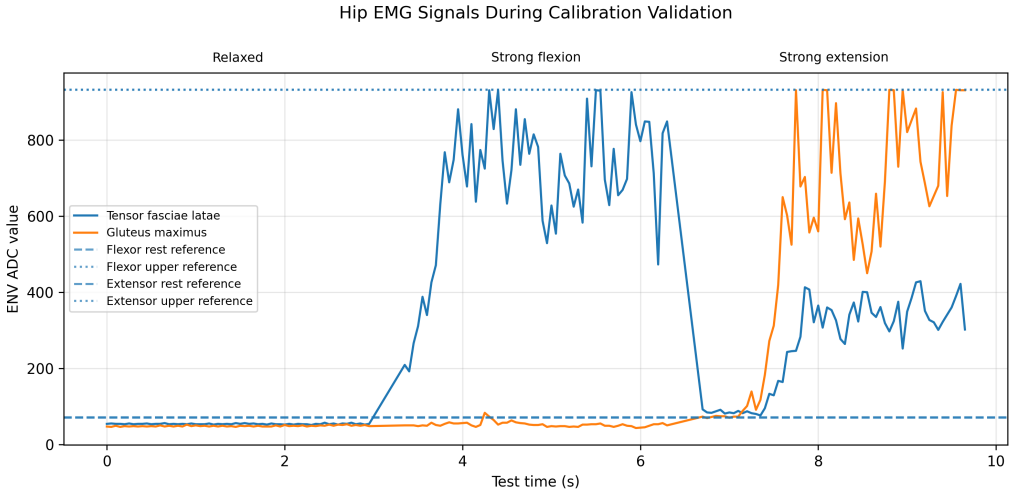


Figure C.9: EMG signals and calibration reference values for the hip muscle pair.

The corresponding normalised muscle activation values are shown in Figure C.10.

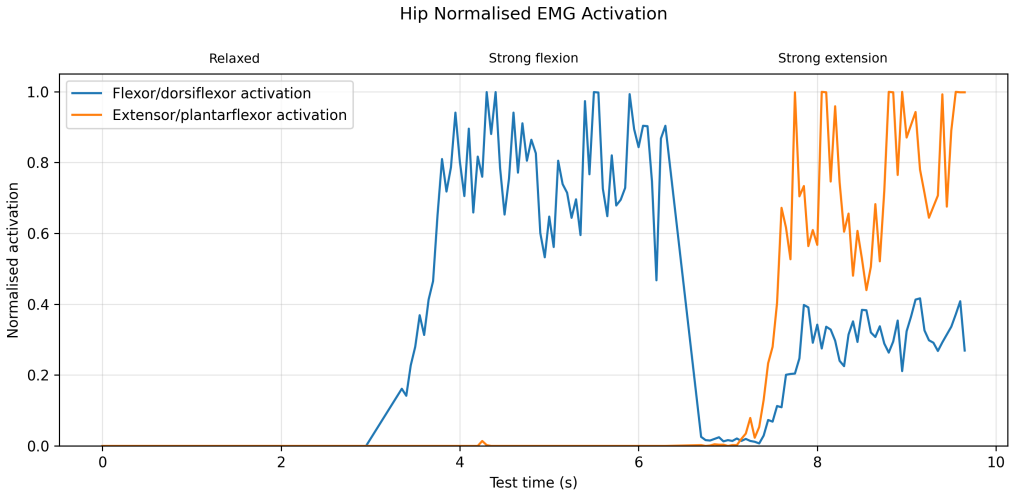


Figure C.10: Normalised flexor and extensor EMG activation for the hip muscle pair.

Figure C.11 shows the expected and detected states during the repeated relaxed, flexion and extension trials.

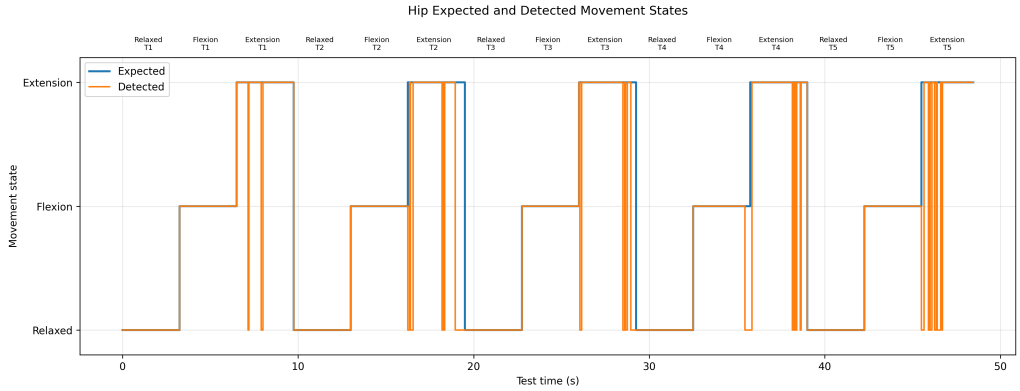


Figure C.11: Comparison between instructed and detected movement states during the hip validation trials.

The corresponding classification percentages are given in Table C.1.

Table C.1: Movement-state classification results for the hip.

State	**Correctly classified samples (%)**
Relaxed	100.0
Flexion	99.0
Extension	84.0

The movement-intensity results obtained for the three voluntary contraction levels are shown in Figure C.12.

C.3.2 Ankle Joint

Figure C.13 shows the acquired ankle EMG signals and the corresponding calibration reference values.

The corresponding normalised muscle activation values are shown in Figure C.14.

Figure C.15 shows the expected and detected states during the repeated relaxed, dorsiflexion and plantarflexion trials.

The corresponding classification percentages are given in Table C.2.

Table C.2: Movement-state classification results for the ankle.

State	**Correctly classified samples (%)**
Relaxed	100.0
Dorsiflexion	100.0
Plantarflexion	95.3

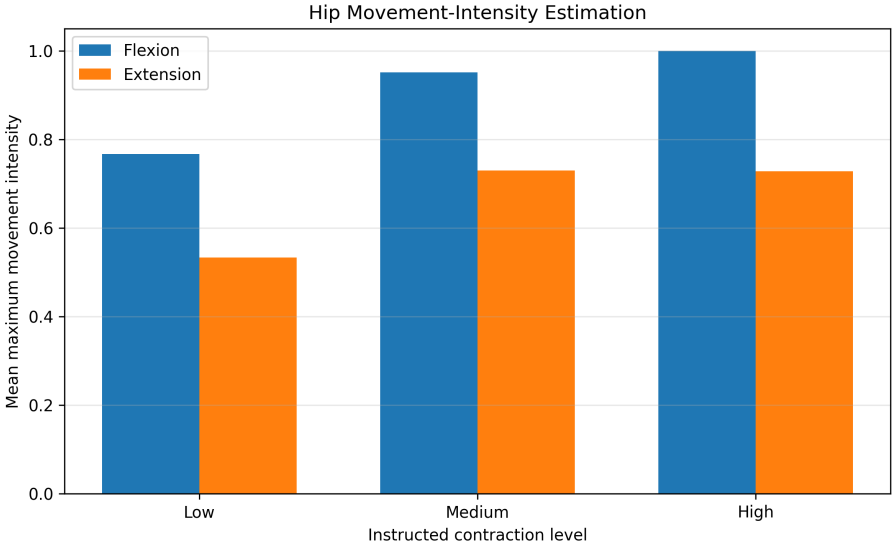


Figure C.12: Mean maximum estimated movement intensity for low, medium and high voluntary hip flexion and extension efforts.

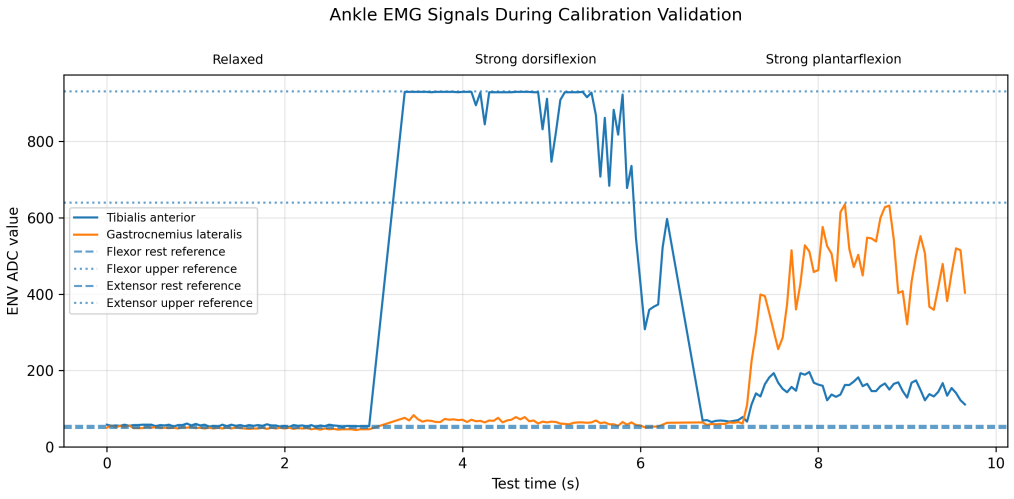


Figure C.13: EMG signals and calibration reference values for the ankle muscle pair.

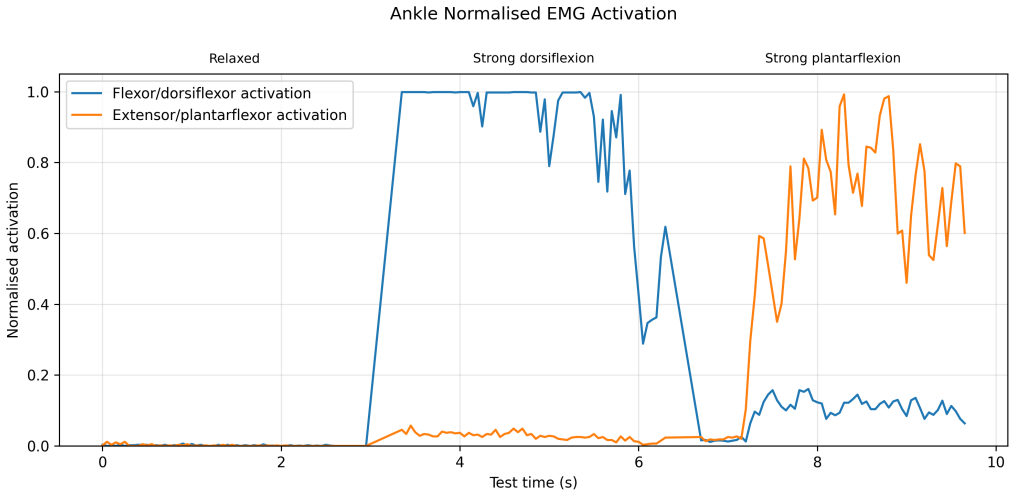


Figure C.14: Normalised dorsiflexor and plantarflexor EMG activation for the ankle muscle pair.

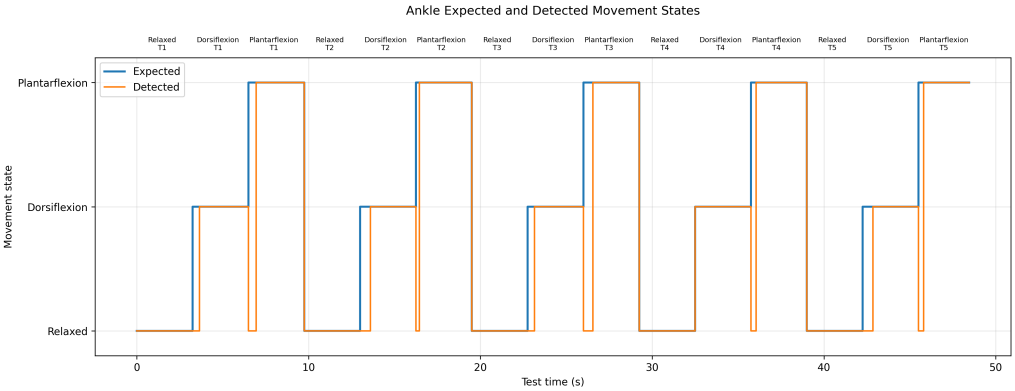


Figure C.15: Comparison between instructed and detected movement states during the ankle validation trials.

The movement-intensity results obtained for the three voluntary contraction levels are shown in Figure C.16.

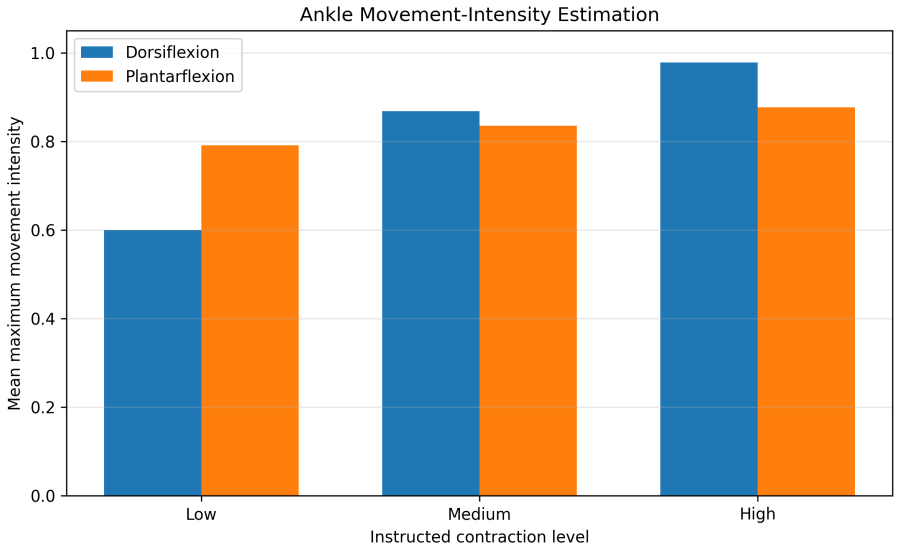


Figure C.16: Mean maximum estimated movement intensity for low, medium and high voluntary ankle dorsiflexion and plantarflexion efforts.

Appendix D

Integrated Validation Circuits

This appendix presents the electrical connections used during the integrated validation tests. Two configurations were used: a single-joint knee circuit and the complete three-joint circuit.

D.1 Single-Joint Knee Circuit

The electrical configuration used for the single-joint integration test is shown in Figure D.1. The main connections are listed in Table D.1.

Table D.1: Main connections used in the single-joint knee circuit.

Subsystem	**Connection**	**Destination**
Knee flexor MyoWare	ENV	Sensing Arduino A2
Knee extensor MyoWare	ENV	Sensing Arduino A3
MyoWare supply	5 V / GND	Sensing Arduino 5 V / GND
Serial communication	TX1 / RX1	Sensing Arduino ↔ actuation Arduino
Common reference	GND	Sensing Arduino ↔ actuation Arduino
Knee encoder	SDA	Actuation Arduino A4
Knee encoder	SCL	Actuation Arduino A5
Knee encoder	A1	5 V
Knee encoder	A2	GND
Knee encoder supply	5 V / GND	Actuation Arduino 5 V / GND
Driver STEP	PUL+	Actuation Arduino D4
Driver DIR	DIR+	Actuation Arduino D5
Driver ENABLE	ENA+	Actuation Arduino D9
Driver signal return	PUL- / DIR- / ENA-	Actuation Arduino GND
Driver supply	V+ / GND	24 V DC supply
Knee motor	A+ / A- and B+ / B-	Two stepper-motor winding pairs

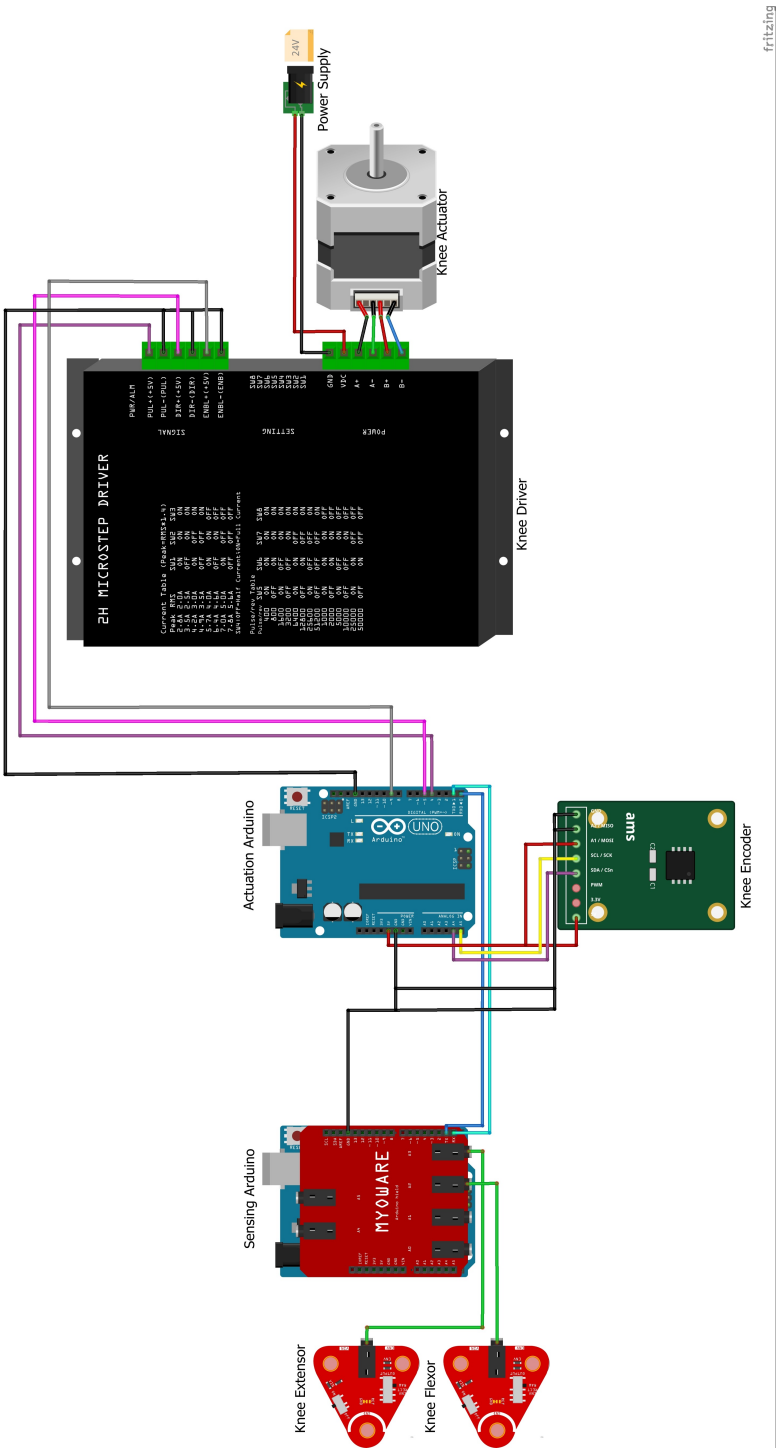


Figure D.1: Circuit used for the single-joint knee integration test.

D.2 Complete Three-Joint Circuit

The complete circuit shown in Figure D.2 was used for the instrumented multi-joint integration test in the seated configuration and for the additional functional check in the lying configuration. The principal motor-control connections are summarised in Table D.2, while the encoder configuration and shared connections are presented in Tables D.3 and D.4, respectively.

Table D.2: Actuation Arduino pins used for the motor-driver control signals.

Joint	**Driver STEP**	**Driver DIR**	**Driver ENABLE**
Hip	D2	D3	D8
Knee	D4	D5	D9
Ankle	D6	D7	D10

The three AS5048B encoders shared the same I^2C communication bus and were distinguished by their individual addresses. The address-selection configuration used for each encoder is shown in Table D.3.

Table D.3: I^2C address configuration of the three AS5048B encoders.

Joint	**I^2C address**	**A1**	**A2**
Hip	`0x40`	GND	GND
Knee	`0x41`	5 V	GND
Ankle	`0x42`	GND	5 V

Table D.4: Shared connections used in the complete three-joint circuit.

Subsystem	**Connection**	**Destination**
Six MyoWare sensors	ENV outputs	Sensing Arduino analogue inputs A0–A5
MyoWare supply	5 V / GND	Sensing Arduino 5 V / GND
Serial communication	TX / RX	Sensing Arduino ↔ actuation Arduino
Common reference	GND	Sensing Arduino ↔ actuation Arduino
Three AS5048B encoders	SDA	Actuation Arduino A4
Three AS5048B encoders	SCL	Actuation Arduino A5
Encoder supply	5 V / GND	Actuation Arduino 5 V / GND
Hip driver	Motor outputs	Hip stepper motor
Knee driver	Motor outputs	Knee stepper motor
Ankle driver	Motor outputs	Ankle stepper motor
Motor-driver supply	24 V / GND	External 24 V DC power supply

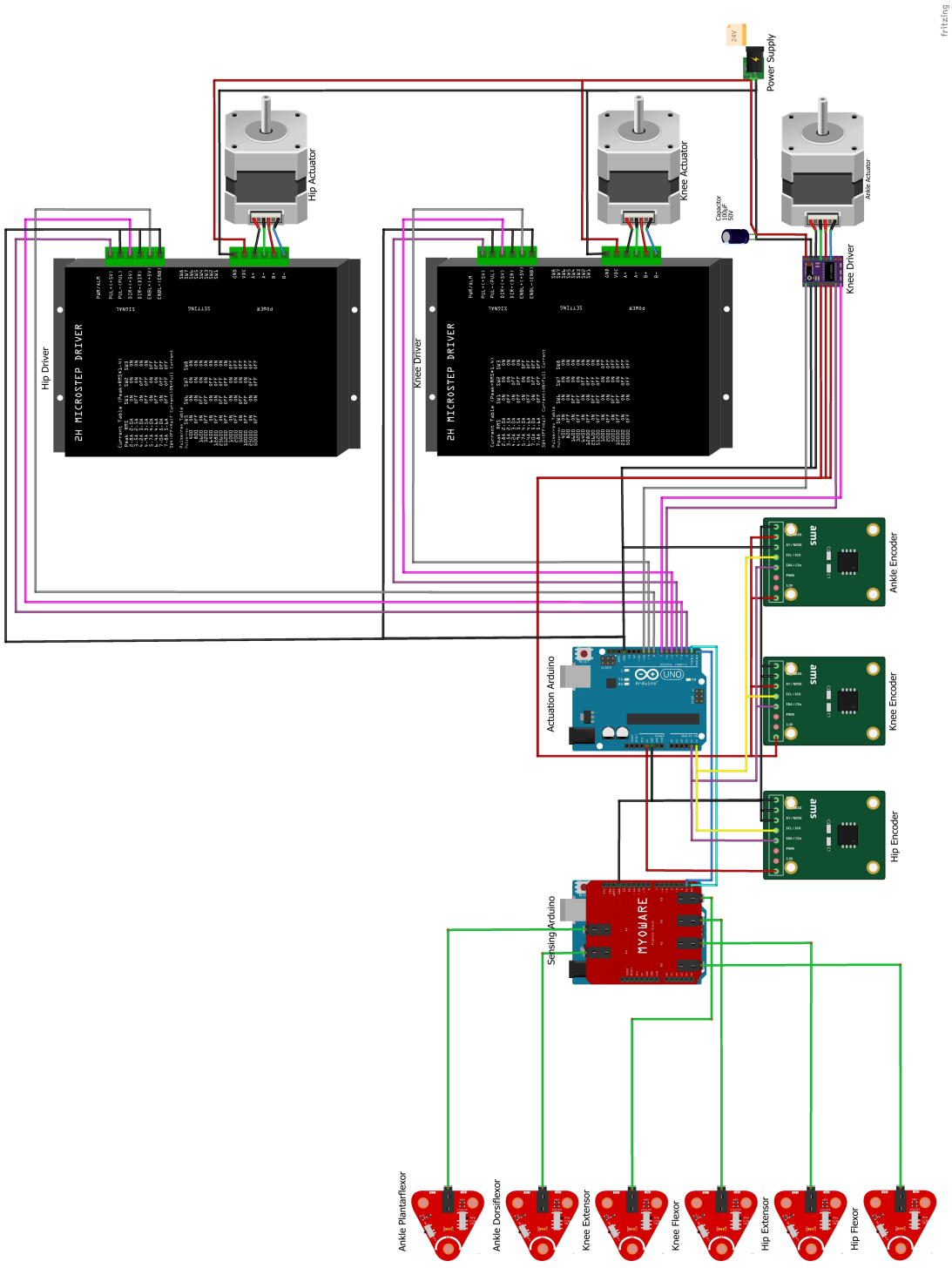


Figure D.2: Circuit used for the multi-joint integration test and the additional lying-configuration functional check.